



รายงานวิจัยฉบับสมบูรณ์

โครงการ อุปกรณ์ใดโอดเรื่องแสงอินทรีย์ที่ใช้สารเรื่องแสงอินทรีย์ชนิดใหม่ Organic Light-Emitting Diodes (OLEDs) Based on Novel Organic Electroluminescent Materials

โดย

รศ.ดร. วินิช พรมอารักษ์

วันสิ้นสุคสัญญา

30 มิถุนายน 2554

รายงานวิจัยฉบับสมบูรณ์

โครงการ อุปกรณ์ใดโอดเรื่องแสงอินทรีย์ที่ใช้สารเรื่องแสงอินทรีย์ชนิดใหม่
Organic Light-Emitting Diodes (OLEDs) Based on Novel Organic
Electroluminescent Materials

รศ.ดร. วินิช พรมอารักษ์

ภาควิชาเคมี คณะวิทยาศาสตร์ มหาวิทยาลัยอุบลราชธานี

สนับสนุนทุนวิจัยโดยสำนักงานคณะกรรมการการอุดมศึกษา

และสำนักงานกองทุนสนับสนุนการวิจัย

)ความเห็นในรายงานนี้เป็นของผู้วิจัย สกอ .และ สกว .ไม่จำเป็นต้องเห็นด้วยเสมอไป(

บทสรุปผู้บริหาร (Excusive Summary) ทุนเพิ่มขีดความสามารถด้านการวิจัยของอาจารย์รุ่นกลางในสถาบันอุดมศึกษา

1. ชื่อโครงการ

(ภาษไทย) อุปกรณ์ใดโอดเรื่องแสงอินทรีย์ที่ใช้สารเรื่องแสงอินทรีย์ชนิดใหม่
(ภาษาอังกฤษ) Organic Light-Emitting Diodes (OLEDs) Based on Novel Organic
Electroluminescent Materials

- **2. คณะผู้วิจัย** รศ.คร. วินิช พรมอารักษ์
- 3. สถาบันต้นสังกัด/สถานที่ติดต่อ

ภาควิชาเคมี คณะวิทยาศาสตร์ มหาวิทยาลัยอุบลราชธานี อ. วารินชำราบ จ .อุบลราชธานี 34190 โทรศัพท์ 081 5930005 โทรสาร 045 288379

- 4. ระยะเวลาโครงการ 3 ปี
- 5. บทสรุปโครงการวิจัย

ในโครงการวิจัยนี้เราทำการสังเคราะห์สารอินทรีย์ที่เป็นสารเรื่องแสง สารส่งผ่านประจุบวก และ สารอินทรีย์ที่เป็นทั้งสารเรื่องแสงและเป็นสารส่งผ่านประจุบวก เช่น อนุพันธ์ของ 9.10-substituted anthracene อนุพันธ์ของ 9,9-bis(4-diphenylaminophenyl)fluorene โมเลกุลของ biphenyl functioned 9,9-โมเลกูลของ bis(4-diphenylaminophenyl)fluorene pyrene-functionalized 9.9-bis(4diphenylaminophenyl)fluorene และโมเลกูลของ bis(4-diphenylaminophenyl)carbazole fluorene สำหรับเป็นทั้งสารเรื่องแสงสีน้ำเงินและเป็นสารส่งผ่านประจุบวก อนุพันธ์ของ oligofluorenethiophenes และ fluorene-oligothiophenes perylenediimide triads สำหรับเป็นสารเรื่องแสง และ carbazole dendronized triphenylamines สำหรับเป็นสารส่งผ่านประจุบวก ทำการพิสูจนเอกลักษ์ด้วยเทคนิค ¹H, ¹³C NMR, FT-IR, UV-vis, PL spectroscopy และ mass spectrometry การศึกษาพบว่าสมบัติทางแสง สมบัติทาง ความร้อน และสมบัติทางไฟฟ้าเคมีของสารที่ได้ สารที่ได้ทุกโมเลกุลมีประสิทธิภาพการเรื่องแสงที่ดี สาร เหล่านี้ถูกใช้เป็นชั้นสารเรื่องแสงในอุปกรณ์ใคโอคเรื่องแสงอินทรีย์ที่มีโครงสร้างเป็น ITO/PEDOT:PSS/ สารเป้าหมาย/BCP/Alq3/LiF:Al และ ITO/PEDOT:PSS/สารเป้าหมาย/BCP/Alq3/LiF:Al อุปกรณ์ใคโอคที่ ทั้งนี้ขึ้นอยู่กับชั้นของสารเรื่องแสงหรือสารเป้าหมายที่ใช้ ได้ทั้งหมดเปล่งแสงตั้งแต่สีน้ำเงินถึงสีเหลือง อนุพันธ์ของ 9,10-substituted anthracene ที่มีหมู่ electron donating triphenylamine เป็นหมู่แทนที่แสดง สมบัติทั้งสารเรื่องแสงสีน้ำเงิน และเป็นสารส่งผ่านประจุบวกสำหรับอุปกรณ์ไคโอคเรื่องแสงอินทรีย์ ความสามารถในการเป็นสารส่งผ่านประจบวกเทียบเท่ากับ NPB ไคโอคเรื่องแสงสีน้ำเงินให้ประสิทธิภาพ เท่ากับ 1.65 cd/A และใดโอดเรื่องแสงสีเขียวให้ประสิทธิภาพเท่ากับ 6.25 cd/A อนุพันธ์ของ 9,9-bis(4diphenylaminophenyl) fluorene ที่มีหมู่ biphenyl เป็นหมู่แทนที่ที่ตำแหน่ง 2,7-ของหมู่ 9,9-bis(4diphenylaminophenyl)fluorene แสคงสมบัติทั้งสารเรื่องแสงสีน้ำเงินและเป็นสารส่งผ่านประจุบวกสำหรับ อุปกรณ์ไดโอดเรื่องแสงอินทรีย์ ความสามารถในการเป็นสารส่งผ่านประจุบวกเทียบเท่ากับ NPB ไดโอด เรื่องแสงสีน้ำเงินให้ประสิทธิภาพเท่ากับ 2.48 cd A^{-1} และ ไดโอดเรื่องแสงสีเขียวให้ประสิทธิภาพเท่ากับ 4.40 cd A^{-1} และ มี turn-on voltage ที่ต่ำเท่ากับ 3.1 และ 2.8 V ตามลำดับ สำหรับอุปกรณ์ไดโอดเรื่องแสงอินทรีย์ ของอนุพันธ์ของ oligofluorene-thiophenes เปล่งแสงตั้งแต่สีน้ำเงินถึงสีส้ม ทั้งนี้ขึ้นอยู่กับชั้นของสารเรื่อง แสงหรือสารเป้าหมายที่ใช้ ให้ประสิทธิภาพเท่ากับ 11.15 cd/A ส่วนสาร carbazole dendronized triphenylamines แสดงสมบัติทางความร้อนที่สูง โดยมี glass transition temperatures (T_g) สูงถึง 401 °C เมื่อ ใช้เป็นสารส่งผ่านประจุบวกในอุปกรณ์ไดโอดเรื่องแสงอินทรีย์ที่มีโครงสร้าง ITO/PEDOT:PSS/HTL/Alq3 /LiF:Al ไดโอดเรื่องแสงสีเขียวให้ประสิทธิภาพเท่ากับ 4.47 cd A^{-1} และมี turn-on voltage ที่ต่ำเท่ากับ 3.0 V

6. สรุปผลลัพธ์จากงานวิจัย (Output)

ผลลัพธ์	ทางตรง (หน่วยนับ)							
องค์ความรู้	- การพัฒนาโมเลกุลสารอินทรีย์ที่มีสมบัติเป็นสารเรื่องแสงอินทรีย์ สำหรับ							
	อุปกรณ์ใดโอดเรื่องแสงอินทรีย์							
	- สมบัติทางกายภาพของโมเลกุลสารอินทรีย์ที่มีสมบัติเป็นสารเรื่องแสง							
	อินทรีย์ที่ได้							
	สมบัติของอุปกรณ์ใคโอคเรื่องแสงอินทรีย์							
	- สร้างต้นแบบของอุปกรณ์ใดโอคเรื่องแสงอินทรีย์							
รางวัล	1. รางวัล Wiley-CST Outstanding Publication Award 2011 ปี 2554 จาก							
	สมาคมเคมีแห่งประเทศไทยในพระบรมราชูปถัมภ์ จากผลงานตีพิมพ์							
	เรื่อง Bifunctional anthracene derivatives as non-doped blue emitters and							
	hole-transporters for electroluminescent devices, Chemical							
	Communications, 2011, 47, 7122-7124. (IF 5.80)							
	ผลงานตีพิพ์ที่ได้รับการลงปกของวารสาร							
	จากผลงานตีพิมพ์ เรื่อง Carbazole Dendronised Triphenylamines as							
	Solution Processed High Tg Amorphous Hole-Transporting Materials for							
	Organic Electroluminescent Devices, Chemical Communications, 2012,							
	48, 3365-3464							
บทความทางวิชาการ	1. A Thangtong, D. Meunmart, T. Sudyoadsuk, S. Jungsuttiwong, N.							
ผลงานตีพิมพ์ใน	Prachumrak, T. Keawin and V. Promarak, Bifunctional anthracene							
วารสารระดับนานาชาติ	derivatives as non-doped blue emitters and hole-transporters for							
	electroluminescent devices, Chemical Communications, 2011, 47, 7122-							
	7124. (IF 5.80)							
	2. A. Thangthong, D. Meunmart, N. Prachumrak, S. Jungsuttiwong, T.							
	Keawin, T. Sudyoadsuk and V. Promarak, Synthesis and							
	characterization of 9,10-substituted anthracene derivatives as blue light-							

- emitting and hole-transporting materials for electroluminescent devices, *Tetrahedron*, **2012**, 68, 1853-1861. (**IF 3.01**)
- A. Thangthong, N. Prachumrak, R. Tarsang, T. Keawin, S. Jungsuttiwong, T. Sudyoadsuk and V. Promarak, Blue Light-Emitting and Hole-Transporting Materials Based on 9,9-Bis(4-diphenylaminophenyl)fluorenes for Efficient Electroluminescent Devices, *Journal of Materials Chemistry*, 2012, 6869–6877. (IF 5.01)
- P. Moonsin, N. Prachumrak, R. Rattanawan, T. Keawin, S. Jungsuttiwong, T. Sudyoadsuk and V. Promarak, Carbazole Dendronised Triphenylamines as Solution Processed High Tg Amorphous Hole-Transporting Materials for Organic Electroluminescent Devices, Chemical Communications, 2012, 48, 3365-3464 (Inside cover image). (IF 5.80)
- J. Khunchalee, R.Tarsang, N. Prachumrak, S. Jungsuttiwong, T. Keawin,
 T. Sudyoadsuk and V. Promarak, Synthesis and Properties of Oligofluorene-thiophenes as Emissive Materials for Organic Electroluminescent Devices, *Tetrahedron*, 2012, submitted
- D. Muenmart, R. Tarsang, S. Jungsuttiwong, T. Keawin, T. Sudyoadsuk and V. Promarak, Synthesis and Properties of Fluorene-oligothiophenes Perylenediimide Triads and Their Electropolymerizations, *Journal of Materials Chemistry*, 2012, submitted
- N. Prachumrak, A. Thangthong, R. Tarsang, T. Keawin, S. Jungsuttiwong, T. Sudyoadsuk, and V. Promarak, Pyrene-Functionalized 9,9-Bis(4-diphenylaminophenyl)fluorene as Solution-Processed Blue Emitting and Hole-Transporting Materials for Efficient Electroluminescent Devices, Organic Electronics, 2012, submitted
- 8. A. Thangthong, N. Prachumrak, S. Namuangruk, S. Jungsuttiwong, T. Keawin, T.Sudyoadsuk and V. Promarak, Synthesis, Properties and Applications of Biphenyl Functioned 9,9-Bis(4-diphenylaminophenyl)fluorene as Bifunctional Materials for Organic Electroluminescent Devices, *Tetrahedron*, 2012, submitted
- D. Meunmart, N. Prachumrak, T. Keawin, S. Jungsuttiwong, T. Sudyoadsuk and V. Promark, Bis(4-diphenylaminophenyl)carbazole end-capped fluorene as solution-processed deep blue light-emitting and

	hole-transporting materials for electroluminescent devices, <i>Tetrahedron</i>						
	Letters, 2012, submitted						
	10. S. Namuangruk, M. Ehara, R.Fukuda, J. Meeprasert, T. Khanasa, S.						
	Morada, T. Kaewin, S. Jungsuttiwong, T. Sudyoadsuk and						
	Promarak , Synthesis, characterization, and theoretical investigation of						
	D-D- π -A type organic dyes for dye-sensitized solar cells, <i>Jouranl of</i>						
	American Chemical Society, 2012, in submission process						
เอกสารประกอบการ	1. V. Promarak, T. Sudyoadsuk, S. Jungsuttiwong, N. Prachumrak, D.						
ประชุม/สัมมนาใน และ	Meunmart, and A. Phansuphon, Novel Blue Electroluminescence						
ต่างประเทศ	Materials Based on 9,10-Disubstituted Anthracenes for OLEDs, The 8th						
	International Conference on Optical Probes of Conjugated Polymers and						
	Organic Nanostructures, China, 2009, 133.						
	2. N. Prachumrak, T. Keawin, S. Jungsuttiwong, T. Sudyoadsuk and V.						
	Promarak , 9,10-Substituted Anthracene Derivatives as Blue Light-						
	Emitting and Hole-Transporting Materials for Electroluminescent						
	Devices, International Symposium on Electronic/Optic Functional						
	Molecules (ISEOFM2012) ระหว่างวันที่ 11 -13 มีนาคม 55 ณ ประเทศ						
	China						
การผลิตบุคลากร							
ุ นักศึกษาระดับปริญญา	1. นางสาวอัจฉราพรรณ โพธิ์ทอง						
์ เตรี	2. นายอิสรา พลนงค์						
	3. นายศักดิ์ระวี พันสาย						
	4. นางสาวทิติยา สุนนท์นาม						
	5. นางสาวศิริพรรณ แก่นสาร์						
 นักศึกษาระดับปริญญา	1. นางสาว อมรรัตน์ พันธุ์สุผล						
โท-เอก	2. นาย นริศ ประชุมรักษ์						
	3. นางสาวจานียา ขันชะถี						
	 4. นางสาวดวงรัชนีกร เหมือนมาตย์						
	5. นายปรีชา มูลสิน						
เอกสารทางวิชาการ							
 รายงานฉบับสมบูรณ์	เรื่อง อุปกรณ์ใดโอดเรื่องแสงอินทรีย์ที่ใช้สารเรื่องแสงอินทรีย์ชนิดใหม่						
v v							

บทคัดย่อ

ในโครงการวิจัยนี้เราทำการสังเคราะห์สารอินทรีย์ที่เป็นสารเรื่องแสง สารส่งผ่านประจุบวก และ สารอินทรีย์ที่เป็นทั้งสารเรื่องแสงและเป็นสารส่งผ่านประจุบวก เช่น อนพันธ์ของ 9.10-substituted anthracene อนพันธ์ของ 9,9-bis(4-diphenylaminophenyl)fluorene โมเลกุลของ biphenyl functioned 9,9bis(4-diphenylaminophenyl)fluorene โมเลกูลของ pyrene-functionalized 9.9-bis(4diphenylaminophenyl)fluorene และ โมเลกุลของ bis(4-diphenylaminophenyl)carbazole end-capped fluorene สำหรับเป็นทั้งสารเรื่องแสงสีน้ำเงินและเป็นสารส่งผ่านประจุบวก อนุพันธ์ของ oligofluorenethiophenes และ fluorene-oligothiophenes perylenediimide triads สำหรับเป็นสารเรื่องแสง และ carbazole dendronized triphenylamines สำหรับเป็นสารส่งผ่านประจุบวก ทำการพิสูจนเอกลักษ์ด้วยเทคนิค ¹H, ¹³C NMR, FT-IR, UV-vis, PL spectroscopy และ mass spectrometry การศึกษาพบว่าสมบัติทางแสง สมบัติทาง ความร้อน และสมบัติทางไฟฟ้าเคมีของสารที่ได้ สารที่ได้ทุกโมเลกุลมีประสิทธิภาพการเรื่องแสงที่ดี สาร เหล่านี้ถูกใช้เป็นชั้นสารเรื่องแสงในอุปกรณ์ใคโอคเรื่องแสงอินทรีย์ที่มีโครงสร้างเป็น สารเป้าหมาย/BCP/Alg3/LiF:Al และ ITO/PEDOT:PSS/สารเป้าหมาย/BCP/Alg3/LiF:Al อุปกรณ์ใดโอดที่ ได้ทั้งหมดเปล่งแสงตั้งแต่สีน้ำเงินถึงสีเหลือง ทั้งนี้ขึ้นอยู่กับชั้นของสารเรื่องแสงหรือสารเป้าหมายที่ใช้ อนพันธ์ของ 9,10-substituted anthracene ที่มีหมู่ electron donating triphenylamine เป็นหมู่แทนที่แสดง สมบัติทั้งสารเรื่องแสงสีน้ำเงิน และเป็นสารส่งผ่านประจุบวกสำหรับอุปกรณ์ใคโอคเรื่องแสงอินทรีย์ ความสามารถในการเป็นสารส่งผ่านประจุบวกเทียบเท่ากับ NPB ไคโอคเรื่องแสงสีน้ำเงินให้ประสิทธิภาพ เท่ากับ 1.65 cd/A และใดโอดเรื่องแสงสีเขียวให้ประสิทธิภาพเท่ากับ 6.25 cd/A อนุพันธ์ของ 9,9-bis(4diphenylaminophenyl) fluorene ที่มีหมู่ biphenyl เป็นหมู่แทนที่ที่ตำแหน่ง 2,7-ของหมู่ 9,9-bis(4diphenylaminophenyl)fluorene แสคงสมบัติทั้งสารเรื่องแสงสีน้ำเงินและเป็นสารส่งผ่านประจุบวกสำหรับ อุปกรณ์ใดโอดเรื่องแสงอินทรีย์ ความสามารถในการเป็นสารส่งผ่านประจุบวกเทียบเท่ากับ NPB ใดโอด เรื่องแสงสีน้ำเงินให้ประสิทธิภาพเท่ากับ 2.48 cd ${f A}^{-1}$ และไดโอคเรื่องแสงสีเขียวให้ประสิทธิภาพเท่ากับ 4.40 cd A^{-1} และมี turn-on voltage ที่ต่ำเท่ากับ 3.1 และ 2.8 V ตามลำดับ สำหรับอุปกรณ์ใดโอดเรื่องแสงอินทรีย์ ของอนพันธ์ของ oligofluorene-thiophenes เปล่งแสงตั้งแต่สีน้ำเงินถึงสีส้ม ทั้งนี้ขึ้นอยู่กับชั้นของสารเรื่อง แสงหรือสารเป้าหมายที่ใช้ ให้ประสิทธิภาพเท่ากับ 11.15 cd/A ส่วนสาร carbazole dendronized triphenylamines แสดงสมบัติทางความร้อนที่สูง โดยมี glass transition temperatures (T_) สูงถึง 401 °C เมื่อ ใช้เป็นสารส่งผ่านประจุบวกในอุปกรณ์ไดโอดเรื่องแสงอินทรีย์ที่มีโครงสร้าง ITO/PEDOT:PSS/HTL/Alq3 /LiF:Al ใดโอดเรื่องแสงสีเขียวให้ประสิทธิภาพเท่ากับ $4.47~\mathrm{cd}~\mathrm{A}^{-1}$ และมี turn-on voltage ที่ต่ำเท่ากับ $3.0~\mathrm{V}$

ABSTRACT

In this project, we carry out the synthesis, characterization, investigation of the physicl properties and applications of 9,10-substituted anthracene derivatives, 9,9-bis(4-diphenylaminophenyl) fluorene derivatives, biphenyl functioned 9,9-bis(4-diphenylaminophenyl)fluorene, pyrene-functionalized 9,9-bis(4diphenylaminophenyl)fluorene and bis(4-diphenylaminophenyl)carbazole end-capped fluorene as blue light-emitting and hole-transporting materials, oligofluorene-thiophenes and fluorene-oligothiophenes perylenediimide triads as emissive materials, and carbazole dendronized triphenylamines as holetransporting materials for organic light-emitting diodes. These materials were characterized by ¹H, ¹³C NMR, FT-IR, UV-vis, PL spectroscopy and mass spectrometry. Their physical and photophysical properties including optical, thermal and electrochemical properties were investigated. These materials were used as active layers in the organic light-emitting diodes with the devices structures of ITO/PEDOT:PSS/Synthesized materials/BCP/Alq3/LiF:Al ITO/PEDOT:PSS/Synthesized and materials/BCP/Alq3/LiF:Al. 9,10-Substituted anthracene derivatives having electron donating triphenylamine as peripheral substituent showed promising potential as both blue light-emitting materials and hole-transporting materials for Alq3-based OELD devices. Their ability as HTL for green OLEDs was comparable to a common hole-transporter NPB. Blue OLEDs with a maximum luminance efficiency of 1.65 cd/A, and green OLEDs with maximum luminance efficiency of 6.25 cd/A were achieved. 9,9-Bis(4diphenylaminophenyl) fluorene derivatives bearing two biphenyl moieties attached to the 2,7-positions of the 9,9-bis(4-diphenylaminophenyl)fluorene showed promising potential as both deep-blue light-emitting and hole-transporting materials for OELD devices. Non-doped deep-blue OLEDs with a maximum luminance efficiency of 2.48 cd A⁻¹, and green OLEDs with maximum luminance efficiency of 4.40 cd A⁻¹ were achieved with low turn-on voltages of 3.1 and 2.8 V, respectively. Notably, the color purities of these deep-blue (CIE coordinate of x = 0.15 and y = 0.07) and green (CIE coordinate of x = 0.28 and y = 0.52) devices were closed to the NTSC blue and green standards. The oligofluorene-thiophenes showed stable electrochemical and thermal properties. OLED devices of these materials emitted brightly in various colors from deep blue to orange. Particularly, deep blue (CIE coordinates of 0.16, 0.14) and green (CIE coordinates of 0.27, 0.61) devices showed high color quality closed to the NTSC standardswith high luminance efficiencies of 1.14 and 11.15 cd/A, respectively. Their triphenylamine dendrimers showed chemically-stable redox and thermally stable amorphous properties with substantially high glass transition temperatures (T_n) up to 401 °C. Alq3-based green OLEDs using these materials as the hole-transporting layer (HTL) with the device configuration of ITO/PEDOT:PSS/HTL/Alq3/LiF:Al emit brightly (λ_{em} 518 nm) from the Alq3 layer with a maximum luminance, maximum efficiency and low turn-on voltage of 25,390 cd m⁻², 4.47 cd A⁻¹ and 3.0 V, respectively.

สารบัญ

	หน้าที่
บทนำ	1
PART I	12
PART II	33
PART III	49
PART IV	69
PART V	79
PART VI	86
PART VII	104
PART VIII	121
PART IX	143
ภาคผนวก	175

เนื้อหางานวิจัย

1. บทน้ำ (Introduction)

ในอนากตเทคโนโลยีหน้าจอแสดงภาพจะได้รับความสนใจเป็นอย่างมาก จากเดิมที่ใช้หลอด แสงแกโทด (cathode ray tube, CRT) ซึ่งจะให้ความสว่างและให้สีที่ชัดเจน แต่ข้อเสียของหลอดแสง แคโทดที่นำมาใช้ในทางการค้านั่นคือ มีประสิทธิภาพในการทำงานต่ำ ราคาแพง มีขนาดใหญ่ ซึ่งทำให้การพกพาเป็นไปได้ยาก จึงทำให้มีการคิดค้นการสร้างหน้าจอแสดงภาพที่มีลักษณะแบน น้ำหนัก เบา ขึ้นมาแทนที่หลอดแสงแคโทด ซึ่งหน้าจอแสดงภาพแบบใหม่ที่กิดค้นขึ้นมานั้นเป็น liquid crystal display, LCD ที่สามารถพกพาได้สะดวกกว่า เพราะมีน้ำหนักเบา ตัวอย่างของ LCD ที่นำมาใช้ เช่น หน้าจอแสดงภาพของคอมพิวเตอร์แบบพกพา (lap-top computer) แต่เมื่อเปรียบเทียบ จอแสดงภาพแบบ LCD กับหลอดแสงแคโทด พบว่ามุมในการมองภาพของจอ LCD จะแคบกว่า หลอดแสงแกโทด และถึงแม้ว่าจอแสดงภาพแบบ LCD จะมีน้ำหนักเบา พกพาได้สะดวก แต่ข้อเสียก็ คือ ประสิทธิภาพในการทำงานต่ำ และขบวนการในการผลิตทำได้ยาก ทำให้มีราคาแพง

นอกจากนี้ยังใค้มีการพัฒนาเทคโนโลยีใคโอคเรื่องแสง (light-emitting diode, LED) ซึ่งคาค ว่าจะใช้เป็นส่วนประกอบในหน้าจอแสดงภาพที่มีข้อดีกว่าทั้งจอแสดงภาพแบบ LCD และหลอดแสง ในแง่งองการใช้พลังงานไฟฟ้าในการทำงานที่ต่ำ และการพกพาทำได้สะควกเนื่องจาก ้น้ำหนักเบา เทคโนโลยีใคโอคเรื่องแสงได้ถูกพัฒนาขึ้นมาครั้งแรกในปี พ.ศ. 2479 โดย Destriau และ คณะ¹ ซึ่งใช้สารอนินทรีย์เป็นชั้นสารเรื่องแสง และจากการศึกษาได้สังเกตเห็นการเรื่องแสงสีแดง ของ ZnS phosphor powder เมื่อนำสารเรื่องแสงนั้นประกบอยู่ระหว่างอิเล็กโทรค 2 อิเล็กโทรค ภายใต้สนามไฟฟ้า ต่อมาก็ได้มีการศึกษาและพัฒนาสารประกอบอนินทรีย์ที่สามารถเรื่องแสงสีอื่น ๆ ได้ โดยสารประกอบอนินทรีย์เหล่านั้นเป็นสารประกอบของธาตุหมู่ 3 และหมู่ 4 ยกตัวอย่างเช่น GaAsP, AlGaAs และ AlInGaP แต่ข้อเสียของการใช้สารอนินทรีย์เป็นสารเรื่องแสงในใคโอคเรื่อง แสง คือการขึ้นรูปสารอนินทรีย์ให้เป็นแผ่นฟิล์มต้องใช้วิธี chemical vapour deposition (CVD) ซึ่ง ทำได้ยากทำให้ผลิตภัณฑ์ที่ได้มีราคาแพง นอกจากนี้การขึ้นรูปเป็นแผ่นฟิล์มขนาดใหญ่ก็ทำได้ยาก และถึงแม้ว่าไคโอคเรื่องแสงที่มีชั้นสารเรื่องแสงเป็นสารอนินทรีย์จะมีลักษณะที่แบน และมีน้ำหนัก เบาก็ตาม ต่อมาในปี พ.ศ. 2532 ได้มีการค้นพบว่าสารโพลิเมอร์ที่มีโครงสร้างแบบคอนจูเกชัน สามารถใช้เป็นชั้นสารเรื่องแสงในใคโอคเรื่องแสงใค้ เช่น poly(p-phenylene vinylene) (PPV) เมื่อ นำเอาสาร PPV มาประกบอยู่ระหว่างสองอิเล็กโทรค และให้กระแสไฟฟ้าผ่านเข้าไปในทั้งสอง อิเล็กโทรค พบว่า PPV ให้แสงสีเขียว 2 หลังจากนั้นได้มีการศึกษาและพัฒนาสารอินทรีย์เพื่อที่จะใช้ เป็นชั้นสารเรื่องแสงในไคโอคเรื่องแสงเป็นอย่างมาก ทั้งนี้เนื่องจากว่ามีความสนใจ เป็นไปได้อย่างสูงในการนำไดโอดเรื่องแสงที่มีชั้นสารเรื่องแสงเป็นสารอินทรีย์ (organic emitting diode, OLED) มาประยุกต์ใช้ในทางการค้า ตัวอย่างเช่น การผลิตหน้าจอของโทรทัศน์ หน้าจอโทรศัพท์มือถือ และหน้าจอคอมพิวเตอร์สี นอกจากนี้การใช้สารอินทรีย์เป็นชั้นสารเรื่องแสง ในไคโอคเรื่องแสงมีข้อดีกว่าการใช้สารอนินทรีย์ที่ใช้ในไคโอคเรื่องแสงแบบคั้งเดิม คือสารอินทรีย์ นั้นสามารถทำให้เป็นแผ่นฟิล์มบาง ๆ ที่มีคุณภาพดีได้ง่ายโดยวิธี spin coating จากสารละลาย ซึ่งจะ ทำให้การสร้างแผ่นฟิล์มบนาดใหญ่เป็นไปได้ง่าย ส่งผลให้สามารถสร้างหน้าจอแสดงภาพบนาดเล็ก และบนาดใหญ่ที่มีราคาถูกได้ และการใช้สารอินทรีย์เป็นชั้นสารเรื่องแสงในไดโอดเรื่องแสง ทำให้ ได้แสงที่มีความสว่างสูง จากการศึกษาที่ผ่านมาพบว่าในปัจจุบัน OLED สามารถมีอายุการใช้งานได้ นานถึง 30,000 ชั่วโมง (อย่างน้อยที่สุด 10,000 ชั่วโมง) นอกจากนี้ยังพบว่าการใช้ OLED เป็น ส่วนประกอบในจอแสดงภาพมีข้อดีมากกว่าจอแสดงภาพแบบ LCD หลายประการคือ

- สารเรื่องแสงที่เป็นสารอินทรีย์ใน OLED สามารถขึ้นรูปเป็นแผ่นฟิล์มได้ง่าย ซึ่งจะทำให้ ต้นทุนการผลิตต่ำ
 - OLED ต้องการพลังงานไฟฟ้าในการทำงานต่ำ เนื่องจากไม่ต้องใช้ backlight
- การแสดงภาพด้วย OLED จะไม่มีปัญหาในเรื่องมุมมองของภาพ และ response time ของ การแสดงภาพ เนื่องจากการแสดงภาพของ OLED เกิดจากการเปล่งแสงของโมเลกุลที่เนื่องมาจาก การลดระดับพลังงานของอิเล็กตรอน

อย่างไรก็ตามการพัฒนาเพื่อที่จะนำ OLED มาใช้เป็นส่วนประกอบของจอแสดงภาพสีนั้น จะต้องมีไดโอดที่มีโมเลกุลที่สามารถเรื่องแสงสีแดง โมเลกุลที่สามารถเรื่องแสงสีเขียว และโมเลกุล ที่สามารถเรื่องแสงสีน้ำเงิน เพื่อให้ครบองค์ประกอบของแม่สีทั้ง 3 สี ดังนั้นจะเห็นได้ว่าในช่วง 10 ปี ที่ผ่านมาได้มีการศึกษาและพัฒนาชั้นสารเรื่องแสงเป็นอย่างมากทั้งของนักวิจัยหลาย ๆ กลุ่มและ บริษัทที่ผลิตหน้าจอแสดงภาพ เพื่อให้ได้โมเลกุลที่เรื่องแสงสีแดง สีเขียว และสีน้ำเงินที่บริสุทธิ์ เพื่อ พัฒนาโครงสร้างของ OLED ให้มีประสิทธิภาพในการทำงานสูง สารอินทรีย์ที่นำมาใช้ใน OLED นั้น โดยมากเป็นสารที่มีโครงสร้างเป็นคอนจูเกชัน ยกตัวอย่างเช่น สารที่เรื่องแสงสีแดง คือ porphyrin สี เขียว คือ PPV และสีน้ำเงิน คือ polyfluorene และเมื่อเร็ว ๆ นี้ได้มีการนำเสนอจอแสดงภาพสี ต้นแบบของโทรทัศน์ คอมพิวเตอร์ และโทรศัพท์มือถือที่ทำด้วย OLED ดังรูปที่ 1

1.1 ใดโอดเรื่องแสงที่มีชั้นสารเรื่องแสงเป็นสารอินทรีย์ (organic light-emitting diode, OLED)

OLED ใค้ถูกสร้างขึ้นครั้งแรกในปี พ.ศ. 2508 โดยใช้สารโมเลกุลเคี่ยวที่เป็นผลึกของ anthracene เป็นสารเรื่องแสง แต่ใดโอดที่ทำด้วย anthracene นี้ไม่ได้รับความสนใจ เนื่องจากว่า ใดโอดมีประสิทธิภาพในการทำงานไม่ค่อยดี จากนั้น OLED ก็เริ่มได้รับความสนใจมากขึ้นในปี พ.ศ. 2530 เมื่อ 8-hydroxyquinoline aluminum (Alq3) ถูกใช้เป็นชั้นสารเรื่องแสง พบว่าเมื่อให้ความ ต่างศักย์เข้าไปใดโอดจะให้แสงสีเขียว ต่อมาในปีพุทธศักราช 2533 ได้มีการค้นพบว่าโพลิเมอร์ (polymer) สามารถนำมาใช้เป็นสารเรื่องแสงในไดโอดเรื่องแสง เช่น ไดโอดเรื่องแสงที่มี PPV เป็น ชั้นสารเรื่องแสงจะให้สีเขียวเช่นกัน และมีประสิทธิภาพสูงเมื่อให้ความต่างศักย์เข้าไป หลังจากนั้น จึงได้มีการศึกษาและใช้โพลิเมอร์ประเภทต่าง ๆ เป็นสารเรื่องแสงเพิ่มมากขึ้น โดยโครงสร้างพื้นฐาน ของ OLED มีองค์ประกอบ 3 ส่วน ได้แก่

- สารอินทรีย์ที่ทำหน้าที่เป็นชั้นสารเรื่องแสง (light-emitting layer)
- โลหะที่มี work function ต่ำ ที่ใช้เป็นขั้วแคโทค เช่น อะลูมิเนียม (aluminum) หรือ แคลเซียม (calcium)

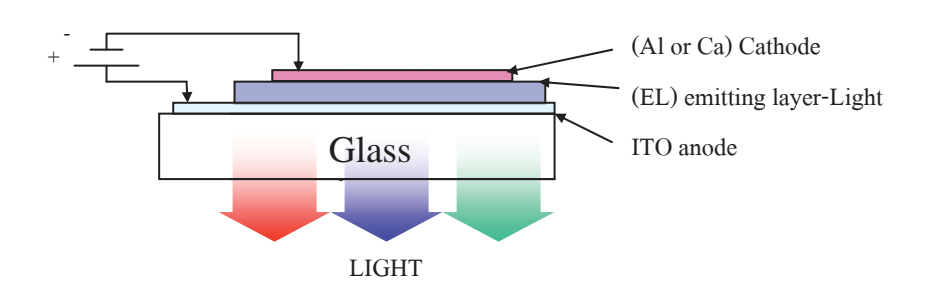
- โลหะหรือสารประกอบที่นำไฟฟ้าได้ และมีลักษณะที่โปร่งใส ที่ใช้เป็นขั้วแอโนด เช่น Indium tin oxide (ITO)



รูปที่ 1 ตัวอย่างหน้าจอแสดงภาพสีที่ทำด้วย OLED

1.1.1 ใดโอดเรื่องแสงแบบชั้นเดียว (single-layer)

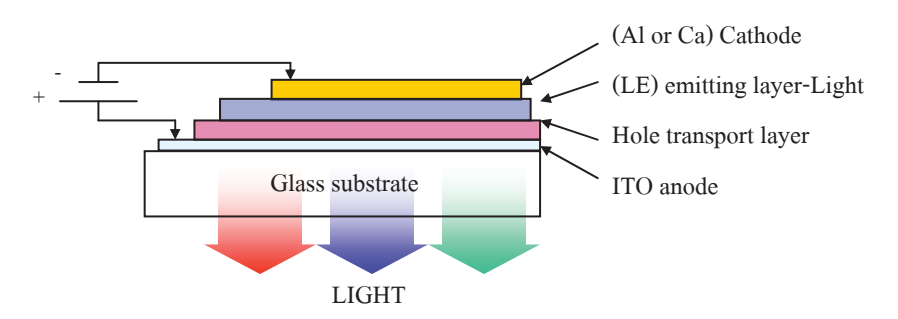
โครงสร้างของใดโอดเรื่องแสงแบบ single-layer โดยทั่ว ๆ ใปมีลักษณะดังแสดงในรูปที่ 2 โดยที่ชั้น ของสารเรื่องแสงจะถูกประกบอยู่ระหว่างขั้วของโลหะแคโทดและแอโนด และแสงที่เปล่งออกมา จากชั้นสารเรื่องแสงจะถูกผ่านออกมาทางขั้วแอโนด ดังนั้นการใช้ขั้วแอโนดที่มีลักษณะโปร่งใส จะ ทำให้แสงที่เกิดขึ้นในชั้นสารเรื่องแสงนั้นสามารถผ่านออกมาได้ การทำงานของไดโอดประเภทนี้เกิด จากการที่เมื่อให้ความต่างศักย์เข้าไปประจุลบ (electron) ที่ขั้วแคโทดถูกใส่เข้าไปในชั้นพลังงาน LUMO ของชั้นสารเรื่องแสงที่อยู่ใกล้กับขั้วแคโทด และในขณะเดียวกันประจุบวก (hole) ที่ ขั้วแอโนดจะถูกใส่เข้าไปในชั้น HOMO ของชั้นสารเรื่องแสงที่อยู่ใกล้ขั้วแอโนด ประจุทั้งสองจะ เคลื่อนที่ผ่านชั้นสารเรื่องแสงภายใต้สนามไฟฟ้าที่ให้เข้าไป เมื่อประจุมารวมกันภายใต้โมเลกุล เดียวกันจะทำให้เกิดเป็นอนุภาค electronic excited state ที่เรียกว่า exciton โดย exciton ที่เกิดขึ้นนี้ เป็นได้ทั้ง singlet หรือ triplet spin state และการลดระดับพลังงานของ singlet excitons จะทำให้เกิด ปรากฏการณ์เรื่องแสงของสารอินทรีย์ที่เรียกว่า ฟลูออเรสเซนซ์ (fluorescence)



รูปที่ 2 โครงสร้างพื้นฐานของใคโอคเรื่องแสงแบบชั้นเคียว

1.1.2 ใดโอดเรื่องแสงแบบหลายชั้น (multi-layer)

การเรื่องแสงของใดโอดเรื่องแสงเกิดจากการรวมกันของประจุลบ (electron) และประจุบวก (hole) ภายในโมเลกูลของสารเรื่องแสงเดียวกัน ซึ่งโดยปกติอัตราการให้ประจุบวกที่ขั้วแอโนดจะไม่ เท่ากับอัตราการให้อิเล็กตรอนที่ขั้วแคโทด แต่เพื่อให้ใดโอคเรื่องแสงมีประสิทธิภาพในการทำงานดี ้ขึ้นต้องทำให้อัตราการให้ประจุบวก (hole) ที่ขั้วแอโนคกับอิเล็กตรอนที่ขั้วแคโทคเท่ากัน โดยการทำ เป็นใคโอคเรื่องแสงที่มีหลายชั้น (multi-layer diodes) ซึ่งการใส่ชั้นของ hole transport เข้าไป ระหว่างขั้วแอโนคกับชั้นของสารเรื่องแสงจะช่วยเพิ่มอัตราการใส่ประจุบวกจากขั้วแอโนคเข้าไปใน ไดโอคดังแสดงในรูปที่ 3 ส่วนการเพิ่มชั้นสารส่งผ่านประจุลบ (electron transport) เข้าไประหว่างขั้ว แกโทคกับชั้นสารเรื่องแสงจะเป็นการช่วยเพิ่มอัตราการใส่อิเล็กตรอนจากขั้วแกโทด ยกตัวอย่างเช่น ใน ไดโอดเรื่องแสงประเภท single-layer ที่มี PPV เป็นชั้นสารเรื่องแสงจะพบว่า ขั้วแอโนคจะให้ประจุบวก ออกมาด้วยอัตราที่มากกว่าที่ขั้วแคโทคให้อิเล็กตรอน ดังนั้นเพื่อเพิ่มประสิทธิภาพในการเรื่องแสงของ ใดโอดที่ใช้ PPV สามารถทำได้โดยการเพิ่มชั้นสารที่เป็นสารส่งผ่านประจุลบเข้าไป จากการศึกษาพบว่าเมื่อ เพิ่มชั้นของ cyano substituted poly(p-phenylene vinylene) (CN-PPV) เข้าไปประสิทธิภาพในการทำงานของ ไคโอคเรื่องแสงจะเพิ่มขึ้น⁸ การใส่ชั้นสารส่งผ่านประจุลบ (electron transport) เข้าไปในไคโอคเรื่องแสง นอกจากจะเพิ่มอัตราการใส่อิเล็กตรอนแล้ว ยังสามารถช่วยกักให้ประจุบวกที่ใส่จากขั้วแอโนคอยู่ที่ชั้นสาร เรื่องแสงได้ ซึ่งจะทำให้โอกาสของทั้งสองอนุภาครวมกันภายในโมเลกุลเดียวกันของสารเรื่องแสงได้มากขึ้น โดยชั้นของสารส่งผ่านประจุลบ (electron transport) ที่เพิ่มเข้ามาเรียกอีกชื่อหนึ่งว่าเป็นชั้น Electron Conducting / Hole Blocking (ECHB) การเตรียมใดโอคเรื่องแสงประเภท multi-layer โดยวิธีการเตรียมจาก สารละลายจะต้องมีสารอินทรีย์เป็นสารเรื่องแสงที่ไม่ละลายในตัวทำละลายเคียวกันกับตัวทำละลายของสาร ที่เป็นสารส่งผ่านประจุลบ (electron transport) หรือสารส่งผ่านประจุบวก (hole transport) เช่นในกรณีของ การทำไดโอดเรื่องแสงที่มีชั้นสารส่งผ่านประจุลบสามารถทำได้ดังนี้ โดยขั้นแรกทำการ spin coating ชั้นของ สารเรื่องแสงลงบน ITO (แอโนค) จากนั้นทำการ spin coating ชั้นของสารส่งผ่านประจุลบทับลงไป ดังนั้น ถ้าสารเรื่องแสงละลายในตัวทำละลายที่ใช้ในขั้นการเตรียมชั้นสารส่งผ่านประจุลบ จะทำให้ชั้นของสารเรื่อง แสงนี้ถูกกำจัดออกไปด้วยเป็นผลทำให้ประเภทของสารที่นำมาใช้ในไคโอดเรื่องแสงประเภท นั้นถูกจำกัดเนื่องจากผลของตัวทำละลาย



รูปที่ 3 โครงสร้างของใคโอคเรื่องแสงแบบหลายชั้น

1.2 สารเรื่องแสงสีน้ำเงิน (blue light-emitting material)

สีน้ำเงินเป็นองค์ประกอบหลักใน 3 แม่สีที่เป็นองค์ประกอบสำคัญในการสร้างสีต่าง ๆ ของ ขอแสดงภาพสี ดังนั้นในการใช้ OLED ในจอแสดงภาพสีก็จะต้องมีไดโอดที่เรื่องแสงสีน้ำเงินอยู่ด้วย หรือหมายความว่าต้องมีโมเลกุลที่เรื่องแสงสีน้ำเงิน โดยทั่วไปสีน้ำเงินจะพบน้อยมากในธรรมชาติ เช่นเคียวกันในทางเคมีโมเลกุลที่เรื่องแสงสีน้ำเงินก็มีจำนวนน้อยเช่นกัน ทั้งนี้เนื่องจากว่าโมเลกุลที่ สามารถเปล่งแสงสีน้ำเงินได้ (fluorophore) โดยพื้นฐานแล้วจะต้องมีโครงสร้างแบบคอนจูเกชัน แต่ สำหรับโมเลกุลที่มีคอนจูเกชันมากขึ้นจะมีสเปกตรัมการดูดกลืนและการเรื่องแสงเคลื่อนไปที่ระดับ พลังงานต่ำลงหรือความยาวคลื่นเพิ่มขึ้น (red shift) ทั้งนี้ขึ้นอยู่กับขนาดของการคอนจูเกชันที่อยู่ใน โมเลกุล ดังนั้นจึงทำให้โมเลกุลที่มีทั้งการคอนจูเกชันและเรื่องแสงสีน้ำเงินมีจำนวนน้อย fluorophore ที่สามารถเรื่องแสงสีน้ำเงินส่วนใหญ่จะมีโครงสร้างทางเคมีเป็น phenylene, fluorene หรือ pyridine ซึ่งจะเห็นได้ว่าโมเลกุลทั้งหมดนี้จะมีคอนจูเกชันภายในวงเท่านั้น

1.2.1 สารโมเลกุลเดี่ยวที่เรื่องแสงสีน้ำเงิน (blue light-emitting molecular material)

จากที่กล่าวมาแล้วข้างต้นทั้ง phenylene, fluorene และ pyridine เป็น fluorophore ที่สามารถ เปล่งแสงสีน้ำเงินได้ แต่อย่างไรก็ตามจะเห็นได้ว่ามีการใช้โมเลกุลเหล่านี้ในไดโอดเรื่องแสงน้อยมาก ทั้งนี้เนื่องมาจากว่าลักษณะโมเลกุลที่แบนราบและมีคอนจูเกชันของสารประกอบเหล่านี้ ทำให้ โมเลกุลมักจะเกิดการซ้อนทับกันแบบ π - π stacking เมื่อถูกขึ้นรูปเป็นแผ่นฟิล์มและยังเกิด concentration quenching ซึ่งจะทำให้ประสิทธิภาพของการเรื่องแสงเหล่านี้ลดลงอย่างมาก อย่างไรก็ ตามได้มีความพยายามที่จะนำโมเลกุลประเภทนี้มาใช้ในไดโอดเรื่องแสงโดยการใส่หมู่แทนที่ที่มี ขนาดใหญ่เข้าไปในโมเลกุลหรือใส่ fluorophore เข้าไปในโครงสร้างของโพลิเมอร์ในรูปของทั้ง แกนกลาง (backbone) และโซ่กิ่ง (side chain) เพื่อป้องกันการซ้อนทับกันของโมเลกุลแบบ π - π stacking หรือโดยการใช้โมเลกุลเหล่านี้ในรูปของสารโพลิเมอร์ซึ่งจะกล่าวโดยละเอียดในหัวข้อ ถัดไป

1.2.2 สารโพลิเมอร์ที่เรื่องแสงสีน้ำเงิน (blue light-emitting polymer)

โพลิเมอร์ชนิดแรกที่ถูกสังเคราะห์ขึ้นที่ใช้เป็นสารเรื่องแสงในไดโอดเรื่องแสงคือ poly(p-phenylene vinylene) (PPV)² แต่การที่หมู่ vinylene เกาะอยู่กับหมู่ phenylene ของ PPV นั้น ทำให้ โครงสร้างของ PPV มีคอนจูเกชันเพิ่มมากขึ้น ส่งผลให้แสงที่เปล่งอออกมานั้นเป็นสีเขียวไม่ใช่สีน้ำ เงิน คังนั้นจะเห็นได้ว่าโดยวิธีนี้สีน้ำเงินสามารถเปลี่ยนเป็นสีเขียวและสีอื่น ๆ จนถึงสีแดงได้ด้วย วิธีการเพิ่มคอนจูเกชันให้กับหมู่ phenylene แต่อย่างไรก็ตามสีเขียวและสีแดงนั้นไม่สามารถ เปลี่ยนเป็นสีน้ำเงินได้ด้วยวิธีเดียวกัน phenylene แต่อย่างไรก็ตามสีเขียวและสีแดงนั้นไม่สามารถ เปลี่ยนเป็นสีน้ำเงินได้ด้วยวิธีเดียวกัน ที่ดังนั้นจึงทำให้สังเคราะห์สารโพลิเมอร์ที่เปล่งแสงสีน้ำเงินได้ยาก และยังคงมีการพัฒนาโพลิเมอร์ที่เรื่องแสงสีน้ำเงินหรือแสงสีเขียวเพื่อที่จะใช้ในทางการค้า ต่อไป และนอกจากนี้โพลิเมอร์ที่ให้แสงสีแดงก็ยังคงต้องมีการปรับปรุงเช่นกัน อย่างไรก็ตามโพลิ เมอร์ที่สามารถเรื่องแสงสีน้ำเงินได้เป็นโพลิเมอร์ที่ต่อกันโดยตรงของ fluorophore ที่เป็น phenylene, fluorene และ pyridine เนื่องจากว่าการต่อกันของ fluorophore เหล่านี้โดยตรงจะไม่เป็นการเพิ่มคอน จูเกชันของ fluorophore มากนัก ทั้งนี้เนื่องจากว่า fluorophore แต่ละตัวไม่เรียงตัวขนานกัน เพราะผล ของความแออัดจากอะตอมไฮโดรเจนที่อยู่ข้างเกียงกันจึงทำให้ fluorophore แต่ละตัวเรียงตัวกันเกือบ

อยู่ในแนวตั้งฉากซึ่งกันและกัน ส่งผลให้ π ออร์บิตัลของแต่ละ fluorophore ไม่ซ้อนเหลื่อมกันมาก นักหมายความว่าไม่เกิดการคอนจูเกชัน ด้วยเหตุนี้จึงไม่มีการเคลื่อนไปของสเปคตรัมการเรื่องแสง มากเท่าไร ทำให้โพลิเมอร์นั้นเรื่องแสงสีน้ำเงินใกล้เคียงกับโมโนเมอร์ของโพลิเมอร์นั้น

1.2.3 โพลิฟลูออรีน และโคโพลิเมอร์ (polyfluorene, PF และ copolymer)

โพลิเมอร์ที่เรื่องแสงสีน้ำเงินถูกใช้ในไดโอดเรื่องแสงเป็นครั้งแรกในปี พ.ส. 2534¹¹ สารละลายของ poly(9,9-bis-n-hexylfluorene) (PDHF) ใน chloroform ถูกทำให้เป็นแผ่นฟิล์มโดยวิธี spin coating บนแผ่น แก้ว ITO จากนั้นทำการเคลื่อบแผ่น magnesium-indium alloy ลงบนแผ่นฟิล์มของโพลิเมอร์โดยวิธี chemical vapour deposition (CVD) ผลจากการศึกษาไดโอดเรื่องแสงที่มี PDHF เป็นชั้นสารเรื่องแสง พบว่า ให้สเปคตรัมการเรื่องแสงสูงสุดที่ความยาวคลื่น 470 nm และพีคมีลักษณะกว้าง โดยมีใหล่พีคที่ 420 nm ส่วนโพลิฟลูออรีนชนิดอื่นนั้นจากการศึกษาสเปคตรัมการเรื่องแสงสูงสุด พบว่าปรากฏที่ตำแหน่งอื่นโดยมีลักษณะที่กว้างและปรากฏใหล่พีคเช่นเดียวกับสเปคตรัมการเรื่องแสงของ PDHF การเกิดสเปคตรัมที่กว้าง เนื่องจากการรวมกันของการเรื่องแสงของ fluorene แต่ละตัวในโพลิเมอร์ ส่วนการเกิดใหล่พีคเกิดเนื่องจากการลดระดับพลังงานของ excimer โดย excimer นั้นเกิดขึ้นจากอันตรกิริยาระหว่างฟลูออรีน 2 หน่วย ผลที่ เกิดจากการเกิดสเปคตรัมการเรื่องแสงของโพลิเมอร์ แต่จะมีส่วนช่วยในการเพิ่มความสามารถในการละลายของโพลิเมอร์ แต่จะมีส่วนช่วยในการเพิ่มความสามารถในการละลายของโพลิเมอร์ ในตัวทำละลายอินทรีย์ และนอกจากนี้ขนาดหรือความยาวของหมู่แอลคิลอังมีผลต่ออุณหภูมิที่สภาวะแก้ว (glass transition temperature, T,) แต่ไม่มีผลต่อสเปคตรัมการเรื่องแสงของโพลิเมอร์

นอกจากการใช้ฟลูออรีนเป็นสารเรื่องแสงแบบโฮโมโพลิเมอร์ (homopolymer) ของ polyfluorene (PF) แล้ว โคโพลิเมอร์ (copolymer) ของฟลูออรีนกับโมเลกุลหลาย ๆ ชนิดก็ถูกสังเคราะห์ขึ้น เพื่อใช้ใน การศึกษาคุณสมบัติการเรื่องแสงในไดโอดเรื่องแสง ซึ่งการใช้โคโพลิเมอร์นี้จะทำให้สามารถปรับสีของการ เรื่องแสงของฟลูออรีนโดยการควบคุมแนวระนาบของฟลูออรีนกับมอนอเมอร์ (monomer) ความสามารถในการละลายของ PF สามารถทำให้เพิ่มขึ้นได้โดยโคโพลิเมอร์ที่ใช้ และประสิทธิภาพในการ เรื่องแสง (external quantum efficiency) ของโมเลกูลยังสามารถทำให้เพิ่มขึ้นได้โดยการใช้โคโพลิเมอร์ที่ เหมาะสมด้วย ตัวอย่างเช่น โคโพลิเมอร์ของ poly(9,9-bis-n-hexylfluorene)phenylene (PDHFP) ซึ่งจะให้ สเปกตรัมการเรื่องแสงสูงสุดที่ 420 nm 13,14 และเมื่อเปรียบเทียบกับโฮโมโพลิเมอร์ของ PF จะเกิด blue shift แสดงว่าการคอนจูเกชั้นลดลง ทั้งนี้เนื่องมาจากว่าหมู่ phenylene มีการจัดเรียงตัวไม่อยู่ใน ระนาบเดียวกับโมเลกุลของฟลูออรีน ซึ่งทำให้ลดความเป็นระนาบเดียวกันระหว่างฟลูออรีนลง นั่นเอง นอกจากนี้ยังพบว่าโคโพลิเมอร์ของ PDHFP มีความสามารถในการละลายเพิ่มขึ้นและการ เรื่องแสงเนื่องจาก excimer ก็ลคลงค้วยเมื่อเทียบกับ $PDHF^{13}$ แสคงให้เห็นว่าการเกิดการซ้อนทับกัน ของฟลออรีนเป็นไปได้น้อยในลักษณะการจัดเรียงตัวเช่นนี้ จากการศึกษายังพบอีกว่าการเติมหม่ แทนที่พวกแอลคิล (alkyl) หรือแอลคอกซี (alkoxy) บนหมู่phenylene ในโคโพลิเมอร์ไม่มีผลทำให้ เกิดการเปลี่ยนแปลงสเปคตรัมการเรื่องแสงของสาร แต่จะเพิ่มความสามารถในการละลายให้ดีขึ้น 15,16,17 แต่ถ้าใช้หมู่ vinylene แทนหมู่ phenylene ในโคโพลิเมอร์จะให้โคโพลิเมอร์ที่เป็น poly(9,9bis-n-hexylfluorene)-viylene (PDHFV) โพลิเมอร์ชนิคนี้จะแสดงสเปคตรัมการเรื่องแสงที่ 475 nm¹³

นั่นแสดงให้เห็นว่าหมู่ใวนิลลีนจะมีการจัดเรียงตัวที่อยู่ในระนาบเดียวกับฟลูออรีนได้ดีกว่าหมู่ฟินิล ส่งผลทำให้การคอนจูเกชันระหว่างหมู่ฟลูออรีนเกิดได้ดีขึ้น ดังแสดงออกมาในรูปของการเกิด red shift ของสเปคตรัมการเรื่องแสง

1.2.4 โพลิ(พารา-ฟินิลลีน) และโคโพลิเมอร์ (poly(p-phenylene), PPP และ coploymer)

จากการศึกษา poly(p-phenylene), PPP ที่เป็นสารเรื่องแสงในได้โอดเรื่องแสงพบว่า PPP สามารถให้แสงสีน้ำเงิน โดยมีสเปคตรัมการเรื่องแสงสูงสุดที่ 485 nm และเนื่องจาก PPP มี ความสามารถในการละลายในตัวทำละลายอินทรีย์ได้ไม่ดี จึงทำให้แผ่นฟิล์มที่ได้ไม่ดีด้วย เนื่องจาก จะต้องเตรียมแผ่นฟิล์มของ PPP โดยวิธี precursor โดย poly(p-phenylene) (PPP) precursor ที่ละลาย ในตัวทำละลายอินทรีย์ได้ดีกว่า PPP จะถูกทำให้เป็นแผ่นฟิล์มจากสารละลายบนแผ่นแก้ว ITO โดย การ spin coating จากนั้นสาร precursor จะถูกเปลี่ยนเป็น PPP โดยการให้ความร้อน แต่อย่างไรก็ ตามจากการศึกษาพบว่าประสิทธิภาพการเรื่องแสง (external quantum efficiency) อยู่ในช่วง 0.01-0.05% และเพื่อเพิ่มความสามารถในการละลายของ PPP จึงได้มีการสังเคราะห์อนุพันธ์ของ PPP ที่มีหมู่แทนที่เป็นหมู่แอลคอกซี (alkoxy) ที่มีขนาดต่าง ๆ จากผลการศึกษาพบว่าโพลิเมอร์ EHO-PPP, DO-PPP และ DB-PPP เหล่านี้ละลายในตัวทำละลายอินทรีย์ได้ดี^{20,21} และมีสเปกตรัมการเรื่อง แสงสูงสุดที่ 420 nm ซึ่งจะเห็นได้ว่าความยาวของการกอนจูเกชัน (conjugation length) ของโพลิ เมอร์เหล่านี้ลดลงเมื่อเทียบกับ PPP ทั้งนี้เนื่องมาจากหมู่แทนที่แอลคอกซีจะไปลดโอกาสของการเกิด การจัดเรียงตัวของหมู่ phenylene ในสายโพลิเมอร์ให้อยู่ในระนาบเดียวกันได้น้อยลง

เพื่อเพิ่มประสิทธิภาพในการเรื่องแสงของ PPP หมู่ฟินิลได้ถูกนำมาสังเคราะห์เป็นโคโพลิ เมอร์กับหน่วยมอนอเมอร์หลาย ๆ ประเภท²² ยกตัวอย่างเช่น การสร้างโคโพลิเมอร์กับหมู่ vinylene ให้เป็น P3V และ acetylene ให้เป็น P3A จากการศึกษาพบว่าโคโพลิเมอร์ทั้ง 2 มีสเปคตรัมการเรื่อง แสงสูงสุดที่ 445 nm และ 420 nm ตามลำดับ จะเห็นได้ว่าโคโพลิเมอร์ที่มีหมู่ acetylene อยู่ด้วยจะมี ความยาวการคอนจูเกชันที่สั้นกว่าโคโพลิเมอร์ที่มีหมู่ vinylene อยู่ด้วยซึ่งจะเห็นได้จากการเกิด red shift ที่น้อยกว่า และจากการศึกษาผลของหมู่ phenylene พบว่าขนาดของความยาวของคอนจูเกชันใน โคโพลิเมอร์ประเภทนี้จะลดลงเมื่อจำนวนของหมู่ phenylene ในโพลิเมอร์เพิ่มขึ้น

1.3 สารส่งผ่านประจุ (charge transport material)

โดยทั่วไปแล้วใดโอดเรื่องแสงที่มีประสิทธิภาพสูงจะต้องเป็นใดโอดที่ให้ค่าประสิทธิภาพการเรื่อง แสงที่สูง ใช้กระแสไฟฟ้าในการทำงานต่ำ และมีอายุการใช้งานที่ยาวนาน จากการศึกษาพบว่าสิ่งหนึ่งที่จะทำ ให้ประสิทธิภาพการเรื่องแสงของไดโอดดีขึ้นคือ ทำให้การใส่ประจุบวก (hole) และประจุลบ (electron) ที่ ขั้วอิเล็กโทรดทั้ง 2 เข้าไปที่ชั้นของสารเรื่องแสงมีอัตราเท่ากัน ส่วนความต่างศักย์ที่จะต้องใช้ในการใส่ประจุ เข้าไปนั้น ขึ้นอยู่กับความแตกต่างของระดับพลังงานของอิเล็กโทรดและชั้นสารเรื่องแสง โดยที่ความต่าง ศักย์ใฟฟ้าที่ใดโอดเรื่องแสงต้องการมีค่าต่ำ ถ้าความแตกต่างระหว่าง work function กับชั้น HOMO หรือ LUMO มีค่าน้อย ถ้าต้องการสร้างใดโอดที่ใช้ความต่างศักย์ในการทำงานต่ำ ระดับพลังงาน HOMO จะต้องมี ค่าใกล้เคียงกับ 4.8 eV ซึ่งเป็นค่าที่ใกล้เคียงกับค่า work function ของ ITO และระดับพลังงาน LUMO จะต้องมีค่าใกล้เคียงกับค่า work function ของขั้วแกโทด ซึ่งเป็น 2.8 eV สำหรับ Ca และ 4.2 eV สำหรับ Al

โดยทั่วไปสารโพลิเมอร์ที่เป็นสารเรื่องแสง ส่วนใหญ่จะมีค่าระดับพลังงาน LUMO ที่น้อย ดังนั้น Ca จึง น่าจะเป็นขั้วแคโทดที่ดี เนื่องจากจะทำให้มีความแตกต่างของระดับพลังงานที่ต่ำ แต่อย่างไรก็ตามในทาง ปฏิบัติ Ca นั้นไม่เหมาะสมที่จะนำมาใช้เพราะเป็นโลหะที่ถูกออกซิไดซ์ได้ง่าย ดังนั้นสารเรื่องแสงหรือสารที่ ส่งผ่านอิเล็กตรอนจึงน่าจะมีระดับพลังงานที่สูง ซึ่งจะทำให้สามารถใช้โลหะที่เสถียรในอากาศและมีค่า work function ที่สูง เช่น Al เป็นขั้วแคโทด เพื่อที่จะให้บรรลุสิ่งที่กล่าวมาข้างต้น สามารถทำได้โดยเพิ่มชั้น ของสารส่งผ่านประจุ (charge transport) เข้าไปอยู่ระหว่างชั้นสารเรื่องแสงและขั้วแคโทดคือ สารส่งผ่าน ประจุลบ (electron transport) หรือระหว่างชั้นสารเรื่องแสงกับขั้วแอโนดคือ สารส่งผ่านประจุบวก (hole transport) โดยที่ในทั้ง 2 กรณีจะมีวัตถุประสงค์เพื่อทำให้อัตราการใส่ประจุจากอิเล็กโทรดทั้ง 2 เท่ากัน หรือ เรียกอีก

อย่างหนึ่งว่าเป็นการสร้างใดโอดเรื่องแสงแบบ multi-layer

1.3.1 สารส่งผ่านประจุลบ (electron transport material)

โดยทั่วไปแล้วโมเลกุลที่จะมีคุณสมบัติที่จะเป็นสารส่งผ่านประจุลบที่ดีนั้นจะต้องมีค่า electron affinity (EA) และ mobility ที่สูง และเป็นที่รู้จักกันดีว่า imine nitrogen (C=N) มีคุณสมบัติ ที่รับอิเล็กตรอนได้ดี ซึ่งทำให้เกิดการรีดักชัน (reduction) ทางเคมีและไฟฟ้าได้ง่ายและเกิดเป็น ตัวส่งผ่านประจุลบได้ดี ดังนั้นสารประเภท oxadiazole จึงนิยมใช้เป็นสารส่งผ่านประจุลบ^{23,24} ยกตัวอย่างเช่น 2-biphenyl-4-yl-5-(4-tert-butylphenyl)-1,3,4-oxadiazole (PBD) และ oxadiazole dendrimer นอกจากโมเลกุลเหล่านี้จะช่วยในการส่งผ่านประจุลบแล้ว ยังช่วยกักประจุบวกให้อยู่ ระหว่างชั้นของชั้นสารเรื่องแสงและชั้นสารส่งผ่านประจุลบ (electron) อีกด้วย

1.3.2 สารส่งผ่านประจุบวก (hole transport material)

โดยทั่วไปโมเลกุลที่จะมีคุณสมบัติที่จะเป็นสารส่งผ่านประจุบวกนั้นจะต้องมีค่า electron affinity (EA) และ mobility ที่ต่ำ โมเลกุลส่วนใหญ่ที่นำมาใช้เป็นสารส่งผ่านประจุบวกเป็นสาร อนุพันธ์ของ arylamine ยกตัวอย่างเช่น N,N'-bis(1-naphthyl)-N,N'-diphenyl-1,1'-biphenyl-4,4'-diamine (NPD) และ N,N'-Diphenyl-N,N'-bis(3-methylphenyl)-1,1'-biphenyl-4,4'-diamine (TPD) โมเลกุลที่นิยมนำมาใช้เป็นสารส่งผ่านประจุบวกนอกจาก arylamine derivatives แล้วยังใช้ สารประกอบของ carbazole ซึ่งมีทั้งในรูปโมเลกุลเดี่ยวและในรูปของ carbazole polymer แต่ carbazole polymer ส่วนใหญ่ที่นำมาศึกษาพบว่ามีคุณสมบัติในการใช้เป็นสารส่งผ่านประจุบวกได้ไม่ ค่อยดี แต่อย่างไรก็ตามได้มีการศึกษาโดยนำโมเลกุลของ carbazole ไปต่อกับโมเลกุลสารเรื่องแสงที่ เป็นทั้งโมเลกุลเดี่ยวและเป็นโพลิเมอร์ พบว่าโมเลกุลของ carbazole นั้นเป็นโมเลกุลที่ส่งผ่านประจุบวกได้เป็นอย่างดี

1.4 วัตถุประสงค์

- 1. เพื่อพัฒนาอุปกรณ์ใคโอคเรื่องแสงอินทรีย์ที่เรื่องแสง สีแคง สีน้ำเงิน และสีเขียว โคยใช้สารเรื่อง แสงอินทรีย์ชนิคใหม่ ให้มีประสิทธิภาพการทำงานสูงเพื่อพัฒนาไปสู่การผลิตในเชิงการค้า
- 2. เพื่อสร้างองค์ความรู้ใหม่ในการสังเคราะห์, การศึกษาสมบัติทางแสง, สมบัติทางไฟฟ้าเคมี และ สมบัติทางความร้อนของสารเรื่องแสงอินทรีย์ที่เรื่องแสงสีแคง เรื่องแสงสีน้ำเงิน และสีเขียวชนิคใหม่

- 3. เพื่อสร้างองค์ความรู้ใหม่ในการสร้าง, การศึกษาสมบัติทางแสง และสมบัติทางไฟฟ้าของ อุปกรณ์ใคโอคเรื่องแสงอินทรีย์ของสารเรื่องแสงสีแคง สีน้ำเงิน และสีเขียวที่สังเคราะห์ได้ และพัฒนาให้ได้ อุปกรณ์ใคโอคเรื่องแสงที่มีประสิทธิภาพสูง (turn-on voltage ต่ำ และค่า quantum efficiency สูง)
- 4. เพื่อเพิ่มผลงานตีพิมพ์ทางวิชาการในวารสารนานาชาติ และสร้างความเข้มแข็งของประเทศใน ด้านอุปกรณ์ใคโอดเรื่องแสงอินทรีย์
- 5. เพื่อสร้างความเข้มแข็งของนักวิจัยไทย โดยเฉพาะอย่างยิ่งทีมนักวิจัยในระดับภูมิภาคให้ ทัดเทียมกับระดับนานาชาติ และสร้างความร่วมระหว่างนักวิจัยในมหาวิทยาลัยระดับภูมิภาคกับนักวิจัยของ สถาบันวิจัยหรือนักวิจัยในต่างประเทศ
- 6. เพื่อสร้างบุคลากรในระดับปริญญาโท-เอกที่มีคุณภาพทั้งในเชิงวิชาการและวิจัย โดยเฉพาะใน ด้านอุปกรณ์ไดโอดเรื่องแสงอินทรีย์เพื่อเป็นนักวิจัยหรืออาจารย์ในมหาวิทยาลัย โดยเฉพาะมหาวิทยาลัยราช ภัฏหรือหน่วยงานเอกชน

1.5 ผลที่คาดว่าจะได้รับ

หากชุด โครงการวิจัยนี้ดำเนินการสำเร็จตามวัตถุประสงค์ จะเกิดประ โยชน์ดังต่อ ไปนี้

- 1. พัฒนาใคโอคเรื่องแสงสีน้ำเงินแบบชั้นเคียว (Single layer OLED) ต้นแบบ ที่มีชั้นสารเรื่องแสงเป็น สารอินทรีย์ โดยใคโอคเรื่องแสงนี้จะสามารถเรื่องแสงเป็นข้อความ และใคโอคเรื่องแสงที่ได้จะเป็นต้นแบบ ในพัฒนาไปสู่การที่จะนำใคโอคเรื่องแสงนี้ไปใช้เป็นส่วนประกอบที่สำคัญของหน้าจอแสคงภาพแบบจอ แบน เช่น จอโทรศัพท์มือถือ เป็นต้น และในที่สุดจะนำไปสู่การผลิตในเชิงพาณิชย์
- 2. พัฒนาเทคนิคการสังเคราะห์ทางเคมีอินทรีย์เพื่อที่จะให้ได้สารเรื่องแสงสีน้ำเงินชนิดใหม่ ที่มี คุณสมบัติเป็นสารส่งผ่านประจุบวกและมีอุณหภูมิกลาสทรานซิชัน (T) สูง สำหรับใช้ในไดโอดเรื่องแสงที่ มีชั้นสารเรื่องแสงเป็นสารอินทรีย์ โดยโมเลกุลจะมีโครงสร้างหลักเป็น oligomer ของ thiophene และ fluorene ที่มีหมู่ปิดท้ายเป็น carbazole ซึ่งผลลัพธ์บั้นปลายจะนำไปสู่การเพิ่มสักยภาพในทางเคมีสังเคราะห์ ของบุคลากรและนักสึกษามหาวิทยาลัยอุบลราชธานี ซึ่งถือว่าเป็นสาสตร์ที่สำคัญทางเคมี
- 3. พัฒนาเทคนิคในการพิสูจน์เอกลักษณ์ของโมเลกุลสารอินทรีย์ เช่น เทคนิค UV-Vis spectroscopy, IR spectroscopy, ¹H-NMR spectroscopy, ¹C-NMR spectroscopy, Mass spectrometry และการหาจุด หลอมเหลว ซึ่งจะนำไปสู่การพัฒนาบุคลากรและนักศึกษา โดยผ่านทางการเรียนการสอนและวิจัยของ มหาวิทยาลัยอุบลราชธานีให้เกิดความเชี่ยวชาญ ชำนาญในเทคนิคการวิเคราะห์ดังกล่าว และในที่สุดจะ นำไปสู่การใช้เครื่องมือวิเคราะห์ดังกล่าวให้เกิดประโยชน์สูงสุดและเป็นศูนย์ในการวิเคราะห์
- 4. พัฒนาเทคนิคและชีดความสามารถในการศึกษาสมบัติทางกายภาพของสารอินทรีย์ต่างๆ เช่น Fluorescence spectroscopy, Cyclic voltammetry (CV), Differential scanning calorimetry (DSC), X-ray diffraction, Scanning electron microscope (SEM) เป็นต้น ซึ่งจะนำไปสู่การพัฒนาบุคลากรและนักศึกษาโดย ผ่านทางการเรียนการสอนและวิจัย ของมหาวิทยาลัยอุบลราชธานีให้เกิดความเชี่ยวชาญ ชำนาญในเทคนิค การวิเคราะห์ดังกล่าว และในที่สุดจะนำไปสู่การใช้เครื่องมือวิเคราะห์ดังกล่าวให้เกิดประโยชน์สูงสุดและ เป็นศูนย์ในการวิเคราะห์
 - 5. พัฒนาเทกนิกในการทำนายกุณสมบัติของโมเลกุลโดยการใช้เทกนิกการใช้เคมีคำนวณเชิงควอนตัม หน้าที่ 9

- 6. จากชุดโครงการวิจัยนี้ประกอบด้วยชุดโครงการย่อยอีก 4 โครงการ จะทำเกิดการสร้างนักวิจัยรุ่น ใหม่ และทำให้เกิดความร่วมความร่วมมือระหว่างหน่วยงานในมหาวิทยาลัยอุบลราชธานี และระหว่าง มหาวิทยาลัยอุบลราชธานีและมหาวิทยาลัยมหิดล
- 7. หากชุดโครงการวิจัยนี้ดำเนินการสำเร็จตามวัตถุประสงค์ผลการวิจัยที่ได้ คือไดโอดเรื่องแสงสีน้ำ เงินต้นแบบ จะผลักดันให้เกิดงานวิจัยต่อเนื่องในมหาวิทยาลัยอุบลราชธานี และเกิดความร่วมมือระหว่าง มหาวิทยาลัยอุบลราชธานี สถาบันการศึกษาอื่น สถาบันวิจัยทั้งในและต่างประเทศ และภาคเอกชน ในการที่ จะพัฒนาต้นแบบนี้ไปสู่การผลิตออกสู่ตลาดเชิงพาณิชย์ เช่น การผลิตเป็นจอแสดงภาพของโทรศัพท์มือถือ เป็นต้น
- 8. การดำเนินชุดโครงการวิจัยนี้จะเป็นแรงผลักดันและส่งเสริมให้เกิดการเรียนการสอนและวิจัยใน ระดับปริญญาโท-เอก ในมหาวิยาลัยอุบลราชธานี
 - 9. นำความรู้ทางเคมีอินทรีย์ไปประยุกต์ใช้ในทางอุตสาหกรรมอิเล็กทรอนิกส์ส์

6. เอกสารอ้างอิง

- 1. G. Destriau, J. Chem. Phys., 1936, 33, 587
- 2. J. H. Burroughes, D. D. C. Bradley, A. R. Brown, R. N. Marks, K. Mackay, R. H. Friend, P. L. Burn and A. B. Holmes, *Nature*, **1990**, 347, 539
- 3. H. Schenk, H. Becker, O. Gelsen, E. Kluge, W. Kreuder and H. Spreitzer, Proc. *EuroDisplay'99*, 1999, 33
- 4. J. N. G. Pillow, M. Halim, J. M. Lupton, P. L. Burn and I. D. W. Samuel, *Macromolecules*, 1999, 32, 5985
- 5. D. Neher, Macromol. Rapid Commun., 2001, 22, 1365
- 6. W. Helfrich and W. G. Schneider, Phys. Rev. Lett., 1965, 14(7), 229
- 7. C. W. Tang and S. A. Vanslyke, Apply. Phys. Lett., 1987, 51(12), 913
- 8. N. C. Greenham, S. C. Moratti, D. D. C. Bradley, R. H. Friend and A. B. Holmes, *Nature*, **1993**, 365, 628
- 9. L. J. Rothberg and A. J. Lovnger, J. Mater. Res., 1996, 11(12), 3174
- 10. T. Virgili, D. G. Lidzey and D. D. C. Bradley, Adv. Mater., 2000, 12(1), 58
- 11. Y. Ohmori, M. Uchida, K. Muro and K. Yoshino, Jpn. J. Appl. Phys., 1991, 30(12B), L1941
- 12. M. Fukuda, K. Sawada and K. Yoshino, J. Polym. Sci., Part A Polym. Chem., 1997, 31, 2465
- 13. H. N. Cho, D. Y. Kim, J. K. Kim and C. Y. Kim, Synth. Met., 1997, 91, 293
- 14. M. Ranger, D. Rondeau and M. Leclerc, Macromolecules, 1997, 30, 7686
- 15. M. Kreyenschmidt, G. Klaerner, T. Fuhrer, J. Ashenhurst, S. Karg, W. D. Chen, V. Y. Lee, J. C. Scott and R. D. Miller, *Macromolecules*, **1998**, 31, 1099
- 16. W. L. Yu, Y. Cao, J. Pei, W. Hyang and A. J. Heeger, Chem. Commun., 1999, 1837

- 17. W. L. Yu, Y. Cao, J. Pei, W. Hyang and A. J. Heeger, J. Appl. Phys. Lett., 1999, 75(21), 3270
- 18. G. Grem, G. Leditzky, B. Ullrich and G. Leising, Adv. Mater., 1992, 4(1), 36
- 19. G. Grem and G. Leising, Synth. Met., 1993, 55-57, 4105
- 20. Y. Yang, Q Pei and A. J. Heeger, J. Appl. Phys., 1996, 79(2), 934
- 21. Y. Yang, Q Pei and A. J. Heeger, Synth. Met., 1996, 78, 263
- 22. M. Remmers, D. Neher, J. Gruner, R. H. Friend, G. H. Gelinck, J. M. Warman, C. Quattrocchi, D. A.

Dos Santos and J. L. Bredas, Macromolecules, 1996, 29(23), 7432

- 23. C. Adachi, T. Tsutsui and S. Saito, Appl. Phys. Lett., 1989, 55, 1489
- 24. J. Bettenhausen, M. Greczmiel, M. Jandke and P. Strohriegl, Synth. Met., 1997, 107, 129.

PART I

Synthesis and characterization of 9,10-substituted anthracene derivatives as blue light-emitting and hole-transporting materials for electroluminescent devices

1. Introduction

The use of π -conjugated organic compounds as electroluminescent materials in organic light-emitting diodes (OLEDs) was originally introduced by van Slyke over two decades ago. Since then, the development of new π -conjugated compounds especially small molecules with superior physical, optical, thermal and electrochemical properties has become one of the most reviving research areas. OLEDs for flat-panel displays are showing great promise, and a related application for a flexible flat-panel display is progressing. Full-color displays are required for red, green, and blue light-emitting materials. Although many fluorescent blue emitters have been reported, such as anthracene derivatives, phenylene derivatives, pyrene derivatives, fluorene derivatives, carbazole derivaties, triarylamine derivatives and phosphorescent iridium complexes, there is still a clear need for further improvements in terms of efficiency and color purity compared to red and green emitters. Due to its unique chemical and electron-rich structure, low electronic band gap and strong blue fluorescence, anthracene has received considerable interest. Anthracene derivatives have been extensively used as fluorescent chromophores in the construction of chemosensors for many applications. Incorporation of anthracene and its 9,10-substituted derivatives into polymer main-chains or linked as pendent groups contributes to solving the problem of preparation of films with good optical quality or to suppress excimer formation. A number of polymeric and molecular 9,10-substituted anthracenes have also been developed and studied as blue light-emitting materials for OLED devices. However, new classes of anthracene based-blue light-emitters with improvements in terms of efficiency and color purity remain to be explored. In this work, the designed 9,10-substituted anthracenes incorporating different characteristic aromatic rings such as fluorene, thiophene and triphenylamine as π -conjugation substituents were synthesized and characterized (Fig. 1). The introduction of planar thiophene would allow a long π -conjugation system to be achieved, while integration of the bulky triphenylamine could suppress aggregation of the planar anthracene ring, as well as increase the hole-transporting capability and thermal stability. Fluorene also has a number of advantages, including its capability to emit in the blue part of the visible spectrum, chemical and photochemical stability. The physical and photophysical properties of these compounds were investigated with the aim of understanding the structure-property relationships and developing novel molecular π -conjugated materials. Investigations on OLED device fabrication and characterization are also demonstrated.

Fig. 1 Chemical structures of 9,10-substituted anthracenes 1-4.

2. Results and discussion

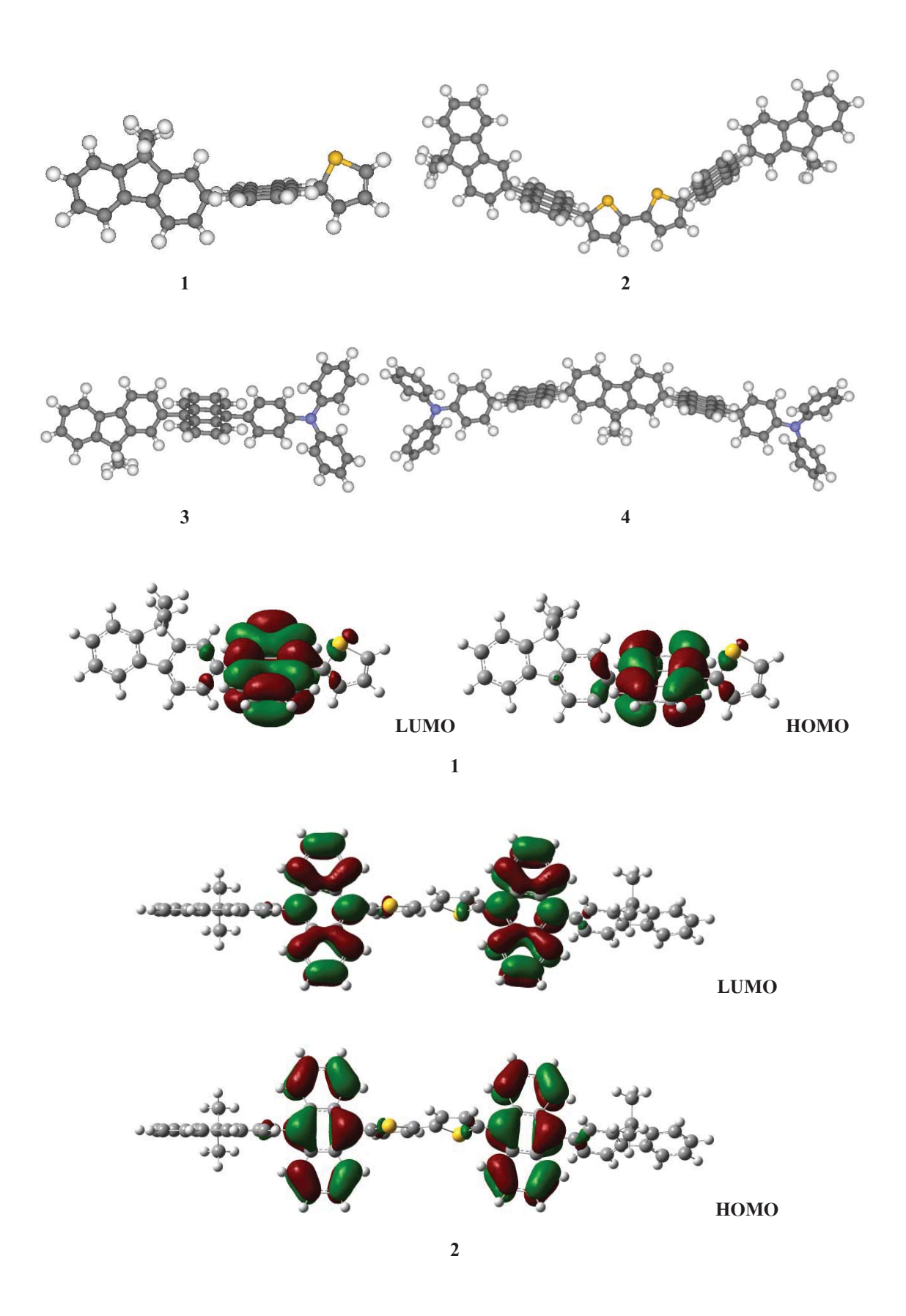
2.1. Synthesis

The molecular structures of the target anthracenes bearing fluorene, thiophene, bithiophene and triphenylamine as 9,10-substituents are shown in Fig. 1. As illustrated in Scheme 1, we began the synthesis with alkylation of 2-iodofluorene 5 at C-9 position of the fluorene ring with dihexyl chains followed by palladium-catalyzed Suzuki cross-coupling of the resultant in excess amounts with 9-bromoanthracene-10boronic acid to give 6 in a fair yield of 52%. Target anthracene 1 bearing fluorene and thiophene rings as 9,10-substituents was formed by Suzuki cross-coupling of 6 with 2-thiopheneboronic acid in 76% yield as light yellow solids. To form the more extended π -conjugation molecule of 2, a two-step synthesis was carried out by regioselective bromination at α-position of thiophene ring of 1 with NBS in THF followed by reductive nickel-catalyzed dimerization reaction of the obtained 7 with the catalytic system of NiCl, zinc powder, PPh, and bipyridine (bpy) in DMAc at 90 °C. Anthracene 2, a dimer of 1, was obtained as a greenish solid in an overall yield of 60%. In the target anthracenes 3 and 4, a substituent group with a holetransporting property was introduced. Compound 3 bearing fluorene and triphenylamine as substituents was obtained as a light yellow solid in a good yield of 79% by Suzuki cross-coupling of readily formed 6 with N,N-diphenyl-N-4-aminophenylboronic acid. Target anthracene 4, a dimer of 3, was successfully synthesized by carrying out double Suzuki cross-coupling of ready dialkylated 2,7-diiodofluorene 8 with 9-bromoanthracene-10-boronic acid (2.11 equiv.) followed by coupling of the obtained 9 with N,Ndiphenyl-N-4-aminophenylboronic acid, and gained as a deep yellow solid in 75% yield. All newly synthesized compounds were fully characterized by standard spectroscopic methods. They had good solubility in most organic solvents at room temperature, resulting from the presence of n-hexyl groups at the C-9 of fluorene ring. As a result, no crystallization thin film should be obtained from a solution casting.

Scheme 1 Synthetic route to 1-4. Reagents and conditions: i) 50% NaOH, *n*-Bu₄NBr, C₆H₁₃Br, DMSO, rt; ii) Pd(PPh₃)₄, 2M Na₂CO₃, THF, reflux; iii) NBS, THF, rt; iv) NiCl₂, Zn, PPh₃, DMAc, bpy, 90 °C.

2.2. Quantum calculation and optical properties

To understand the electronic properties and the geometries of 1-4, quantum chemical calculations were performed using the TDDFT/B3LYP/6-31G (d,p) method. The optimized structures of these compounds revealed that all molecules adopted non coplanar conformations. Particularly, the planar anthracene unit was twisted nearly perpendicular to the adjacent thiophene, fluorene and triphenylamine moieties because of a steric repulsion between anthracene peri-hydrogen atoms (1,8 and 4,5 positions) and hydrogen atoms of those aromatic rings. Such structural characteristics can influence some of their electronic and physical properties such as a suppression of the conjugation. As demonstrated in Fig. 2, in the highest occupied molecular orbitals (HOMO) of 1 and 2, π-electrons located on anthracene and thiophene moieties, while in the HOMO orbitals of 3 and 4, π -electrons delocalized over anthracene and donor triphenylamine segments. The participation of fluorene ring in the π -conjugation system was diminished in all cases. In the lowest unoccupied molecular orbitals (LUMO) of all compounds, electrons located only on anthracene rings. The HOMO-LUMO energy gaps (Eg cal.) were calculated and presented in Table 1. These calculated values were slightly deviated from those obtained from the experimental results (\sim 0.01-0.18 eV). There are factors responsible for the errors because the orbital energy difference between HOMO and LUMO is still an approximate estimation to the transition energy since the transition energy also contains significant contributions from some two-electron integrals. The real situation is that an accurate description of the lowest singlet excited state requires a linear combination of a number of excited configurations.



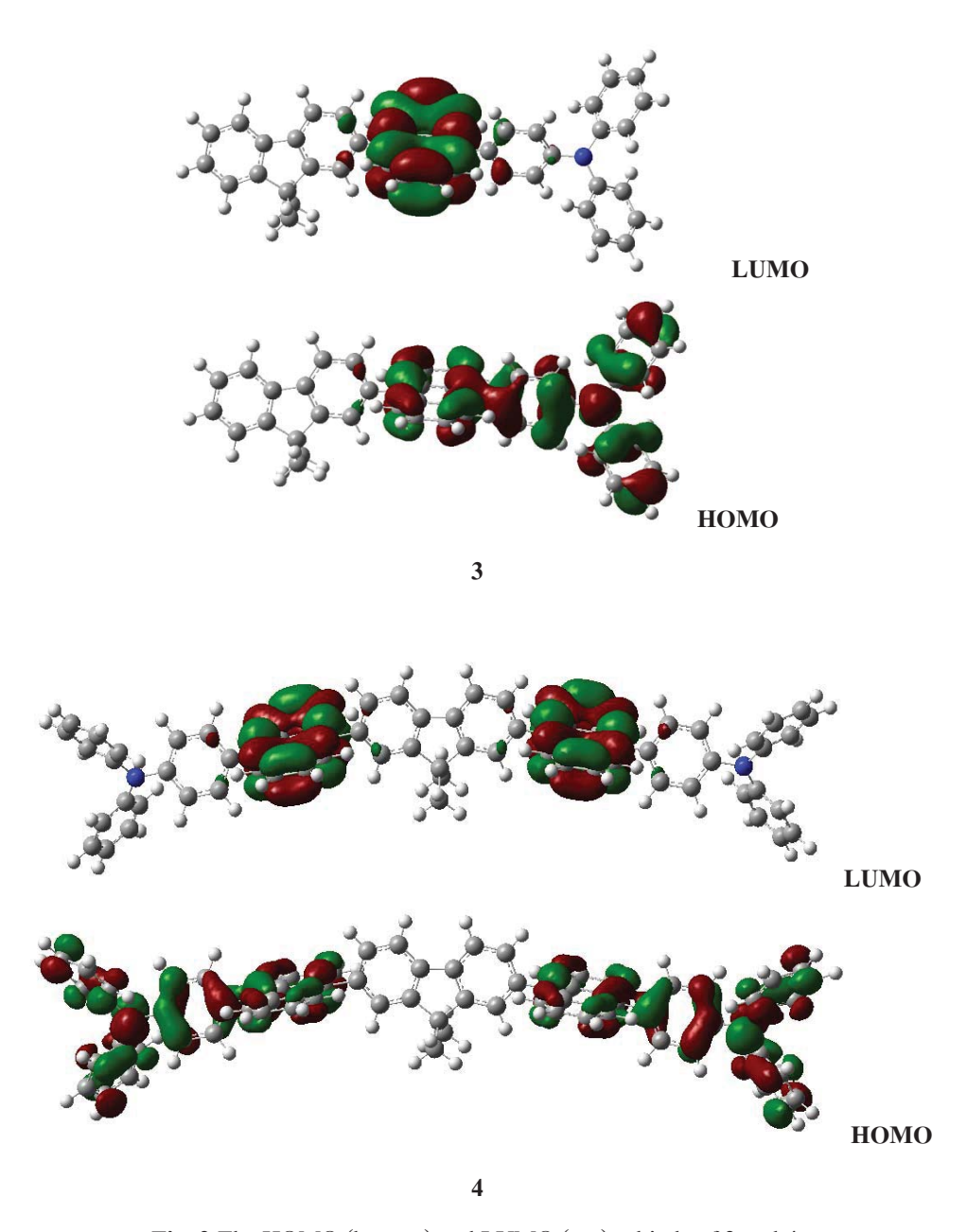


Fig. 2 The HOMO (bottom) and LUMO (top) orbitals of 2 and 4.

Photophysical properties of 1-4 were investigated in dilute CH_2Cl_2 solution and thin film obtained by thermal evaporation on quart substrate. The pertinent data are presented Fig. 3 and 4, and summarized in Table 1. Their UV-vis spectra showed two absorption bands, which were assigned in terms of the strong absorption band in the region of 250-310 nm corresponding to the π - π * local electron transition of the individual aromatic units and the less intense three absorption bands in the region of 350-400 nm attributed to the characteristic π - π * electron transition of the anthracene. Their HOMO-LUMO energy gaps (E_g) were estimated from the onset of the absorption spectra to be 2.96, 2.87, 2.90 and 2.89 eV, respectively. The E_gs of 3 and its corresponding dimer 4 were nearly identical, despite somewhat different molecular sizes, indicating they had comparable π -conjugation length. This can be explained by an out of plane twisting of the fluorene unit from adjacent anthracene rings as mentioned earlier (Fig. 2) limiting the

delocalization of π -electrons on the anthracene and triphenylamine units only. In contrast, the E_g of 1 is noticeably higher than that of its corresponding dimer 2 indicating remarkably longer π -conjugation length in 2. This is due to less hindered thiophene ring in the molecules allowing extended π -electron delocalization over the anthracene and bithiophene moieties.

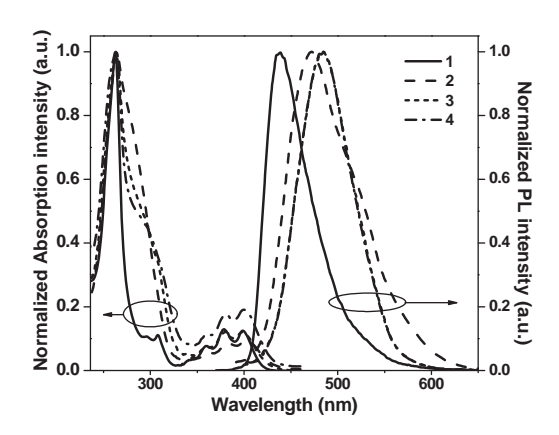


Fig. 3 UV-Vis absorption and PL spectra of 1-4 measured in dilute CH₂Cl₂ solution.

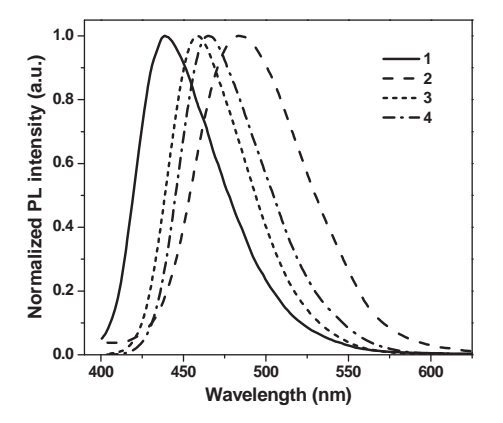


Fig. 4 PL spectra of 1-4 measured as thin film obtained by vapour deposition on quart substrate.

These compounds in solution fluoresced ranging from bright blue to blue-green colors with featureless photoluminescence (PL) spectra (Fig. 3) which is similar to what was observed for most 9,10-diphenylanthracenes. The solution PL spectrum of the dimer 2 red-shifted with respect to that of 1, whereas the PL spectra of 3 and dimer 4 were duplicate. These results were in agreement to what was observed from the theoretical and UV-vis experiments. These materials showed slight stokes shift (41-85 nm) suggesting less energy loss during the relaxation process and efficient fluorescence. The thin film PL emission spectrum of 1, shown in Fig. 4, was similar to its solution PL spectrum in term of line shape, emission λ_{max} and full with at a half-maximum, thus indicating no or less if any solid state packing occurred in this case due to its bulky molecular structure. However, thin film PL spectrum of 2 exhibited bathochromic shift caused by solid state packing, thus indicating greater planarity between the anthracene and bithiophene unit and better π -electron delocalization in the conjugated system. So that in the cases of 3 and 4 having bulky structures, their thin film PL spectra exhibited hypsochromic shift of about 19-26 nm

compared to their corresponding solution spectra. This result may also be attributed to the aforementioned solid state packing force which prohibits the electron-vibration coupling between triphenylamine substituent and the anthracene photoactive unit.

Table 1 Physical and photophysical data of 1-4.

co	$\lambda_{abs} (nm)^a$	$\lambda_{_{em}}$	$\lambda_{_{em}}$	Stoke	$\Phi_{\scriptscriptstyle F}^{\ d}$	$T_g/T_c/T_m/T_{5d}$ (°C) ^e	E_g	E _g cal.	$E_{1/2}(V)^h$	E _{onset}	HOMO/LUM
		(nm)	$(nm)^b$	s			$(eV)^{f}$	$(eV)^g$		$(V)^h$	O (eV)
		a		shift							
				(nm) ^c							
1	359,378,398	439	439	41	0.12	- /115/209/330	2.96	3.11	1.20, 1.45	1.12	-5.56/-2.60
2	363,383,402	474	483	72	0.04	- / - /326/370	2.87	3.05	1.15, 1.40	1.08	-5.52/-2.65
3	359,380,399	484	458	85	0.73	79/ - / - /397	2.90	2.93	0.95, 1.21	0.88	-5.32/-2.42
4	360,380,400	485	466	85	0.77	155/225/338/424	2.89	2.90	0.96, 1.25	0.88	-5.32/-2.43

^a Measured in a dilute CH₂Cl₂ solution.

Fluorescence quantum yields ($\Phi_{\rm F}$) of **1-4** measured in dilute solution using quinine sulfate solution in 0.01 M H₂SO₄ ($\Phi_{\rm F}$ = 0.54) as a standard were 0.12, 0.04, 0.73 and 0.77, respectively. The results indicated that direct attachment of the thiophene ring to the luminous anthracene moiety in compound **1** lowered the $\Phi_{\rm F}$ (0.12) and the value was rather reduced in compound **2** ($\Phi_{\rm F}$ = 0.04) having two thiophene rings. The decrease of $\Phi_{\rm F}$ value with the increasing of the thiophene units is usually observed in most of the thiophene oligomers as the molecule becoming more planar and likely to fluorescence quenching by intermolecular π - π stacking. In contrast, replacing thiophene ring with electron donating triphenylamine in compound **3** significantly increased the $\Phi_{\rm F}$ (0.73) and the value was slightly higher in the dimer **4** ($\Phi_{\rm F}$ = 0.77).

^b Measured on a vapor deposition thin film and excited at 390 nm.

 $^{^{}c}$ Stokes shift calculated from the difference between λ_{max} of the absorption and emission spectra.

^d Determined in CH_2Cl_2 solutions (A < 0.1) at room temperature using quinine sulfate solution in 0.01 M H_3SO_4 ($\Phi_E = 0.54$) as a standard.²²

 $^{^{\}circ}$ Obtained from DSC on the 2 $^{\rm nd}$ heating cycle and TGA measurements under N_2 at a heating rate of 10 $^{\circ}$ C/min.

Estimated from the onset of the absorption spectra ($E_g = 1240/\lambda_{onset}$).

^g Obtained from quantum chemical calculation using TDDFT/B3LYP/6-31G (d,p).

^h Measured using a three electrode system fitted with a glassy carbon working electrode, a platinum rod counter electrode and SCE reference electrode in degassed CH₂Cl₂ containing 0.1 M *n*-Bu₄NPF₆ as a supporting electrolyte at a scan rate of 50 mV/s.

ⁱ Calculated using the empirical equation: $HOMO = -(4.44 + E_{onset})$ and $LUMO = HOMO + E_{g}$.

2.3. Electrochemical and thermal properties

Electrochemical behaviors of all compounds were investigated by cyclic voltammetry (CV), and the resulting data are shown in Fig. 5 and summarized in Table 1. The experiment was carried out in degassed CH₂Cl₂ containing 0.1 M n-Bu₄NPF₆ as a supporting electrolyte under argon atmosphere. Compound 3 and its corresponding dimer 4 were found to exhibit two quasi-reversible oxidation processes at 0.95 and 1.21 V, and 0.96 and 1.26 V, respectively. The first oxidation wave assigned to the removal of electrons from the peripheral triphenylamines resulting radical cations, while the second attributed to the formation of anthracene radical cation. The onset oxidation potentials (E_{onset}) of 3 and 4 estimated from the first anodic oxidation wave were at the same value of 0.88 V, which is very close to the data reported for most triphenylamine derivatives (0.90 V). Their multiple CV scans revealed identical CV curves with no additional peak at lower potential on the cathodic scan (E_{pc}) being observed (see supporting information). This indicates no oxidative coupling or a weak oxidative coupling if any at p-phenyl rings of the peripheral triphenylamine led to electro-polymerization and they are electrochemically stable molecules. Usually, this type of electrochemical coupling reaction is detected in most triphenylamine derivatives with unsubstituted p-position of the phenyl ring such as in case of 2,7-bis[2-(4-diphenylaminophenyl)-1,3,4-oxadiazol-5-yl]-9,9-bis-n-hexylfluorene. Steric hindrance of an adjacent anthracene ring might play a key role to prevent such electrochemical reactions in both molecules. CV curves of 1 and 2 showed two irreversible oxidation processes. Duplicate CV curves of each compound were noticed under multiple scans demonstrating stable molecules (see supporting information). In case of 1, the first oxidation wave corresponds to the removal of electrons from the terminal thiophene ring to form the radical cation. No oxidation peak at lower potential due to a dimerization coupling of such species was detected unlike what was observed in most cases of α-unsubstituted short oligothiophenes. In our case, this electrochemical dimerization coupling could be prevented by a steric hindrance of the nearby anthracene moiety. Moreover, under these CV experiment conditions, no distinct reduction process was observed in all cases. The HOMO and LUMO energy levels of 1-4 were calculated from the oxidation onset potentials (E_{onset}) and energy gaps (E_g) and the results are summarized in Table 1. The HOMO levels of these materials ranged from -5.56 to -5.32 eV matching well with the work functions of the gold (Au) or indium tin oxide (ITO) electrodes and favoring the injection and transport of holes.

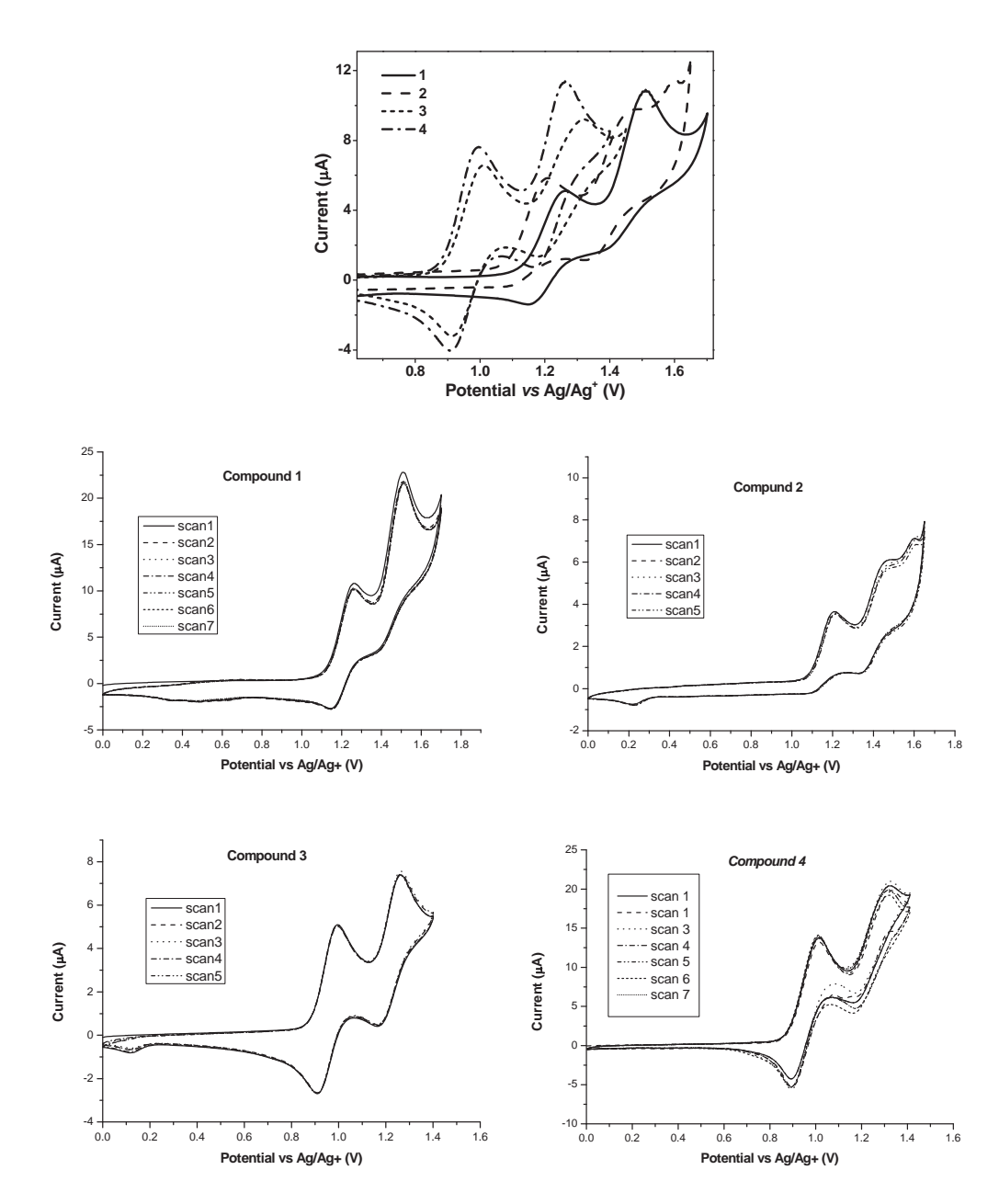


Fig. 5 CV curves of 1-4 measured in CH₂Cl₂ at a scan rate of 50 mV/s.

The thermal properties of **1-4** were investigated by the thermogravimetric analysis (TGA) and differential scanning calorimetry (DSC), and the results are shown in Fig. 5 and summarized in Table 1. Those results suggested that all compounds were thermally stable materials with 5% weight loss temperatures (T_{5d}) well over 330 °C. During the 1st heating DSC scan of crystalline samples **1** and **2**, only endothermic melting peaks (T_m) at 209 and 328 °C were detected, respectively. In their DSC 2nd heating scan, thermogram of **1** showed broad exothermic peaks due to the crystallization (T_c) at 115 °C followed by the melting peak, while the 2nd heating thermogram of dimer **2** was the same as the 1st cycle. Compounds **3** and **4** bearing triphenylamine as substituent exhibited different thermal behaviour. The asymmetric nature of this group may play additional role to the molecular packing. DSC thermogram (1st scan) of **3** revealed only endothermic peak at 155 °C due to melting of crystalline sample, while under 2nd

heating cycle, only endothermic baseline shift owing to glass transition (T_g) at 79 °C was detected with no crystallization and melting peaks at higher temperature being observed. The thermogram (2^{nd} scan) of 4 displays T_g at 155 °C and T_c around 225 °C to give the same crystal as obtained by crystallization from solution, which then melted at 338 °C. The ability of 3 and 4 to form a molecular glass with the possibility to prepare thin films from these materials both by evaporation and by solution casting is highly desirable for applications in electroluminescent devices.

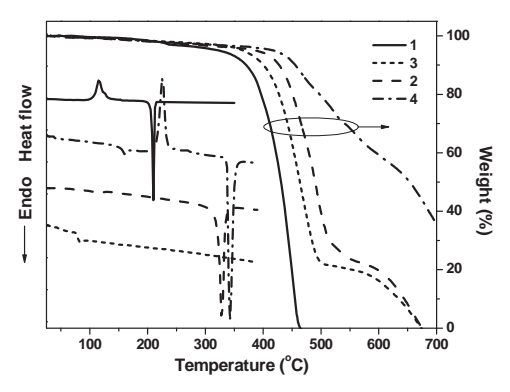


Fig. 6 DSC (2nd heating) and TAG thermograms of 1-4 measured under N₂ at heating rate of 10 °C/min.

2.4. Electroluminescence properties

In order to investigate the electroluminescence properties of 1-4, OLED devices were fabricated with the following device structure: indium tin oxide (ITO)/PEDOT:PSS/EML(50 nm)/BCP(40 nm)/LiF(0.5 nm):Al(150 nm), where these materials were used as emitting layer (EML). Conductive polymer poly(3,4ethylenedioxythiophene):poly(4-styrenesulfonate) (PEDOT:PSS) as hole injection layer and 2,9-dimethyl-4,7-diphenyl-1,10-phenanthroline (BCP) as hole blocking layer were also used to enable high-performance devices. The voltage-luminance and voltage-current density (J-V-L) characteristics of the devices are shown in Fig. 7 and 8, and their electrical parameters are summarized in Table 2. The results revealed that 3 and 4 owing electron donating triphenylamine in the molecules had the best EML properties among these four materials. Device IV having 4 as EML showed the best performance with a high maximum brightness of 4.586 cd/m² at 8.8 V, a low turn-on voltage of 4.6 V, a maximum luminous efficiency of 1.65 cd/A and a maximum external quantum efficiency of 0.34%. A slightly lower device performance was observed from device III displaying maximum brightness of 2,621 cd/m² at 8.6 V, turn-on voltage of 4.4 V, a maximum luminous efficiency of 1.28 cd/A and a maximum external quantum efficiency of 0.26%. Device I and II exhibited poorer device performance. The trend in device luminous efficiencies matches very well with the observed decrease in PL quantum efficiencies in going from 4 to 3 to 1 to 2 (Table 1). Fluorescence quantum yields (Φ_v) of both 3 and 4 were significantly higher than those of 1 and 2. The efficiency of an OLED depends both on the balance of electrons and holes and the $\Phi_{\scriptscriptstyle E}$ of the emitter. Analysis of band energy diagrams of all devices also revealed that the HOMO levels of all compounds

(5.32-5.56 eV) lied between those of PEDOT:PSS (5.00 eV) and BCP (6.50 eV) (see supporting information). However, there is a barrier around 0.32 eV for holes to migrate from the PEDOT:PSS/EML interface in devices III and IV, while such energy barrier (0.52-0.56 eV) is wider in devices I and II. This suggests that a migration of hole from the PEDOT:PSS to EML layer is more effective in devices III and IV resulting the charge efficiently recombine in the emitting layer and better device performance. Fig. 9 showed the normalized electroluminescence (EL) spectra of all diodes. In device III and IV, the EL emission was very similar to their corresponding PL emission with emission λ_{max} of 457 and 465 nm, respectively. However, we observed a spectral shift in the EL spectra for compounds 1 and 2. The EL spectrum of device I (1 as EML) displayed an emission peak at 440 nm corresponding PL emission of compound 1 and shoulder emission owing to exciplex species at the longer wavelength, while EL spectrum of device II (2 as EML) presented a totally red shifted emission peak (498 nm) from the exciplex species. However, stable emission was obtained from the all diodes with the EL spectra did not change much over the entire drive voltages (see supporting information).

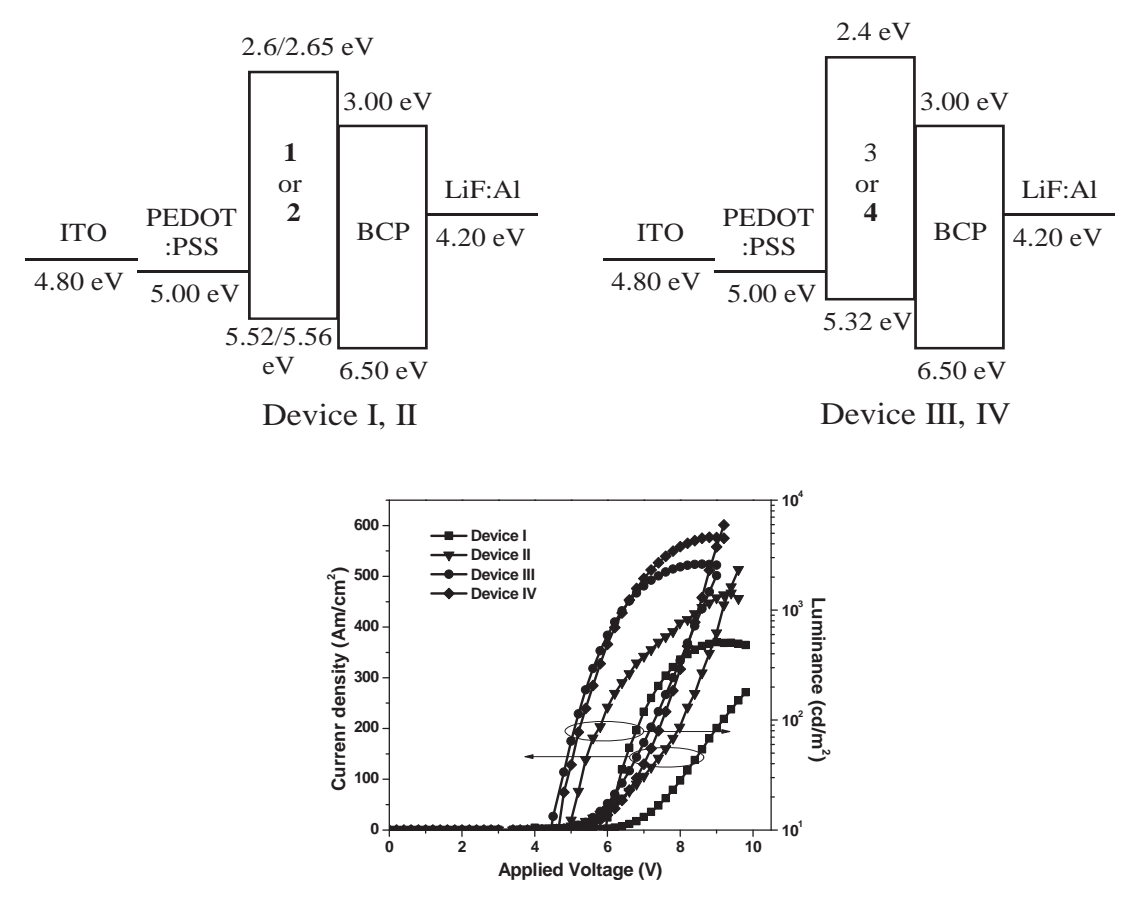


Fig. 7 J-V-L characteristics of OLED devices with 1-4 as EML.

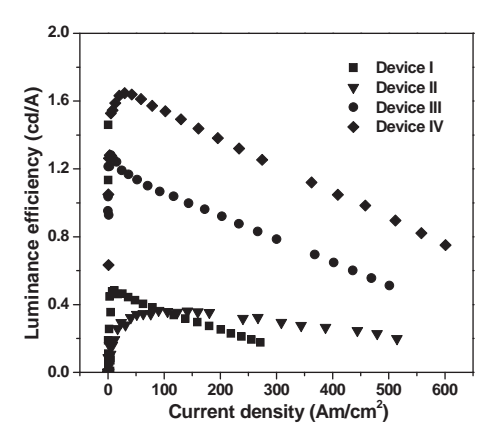


Fig. 8 Variation in luminance efficiency with current density of OLED devices with 1-4 as EML.

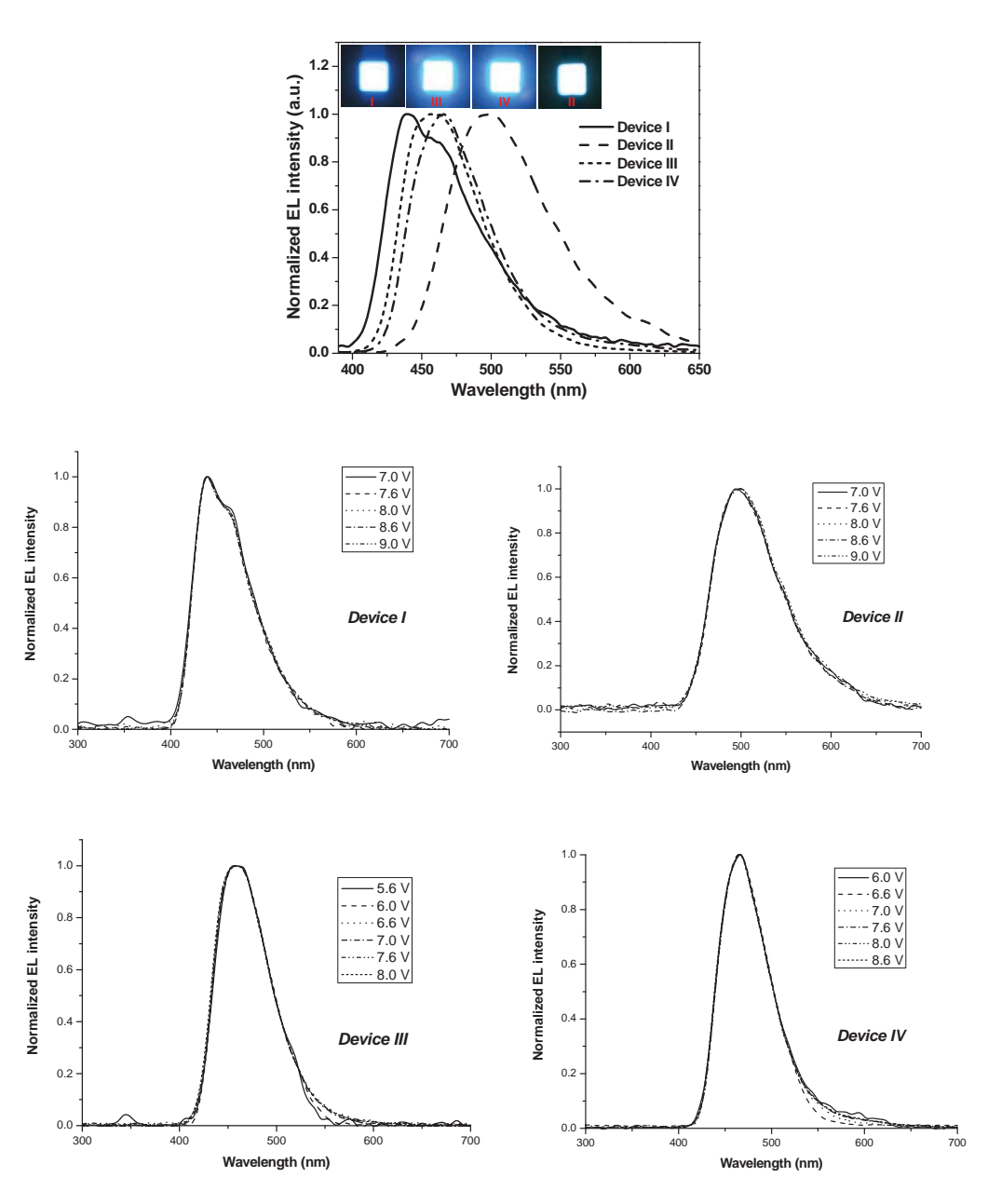


Fig. 9 EL spectra of OLED devices with 1-4 as EML.

As the HOMO levels of both **3** and **4**, having hole-transporting moiety in the molecules, matching well with the work function of ITO (4.8 eV), these compounds may potentially serve as hole-transporting material (HTM). To test this hypothesis, double-layer green OLED devices with the structure of ITO/PEDOT:PSS/HTL(40 nm)/Alq3(50 nm)/LiF(0.5 nm):Al(150 nm) were fabricated, where these materials were used as hole-transporting layer (HTL) and tris-(8-hydroxyquinoline)aluminum (Alq3) as the green light-emitting (EML) and electron-transporting layers (ETL). The reference device with the same structure based on commonly used commercial HTM, *N*,*N*'-diphenyl-*N*,*N*'-bis(1-naphthyl)-(1,1'-biphenyl)-4,4'-diamine (NPB), as HTL was made for comparison.

Table 2 Device characteristics of OLEDs with 1-4 and NBP as either EML or HTL.

Device	Structure	$V_{ m on}^{a}$	$\lambda_{\rm em}^{^{b}}$	$L_{\rm max}^{}$	\mathcal{J}^{d}	$\eta^{\mathfrak{e}}$	EQE^{f}	CIE ^g
I	ITO/PEDOT:PSS/1/BCP/LiF:A1	5.7	440	504	237	0.48	0.10	0.15, 0.13
II	ITO/PEDOT:PSS/2/BCP/LiF:Al	4.7	498	1427	479	0.37	0.03	0.22, 0.44
III	ITO/PEDOT:PSS/3/BCP/LiF:Al	4.4	457	2621	436	1.28	0.26	0.14, 0.13
IV	ITO/PEDOT:PSS/4/BCP/LiF:Al	4.6	465	4586	512	1.65	0.34	0.15, 0.16
V	ITO/PEDOT:PSS/3/Alq3/LiF:Al	3.8	515	18035	891	4.13	0.20	0.27, 0.52
VI	ITO/PEDOT:PSS/4/Alq3/LiF:Al	4.0	509	32270	894	6.25	0.30	0.26, 0.49
VII	ITO/PEDOT:PSS/NPB/Alq3/LiF:Al	3.4	515	30044	1362	4.45	0.22	0.25, 0.47

^a Turn-on voltage (V) at luminance of 10 cd/m².

g CIE coordinates (x, y)

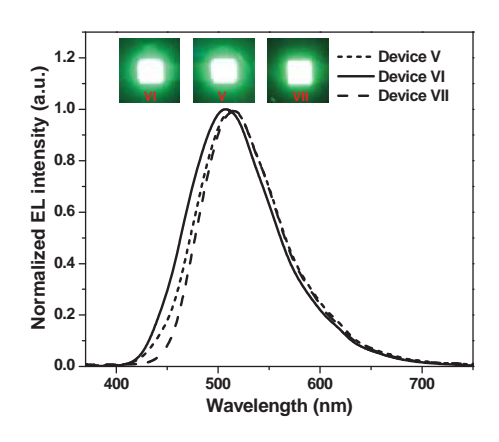


Fig. 10 EL spectra of green OLED devices with 3, 4 and NPB as HTL.

^b Emission maximum.

^c Maximum luminance (cd/m²) at the applied voltage (V).

^d Current density (mA/cm²).

^e Luminance efficiency (cd/A).

^f External quantum efficiency (%).

When comparison of HOMO and LUMO levels of layers for the devices, it was found that the HOMO levels of compounds 3 and 4 (5.32 eV) lied between those of PEDOT:PSS (5.00 eV) and Alq3 (5.80 eV), while the LUMO level of Alq3 (3.00 eV) lied between those of 3 and 4 (2.43-2.43 eV) and LiF:Al (4.20 eV) (see supporting information). There is a barrier around 0.32 eV for holes to migrate from the HTL layer to Alq3 layer, while that for electron to transport from the Alq3 to the HTL layer is about 0.57 eV. According to this band diagram and device configuration, both compounds can transport a hole injected from ITO/PEDOT:PSS to the Alq3 emitting layer. Under applied voltage, all devices emitted a bright green luminescence with EL spectra (λ_{max} 507-515 nm) matching with the PL spectrum of Alq3 and also other reported EL spectra of Alq3 devices (Fig. 10). No emission at the longer wavelength owing to exciplex species formed at the interface of HTL and ETL materials, which is often occurred in the devices fabricated from HTL with planar molecular structure, was detected. In our case, the formation exciplex species could be prevented by the bulky nature of both the anthracene core and triphenylamine at the peripheral of the molecules. From these results and in view of the fact that barrier for electron-migration at the Alq3/HTL interface (0.57 eV) is nearly twice higher than those for hole-migration at the HTL/Alq3 interface (0.32 eV), thus these compounds act only as HTM and Alq3 would act preferably as an electron blocker more than as a hole blocker and charge recombination thus confined to Alq3 layer.

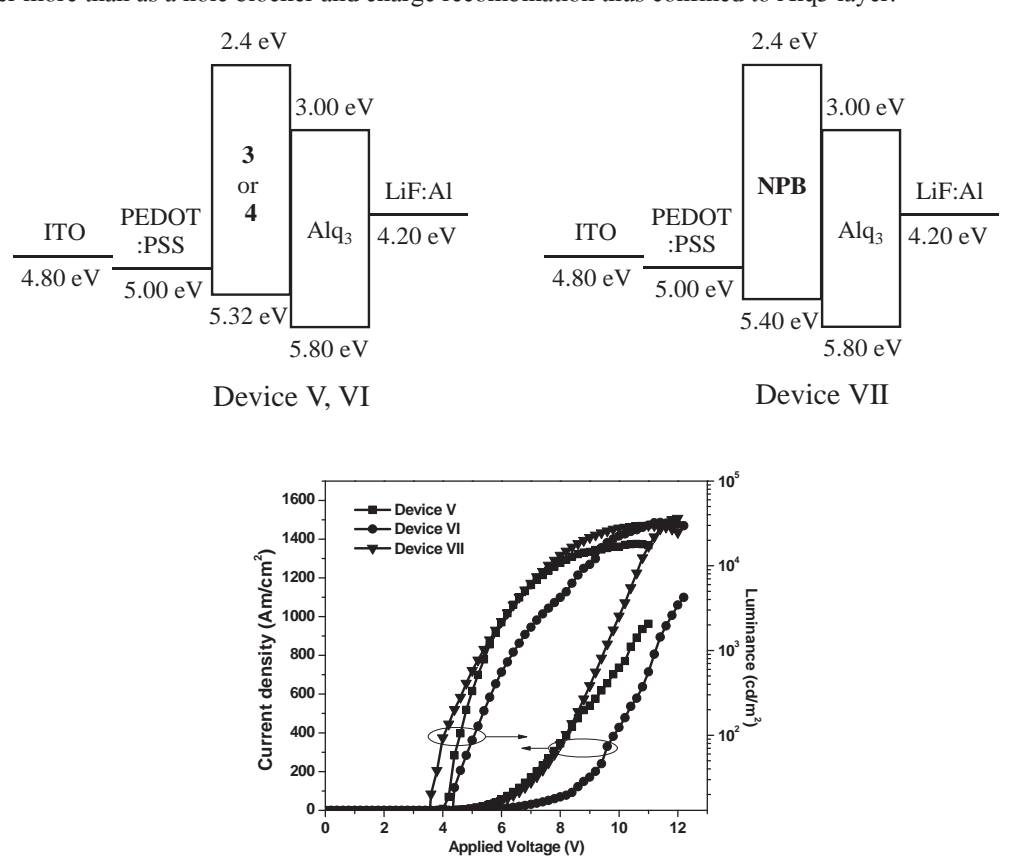


Fig. 11 J-V-L characteristics of green OLED devices with 3, 4 and NPB as HTL.

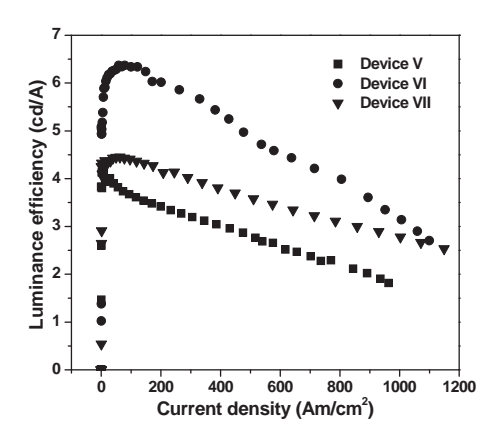


Fig. 12 Variation in luminance efficiency with current density of green OLED devices with 3, 4 and NPB as HTL.

The voltage-luminance and voltage-current density (*J-V-L*) characteristics of the devices are shown in Fig. 11 and 12, and their electrical parameters are summarized in Table 2. These results clearly demonstrated the hole-transporting ability of 3 and 4 with superior device performance (maximum brightness and efficiency) comparable to NPB-based device (device VII). Device VI having compound 4 as HTL exhibited the best performance with a high maximum brightness of 32,270 cd/m² for green OLED at 11.4 V, a low turn-on voltage of 4 V, a maximum luminous efficiency of 6.25 cd/A and a maximum external quantum efficiency of 0.30%. A slightly lower device performance was observed from compound 3-based device (device VI) showing maximum brightness of 18,035 cd/m² at 10.6 V, turn-on voltage of 3.8 V, a maximum luminous efficiency of 4.13 cd/A and a maximum external quantum efficiency of 0.20%.

3. Conclusions

In conclusion, we have successfully synthesized four new 9,10-substituted anthracenes with the combined characteristics of light-emitting and hole-transporting materials. These materials showed blue emission with high emission quantum efficiency over 70% in the solution and strong luminance in solid state. All of them were electrochemically and thermally stable with degradation temperature well above 330 °C. Most importantly, two of these materials having electron donating triphenylamine as peripheral substituent showed promising potential as both blue light-emitting materials and hole-transporting materials for Alq3-based OELD devices. Their ability as HTL for green OLEDs was comparable to a common hole-transporter NPB. Blue OLEDs with a maximum luminance efficiency of 1.65 cd/A, and green OLEDs with maximum luminance efficiency of 6.25 cd/A were achieved.

4. Experimental

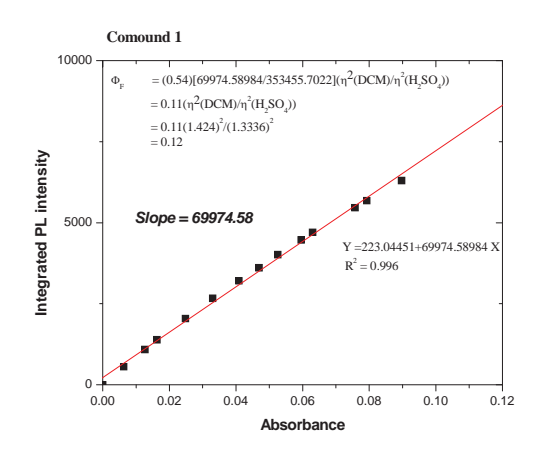
4.1. General procedure

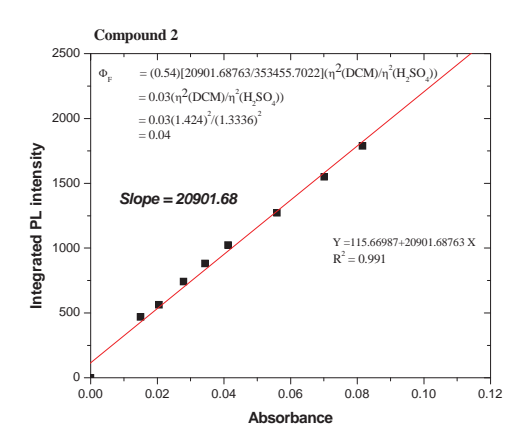
All reagents were purchased from Aldrich, Acros or Fluka and used without further purification. All solvents were supplied by Thai companies and used without further distillation. Tetrahydrofuran (THF) was refluxed with sodium and benzophenone, and freshly distilled prior to use. Dichloromethane for cyclic voltammetry (CV) measurements was washed with conc. H₂SO₄ and distilled twice from calcium hydride.

 1 H and 13 C nuclear magnetic resonance (NMR) spectra were recorded on a Brüker AVANCE 300 MHz spectrometer with tetramethylsilane as the internal reference using CDCl₃ as solvent in all cases. High resolution mass spectrometry (HRMS) was performed by Mass Spectrometry Unit at Chulabhorn Research Institute (CRI). Infrared (IR) spectra were measured on a Perkin-Elmer FTIR spectroscopy spectrum RXI spectrometer as potassium bromide (KBr) disc. Ultraviolet-visible (UV-Vis) spectra were recorded as a diluted solution in spectroscopic grade dichloromethane on a Perkin-Elmer UV Lambda 25 spectrometer. Photoluminescence spectra and the fluorescence quantum yields (Φ_F) were recorded with a Perkin-Elmer LS 50B Luminescence Spectrometer as a dilute solution in spectroscopic grade dichloromethane and thin film obtained by thermal deposition. The fluorescence quantum yields (Φ_F) were determined by comparison with a fluorescence standard of known fluorescence quantum yield value according to the following equation:

$$\Phi_{X} = \Phi_{ST} \left(\frac{Slope_{X}}{Slope_{ST}} \right) \left(\frac{\eta_{X}^{2}}{\eta_{ST}^{2}} \right)$$
(1)

Where the subscripts x refer to the unknown samples and ST refers to the standard quinine sulfate solution in 0.01 M $\rm H_2SO_4$, whose fluorescence quantum yield is known to be 0.54. Φ is the fluorescence quantum yield, Slope is the slope from the plot of integrated fluorescence intensity vs absorbance, and η is the refractive index of the solvent. The refractive indexes of the solvents were taken as 1.424 and 1.333 for CH₂Cl₂ and 0.01 M $\rm H_2SO_4$, respectively.





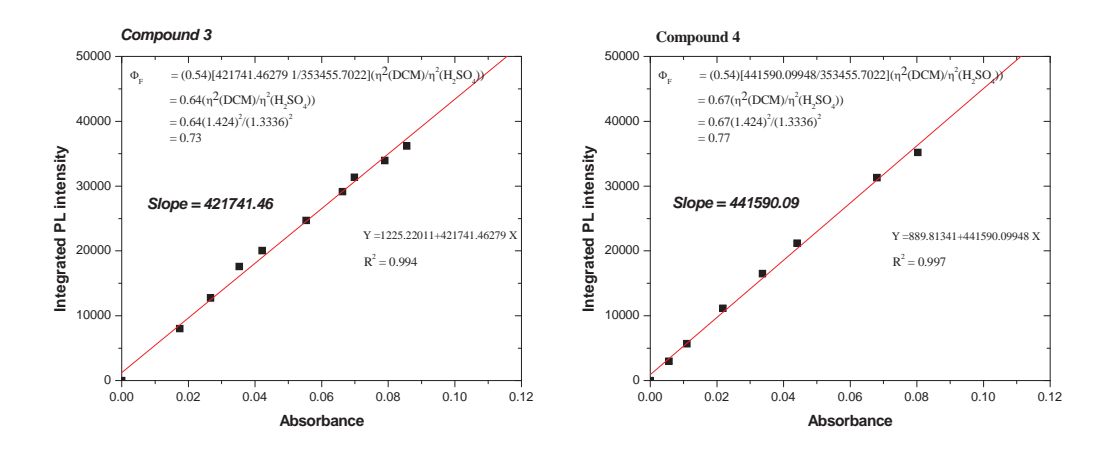


Fig. 13 Plots of integrated fluorescence intensity vs absorbance and calculation

Differential scanning carolimetry (DSC) analysis and thermogravimetry analysis (TGA) were performed on a METTLER DSC823e thermal analyzer and a Rigaku TG-DTA 8120 thermal analyzer, respectively, with heating rate of 10 °C/min under nitrogen atmosphere. Cyclic voltammetry (CV) measurements were carried out on an Autolab Potentiostat PGSTAT 12 with a three electrode system (platinum counter electrode, glassy carbon working electrode and Ag/Ag⁺ reference electrode) at scan rate of 50 mV/s in dichloromethane under argon atmosphere. The concentrations of an analytical material and supporting electrolyte tetrabutyl ammonium hexafluorophosphate (*n*-Bu₄NPF₆) were 10⁻³ M and 0.1 M, respectively. High resolution mass spectrometry (HRMS) analysis was performed by Mass Spectrometry Unit, Mahidol University, Thailand.

The ground state geometries were fully optimized using density functional theory (DFT) at the B3LYP/6-31G (d,p) level, as implemented in Gaussian 03. TDDFT/B3LYP calculation of lowest excitation energies were performed at the optimized geometries of the ground states.

4.2. Fabrication and characterization of OLEDs

OLED devices using 1-4 as EL with configuration of ITO/PEDOT:PSS/EML(50 nm)/BCP(40 nm)/LiF(0.5 nm):Al(150 nm) and double-layer green OLED devices using 3, 4 and NPB as HTL with configuration ITO/PEDOT:PSS/HTL(40 nm)/Alq3(50 nm)/LiF(0.5 nm):Al(150 nm) were fabricated and characterized as followed. The patterned indium tin oxide (ITO) glass substrate with a sheet resistance 14 Ω/\Box (purchased from Kintec Company) was thoroughly cleaned by successive ultrasonic treatment in detergent, deionized water, isopropanol, and acetone, and then dried at 60 °C in a vacuum oven. A 50 nm thick PEDOT:PSS hole injection layer was spin-coated on top of ITO from a 0.75 wt.% dispersion in water at a spin speed of 3000 rpm for 20 s and dried at 200 °C for 15 min under vacuum. Thin films of each organic EML or HTL were deposited on top of PEDOT:PSS layer by evaporation from resistively heated alumina crucibles at evaporation rate of 0.5-1.0 nm/s in vacuum evaporator deposition (ES280, ANS Technology) under a base pressure of ~10⁻⁵ mbar. The film thickness was monitored and recorded by

quartz oscillator thickness meter (TM-350, MAXTEK). A 40 nm thick hole-blocking layer of BCP or a 50 nm thick green-emitting layer of Alq3 was then deposited on the organic EML or HTL, respectively, without breaking the vacuum chamber. The chamber was vented with dry air to load the cathode materials and pumped back; a 0.5 nm thick LiF and a 150 nm thick aluminum layers were the subsequently deposited through a shadow mask on the top of EML/HTL film without braking vacuum to from an active diode areas of 4 mm². The measurement of device efficiency was performed according to M.E. Thomson's protocol and the device external quantum efficiencies were calculated using procedure reported previously. Current density-voltage-luminescence (*J-V-L*) characteristics were measured simultaneous by the use of a Keithley 2400 source meter and a Newport 1835C power meter equipped with a Newport 818-UV/CM calibrated silicon photodiode. The EL spectra were acquired by an Ocean Optics USB4000 multichannel spectrometer. All the measurements were performed under ambient atmosphere at room temperature.

4.3. Synthesis and characterization

4.3.1. 9-Bromo-10-(9,9-dihexylfluoren-2-yl) anthracene (6)

A mixture of 2-iodo-9,9-bis-n-hexylfluorene (1.28 g, 2.79 mmol), 9-bromoanthracen-10-boronic acid (0.84 g, 2.79 mmol) and Pd(PPh₃)₄ (0.065 g, 0.12 mmol) and 2 M Na₂CO₃ (8 ml,) aqueous solution in THF (12 ml) was degassed with N₂ for 5 min. The reaction mixture was stirred at reflux under N₂ for 18 h. After being cooled to room temperature, water (50 ml) was added and extracted with CH₂Cl₂ (50 ml x 2). The combined organic phase was washed with water (50 ml), brine solution (50 ml), dried over anhydrous Na₂SO₄, filtered, the solvents were removed to dryness. Purification by column chromatography over silica gel eluting with a mixture of CH₂Cl₂ and hexane (1:4) followed by recrystallization from a mixture of CH₂Cl₂ and methanol afforded light yellow solid (0.66 g, 52%); ¹H-NMR (300 MHz, CDCl₃) δ 0.76-0.88 (10 H, m), 1.09-1.14 (12 H, m), 1.95-2.01 (4H, m), 7.34-7.40 (7 H, m), 7.59 (2 H, t, J = 8.8 Hz), 7.72 (2 H, d, J = 9.0 Hz), 7.81 (1 H, dd, J = 3.3 Hz, J = 2.7 Hz), 7.89 (1 H, d, J = 7.5 Hz) and 8.62 (2 H, d, J = 8.7 Hz); ¹³C-NMR (75Hz, CDCl₃) δ 13.99, 22.47, 23.85, 29.60, 31.52, 40.37, 55.26, 119.62, 119.83, 122.92, 124.87, 125.46, 125.91, 126.54, 126.92, 127.32, 127.44, 129.73, 130.30, 131.20, 136.90, 140.81 and 150.95; HRMS-ESI m/z: [MH⁺] calcd. for C₃₀H₄₇Br, Exact Mass: 589.2432; found, 589.3042.

4.3.2. 9-(9,9-Dihexylfluoren-2-yl)-10-thiophen-2-yl-anthracene (1)

A mixture of $\mathbf{6}$ (0.67 g, 1.14 mmol), 2-thiophene boronic acid (0.16 g, 1.25 mmol), Pd(PPh₃)₄ (0.025 g, 0.023 mmol) and 2 M Na₂CO₃ aqueous solution (6 ml) in THF (10 ml) was degassed with N₂ for 5 min. The reaction mixture was stirred at reflux under N₂ for 20 h. After being cooled to room temperature, water (50 ml) was added and extracted with CH₂Cl₂ (50 ml x 2). The combined organic phase was washed with water (50 ml), brine solution (50 ml), dried over anhydrous Na₂SO₄, filtered, the solvents were removed to dryness. Purification by column chromatography over silica gel eluting with a mixture of CH₂Cl₂ and hexane (1:4) followed by recrystallization from a mixture of CH₂Cl₂and methanol afforded

light yellow solids (0.51 g, 76%); 1 H-NMR (300 MHz, CDCl₃) δ 0.78-0.82 (10 H, m), 1.12-1.18 (12 H, m), 2.03 (4 H, t, J = 9.0 Hz), 7.34-7.47 (11 H, m), 7.66 (1 H, d, J = 4.8 Hz), 7.79 (2 H, d, J = 8.7 Hz), 7.84 (1 H, d, J = 7.8 Hz) and 7.92-7.98 (3 H, m); 13 C-NMR (75 MHz, CDCl₃) δ 14.03, 22.51, 23.89, 29.66, 31.55, 40.45, 55.27, 119.64, 119.82, 122.92, 125.10, 125.57, 126.03, 126.73, 126.91, 127.03, 127.20, 127.26, 128.66, 129.50, 129.75, 131.65, 137.40, 139.17, 139.31, 140.87, 141.05, 150.91 and 151.02; IR (KBr) 2925, 1517, 1463, 1377, 1025, 822 and 767 cm ${}^{-1}$; HRMS-ESI m/z: [MH ${}^{+}$] cald. for C₄₃H₄₅S, 593.3197; found, 593.3186.

4.3.3. 2-Bromo-5-(10-(9,9-dihexylfluoren-2-yl)anthracen-9-yl)thiophene (7)

To a solution of **1** (0.60 g, 1.01 mmol) in tetrahydrofuran (15 ml) was added NBS (0.18 g, 1.01 mmol) in small portions. While adding NBS, the reaction was monitored by TLC. Soon after all starting material was consumed, water was added and the mixture was extracted with CH_2Cl_2 (50 ml x 2). The combined organic phase was washed with water (50 ml), a dilute NaHCO₃ aqueous solution (50 ml), brine solution (50 ml), dried over anhydrous Na_2SO_4 , filtered, the solvents were removed to dryness. Purification by recrystallization a mixture of CH_2Cl_2 and methanol gave light yellow solid (0.64 g, 95%); ¹H NMR (300 MHz, CDCl₃) δ 0.74-0.92 (10 H, m), 1.08-1.15 (12 H, m), 1.97-2.05 (4 H, m), 6.99 (1 H, d, J = 3.9 Hz), 7.29-7.47 (10 H, m), 7.75 (2 H, d, J = 8.7Hz), 7.81-7.84 (1 H, m) and 7.92-7.97 (3 H, m); ¹³C NMR (75 MHz, CDCl₃) δ 14.00, 22.49, 23.87, 29.63, 31.53, 40.42, 55.26, 112.83, 119.65, 119.82, 122.92, 125.17, 125.91, 126.37, 126.91, 127.13, 127.30, 128.87, 129.67, 129.94, 130.14, 131.56, 134.10, 137.16, 139.81, 140.76, 140.87, 141.18, 150.91 and 150.96; HRMS-ESI m/z: [MH⁺] calcd. for $C_{43}H_{44}$ BrS, Exact Mass: 671.2349; found, 671.5429.

4.3.4. 5,5'-Bis(10-(9,9-dihexylfluoren-2-yl)anthracen-9-yl)-2,2'-bithiophene (2)

A mixture of 7 (0.65 g, 0.96 mmol), NiCl₂ (0.75 g, 5.78 mmol), Zn powder (0.11 g, 1.73 mmol), PPh₃ (0.15 g, 0.57 mmol), bipyridine (bpy) (0.06 g, 0.38 mmol) in DMAc (10 ml) was degassed with N₂ for 10 min. The reaction mixture was stirred at reflux under N₂ for 24 h. After being cooled to room temperature, water (50 ml) was added and extracted with CH₂Cl₂ (50 ml x 2). The combined organic phase was washed with water (50 ml), brine solution (50 ml), dried over anhydrous Na₂SO₄, filtered, the solvents were removed to dryness. Purification by column chromatography over silica gel eluting with a mixture of CH₂Cl₂ and hexane (1:5) followed by recrystallization from a mixture of CH₂Cl₂ and methanol afforded greenish solids (0.35 g, 63%); ¹H-NMR (300 MHz, CDCl₃) δ 0.78-0.82 (20 H, m), 1.12-1.18 (24 H, m), 2.03 (8 H, t, J = 8.1 Hz), 7.22 (2 H, d, J = 3.3 Hz), 7.36-7.55 (20 H, m), 7.80-7.87 (6 H, m), 7.95 (2 H, d, J = 8.1 Hz) and 8.12 (4 H, d, J = 9.0 Hz); ¹³C-NMR (75 MHz, CDCl₃) δ 14.01, 22.50, 23.89, 29.65, 31.54, 40.44, 55.28, 119.65, 119.82, 122.93, 123.88, 125.18, 125.78, 126.02, 126.69, 127.13, 127.27, 128.04, 129.75, 130.04, 130.49, 131.60, 137.33, 138.50, 138.73, 139.48, 140.73, 140.92, 150.91 and 150.99; IR

(KBr) 2922, 1557, 1447, 1369 1270, 1018, 824 and 764cm $^{-1}$; HRMS-ESI m/z: [MH $^{+}$] calcd. for C₈₆H₈₇S₂, 1183.6244; found, 1183.6210.

4.3.5. 9-(9,9-Dihexylfluoren-2-yl)-10-(4-diphenylaminophenyl) anthracene (3)

A mixture of **6** (0.52 g, 0.88 mmol), N_iN -diphenyl- N_i -4-aminophenylboronic acid (0.28 g, 0.97 mmol), Pd(PPh₃)₄ (0.021 g, 0.017 mmol) and 2 M Na₂CO₃ aqueous solution (6 ml) in THF (10 ml) was degassed with N₂ for 5 min. The reaction mixture was stirred at reflux under N₂. After being cooled to room temperature, water (50 ml) was added and extracted with CH₂Cl₂ (50 ml x 2). The combined organic phase was washed with water (50 ml), brine solution (50 ml), dried over anhydrous Na₂SO₄, filtered, the solvents were removed to dryness. Purification by column chromatography over silica gel eluting with a mixture of CH₂Cl₂ and hexane (1:4) followed by recrystallization from a mixture of CH₂Cl₂ and methanol afforded light yellow solids (0.52 g, 79%); ¹H-NMR (300 MHz, CDCl₃) δ 0.75-0.80 (10 H, m), 1.09-1.16 (12 H, m), 1.98-2.03 (4 H, m), 7.07-7.12 (2 H, t, J = 7.0 Hz), 7.26-7.46 (21 H, m), 7.77-7.95 (6 H, m); ¹³C-NMR (75 MHz, CDCl₃) δ 14.02, 22.51, 23.89, 31.55, 40.47, 55.26, 119.61, 119.78, 122.91, 123.10, 123.13, 124.71, 124.97, 126.16, 126.88, 127.10, 127.19, 129.40, 129.89, 130.10, 130.15, 132.14, 132.69, 136.92, 137.70, 140.54, 141.00, 147.17, 147.84, 150.86 and 150.98; IR (KBr) 2929, 1590, 1494, 1380, 1273, 1019, 823 and 746 cm⁻¹; HRMS-ESI m/z: [MH⁺] calcd. for C₅₇H₅₆N, 754.4407; found, 754.4386.

4.3.6. 2,7-Bis(9-bromoanthracene-10-yl)-9,9-dihexylfluorene (9)

A mixture of 2,7-diiodo-9,9-bis-n-hexylfluorene (1.11 g, 1.90 mmol), 9-bromoanthracen-10-boronic acid (1.20 g, 3.99 mmol) and Pd(PPh₃)₄ (0.11 g, 0.10 mmol) and 2 M Na₂CO₃ (10 ml,) aqueous solution in THF (15 ml) was degassed with N₂ for 5 min. The reaction mixture was stirred at reflux under N₂ for 20 h. After being cooled to room temperature, water (50 ml) was added and extracted with CH₂Cl₂ (50 ml x 2). The combined organic phase was washed with water (50 ml), brine solution (50 ml), dried over anhydrous Na₂SO₄, filtered, the solvents were removed to dryness. Purification by column chromatography over silica gel eluting with a mixture of CH₂Cl₂ and hexane (1:4) followed by recrystallization from a mixture of CH₂Cl₂ and methanol afforded light yellow solid (0.90 g, 56%); ¹H-NMR (300 MHz, CDCl₃) δ 0.8 (6 H, t, J = 6.9 Hz), 0.94 (4 H, m), 1.14-1.27 (12 H, m), 2.04 (4 H, t, J = 7.8 Hz), 7.40-7.48 (8 H, m), 7.65 (4 H, t, J = 8.4 Hz), 7.79 (4 H, d, J = 9.0 Hz), 8.04 (2 H, d, J = 8.1 Hz) and 8.66 (4 H, d, J = 9.0 Hz); ¹³C-NMR (75Hz, CDCl₃) δ 14.02, 22.40, 24.06, 29.55, 31.57, 40.34, 55.51, 119.86, 122.70, 125.56, 126.04, 126.97, 127.40, 127.95, 130.01, 130.34, 131.21, 137.32, 138.229, 140.53 and 151.21; HRMS-ESI m/z: [MH[†]] calcd. for C₅₃H₄₀Br₂, Exact Mass: 843.2193; found, 843.8920.

4.3.7. 2,7-Bis(9-(4-diphenylaminophenyl) anthracene-10-yl)-9,9-dihexylfluorene (4)

A mixture of 9 (0.51g, 0.60 mmol), N_1N_2 -diphenyl- N_2 -aminophenylboronic acid (0.37 g, 1.27 mmol), $Pd(PPh_3)_4$ (0.01 g, 0.01 mmol) and 2 M Na_2CO_3 aqueous solution (6 ml) in THF (10 ml) was degassed with N_2 for 5 min. The reaction mixture was stirred at reflux under N_2 . After being cooled to room

temperature, water (50 ml) was added and extracted with CH_2Cl_2 (50 ml x 2). The combined organic phase was washed with water (50 ml), brine solution (50 ml), dried over anhydrous Na_2SO_4 , filtered, the solvents were removed to dryness. Purification by column chromatography over silica gel eluting with a mixture of CH_2Cl_2 and hexane (1:6) followed by recrystallization from a mixture of CH_2Cl_2 and methanol afforded deep yellow solids (0.45 g, 75%); 1H -NMR (300 MHz, $CDCl_3$) δ 0.82 (6 H, t, J = 6.9 Hz), 0.91 (4 H, bs), 1.17-1.28 (12 H, m), 2.06 (4 H, t, J = 7.8 Hz), 7.12 (4 H, t, J = 6.9 Hz), 7.31-7.48 (32 H, m), 7.55-7.56 (4 H, m), 7.85 (4 H, d, J = 8.7 Hz), 7.90 (4 H, d, J = 8.4 Hz) and 8.07 (2 H, d, J = 8.1 Hz); ^{13}C -NMR (75 MHz, $CDCl_3$) δ 14.05, 22.48, 24.10, 29.65, 31.62, 40.51, 55.50, 119.77, 123.12, 124.73, 125.02, 126.28, 127.07, 127.16, 129.41, 130.14, 130.20, 132.16, 132.70, 137.00, 137.55, 137.96, 140.43, 147.20, 147.85 and 151.18; IR (KBr) 2922, 1590, 1491, 1384, 1273, 1019, 823 and 764 cm $^{-1}$; HRMS-ESI m/z: [MH $^+$] calcd. for $C_{89}H_{77}N_7$, 1173.6081; found, 1173.6070.

PART II

Blue Light-Emitting and Hole-Transporting Materials Based on 9,9-Bis(4-diphenylaminophenyl) fluorenes for Efficient Electroluminescent Devices

1. Introduction

Organic light-emitting diodes (OLEDs) have attracted a great deal of attention due to their applications, such as full-color or large-area flat panel displays, backlight, and general illumination. In the past decade, we have seen great progress in both materials development and device fabrication techniques. One area of continuing research is the pursuit for a stable-blue emitting material. Poly(p-phenylene) (PPP) and related polymers, such as ladder-type PPP and polyfluorenes (PFs), have received strong interest in recent years. Although, PFs in particular have been used to make efficient blue light-emitting devices, they still have a number of deficiencies as potential candidates for blue OLEDs including low colour purity due to side emission from the aggregates and defect sites, and requiring the use of hole-transporting layers to obtain a balance in charge carriers. The hole-injection ability of these PFs has been successfully improved by many approaches such as blending with hole-transporting triarylamines, end-capping the polymer chain with triarylamines, copolymerization with triarylamine-containing monomers and substitutions at the C-9 position of the fluorene block with triarylamines. The latter approach was proven to be more effective and complex synthesis required. For example, 9,9-bis(4-diphenylaminophenyl)fluorene (9,9bis(triphenylmine)fluorene) has been successfully used as a building block for the synthesis of many blue emitting PFs and copolymers with improving hole-injection and suppressing aggregation. It has been shown that the formation of molecular fluorenes or oligofluorenes efficiently improved colour purity of these polymers. Hence, using this fluorene building block to construct new molecular materials might be a simple solution to develop efficient pure blue emitters.

Owing to its high photoluminescence efficiency in blue, high carrier mobility, and improved the hole-injection ability than other blue chromophores such as oligofluorenes, PFs or PPP, pyrene has been used as a building block to form many emissive materials. Recently, many kinds pyrene-functionalized materials have been synthesized and considered for several applications, and some of them were proven to be promising blue emitters for OLEDs. Pyrene-based molecules as bifunctioned materials, blue emitters and hole-transporters, remain rare and largely unexplored in OLEDs. Therefore, we herein implemented all required aspects in the synthesized molecules (Fig. 1). The use of 9,9-bis(4-diphenylaminophenyl)fluorene as a molecular framework offers a perfect bulky molecule with high thermal stability and an improved hole

injection and transport ability from the substituted triphenylamine units. Incorporation of pyrene unit into cruciform of this platform is an effective way to control the π - π stacking interactions and maintain the high blue emissive ability of pyrene in the solid state, which significantly impact the emission behaviour of devices. The high steric hindrance in the molecule also offers good solubility and thereby thermally stable amorphous thin film could be deposited by cheap solution process. Fluorene also has a number of advantages, including its capability to emit in the blue part of the visible spectrum, chemical and photochemical stability. Accordingly, this would result in new bifunctioned materials with combined blue emitting and hole-transporting properties. An investigation of their physical and photophysical properties, and blue OLED fabrication and characterization are also reported.

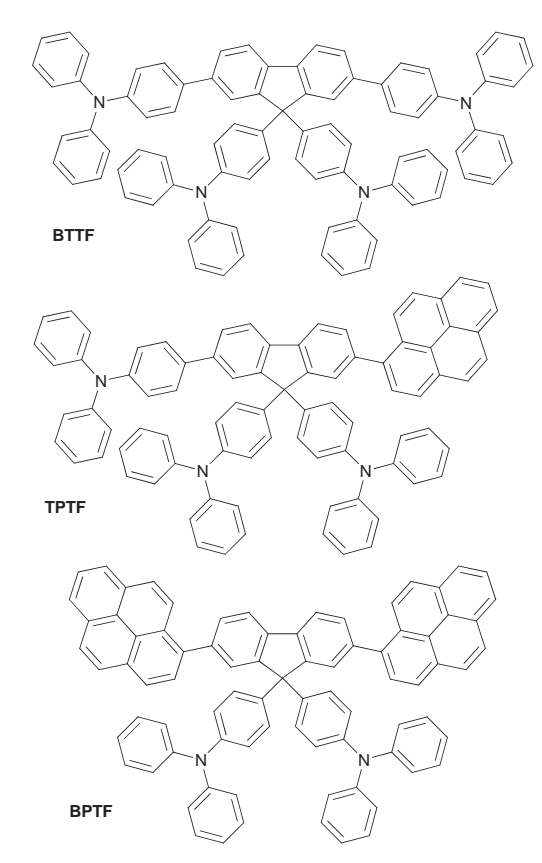


Fig. 1 Molecular structures of BTTF, TPTF and BPTF.

2. Results and discussion

2.1 Synthesis

The target molecules were synthesized as outlined in Scheme 1. Firstly, an intermediate 2 was synthesized *via* a tandem protocol of ready obtained 2,7-dibrofluorenone (1) with an excess of triphenylamine catalysed by methanesulfonic acid at 190 °C. Coupling of 2 with either pyrene-1-boronic acid or triphenylamine-4-boronic acid under Suzuki cross-coupling reaction catalysed by Pd(PPh₃)₄ afforded **BPTF** and **BTTF** in good yields as yellow and white solids, respectively. Under the same Pd-

catalysed coupling conditions, a stepwise coupling of **2** with triphenylamine-4-boronic acid followed by 1-pyreneboronic acid gave **TPTF** as light yellow solid in 54% yield over two steps. Their chemical structures were characterized unambiguously with ¹H-NMR, ¹³C-NMR spectroscopy and mass spectrometry. These materials showed good solubility in organic solvents, opening the door to solution processing techniques.

Scheme 1. Synthesis of **BTTF**, **TPTF** and **BPTF**; (a) triphenylamine, MeSO₃H, 190 °C. (b) pyrene-1-boronic acid, (c) triphenylamine-4-boronic acid, Pd(PPh₃)₄, 2M Na₂CO₃, THF, reflux.

2.2 Quantum calculation and optical properties

To understand the electronic properties and the geometries of the synthesized molecules, quantum chemical calculations were performed using TDDFT/B3LYP/6-31G (d,p) method. The optimized structures of these compounds revealed that both triphenylamine moieties at the C-9 position of the fluorene ring generated a highly steric hindrance, resulting a bulky molecular structure and thereby preventing a closed π - π stacking interaction of the molecule. The molecules (**TPTF** and **BTTF**) became more steric when the C-2 or -7 positions of the fluorene ring being attached by extra triphenylamine units. In the highest occupied molecular orbitals (HOMO) of **BTTF** and **TPTF**, π -electrons delocalized over the π -conjugated 2-(4-diphenylaminophenylfluorene) backbone and also located on triphenylamine pendant groups, while in the HOMO orbital of **BPTF**, π -electrons localized only on the triphenylamine (Fig. 2). This suggested that there is no π -electron interaction between fluorene and pyrene moieties. In the lowest unoccupied molecular orbitals (LUMO) of all compounds, the excited electrons delocalized over the quinoid-like pyrene-fluorene plane, creating in case of **TPTF** a donor-acceptor molecule with triphenylamine acting as donor and pyrene acting as acceptor. The HOMO-LUMO energy gaps (E_g cal.)

were calculated and presented in Table 1. These calculated values slightly deviated from those obtained from the experimental results (~0.03-0.11 eV). There are factors responsible for the errors because the orbital energy difference between HOMO and LUMO is still an approximate estimation to the transition energy since the transition energy also contains significant contributions from some two-electron integrals. The real situation is that an accurate description of the lowest singlet excited state requires a linear combination of a number of excited configurations.

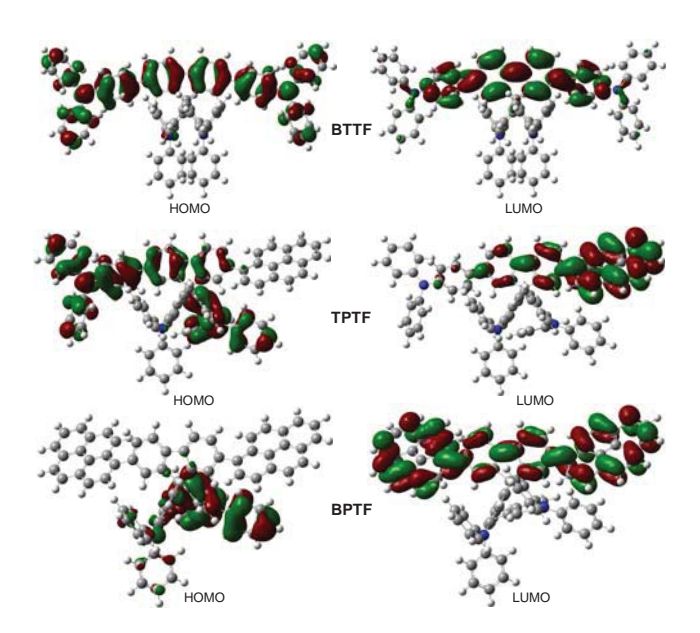


Fig. 2 The HOMO (right) and LUMO (left) orbitals of BTTF, TPTF and BPTF.

The optical properties of BTTF, TPTF and BPTF were investigated in dilute CH_2CI_2 solution and thin film obtained by thermal evaporation on a quart substrate. The pertinent data are presented Fig. 3a and summarized in Table 1. Their solution absorption spectra showed two absorption bands: a strong absorption band at 303 nm corresponding to the π - π * local electron transition of the pendant triphenylamine moieties and a less intense absorption band at longer wavelength (350-400 nm) assigning to the π - π * electron transition of the π -conjugated backbone. In solid state, the similar absorption features with a slight red shift compared to their corresponding solution spectra were observed. These materials exhibited a strong blue fluorescence in both solution and solid state. Fluorescence quantum yields (Φ_F) of BTTF, TPTF and BPTF measured in dilute solution using quinine sulfate solution in 0.01 M H_2SO_4 (Φ_F = 0.54) as a standard were 0.43, 0.64 and 0.74, respectively. The results indicated that direct attachment of the pyrene ring to the molecule boosted the Φ_F of these materials. Their solution photoluminescence (PL) spectra showed a featureless emission peak in the blue region (430-470 nm). The PL spectrum of TPTF red-shifted of 28 nm with respect to those of BTTF and BPTF, resulting from its donor-acceptor character as indicated in quantum calculation. These materials showed small stoke shifts (66-89 nm) suggesting less energy loss during the relaxation process and thereby ensuing efficient fluorescence. The thin film PL

emission spectra of **BTTF** and **BPTF** were similar to their solution PL spectra, hence indicating no or less if any solid state packing occurred in this case due to their bulky molecular structures.

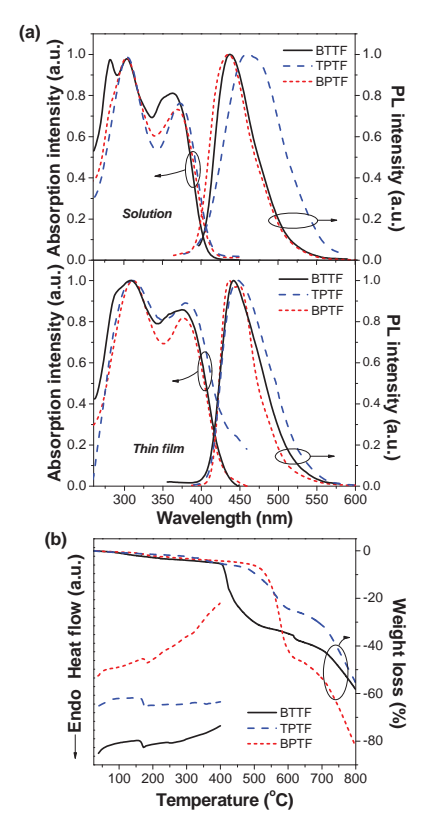


Fig. 3 (a) UV-vis absorption and PL spectra measured in CH_2Cl_2 solution and as thin film obtained by thermal deposition on quart substrate. (b) DSC (2^{nd} heating scan) and TGA thermograms measured under N_2 at heating rate of 10 °C/min.

2.3 Thermal and electrochemical properties

For OLED applications, thermal stability of organic materials is crucial for device stability and lifetime. The thermal instability or low glass transition temperature (T_g) of the amorphous organic layer may result in the degradation of organic devices due to morphological changes. The thermal properties of **BTTF**, **TPTF** and **BPTF** were investigated by the thermogravimetric analysis (TGA) and differential scanning calorimetry (DSC), and the results are shown in Fig. 3b and summarized in Table 1. Those results suggested that all compounds were thermally stable materials with 5% weight loss temperatures (T_{5d}) well over 390 °C. In the 1st and 2nd heating scans, DSC thermograms of all compounds displayed only baseline shift due to glass transition temperatures (T_g) ranged from 171 to 179 °C with no crystallization and melting peaks at higher temperature being observed. These results indicated that these materials were stable amorphous materials with high T_g which was higher those of the commonly used HTMs such as NPB ($T_g = 100$ °C) and *N,N'*-bis(3-methylphenyl)-*N,N'*-bis(phenyl)benzidine (TPD) ($T_g = 63$ °C), and other triphenylamine derivatives. The results proved that the use of 9,9-bis(4-diphenylaminophenyl)fluorene as a

molecular platform could reduce the crystallization of pyrene and improve the amorphous stability of the materials, which in turn could increase the service time in device operation and enhance the morphological stability to the thin film. Moreover, the abilities of these materials to form molecular glass and dissolve in organic solvents offers the possibility to prepare good thin films by both thermal evaporation and solution casting techniques which are highly desirable for fabrication of OLED device.

Electrochemical behaviours of all compounds were investigated by cyclic voltammetry (CV), and the resulting data are shown in Fig. 4 and summarized in Table 1. The experiment was carried out in degassed CH₂Cl₂ containing 0.1 M n-Bu₄NPF₆ as a supporting electrolyte under argon atmosphere. BTTF was found to exhibit one quasi-reversible oxidation process at 0.96 V, while both TPTF and BPTF showed two quasi-reversible oxidation processes with additional peak at lower potential (0.74 V) on the cathodic scan (E₂₀) being observed. The first oxidation potentials of all compounds were nearly identical (0.96-0.98 V) and assigned to the removal of electrons from the triphenylamines resulting radical cations as demonstrated in Fig 5. The multiple CV scans of BTTF revealed identical CV curves, indicating no oxidative coupling or a weak oxidative coupling if any at p-phenyl rings of the peripheral triphenylamine led to electro-polymerization and BTTF is electrochemically stable molecule. However, this type of electrochemical reaction was detected in both TPTF and BPTF as indicated by the presence of the cathodic peak at 0.74 V in their first CV scan. The repeated CV scans of these compounds also revealed an increasing change in their CV curves as illustrated in Fig. S1 (ESI†). Usually, this type of electrochemical coupling reaction is detected in most triphenylamine derivatives with unsubstituted p-position of the phenyl ring such as in case of 2,7-bis[2-(4-diphenylaminophenyl)-1,3,4-oxadiazol-5-yl]-9,9-bis-nhexylfluorene. A proposed oxidation and electrochemical coupling reaction of these materials is outlined in Fig. 5. During the first oxidation, the electrons are removed from N-atom of all available triphenylamine moieties to give radical cations form A which undergoes electron delocalization to get resonance forms B, C and D, respectively. These radical cations are highly reactive species and readily undergo dimerization coupling to stable neutral molecule. Resonance forms A, B and D having a radical on N atom, ortho-C atoms, respectively, are less reactive to a dimerization coupling reaction due to high steric hindrance and thereby this electrochemical reaction would take place through the resonance form C. However, triphenylamine units X and Y are unlikely to undergo such coupling reaction due to the radical cation formed is stabilized by electron delocalization through the attached fluorene ring and is prevented by steric hindrance of the adjacent triphenylamine unit, respectively. Hence, the oxidative coupling of the triphenylamine occurs only with the unstable and less steric triphenylamine unit Z. Steric hindrance and stability of triphenylamine moieties therefore played an important role to prevent such electrochemical reaction in BTTF. While in cases of TPTF and BPTF having one or both of C-2 and -7 positions of the fluorene ring being substituted by pyrene ring which is less bulk than triphenylamine unit (in BTTF), the

coupling reaction took place through less steric triphenylamine pendant groups (\mathbf{X}). However, this type of electrochemical reaction will become inactive in non-diffusion system or solid state. Moreover, under these CV experiment conditions, no distinct reduction process was observed in all cases. The HOMO and LUMO energy levels of BTTF, TPTF and BPTF were calculated from the oxidation onset potentials (\mathbf{E}_{onset}) and energy gaps (\mathbf{E}_{g}) and the results are summarized in Table 1. The HOMO levels of these materials ranged from 5.29 to 5.31 eV matching well with the work functions of the gold (Au) or indium tin oxide (ITO) electrodes and hence favouring the injection and transport of holes.

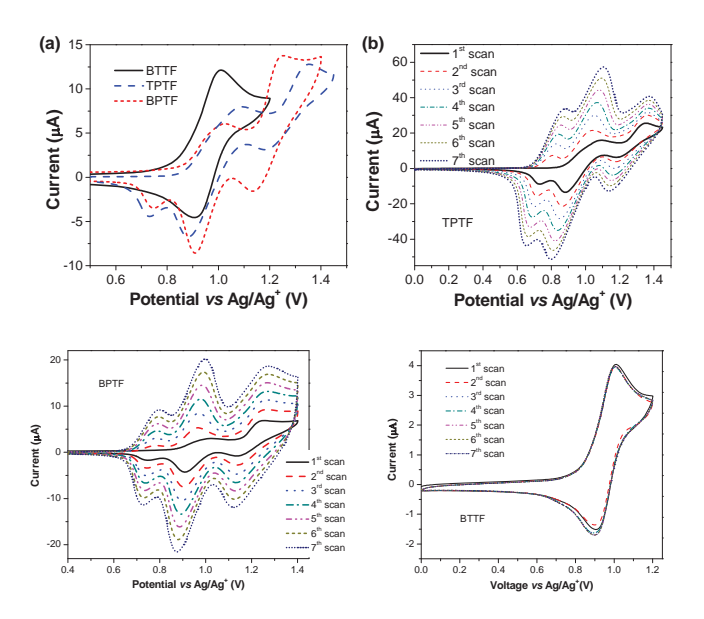


Fig. 4 (a) CV curves of **BTTF**, **TPTF** and **BPTF** and (b) multiple CV scans of **TPTF**, **BPTF** and **BTTF** measured in CH₂Cl₂ at a scan rate of 50 mV/s.

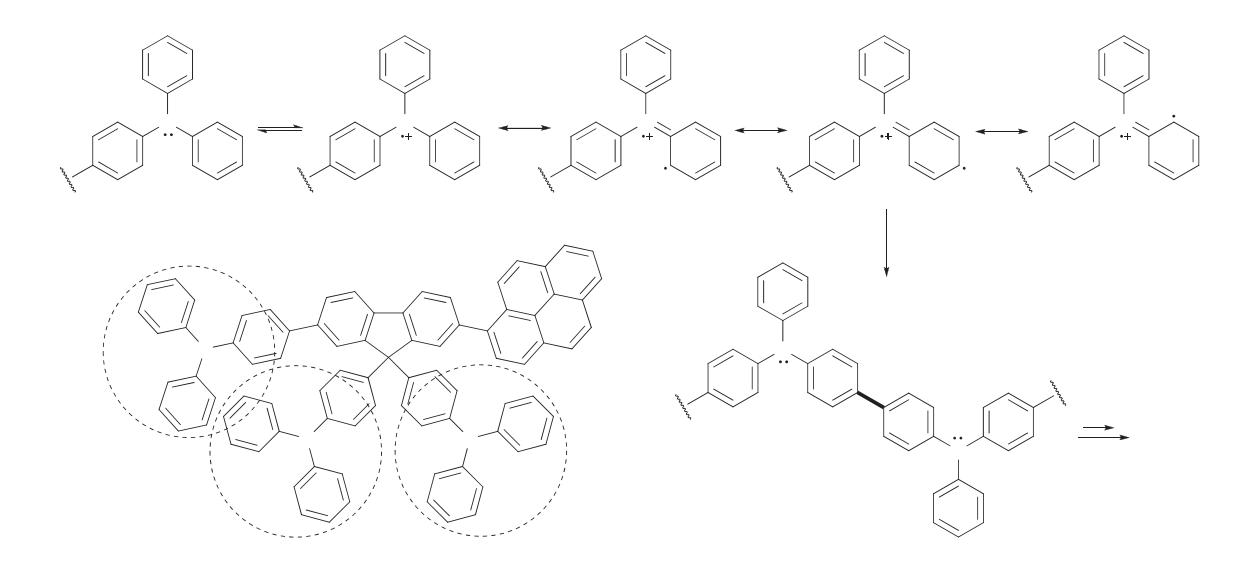


Fig. 5 A proposed oxidation and electrochemical reaction of triphenylamine moiety.

Table 1. Physical data of the synthesized molecules.

Comp.	Solution (nm) ^a		Thin film (nm) ^c		$\Phi_{\scriptscriptstyle F}^{^{\;d}}$	$\rm T_g/T_{5d}$	$E_{1/2}(E_{onset})(V)^{f}$	E_g	E _g cal.	HOMO/LUMO	
•	λ_{abs}	$\lambda_{_{em}}$	Stoke	λ_{abs}	$\boldsymbol{\lambda}_{_{em}}$	-"	(°C) ^e		(eV) ^g	$(eV)^h$	(eV) ⁱ
			shift ^b								
BTTF	303, 363	437	71	310, 375	436	0.43	171/390	0.96 (0.85)	3.06	3.11	-5.29/-2.23
TPTF	303, 373	462	89	310, 380	447	0.64	174/405	0.98, 1.27 (0.87)	3.01	3.04	-5.31/-2.30
BPTF	303, 369	436	66	310, 375	441	0.74	179/472	0.97, 1.13 (0.87)	3.02	3.13	-5.31/-2.28

^aMeasured in CH₂Cl₂ solution; ^bStokes shift calculated from the difference between λ_{max} of the absorption and emission spectra. ^cMeasured on thermal evaporated film on quartz substrate; ^dDetermined in CH₂Cl₂ solutions (A < 0.1) at room temperature using quinine sulfate solution in 0.01 M H₂SO₄ (Φ_F = 0.54) as a standard. ^cObtained from DSC (2nd heating scan) and TGA at heating rate of 10 °C/min; ^fMeasured by CV (Pt counter, glassy carbon working and SCE reference electrodes) in CH₂Cl₂ containing *n*-Bu₄NPF₆ as a supporting electrolyte; ^gEstimated from the optical absorption edge; ^hObtained from quantum chemical calculation using TDDFT/B3LYP/6-31G (d,p). ⁱCalculated by HOMO = -(4.44 + E_{onset}), and LUMO = HOMO- E_g, where E_{onset} is the onset potential of the oxidation peak

2.4 Electroluminescent properties

Owning to their high blue fluorescence ($\Phi_F = 0.43-0.74$) and their HOMO levels (5.30 eV) lying between those of PEDOT:PSS (5.00 eV) and Alq3 (5.80 eV), the new synthesized materials BTTF, TPTF and BPTF could be used as bifunctioned materials namely blue light-emitting and hole-transporting materials. This encouraged us to investigate the use of these compounds as emissive layer (EML) for blue OLED and hole-transporting layer (HTL) for Alq3-based green OLED. The blue light-emitting diodes with the device structure of indium tin oxide (ITO)/PEDOT:PSS/EML(50 nm)/BCP(40 nm)/LiF(0.5 nm):Al(150 nm) and green light-emitting diodes with the device structure of ITO/PEDOT:PSS/HTL(40 nm)/Alq3(50 nm)/LiF(0.5 nm):Al(150 nm) were fabricate. Tris-(8-hydroxyquinoline) aluminum (Alq3) act as the green light-emitting (EML) and electron-transporting layers (ETL). Conductive polymer, poly(3,4ethylenedioxythiophene):poly(4-styrenesulfonate) (PEDOT:PSS), as hole injection layer and 2,9-dimethyl-4,7-diphenyl-1,10-phenanthroline (BCP) as hole blocking layer (HBL) were integrated to enable highperformance devices. From our study and other reports, it was found that the incorporation of PEDOT:PSS in the device as hole injection layer not only increased the maximum luminance from 1236 cd/m² (η of 1.24 cd/A) in device IX to 30760 cd/m² (η of 4.94 cd/A) in device VII, but also significantly decreased the turn-on voltage from 5.9 V to 3.0 V (Table 2). Moreover, their EL spectra were near identical. It has been pointed out that the lower operating voltage of PEDOT:PSS-based device can be attributed to the rough and porous surface of spin-coated PEDOT:PSS polymer layer, which increases the contact area to enhance hole injection and lowers barrier at the organic-organic interface by relocating the barrier to the more conductive PEDOT:PSS layer. To enable high-performance devices therefore PEDOT:PSS as hole injection layer was integrated into all devices. To compare blue light-emitting and hole-transporting abilities of the synthesized materials, N,N'-diphenyl-N,N'-bis(1-naphthyl)-(1,1'-biphenyl)-4,4'-diamine (NPB), a commonly used commercial HTM, was employed as reference EML and HTL materials and the reference devices (IV and VIII) of the same structure were fabricated.

As non-doped blue emitters, under applied voltage, devices I-III emitted a bright blue emission with peaks centered at 427, 437 and 438, respectively (Fig. 6a). The electroluminescence (EL) spectra of all diodes matched with their corresponding PL spectra with the EL of device I being slightly blue shifted (9 nm) from the PL of BTTF. Moreover, no emission shoulder at the longer wavelength owing to excimer and exciplex species formed at the interface of EML and HBL materials, which often occurs in the devices fabricated from EML with planar molecular structure, was detected. In our case, the formation of these species could be prevented by the bulky nature of the 9,9-bis(4-diphenylaminophenyl)fluorene implemented as molecular platform. Additionally, stable emission was obtained from all devices with the EL spectra did not change much over the entire drive voltages. Device I emitted a deep blue (427 nm) light with CIE coordinates of (0.16, 0.08), which is close to the National Television System Committee (NTSC) deep blue (0.14, 0.10) standard. The voltage-luminance and voltage-current density (J-V-L) characteristics of the devices are shown in Fig. 6b-d, and their electrical parameters are summarized in Table 2. The light turn-on voltage at 1 cd/m² for all devices was in the range of 3.3-3.4 V and the operating voltage at 100 cd/m² was in the range of 4.0-5.0 V, indicating good performance is achieved for all the devices. The device characteristics in terms of maximum brightness, turn-on voltage and maximum luminous efficiency clearly verified that the blue-emitting abilities of these newly synthesized materials were greater than NPB-based device (device IV). The results also revealed that BPTF bearing two pyrene rings attached to the fluorene ring of the 9,9-bis(4-diphenylaminophenyl)fluorene had the best EML properties among these three materials. The device (III) showed a high maximum brightness of 6245 cd/m² at 8.8 V, a low turn-on voltage of 3.4 V, a maximum luminous efficiency of 2.06 cd/A and a maximum external quantum efficiency of 0.56%. A reasonably lower device performance was observed from devices I (BTTF as EML) and II (TPTF as EML) displaying a maximum luminous efficiency of 0.83 and 0.88 cd/A, respectively. The trend in device luminous efficiencies matched very well with the observed decrease in PL quantum efficiencies in going from **BPTF** to **TPTF** to **BTTF** (Table 1). Fluorescence quantum yield $(\Phi_{\rm p})$ of **BPTF** was significantly higher than those of **TPTF** and **BTTF**. It has been demonstrated that the efficiency of an OLED depends both on the balance of electrons and holes and the $\Phi_{\rm F}$ of the emitter. Analysis of the band energy diagrams of these diodes also revealed that the HOMO levels of BTTF, TPTF and BPTF (5.28-5.31 eV) sat perfectly between those of the hole injection layer (PEDOT:PSS, 5.00 eV) and HBL (BCP, 6.50 eV), resulting the charge efficiently recombine in the emitting layer and better device performance.

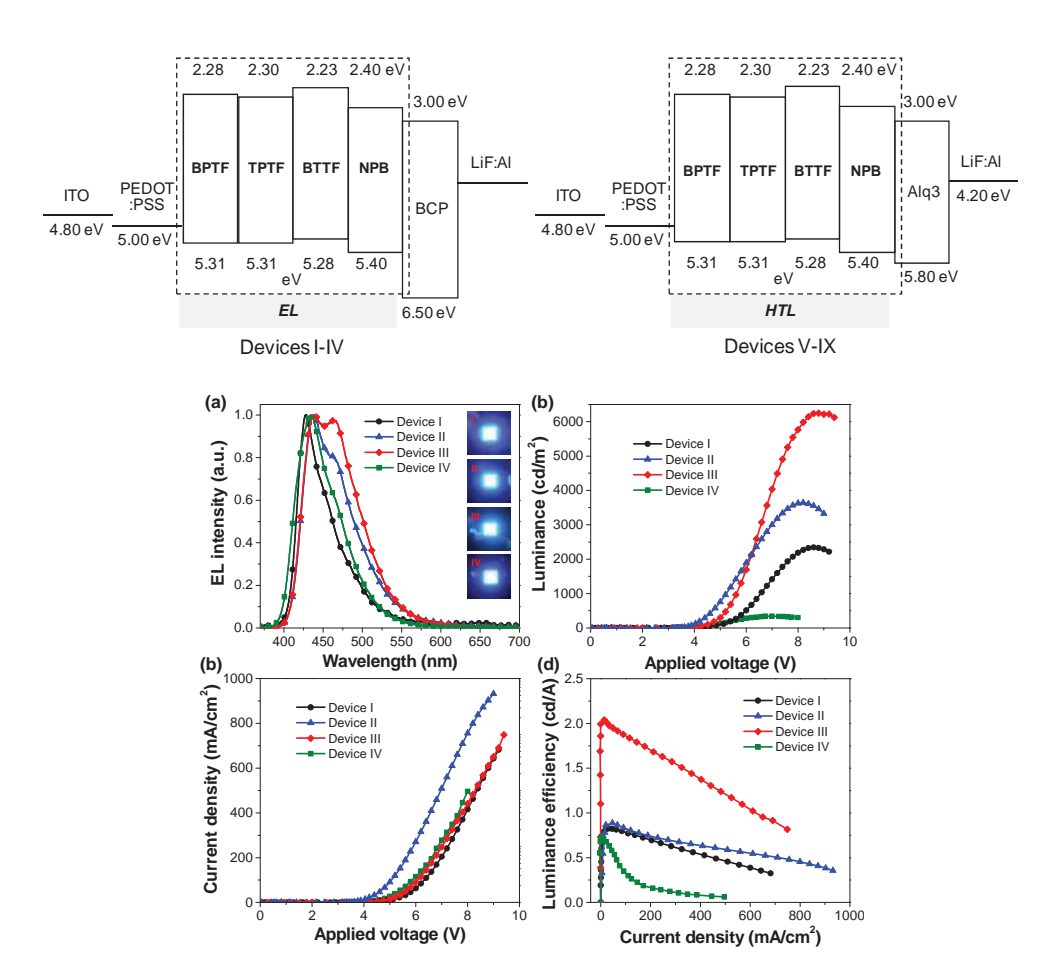


Fig. 6 (a) EL spectra, (b) *V-L* characteristics, (c) *I-V* characteristics, (d) variation of luminance efficiency with current density of the fabricated blue OLED devices using the synthesized materials as EML.

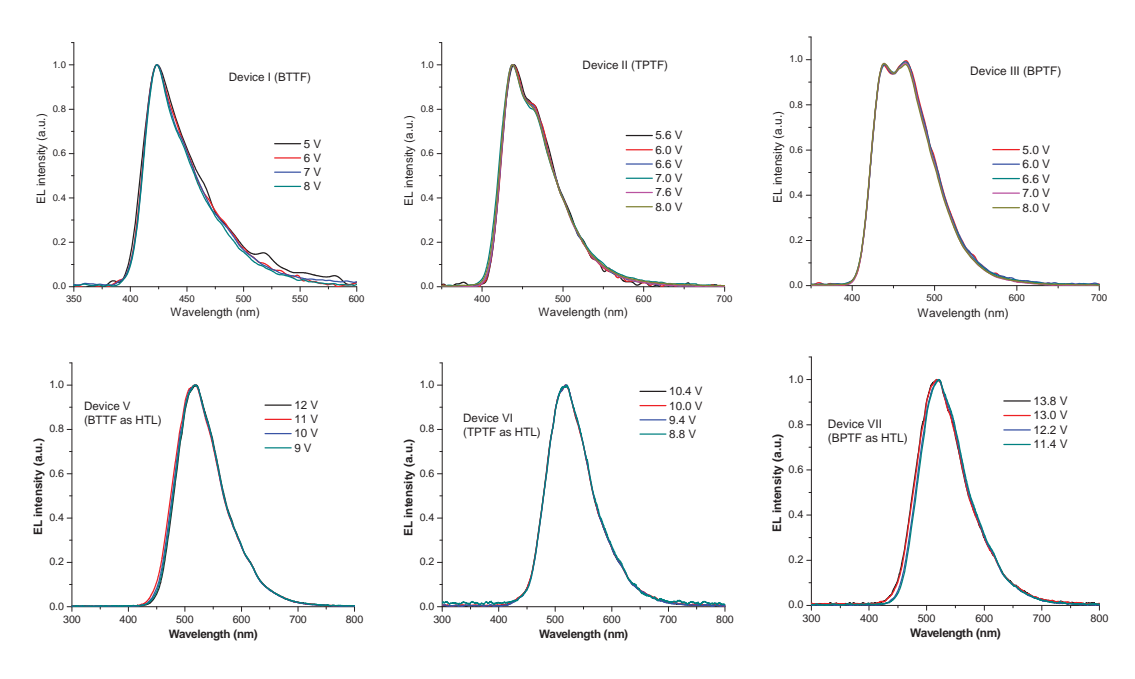


Fig. S3 Normalized EL spectra of OLED devices under different applied voltages.

As HTLs, devices (V-VII) exhibited the light turn-on voltage at 1 cd/m² in the range of 3.0-3.1 V and

the operating voltage at 100 cd/m² in the range of 4.2-4.6 V, indicating good performance is achieved for all the devices (Fig. 7 and Table 2). By comparison with the reference device X, it was found that the incorporation of BTTF, TPTF and BPTF in the device as HTL not only increased the maximum luminance from 4961 cd/m² (η of 0.91 cd/A) to 26375-30760 cd/m² (η of 4.78-4.94 cd/A) in device III, but also significantly decreased the turn-on voltage from 4.2 V to 3.0-3.2 V. Besides, their EL spectra were nearly identical. Moreover, the device characteristics in terms of luminous efficiency clearly demonstrated that the HTM abilities of these materials were greater than NPB-based device (device VIII). Device VII having compound BPTF as HTL exhibited the best performance with a high maximum brightness of 30760 cd/m² for green OLED at 10.6 V, a low turn-on voltage of 3.0 V, a maximum luminous efficiency of 4.94 cd/A and a maximum external quantum efficiency of 0.24%. A comparable device performance was observed from devices V (BTTF as HTL) and VI (TPTF as HTL) (Table 1). Under applied voltage, all devices (V-VII) exhibited a bright green emission with peaks centered at 519 nm and CIE coordinates of (0.29, 0.53) (Fig. 7a). The electroluminescence (EL) spectra of these diodes were identical, and matched with the PL spectrum of Alq3, the EL of the reference devices (VII and X) and also other reported EL spectra of Alq3-based devices. No emission at the longer wavelength owing to exciplex species formed at the interface of HTL and ETL materials, which often occurs in the devices fabricated from HTL with planar molecular structure, was detected. In our case, the formation of exciplex species could be prevented by the bulky nature of the 9,9-bis(4-diphenylaminophenyl)fluorene. From these results and in view of the fact that a barrier for electron-migration at the Alq3/HTL interface (~0.7 eV) is higher than those for holemigration at the HTL/Alq3 interface (~0.5 eV). Hence, under the present device configuration of ITO/PEDOT:PSS/HTL(50 nm)/Alq3(50 nm)/LiF(0.5 nm):Al(200 nm), BTTF, TPTF and BPTF would act only as HTL, and Alq3 would act preferably as an electron blocker more than as a hole blocker and charge recombination thus confined to Alq3 layer. More importantly, a stable emission was obtained from all diodes (V-VII) with the EL spectra and CIE coordinates did not change over the entire applied voltages (Fig. S4, ESI†).

Although, many blue emitting and hole-transporting materials have been reported, in terms of the amorphous morphology, high T_g and device efficiency, **BPTF** is among the good bifunctioned materials reported.

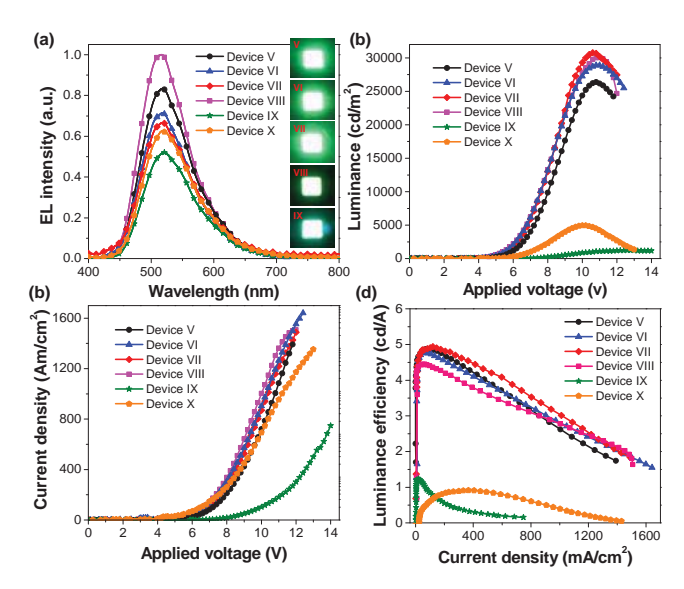


Fig. 7 (a) EL spectra, (b) *V-L* characteristics, (c) *I-V* characteristics, (d) variation of luminance efficiency with current density of the fabricated green OLED devices using the synthesized materials as HTL.

Table 2. Device characteristics of the fabricated OLED devices.

Device	Structure	$V_{ m on}^{a}$	$\lambda_{\text{max}}^{ b}$	$L_{\mathrm{max}}^{}\mathrm{c}}$	$\eta^{^{\scriptscriptstyle d}}$	EQE^{e}	CIE^{f}
I	ITO/PEDOT:PSS/BTTF/BCP/LiF:Al	3.3	427	2340	0.83	0.22	0.16, 0.08
II	ITO/PEDOT;PSS/TPTF/BCP/LiF;A1	3.3	437	3639	0.88	0.29	0.15, 0.12
III	ITO/PEDOT;PSS/BPTF/BCP/LiF;A1	3.4	438	6245	2.06	0.56	0.15, 0.13
IV	ITO/PEDOT:PSS/NPB/BCP/LiF:Al	3.4	436	343	0.73	0.24	0.15, 0.07
V	ITO/PEDOT:PSS/BTTF/Alq3/LiF:Al	3.1	519	28895	4.78	0.23	0.29, 0.53
VI	ITO/PEDOT:PSS/ TPTF /Alq3/LiF;Al	3.2	518	26375	4.88	0.24	0.28, 0.53
VII	ITO/PEDOT:PSS/BPTF/Alq3/LiF;Al	3.0	519	30760	4.94	0.24	0.29, 0.52
VIII	ITO/PEDOT:PSS/NPB/Alq3/LiF:Al	3.1	516	30044	4.45	0.22	0.30, 0.54
IX	ITO/BPTF/Alq3/LiF:Al	5.9	520	1236	1.24	0.06	0.27, 0.53
X	ITO/PEDOT:PSS/Alq3/LiF:Al	4.2	518	4961	0.91	0.05	0.30, 0.54

^aTurn-on voltage (V) at luminance of 1 cd/m²; ^bEmission maximum; ^cMaximum luminance (cd/m²) at the applied voltage (V); ^dLuminance efficiency (cd/A); ^eExternal quantum efficiency (%); ^fCIE coordinates (x, y)

4. Conclusions

In conclusion, we successfully designed and synthesized three bifunctioned materials namely **BTTF**, **TPTF** and **BPTF**. By the use of 9,9-bis(4-diphenylaminophenyl)fluorene as a molecular platform, we were able to reduce the crystallization and maintained high blue emissive ability of pyrene in the solid state, and improve the amorphous stability of these materials. Strong blue emission in both solution and solid state with solution fluorescence quantum efficiency up to 74% was obtained. All of them were thermally stable amorphous materials with glass transition temperature well above 170 °C. Their abilities

as both blue light-emitting materials for blue OLEDs and hole-transporting materials for green OLEDs in terms of device performance and thermal property were greater than a commonly used NPB. Importantly, BPTF having two pyrene rings as terminal substituents showed promising potential as both blue light-emitting and hole-transporting materials for OELD devices. Non-doped blue OLEDs with a maximum luminance efficiency of 2.06 cd/A, and green OLEDs with maximum luminance efficiency of 4.94 cd/A were achieved. The use of this type of molecular platform might be an effective way to prepare high T_g amorphous materials for long-lifetime device applications, especially for high-temperature applications in OLEDs or other organic optoelectronic devices.

5. Experimental Section

5.1 General procedure

¹H and ¹³C nuclear magnetic resonance (NMR) spectra were recorded on a Brüker AVANCE 300 MHz spectrometer with tetramethylsilane as the internal reference using CDCl, as solvent in all cases. Infrared (IR) spectra were measured on a Perkin-Elmer FTIR spectroscopy spectrum RXI spectrometer as potassium bromide (KBr) disc. Ultraviolet-visible (UV-Vis) spectra were recorded as a dilute solution in dichloromethane on a Perkin-Elmer UV Lambda 25 spectrometer. Photoluminescence spectra and the fluorescence quantum yields (Φ_p) were recorded with a Perkin-Elmer LS 50B Luminescence Spectrometer as a dilute solution in dichloromethane and thin film obtained by thermal evaporation. Quinine sulfate solution in 0.01 M H_2SO_4 ($\Phi_F = 0.54$) was used as a reference standard. Differential scanning carolimetry (DSC) analysis and thermogravimetry analysis (TGA) were performed on a METTLER DSC823e thermal analyzer and a Rigaku TG-DTA 8120 thermal analyzer, respectively, with heating rate of 10 °C/min under nitrogen atmosphere. Cyclic voltammetry (CV) measurements were carried out on an Autolab potentiostat PGSTAT 12 with a three electrode system (platinum counter electrode, glassy carbon working electrode and Ag/Ag⁺ reference electrode) at scan rate of 50 mV/s in the presence of tetrabutyl ammonium hexafluorophosphate (n-Bu₄NPF₆) as a supporting electrolyte in dichloromethane under argon atmosphere. Melting points were measured using an Electrothermal IA 9100 series of digital melting point instrument and are uncorrected. High resolution mass spectrometry (HRMS) analysis was performed on Brüker micrOTOF (Q-ToF II) mass spectrometer. Elemental analysis was analyzed on PerkinElmer 2400 Series II CHNS/O Elemental Analyzer at Chulalongkorn University.

5.2 Synthesis

Synthesis of 2,7-Dibromo-9, 9-bis(4-diphenylaminophenyl)fluorene (2)

A mixture of 2, 7-dibromofluorenone (2.57 g, 6.79 mmol), triphenylamine (16.67 g, 67.99 mmol), and methanesulfonic acid (0.45 ml) was heated at 190 °C for 6 h. The cooled mixture was poured into water. The greenish precipitate was filtered, washed with water and dried to afford crude compound 3. Purification by column chromatography using silica gel eluting with a mixture of CH₂Cl₂ and hexane

followed by recrystallized from methanol/CH₂Cl₂ afforded light white solids (3.72 g, 61%); ¹H NMR (300.13 MHz, CDCl₃) δ 6.99 ppm (4H, d, J = 9.01 Hz), 7.00 (8H, t, J = 9.01 Hz), 7.09 (8H, d, J = 9.01 Hz), 7.26 (8H, t, J = 9.01 Hz), 7.55 (4H, t, J = 9.01 Hz), 7.58 (2H, d, J = 9.01 Hz); ¹³C NMR (75 MHz, CDCl₃) δ 64.65 ppm, 121.55, 121.76, 122.77, 123.06, 124.5, 124.68, 128.69, 129.27, 129.38, 130.82, 137.66, 137.98, 146.74, 147.52 and 153.47; HRMS m/z calcd for C₄₉H₃₄Br₂N₂, 808.1089; found, 809.1169 [MH⁺].

2,7,9,9-Tatrakis(4-diphenylaminophenyl)fluorene (BTTF)

A mixture of **2** (1.00 g, 0.55 mmol), triphenylamine-4-boronic acid (0.39 g, 1.35 mmol), Pd(PPh₃)₄ (21 mg, 0.13 mmol) and an aqueous Na₂CO₃ solution (2 M, 10 ml) in THF (15 ml) was degassed with N₂ for 5 min. The mixture was heated at reflux under N₂ atmosphere for 20 h. After the mixture was cooled to room temperature water (50 ml) was added. The mixture was extracted with CH₂Cl₂ (50 ml x 2). The combined organic phase was washed with water (50 ml), brine solution (50 ml), dried over anhydrous Na₂SO₄, filtered, and the solvents were removed to dryness. Purification by column chromatography using silica gel eluting with a mixture of CH₂Cl₂ and hexane followed by recrysatllisation in a mixture of CH₂Cl₂ and methanol afforded white solids (1.09 g, 78%): m.p. 200-201 °C; ¹H NMR (300 MHz, CDCl₃) δ 6.92–7.09 (20H, m), 7.16–7.31 (32H, m), 7.47 (4H, d, J = 8.40 Hz), 7.50 (2H, d, J = 9.01 Hz), 7.61 (2H, s), 7.8 (2H, d, J = 7.8 Hz); ¹³C NMR (75 MHz, CDCl₃) δ 64.68, 120.35, 122.77, 122.99, 123.09, 123.81, 124.45, 126.15, 127.79, 129.00, 129.17, 129.29, 135.24, 138.62, 139.62, 140.01, 146.27, 147.19, 147.65, 147.71, 152.52; IR (KBr disc) 3415, 3031, 1600, 1505, 1250, 1177, 813; Found: C, 89.71; H, 5.34; N, 5.65%; HRMS (m/z) M⁺, 1139.5376. C₈₅H₆₇N₄ requires C, 89.60; H, 5.48; N, 4.92%; M⁺, 1138.4977.

2,7-Bis(pyren-1-yl)-9,9-bis(4-diphenylaminophenyl)fluorene (BPTF)

BPTF was synthesized in the same manner as **BTTF** from **2** and pyrene-1-boronic acid, and obtained as yellow solids (0.56 g, 68%); m.p. >250 °C; ¹H NMR (300 MHz, CDCl₃) δ 6.98 ppm (8H, t, J = 9.01 Hz), 7.07 (8H, d, J = 7.69 Hz), 7.15-7.29 (20H, m), 7.51 (2H, d, J = 8.18 Hz), 7.67 (2H, d, J = 7.85 Hz), 7.77 (2H, s), 7.89–8.00 (2H, m), 8.03–8.06 (2H,m), 8.10 (4H, t J = 7.23 Hz), 8.22 (2H, t, J = 8.10 Hz); ¹³C NMR (75 MHz, CDCl₃) δ 50.50, 120.44, 122.73, 123.45, 124.30, 124.72, 124.80, 124.94, 125.12, 125.18, 125.26, 126.07, 127.44, 127.50, 127.69, 128.48, 128.83, 129.05, 129.21, 130.05, 130.64, 130.97, 131.53, 137.77, 138.96, 140.51, 146.39, 147.73; IR (KBr disc) 3415, 3031, 1589, 1510, 1260, 813; Found: C, 92.32; H, 5.28; N, 2.59%; HRMS (m/z) M⁺, 1052.4506. C₈₁H₅₂N₂ requires C, 92.36; H, 4.98; N, 2.66%; M⁺, 1052.4130.

7-Bromo-2,9,9-tris(4-diphenylaminophenyl)fluorene (3)

3 was synthesized in the same manner **BTTF** from **2** and triphenylamine-4-boronic acid, and obtained as white solids (1.02 g, 72%); m.p. 167-170 °C; ¹H NMR (300 MHz, CDCl₃) δ 6.93 ppm (4H, d, J = 9.01), 7.00 (5H, t, J = 8.10), 7.15-7.07 (19H, m), 7.31–7.21 (12H, m), 7.46 (2H, d, J = 7.8.40), 7.51 (1H, s) 7.58

(1H, s),7.62 (2H, d, J = 5.10), 7.64 (1H, s), 7.77 (1H, d, J = 7.8 Hz); ¹³C NMR (75 MHz, CDCl₃) δ 64.66, 120.45, 120.45, 121.16, 121.42, 122.92, 123.07, 123.70, 124.40, 124.56, 126.25, 127.77, 128.84, 129.22, 129.30, 129.37, 130.66, 137.68, 138.65, 138.87, 140.58, 146.48, 147.60, 152.09, 153.88; IR (KBr disc) 3415, 3030, 1600, 1520, 1256, 1170, 813; Found: C, 82.44; H, 5.31; N, 4.37%; HRMS (m/z) M⁺, 973.3099. $C_{67}H_{48}BrN_3$, requires C, 82.53; H, 4.96; N, 4.31%; M⁺, 973.3032.

7-(Pyren-1-yl)-2,9,9-tris(4-diphenylaminophenyl)fluorene (TPTF)

TPTF was synthesized in the same manner **BTTF** from **3** and pyrene-1-boronic acid, and obtained as light yellow solids (0.48 g, 75%); m.p. 189-199 °C; ¹H NMR (300 MHz, CDCl₃) δ 6.99 ppm (8H, t, J = 6.90 Hz), 7.12 (10H, d, J = 7.00 Hz), 7.29 (24H, m), 7.48 (2H, d, J = 12 Hz), 7.62 (3H, t, J = 12 Hz), 7.68 (1H, s), 7.87–7.95 (3H, m), 7.98–8.03 (2H, m), 8.08 (4H, t, J = 12 Hz); ¹³C NMR (75 MHz, CDCl₃) δ 64.74, 120.24, 120.63, 122.76, 123.30, 124.38, 124.70, 124,77, 124.93, 125.09, 125.15, 125.26, 126.05, 127.45, 127.67, 128.45, 128.70, 129.02, 129.19, 129.91, 130.59, 130.95, 131.51, 137.79, 138,89, 139.68, 140.25, 146.30, 147.69, 152.38; IR (KBr disc) 3415, 3031, 1602, 1504, 1260, 813; Found: C, 91.13; H, 5.36; N, 3.89%; HRMS (m/z) M⁺, 1096.4537. $C_{83}H_{59}N_3$ requires C, 90.93; H, 5.24; N, 3.83; M⁺, 1097.4709.

5.3 Quantum calculation

The ground state geometries of all molecules were fully optimized using density functional theory (DFT) at the B3LYP/6-31G (d,p) level, as implemented in Gaussian 03. TDDFT/B3LYP calculation of lowest excitation energies were performed at the optimized geometries of the ground states.

5.4 Fabrication and characterisation of OLEDs

OLED devices using BTTF, TPTF and BPTF as EML with configuration of ITO/PEDOT:PSS/EML(50 nm)/BCP(40 nm)/LiF(0.5 nm):Al(150 nm) and double-layer green OLED devices using BTTF, TPTF, BPTF and NPB as HTL with configuration of ITO/PEDOT:PSS/HTL(40 nm)/Alq3(50 nm)/LiF(0.5 nm):Al(150 nm) were fabricated and characterized as followed. The patterned indium tin oxide (ITO) glass substrate with a sheet resistance 14 Ω / \square (purchased from Kintec Company) was thoroughly cleaned by successive ultrasonic treatment in detergent, deionised water, isopropanol, and acetone, and then dried at 60 °C in a vacuum oven. A 50 nm thick PEDOT:PSS hole injection layer was spin-coated on top of ITO from a 0.75 wt.% dispersion in water at a spin speed of 3000 rpm for 20 s and dried at 200 °C for 15 min under vacuum. Thin films of each organic EML or HTL were deposited on top of PEDOT:PSS layer by evaporation from resistively heated alumina crucibles at evaporation rate of 0.5-1.0 nm/s in vacuum evaporator deposition (ES280, ANS Technology) under a base pressure of ~10⁻⁵ mbar. The film thickness was monitored and recorded by quartz oscillator thickness meter (TM-350, MAXTEK). A 40 nm thick hole-blocking layer of BCP or a 50 nm thick green-emitting layer of Alq3 was then deposited on the organic EML or HTL, respectively, without breaking the vacuum chamber. The chamber

was vented with dry air to load the cathode materials and pumped back; a 0.5 nm thick LiF and a 150 nm thick aluminium layers were the subsequently deposited through a shadow mask on the top of EML/HTL film without braking vacuum to from an active diode areas of 4 mm². The measurement of device efficiency was performed according to M.E. Thomson's protocol and the device external quantum efficiencies were calculated using procedure reported previously. Current density-voltage-luminescence (*J-V-L*) characteristics were measured simultaneous by the use of a Keithley 2400 source meter and a Newport 1835C power meter equipped with a Newport 818-UV/CM calibrated silicon photodiode. The EL spectra were acquired by an Ocean Optics USB4000 multichannel spectrometer. All the measurements were performed under ambient atmosphere at room temperature.

PART III

Synthesis, Properties and Applications of Biphenyl Functioned 9,9-Bis(4-diphenylaminophenyl)fluorene as Bifunctional Materials for Organic Electroluminescent Devices

1. Introduction

Organic light-emitting diodes (OLEDs) have attracted a great deal of attention due to their potential applications in full-color or large-area flat panel displays, backlight and general illumination. In the past decades, we have seen great progresses in the development of electroluminescent materials with high luminescent efficiency, good thermal/optical stability, excellent charge-carrier injection and transport, and designed film morphology, as well as in the fabrication of high-performance devices. For full-color display applications, blue, green and red materials and devices with high emission efficiency and high color purity are required. The performance of deep-blue OELDs usually inferior to that of green and red OLEDs due to poor carrier injection into the emitters, and hence the electroluminescent (EL) properties of the blue ones need to be improved, particularly in terms of EL efficiencies and color purity. The materials that emit a deep-blue color with excellent Commission International De L'Eclairage (CIE) coordinates of x = 0.14and y = 0.08 for the National Television Standards Committee (NTSC) standard blue need to have excited energies near 3.1 eV. Such deep-blue emitters have high ionization potentials and low electron affinities. Although many blue light-emitting materials based on pyrene, antharcene, fluorenes, aromatic hydrocarbon and triarylamine derivatives have been reported, EL efficiencies of these deep-blue OLEDs (CIE coordinates of x = 0.15 and y = 0.10) are rather poorer compared to those of sky-blue OLEDs (CIE coordinates of x = 0.15 and y > 0.15). Therefore, searching for new efficient deep-blue fluorescent materials with high performance remains one of the major challenges and is still required.

Among the blue emitters, fluorenes, spirofluorenes, oligomeric fluorenes, polyfluorenes (PFs) and their derivatives have been intensively investigated and are regarded as the most promising candidates for blue OLEDs. However, these materials as potential candidates for deep-blue OLEDs still have a number of deficiencies including low color purity due to unwanted emission at longer wavelengths from the aggregates, excimers and fluorenone defects, and inefficient hole-injection that requires the use of hole-transporting layers to obtain a balance in charge carriers leading to a complex device structure. The hole-injection ability of these fluorene derivatives has been successfully improved by many approaches such as blending with hole-transporting triarylamines, end-capping the polymer chain with triarylamines,

copolymerization with triarylamine-containing monomers and substitutions at the C-9 position of the fluorene block with triarylamines. The latter approach was proven to be more effective and less complex synthesis required. For example, 9,9-bis(4-diphenylaminophenyl)fluorene (9,9-bis(triphenylmine) fluorene) has been successfully used as a building block for the synthesis of many blue emitting PFs and derivatives with improving hole-injection and suppressing aggregation. Hence, using this fluorene building block to construct new molecular materials might be a simple solution to develop efficient deep-blue emitters. Therefore, we herein implemented all required aspects in the synthesized molecules (Scheme. 1). The use of 9,9-bis(4-diphenylaminophenyl)fluorene as a molecular framework offers a perfect bulky molecule with high thermal stability and an improved hole injection and transport ability from the pendent triphenylamine units. The presence of such bulky groups at C-9 position of the framework would also suppress the aggregation phenomena and reduce the excimer formation resulting in a stable blue emission. Incorporation of biphenyl moiety into cruciform of this platform is to assure high deep-blue emissive ability. Fluorene and biphenyl have a number of advantages, including its capability to emit in the blue part of the visible spectrum, chemical and photochemical stability. The high steric hindrance in the molecule also offers good solubility and thereby thermally stable amorphous thin film could be deposited by cheap solution process. Accordingly, this would result in new bifunctioned materials with combined blue emitting and hole-transporting properties. An investigation of their physical and photophysical properties, and blue OLED fabrication and characterization are also reported. One of these materials, namely BPTF having two biphenyl substituents, showed great potential as bifunctioned materials. Using this molecule as active layers, efficient, and bright non-doped deep-blue and Alq3-based green OLEDs with maximum luminance efficiencies and CIE coordinates of 2.48 cd A^{-1} and x = 0.15 and y = 0.07, and 4.40 cd A^{-1} and x = 0.15 and y = 0.07, and 4.40 cd A^{-1} and x = 0.15 and y = 0.07, and 4.40 cd A^{-1} and x = 0.15 and y = 0.07, and 4.40 cd A^{-1} and x = 0.15 and y = 0.07, and 4.40 cd A^{-1} and x = 0.15 and y = 0.07, and 4.40 cd A^{-1} and x = 0.15 and y = 0.07, and 4.40 cd A^{-1} and x = 0.15 and y = 0.07, and 4.40 cd A^{-1} and x = 0.15 and y = 0.07, and 4.40 cd A^{-1} and x = 0.15 and y = 0.07, and 4.40 cd A^{-1} and x = 0.15 and y = 0.07, and 4.40 cd A^{-1} and x = 0.15 and y = 0.07, and 4.40 cd A^{-1} and x = 0.15 and y = 0.07, and 4.40 cd A^{-1} and x = 0.15 and y = 0.07, and 4.40 cd A^{-1} and x = 0.15 and y = 0.07, and 4.40 cd A^{-1} and x = 0.15 and y = 0.07, and 4.40 cd A^{-1} and x = 0.15 and y = 0.07, and 4.40 cd A^{-1} and x = 0.15 and y = 0.07, and 4.40 cd A^{-1} and x = 0.07 and 4.40 cd A^{-1} and x = 0.07 and 4.40 cd A^{-1} and 4.40 cd A^{-1} = 0.28 and y = 0.52 were achieved, respectively. Both devices showed low turn-on voltages of 3.1 and 2.8 V, respectively.

2. Results and Discussion

The designed molecules were synthesized as outlined in Scheme 1. Firstly, a 9,9-bis(4-diphenylaminophenyl)fluorene (2) intermediate was synthesized via a tandem protocol of ready obtained 2,7-dibrofluorenone (1) with an excess of triphenylamine catalyzed by CH₃SO₃H at 190 °C. Coupling of 2 with available 4-biphenylboronic acid and 4-biphenylvinylboronic acid under Suzuki cross-coupling reaction catalyzed by Pd(PPh₃)₄ afforded BPTF and BPVTF as white solids in good yields of 90% and 70%, respectively, while coupling of 2 with 4-carbazol-9-ylbiphenyldioxaborolanes 3 and 4 under the same conditions gave CBPTF and CMBPTF in good yields as white and yellow solids, respectively. The borolane 3 was prepared from an Ullmann coupling of 4,4'-dibromobiphenyl (7) with carbazole followed by treatment of the resultant compound 8 with *n*-BuLi lithiation and trapping the anion formed with 2-isopropoxy-4,4,5,5-tetramethyl 1,3,2-dioxaborolane. Suzuki cross-coupling of 5-bromo-2-iodotoluene (9)

with boronic acid **10** followed by treatment of the resultant compound **11** with *n*-BuLi/2-isopropoxy-4,4,5,5-tetramethyl-1,3,2-dioxaborolane afforded the borolane **4** in 71% yield. The chemical structures and purities of these materials were characterized unambiguously with NMR spectroscopy, mass spectrometry and elemental analysis. They showed good solubility in organic solvents, opening the door to solution processing techniques

Scheme 1. Synthesis of the target molecules: i) triphenylamine, MeSO₃H, 190 °C; ii) Pd(PPh₃)₄, 2M Na₂CO₃, THF, heat; iii) carbazole, CuI, K₃PO₄, *trans*-1,2-diaminocyclohexane, toluene; iv) *n*-BuLi, THF, -78 °C then 2-isopropoxy-4,4,5,5-tetramethyl-1,3,2-dioxaborolane, -78 °C to rt and acidic work up.

To understand the electronic properties and the geometries of the synthesized molecules, quantum chemical calculations were performed using TDDFT/B3LYP/6-31G (d,p) method. The optimized structures of these compounds revealed that both triphenylamine moieties at the C-9 position of the fluorene ring generated a highly steric hindrance, resulting a bulky molecular structure and thereby preventing a closed π - π stacking interaction of the molecule. In the higher occupied molecular orbitals (HOMO) of BPTF, CBPTF, CMBPTF and BPVTF, π -electrons localized on triphenylamine pendant groups, while in their lowest unoccupied molecular orbitals (LUMO), the accited electrons delocalized over the quinoid-like fluorene-biphenyl plane. The HOMO-LUMO energy gaps (E_g cal.) were calculated to be in the range of 3.06-3.49 eV. These values were slightly higher than those estimated from the optical absorption edge (E_g) (Table 1). There are factors responsible for the errors because the orbital energy

difference between HOMO and LUMO is still an approximate estimation to the transition energy since the transition energy also contains significant contributions from some two-electron integrals. The real situation is that an accurate description of the lowest singlet excited state requires a linear combination of a number of excited configurations.

Table HOMO, LUMO and HOMO-LUMO energy gap for dyes in CH₂Cl₂ calculated by B3LYP/6-31G(d,p) using C-PCM model. Energies are in eV.

Compd	номо	LUMO	$\Delta m E_{ m HOMO-LUMO}$ (E $_{ m g}$ cal.)
Сотра	eV	eV	eV
BPTF	-5.03	-1.56	3.47
CBTF	-5.04	-1.65	3.39
CMBTF	-5.03	-1.55	3.49
BVTF	-5.03	-1.97	3.06

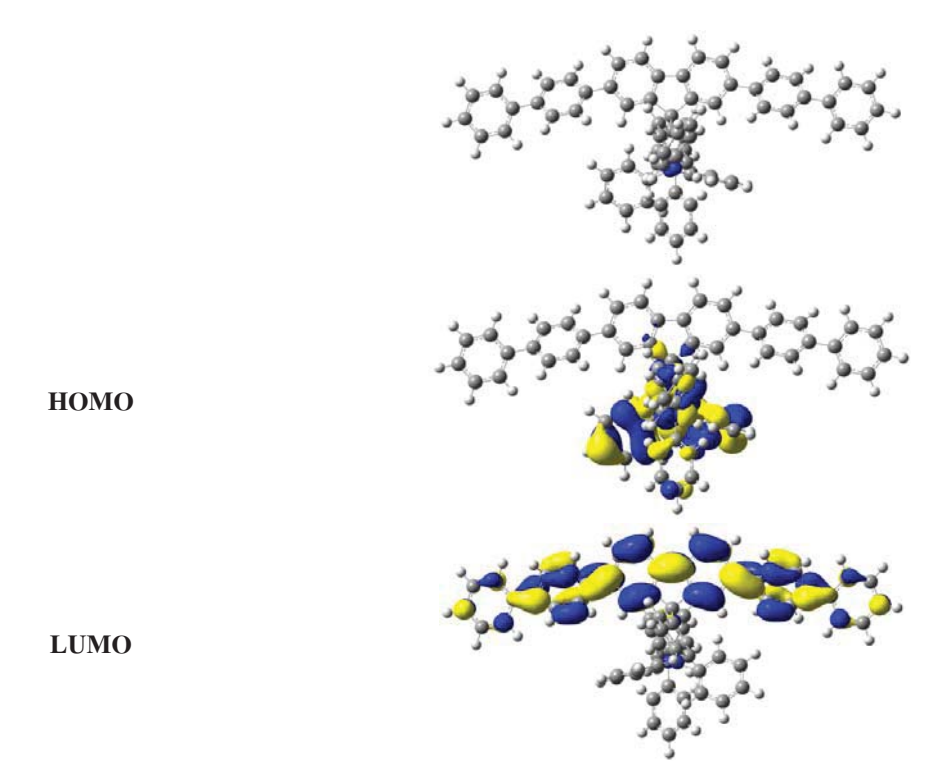
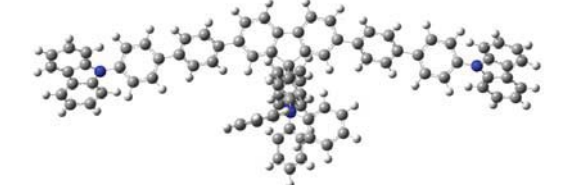


Fig. S1 Optimized structure, HOMO, and LUMO of BPTF calculated by B3LYP/6-31G(d,p).



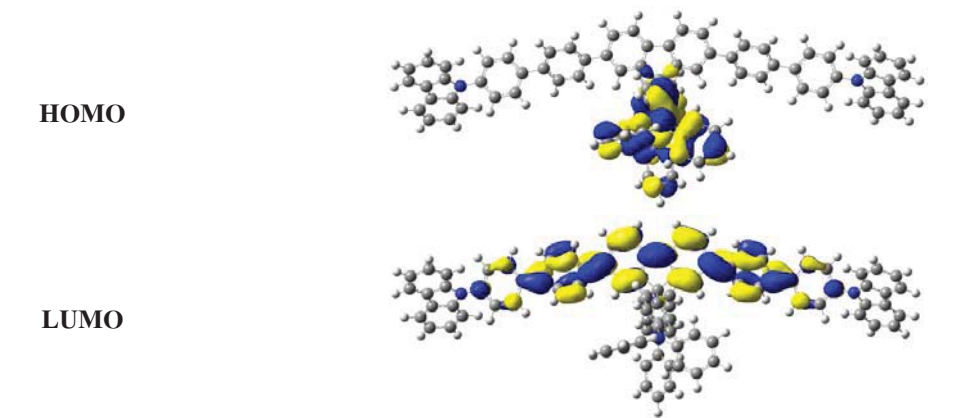


Fig. S2 Optimized structure, HOMO, and LUMO of CBTF calculated by B3LYP/6-31G(d,p).

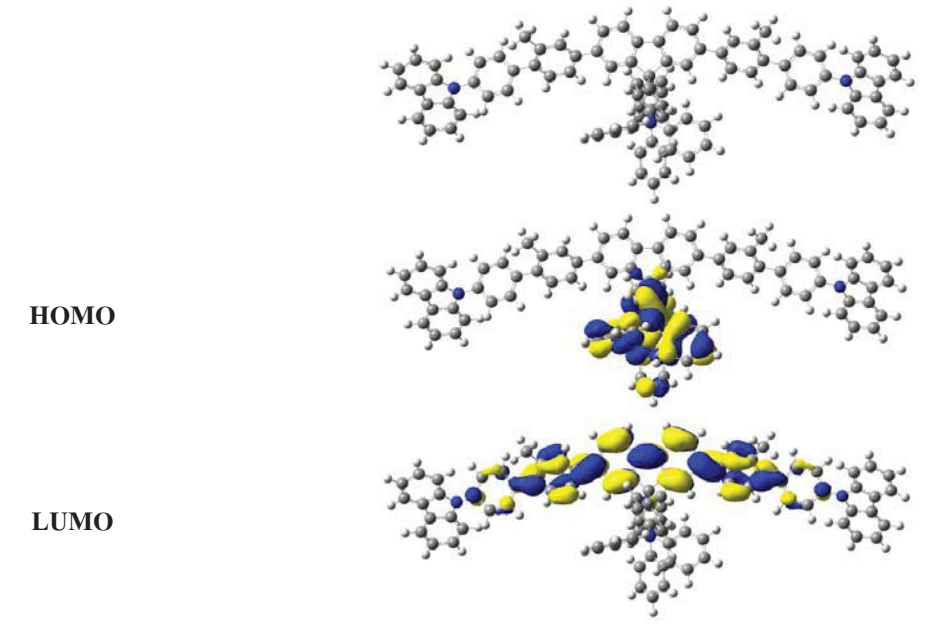
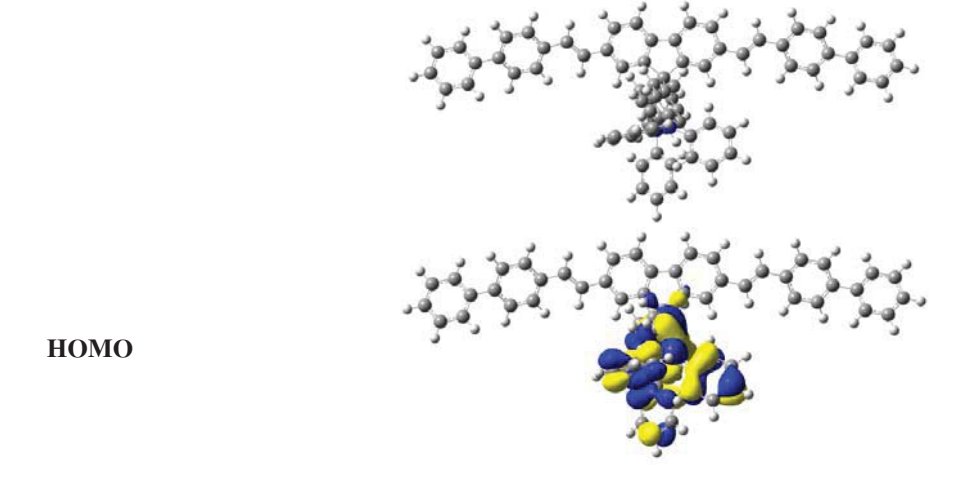


Fig. S3 Optimized structure, HOMO, and LUMO of CMBTF calculated by B3LYP/6-31G(d,p).



LUMO

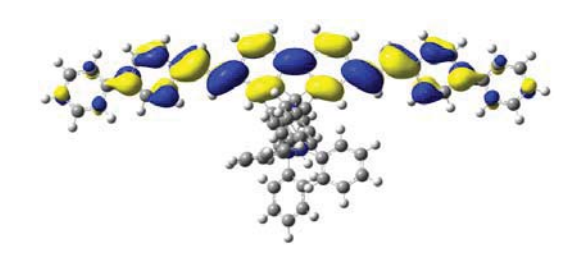


Fig. S4 Optimized structure, HOMO, and LUMO of BVTF calculated by B3LYP/6-31G(d,p).

The optical properties of BPTF, CBPTF, CMBPTF and BPVTF were investigated in dilute CH2Cl2 solution and thin film obtained by thermal evaporation on a quart substrate (Figure 3, Table 1). Their solution absorption spectra showed two absorption bands: absorption band at ~300 nm assigning to the $\pi - \pi^*$ local electron transition of the pendant triphenylamine moieties and strong absorption band at longer wavelengths (327-395 nm) corresponding to the π - π * electron transition of the fluorene-biphenyl conjugated backbone. The latter absorption band of CBPTF was red-shifted comparison to that of BPTF due to the π -electrons in the ground sate are able to delocalize over the fluorene-biphenyl backbone and carbazole through the lone electron pair of the N-atom of the carbazole. Though, such absorption band of CMBPTF was nearly identical and blue shifted to those of BPTF and CBPTF, respectively. This is due to a methyl substituent of the biphenyl moiety in CMBPTF restricted a free rotation of such unit limiting an interaction between fluorene-biphenyl and carbazole moieties. However, BPVTF possessed more extended π-conjugation backbone due to the presence of vinyl bond in between fluorene and biphenyl units as observed in the DFT calculation and its absorption spectrum was further red-shifted. In solid state, the similar absorption features with a slight red shift compared to their corresponding solution spectra were observed. These materials exhibited a strong emission intensity and deep-blue emission in both solution and solid state. Their fluorescence quantum yields (Φ_v) measured in CH₂Cl₂ solution using quinine sulfate solution in 0.01 M H_3SO_4 ($\Phi_F = 0.54$) ranged from 0.20 to 0.49. The solution photoluminescence (PL) spectra of BPTF, CBPTF and CMBPTF showed a featureless emission peak in the blue region (448-454 nm), while the spectrum of **BPVTF** exhibited two emission peaks at 459 and 482 nm. The thin film PL emission spectra of these materials appeared at the same region to their solution PL spectra, hence indicating no or less if any solid state packing occurred in this case due to their bulky molecular structures. These materials showed small stoke Shifts (61-100 nm) suggesting less energy loss during the relaxation process and thereby ensuing efficient fluorescence.

Table 1. Physical and photophysical properties of the synthesized molecules.

compd	thin film (nm) ^[a]		- Ф ^[b]	$T_g/T_c/T_m/T_{5d}(^{\circ}C)^{[c]}$ -	E _{1/2} vs SCE	\mathbf{E}_{g}	E _g cal.	HOMO/LUMO	
	λ_{abs}	$\lambda_{_{\rm em}}$	$-\Phi_{ m F}$	$I_g/I_c/I_m/I_{5d}(C)$	E^{10}, E^{20}, E^{30}	E_{pc}	$(eV)^{[e]}$	$(eV)^{[f]}$	$(eV)^{[g]}$
BPTF	327	426	0.35	166/ - / - /456	0.98, 1.51	0.73	3.31	3.47	-5.32/-2.01
CBPTF	346	438	0.24	207/324/359/487	0.98, 1.23	0.74, 0.83	3.19	3.39	-5.32/-2.13

CMBPTF	327	408, 426	0.20	192/270/320/343	0.98, 1.30	0.74, 0.81	3.26	3.49	-5.33/-2.07
BPVTF	395	446, 467	0.49	164/246/320/330	0.96, 1.22, 1.37	-	2.88	3.06	-5.29/-2.91

^[a]Measured as thin film obtained by thermal evaporation. ^[b]Determined in CH_2Cl_2 solutions. ^[c]Obtained from DSC and TGA measurements. ^[d]Obtained from CV and DPV at a scan rate of 50 mV/s. ^[e]Estimated from the optical absorption edge; ^[f]Obtained from quantum calculation using TDDFT/B3LYP/6-31G (d,p). ^[g]Calculated by HOMO = -(4.44 + E_{onset}), and LUMO = HOMO- E_g , where E_{onset} is the onset potential of the oxidation.

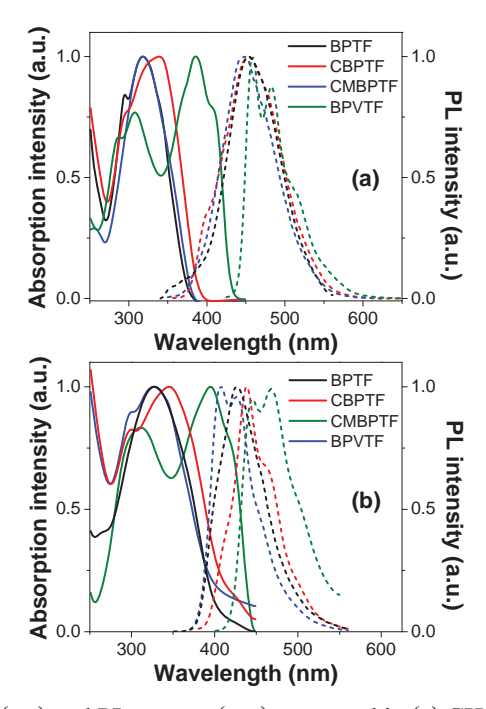


Figure 1. UV-vis absorption (—) and PL spectra (----) measured in (a) CH₂Cl₂ solution and (b) thin film obtained by thermal deposition on quart substrate.

For OLED applications, thermal stability of organic materials is crucial for device stability and lifetime. The thermal instability or low glass transition temperature (T_g) of the amorphous organic layer may result in the degradation of organic devices due to morphological changes. The thermal properties of **BPTF**, **CBPTF**, **CMBPTF** and **BPVTF** were investigated by the thermogravimetric analysis (TGA) and differential scanning calorimetry (DSC) (Table 1). Those results suggested that all compounds were thermally stable materials with 5% weight loss temperatures (T_{5d}) well over 330 °C. DSC thermograms of all compounds displayed baseline shift due to glass transition temperatures (T_g) ranged from 166 to 207 °C. These results indicated that these materials were stable amorphous materials with high T_g which was higher than those of the commonly used HTMs such as N,N'-diphenyl-N,N'-bis(1-naphthyl)-(1,1'-biphenyl)-4,4'-diamine (NPB) ($T_g = 100$ °C) and N,N'-bis(3-methylphenyl)-N,N'-bis(phenyl)benzidine (TPD) ($T_g = 63$ °C), and other triphenylamine derivatives. The results proved that the use of 9,9-bis(4-diphenylaminophenyl)fluorene as a molecular platform could improve the amorphous stability of the

materials, which in turn could increase the service time in device operation and enhance the morphological stability to the thin film. Moreover, the abilities of these materials to form molecular glass and dissolve in organic solvents offers the possibility to prepare good thin films by both thermal evaporation and solution casting techniques which are highly desirable for fabrication of OLED devices.

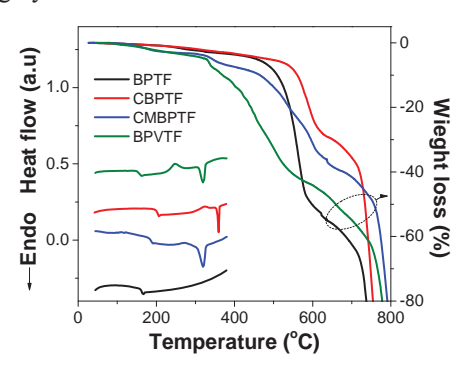


Fig. S5 DSC (2nd heating scan) and TGA thermograms measured under N₂ at heating rate of 10 °C/min

Electrochemical behaviors of all compounds were investigated by cyclic voltammetry (CV) (Figure 2, Table 1). In all cases, the first quasi-reversible oxidation wave appeared at nearly the same position (0.96-0.98 V) and assigned to the removal of electrons from the triphenylamines and carbazoles resulting radical cations, while the rest oxidation waves denoted to the removal of electrons from the fluorene-biphenyl backbones. CV curves of BPTF, CBPTF and CMBPTF showed additional peaks at lower potential on the cathodic scan (E_{pc}) at 0.73 V and 0.83V which corresponded to electrochemical coupling reactions of the triphenylamine and carbazole radical cations, respectively. The repeated CV scans of these compounds also revealed an increasing change in their CV curves, demonstrating a series of electrochemical reactions led to electro-polymerization of those radical cation species taking place on the glassy carbon electrode surface. The multiple CV scans of BPVTF revealed a weakly change in CV curves, indicating a weak oxidative coupling of the pendent triphenylamines and among the synthesized materials, BPVTF is relative more electrochemically stable molecule. Usually, this type of electrochemical coupling reaction is detected in most triphenylamine and carbazole derivatives with unsubstituted p-position of the phenyl ring and unsubstituted 3,6-positions such as in case of 2,7-bis[2-(4-diphenylaminophenyl)-1,3,4-oxadiazol-5yl]-9,9-bis-n-hexylfluorene. A proposed oxidation and electrochemical coupling reaction of these materials is outlined in Figure 3. During the first oxidation, the electrons are removed from N-atom of both triphenylamine and carbazole moieties to give radical cations form A which undergoes electron delocalization to get resonance forms B, C and D, respectively. These radical cations are highly reactive species and readily undergo dimerization coupling to stable neutral molecule. Resonance forms A, B and D having a radical on N atom, ortho-C atoms, respectively, are less reactive to a dimerization coupling reaction due to high steric hindrance and thereby this electrochemical reaction would take place through the resonance form C. However, triphenylamine units of BPVTF are faintly to undergo such

electrochemical reaction due to steric hindrance from the adjacent 4-biphenylvinyl moiety keep them away from each other to prevent the coupling. However, this type of electrochemical reaction will become inactive in non-diffusion system or solid state. Moreover, under these CV experiment conditions, no distinct reduction process was observed in all cases. The HOMO and LUMO energy levels of **BPTF**, **CBPTF**, **CMBPTF** and **BPVTF** were calculated from the oxidation onset potentials (E_{onset}) and energy gaps (E_g) and the results are summarized in Table 1. The HOMO levels of these materials ranged from 5.29 to 5.33 eV matching well with the work functions of the gold (Au) or indium tin oxide (ITO) electrodes and hence favouring the injection and transport of holes.

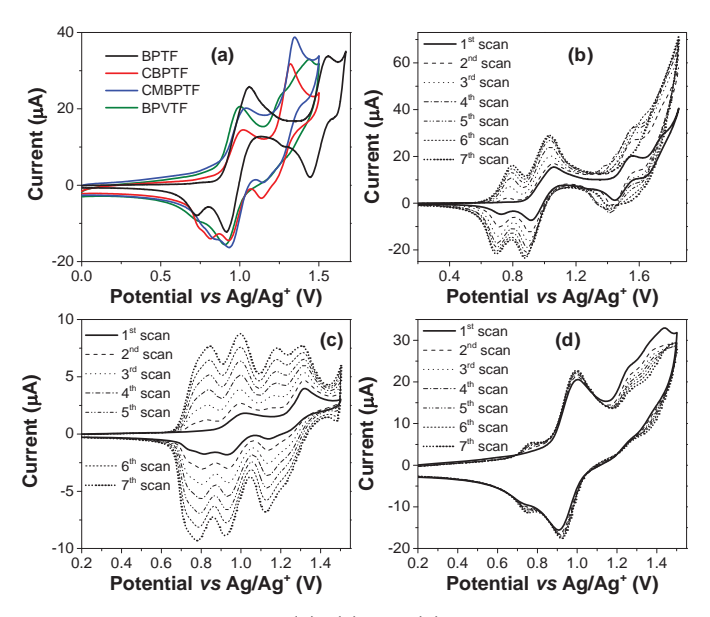


Figure 2. (a) CV curves of all materials, and (b), (c) and (d) multiple CV scans of **BPTF**, **CBPTF** and **BPVTF**, respectively, measured in CH₂Cl₂ at a scan rate of 50 mV/s.

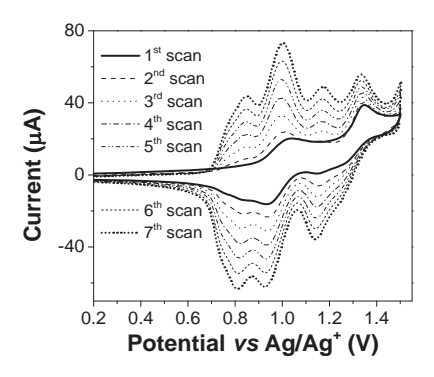


Fig. S6 Multiple CV scans of CMBPTF measured in CH₂Cl₂ at a scan rate of 50 mV/s.

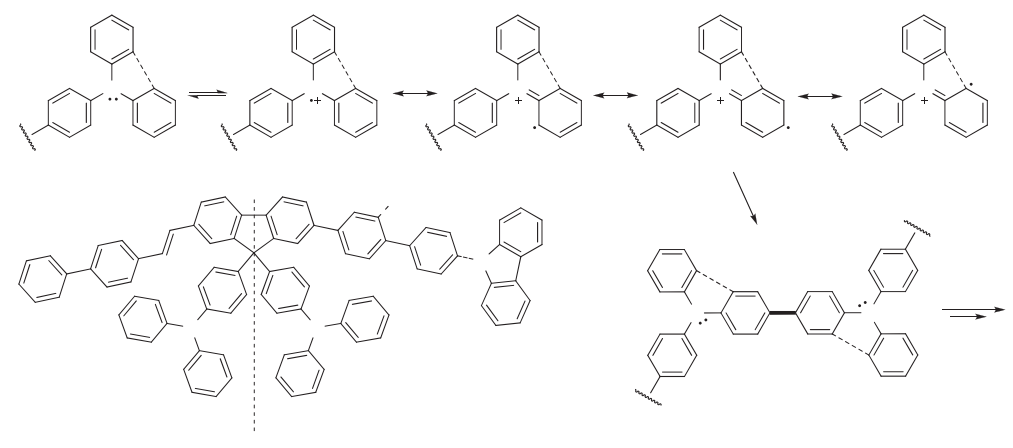


Figure 3. A proposed oxidation and electrochemical reaction of triphenylamine and carbazole moieties.

Ν

BPVTF

high steric TPA (more stable radical cation)

Owning to their high blue fluorescence and their HOMO levels (5.3 eV) lying between those of PEDOT:PSS (5.00 eV) and Alq3 (5.80 eV), the new synthesized materials BPTF, CBPTF, CMBPTF and BPVTF could be used as bifunctioned materials namely blue light-emitting and hole-transporting materials. This encouraged us to investigate the use of these compounds as emissive layer (EML) for blue OLED and hole-transporting layer (HTL) for Alq3-based green OLED. The blue light-emitting diodes with the device structure of indium tin oxide (ITO)/PEDOT:PSS/EML(50 nm)/BCP(40 nm)/LiF(0.5 nm):Al(150 nm) and green light-emitting diodes with the device structure of ITO/PEDOT:PSS/HTL(40 nm)/Alq3(50 nm)/LiF(0.5 nm):Al(150 nm) were fabricated. Tris-(8-hydroxyquinoline) aluminum (Alq3) act as the green light-emitting (EML) and electron-transporting layers (ETL). Conductive polymer, poly(3,4-ethylenedioxythiophene):poly(4-styrenesulfonate) (PEDOT:PSS), as hole injection layer and 2,9dimethyl-4,7-diphenyl-1,10-phenanthroline (BCP) as hole blocking layer (HBL) were integrated to enable high-performance devices. From our study and other reports, it was found that the incorporation of PEDOT:PSS in the device as hole injection layer not only increased the maximum luminance from 6127 cd m⁻² (η of 1.29 cd A⁻¹) in device XI to 26067 cd m⁻² (η of 4.40 cd A⁻¹) in device VI, but also significantly decreased the turn-on voltage from 5.8 V to 2.8 V (Table 2). Moreover, their EL spectra were almost identical. It has been pointed out that the lower operating voltage of PEDOT:PSS-based device can be attributed to the rough and porous surface of spin-coated PEDOT:PSS polymer layer, which increases the contact area to enhance hole injection and lowers barrier at the organic-organic interface by relocating the barrier to the more conductive PEDOT:PSS layer. To enable high-performance devices therefore PEDOT:PSS as hole injection layer was integrated into all devices. To compare blue light-emitting and hole-transporting abilities of the synthesized materials, NPB, a commonly used commercial HTM, was employed as reference EML and HTL materials and the reference devices (V and X) of the same structure were fabricated.

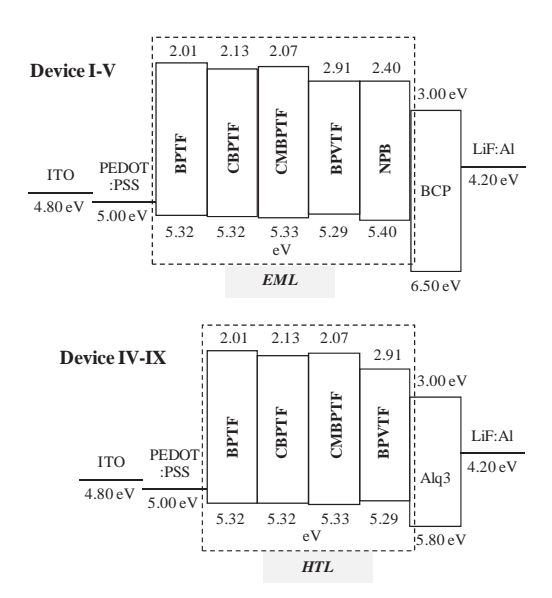


Fig. S7 (a) A schematic of the energy band diagram of the devices

As non-doped blue emitters, under applied voltage, devices I-III emitted bright deep-blue light with a maximum peaks centered at 420, 419 and 428, respectively, while device IV emitted a sky blue light with peak centered at 467 nm (Figure 4a). The electroluminescence (EL) spectra of all diodes matched with their corresponding PL spectra. No emission shoulder at the longer wavelength owing to excimer and exciplex species formed at the interface of EML and HBL materials, which often occurs in the devices fabricated from EML with planar molecular structure, was detected in EL spectra of devices I-III. EL spectrum of device IV having BPVTF as EML displayed emission shoulder corresponding to excimer and exciplex emissions. The former might arise from the ladder type aggregate of the planar 2,7-bis(4-(biphenyl-4-yl)vinyl)fluorene moiety. The latter is often observed at the interface of organic/organic layers in an OLED and can be tuned by adjusting the thickness of those layers. In devices I-III, the formation of these species could be prevented by the bulky nature of the 9,9-bis(4-diphenylaminophenyl)fluorene implemented as molecular platform and the non-planar nature of the biphenyl-fluorene backbone. Additionally, stable emission was obtained from all devices with the EL spectra did not change much over the entire driven voltages (Supporting information).

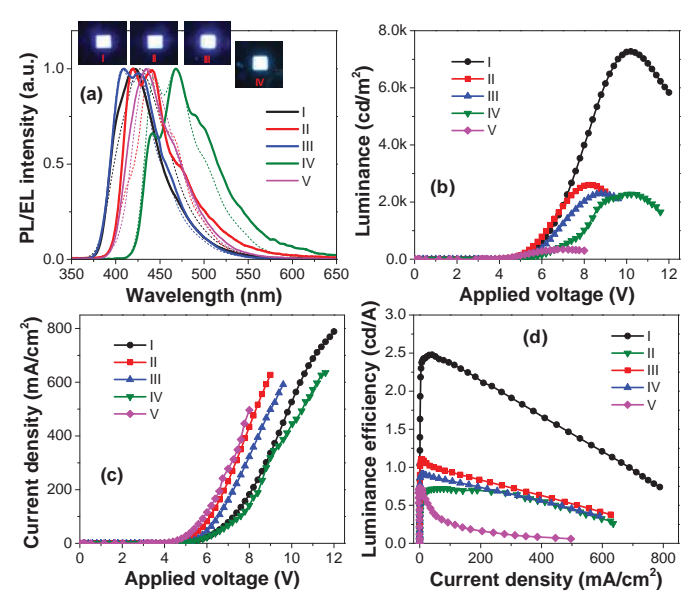


Figure 4. (a) PL (—) and EL (----) spectra, (b) *V-L* characteristics, (c) *I-V* characteristics, (d) variation of luminance efficiency with current density of the fabricated blue OLED devices using the synthesized materials as EML.

The current density-voltage-luminance (*I-V-L*) characteristics of the devices are shown in Figure 4b-d, and their electrical parameters are summarized in Table 2. The light turn-on voltage at 1 cd m⁻² for all devices was in the range of 3.1-3.5 V and the operating voltage at 100 cd m⁻² was in the range of 4.9-5.7 V, indicating good performance is achieved for all the devices. The device characteristics in terms of maximum brightness, turn-on voltage and maximum luminous efficiency clearly verified that the blue-

emitting abilities of these newly synthesized materials were greater than NPB-based blue device (device V). The results also revealed that **BPTF** bearing two biphenyl moieties attached to the 2,7-positions of the 9,9-bis(4-diphenylaminophenyl)fluorene framework had the best EML properties among these four materials in terms of both device performance and purity of emission color. The device I showed a high maximum brightness of 7277 cd m⁻² at 10.2 V, a maximum luminous efficiency of 2.48 cd A⁻¹, a maximum external quantum efficiency of 0.35% and a low turn-on voltage of 3.1 V, which is considered to be one of the lowest turn-on voltage for deep-blue OLED. This device also emitted intense deep-blue color (420 nm) with CIE coordinates of x = 0.15 and y = 0.07), which is close to the National Television System Committee (NTSC) deep-blue (CIE coordinates of x = 0.14 and y = 0.08) standard. A reasonably lower device performance was observed from devices II (CBPTF as EML) and III (CMBPTF as EML) displaying a maximum luminous efficiency of 1.06 and 0.93 cd A⁻¹, respectively. The trend in device luminous efficiencies of devices I-III matched very well with the observed decrease in PL quantum efficiencies of the EML in going from BPTF to CBPTF to CMBPTF (Table 1). Fluorescence quantum yield $(\Phi_{\rm p})$ of **BPVTF** was higher than **BPTF** and also significantly higher than those of **CBPTF** and CMBPTF. However, the emission efficiency of device V having BPVTF as EML was relatively low among these four EMLs. It has been demonstrated that the efficiency of an OLED depends both on the balance of electrons and holes and the $\Phi_{\scriptscriptstyle F}$ of the emitter. Analysis of the band energy diagrams of these diodes also revealed that the HOMO levels of BPTF, CBPTF, CMBPTF and BPVTF (5.29-5.33 eV) sat perfectly between those of the hole injection layer (PEDOT:PSS, 5.00 eV) and HBL (BCP, 6.50 eV), resulting the charge efficiently recombine in the emitting layer and better device performance (Supporting information). The reason for the device IV's poor performance might come from the presence of excimer and exciplex emission at longer wavelength side in the EL spectrum. The excimer formation has also been found on polyfluorenes (PFs).

Table 2. Device characteristics of OLEDs.

device	structure	$V_{\mathrm{on}}^{[a]}$	$V_{100}^{[b]}$	$\lambda_{\text{max}}^{ [c]}$	$L_{\rm max}^{ [\rm d]}$	$I^{[\mathrm{e}]}$	$\eta^{\rm [f]}$	EQE ^[g]	CIE ^[h]
I	ITO/PEDOT:PSS/BPTF/BCP/LiF;Al	3.1	4.9	420	7277	564	2.48	0.35	0.15, 0.07
II	ITO/PEDOT:PSS/CBPTF/BCP/LiF:Al	3.3	4.9	419	2603	476	1.06	0.35	0.16, 0.10
III	ITO/PEDOT:PSS/CMBPTF/BCP/LiF:Al	3.5	5.3	428	2230	467	0.91	0.30	0.16, 0.04
IV	ITO/PEDOT:PSS/BPVTF/BCP//LiF;Al	3.4	5.7	467	2248	411	0.72	0.12	0.17, 0.23
V	ITO/PEDOT:PSS/NPB/BCP/LiF:A1	3.4	5.5	436	343	241	0.73	0.24	0.15, 0.07
VI	ITO/PEDOT:PSS/BPTF/Alq3/LiF:Al	2.8	4.9	516	26067	1075	4.40	0.22	0.28, 0.52
VII	ITO/PEDOT:PSS/CBPTF/Alq3/LiF:Al	2.8	4.5	516	24000	1197	4.31	0.21	0.28, 0.52
VIII	ITO/PEDOT:PSS/CMBPTF/Alq3/LiF:Al	3.1	5.3	517	23802	917	4.13	0.20	0.29, 0.53
IX	ITO/PEDOT:PSS/BPVTF/Alq3/LiF:Al	3.3	5.5	516	21675	919	3.85	0.19	0.28, 0.52
X	ITO/PEDOT:PSS/NPB/Alq3/LiF:Al	3.1	4.1	516	30044	1362	4.45	0.22	0.30, 0.54

XI	ITO/ BPTF /Alq3/LiF:Al	5.8	6.5	516	6127	1114	1.29	0.10	0.28, 0.52
XII	ITO/PEDOT:PSS/Alq3/LiF:Al	4.2	5.4	518	4961	693	0.91	0.05	0.30, 0.54

[a] Turn-on voltage (V) at luminance of 1 cd m⁻². [b] Voltage (V) at luminance of 100 cd m⁻². [c] Emission maximum (nm). [d] Maximum luminance (cd m⁻²). [e] Current density at maximum luminance (mA cm⁻²). [f] Luminance efficiency (cd A⁻¹). [g] External quantum efficiency (%). [h] CIE coordinates (x, y).

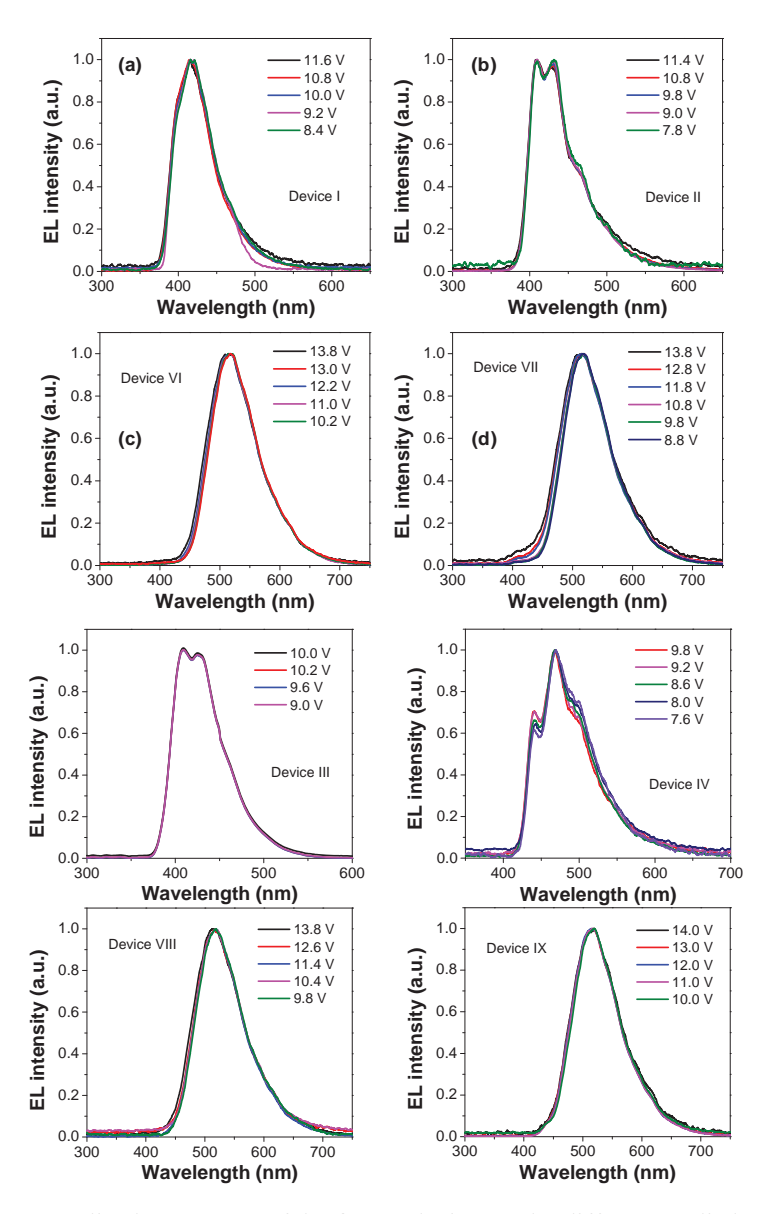


Fig. S8 Normalized EL spectra of the OLED devices under different applied voltages

As HTLs, devices (VI-IX) exhibited the light turn-on voltage at 1 cd m⁻² in the range of 2.8-3.3 V and the operating voltage at 100 cd m⁻² in the range of 4.9-5.5 V, indicating good performance is achieved for all the devices (Figure 5, Table 2). By comparison with the reference device XII, it was found that the incorporation of **BPTF**, **CBPTF**, **CMBPTF** and **BPVTF** in the devices as HTL not only increased the maximum luminance from 4961 cd m⁻² (η of 0.91 cd A⁻¹) to 21675-26067 cd m⁻² (η of 3.85-4.40 cd A⁻¹) in

devices VI-IX, but also significantly decreased the turn-on voltage from 4.2 V to 2.8-3.3 V. Besides, their EL spectra were nearly identical. Moreover, the device characteristics in terms of luminous efficiency clearly demonstrated that the hole-transporting material abilities of these materials were comparable to NPB-based device (device X). Device VI having compound BPTF as HTL exhibited the best performance with a high maximum brightness of 26067 cd m⁻² for green OLED at 10.4 V, a low turn-on voltage of 2.8 V, a maximum luminous efficiency of 4.40 cd A⁻¹ and a maximum external quantum efficiency of 0.22%. A comparable device performance was observed from devices VII (CBPTF as HTL) and VIII (CMBPTF as HTL) (Table 2). Under applied voltage, all devices (VI-VIII) exhibited a bright green emission with peaks centered at 516 nm, and CIE coordinates of x = 0.28 and y = 0.52 (Figure 5a). The electroluminescence (EL) spectra of these diodes were identical, and matched with the PL spectrum of Alq3, the EL of the reference devices (X-XII) and also other reported EL spectra of Alq3-based devices. No emission at the longer wavelength owing to exciplex species formed at the interface of HTL and ETL materials, which often occurs in the devices fabricated from HTL with planar molecular structure, was detected. In our case, the formation of exciplex species could be prevented by the bulky nature of the 9,9-bis(4-diphenylaminophenyl)fluorene.

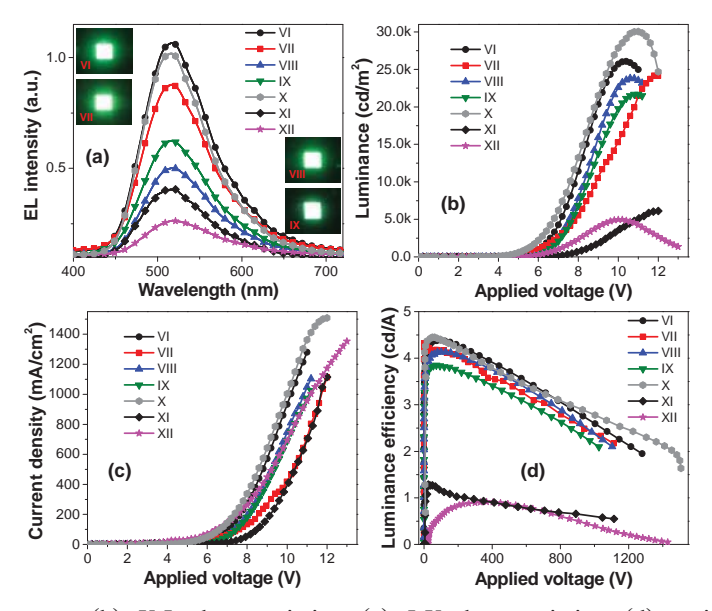


Figure 5. (a) EL spectra, (b) *V-L* characteristics, (c) *I-V* characteristics, (d) variation of luminance efficiency with current density of the fabricated green OLED devices using the synthesized materials as HTL.

From these results and in view of the fact that a barrier for electron-migration at the Alq3/HTL interface (~0.9 eV) is higher than those for hole-migration at the HTL/Alq3 interface (~0.5 eV). Hence, under the present device configuration of ITO/PEDOT:PSS/HTL(50 nm)/Alq3(50 nm)/LiF(0.5 nm):Al(200 nm), BPTF, CBPTF, CMBPTF and BPVTF would act only as HTL, and Alq3 would act

preferably as an electron blocker more than as a hole blocker and charge recombination thus confined to Alq3 layer. More importantly, a stable emission was obtained from all diodes (VI-VIII) with the EL spectra and CIE coordinates did not change over the entire applied voltages (Supporting information). Although, many blue emitting and hole-transporting materials have been reported, in terms of the amorphous morphology, high T_g and device efficiency, **BPTF** is among the good bifunctioned materials reported.

4. Conclusion

In conclusion, we have successfully designed and synthesized four new bifunctioned materials, namely BPTF, CBPTF, CMBPTF and BPVTF, as non-doped deep-blue light-emitting and hole-transporting materials for OLEDs. By the use of 9,9-bis(4-diphenylaminophenyl)fluorene as a molecular platform, we were able to maintained high blue emissive ability of fluorene in the solid state, and improve the amorphous stability of these materials. Strong deep-blue emission in both solution and solid state was obtained. All of them were thermally stable amorphous materials with glass transition temperature well above 166 °C. Their abilities as both blue light-emitting materials for blue OLEDs and hole-transporting materials for green OLEDs in terms of device performance and thermal property were greater than a commonly used NPB. Importantly, BPTF bearing two biphenyl moieties attached to the 2,7-positions of the 9,9-bis(4-diphenylaminophenyl)fluorene showed promising potential as both deep-blue light-emitting and hole-transporting materials for OELD devices. Non-doped deep-blue OLEDs with a maximum luminance efficiency of 2.48 cd A⁻¹, and green OLEDs with maximum luminance efficiency of 4.40 cd A⁻¹ were achieved with low turn-on voltages of 3.1 and 2.8 V, respectively. Notably, the color purities of these deep-blue (CIE coordinate of x = 0.15 and y = 0.07) and green (CIE coordinate of x = 0.28 and y = 0.52) devices were closed to the NTSC blue and green standards. The use of this type of molecular platform might be an effective way to prepare high T_g amorphous materials for long-lifetime device applications, especially for high-temperature applications in OLEDs or other organic optoelectronic devices.

5. Experimental Section

General procedure

¹H and ¹³C NMR spectra were recorded on a Brüker AVANCE 300 MHz spectrometer. Infrared (IR) spectra were measured on a Perkin-Elmer FTIR spectroscopy spectrum RXI spectrometer. Ultraviolet-visible (UV-Vis) spectra were recorded on a Perkin-Elmer UV Lambda 25 spectrometer and photoluminescence spectra and the fluorescence quantum yields (Φ_F) were recorded with a Perkin-Elmer LS 50B Luminescence Spectrometer as dilute CH_2Cl_2 solution and thin film obtained by thermal evaporation. Quinine sulfate solution in 0.01 M H_2SO_4 ($\Phi_F = 0.54$) was used as a reference standard. Differential scanning calorimetric (DSC) analysis and thermogravimetric analysis (TGA) were performed on a METTLER DSC823e thermal analyzer and a Rigaku TG-DTA 8120 thermal analyzer, respectively,

with heating rate of 10 °C/min under nitrogen atmosphere. Cyclic voltammetry (CV) measurements were carried out on an Autolab potentiostat PGSTAT 12 with a three electrode system (platinum counter electrode, glassy carbon working electrode and Ag/Ag⁺ reference electrode) at scan rate of 50 mV/s in the presence of tetrabutyl ammonium hexafluorophosphate (*n*-Bu₄NPF₆) as a supporting electrolyte in CH₂Cl₂ under argon atmosphere. Melting points were measured using an Electrothermal IA 9100 series of digital melting point instrument and are uncorrected. High resolution mass spectrometry (HRMS) analysis was performed on Brüker micrOTOF (Q-ToF II) mass spectrometer. Elemental analysis was analyzed on PerkinElmer 2400 Series II CHNS/O Elemental Analyzer at Chulalongkorn University.

Synthesis

2,7-Bis(4-(biphenyl-4-yl))-9,9-bis(4-diphenylaminophenyl)fluorene (**BPTF**)

A mixture of **2** (0.70 g, 0.86 mmol), 4-biphenylboronic acid (0.43 g, 2.16 mmol), Pd(PPh₃)₄ (99 mg, 0.086 mmol) and an aqueous Na₂CO₃ solution (2 M, 10 ml) in THF (15 ml) was degassed with N₂ for 5 min. The mixture was heated at reflux under N2 atmosphere for 20 h. After the mixture was cooled to room temperature water (50 ml) was added. The mixture was extracted with CH₂Cl₂ (50 ml x 2). The combined organic phase was washed with water, brine solution, dried over anhydrous Na₂SO₄, filtered, and the solvents were removed to dryness. Purification by column chromatography using silica gel eluting with a mixture of CH₂Cl₂ and hexane followed by recrystallization from methanol/CH₂Cl₂ afforded a white solid (0.74 g, 90%). m.p. >250 °C; IR (KBr); 3415, 3030, 1600, 1480, 1300, 813 and 751cm⁻¹; ¹H NMR (300 MHz, CDCl₃) δ 6.94-7.01 (8H, m) 7.08 (8H, d, J = 7.80 Hz), 7.19-7.25 (12H, m), 7.35-7.40 (2H, m), 7.48 (t, 4H, J = 7.80 Hz) 7.64-7.73 (16H, m) and 7.80 (2H, d, J = 7.80 Hz) ppm; ¹³C NMR (75 MHz, CDCl₃) δ 64.76, 120.58, 122.83, 123.07, 124.51, 124.88, 126.64, 127.08, 127.40, 127.55, 127.59, 128.87, 128.98, 139.08, 139.44, 140.19, 140.30, 140.70, 146.35, 147.67 and 152.65 ppm; HRMS calcd for C₇₃H₅₂N₂: m/z 956.4130; found: 955.1625 [M⁺]; Anal. calcd for C₇₃H₅₂N₂: C 91.60, H 5.48 N 2.93; found: C 91.69, H 5.47 N 2.80.

$2,7-Bis (4-(carbazol-9-yl)-4-biphenyl-4-yl)-9,9-bis (4-diphenylaminophenyl) fluorene \ (\textbf{\textit{CBPTF}})$

CBPTF was synthesized from **2** (0.50 g, 0.62 mmol), **3** (0.64 g, 1.35 mmol) in similar manner to **BPTF**, and obtained as a white solid (0.60 g, 75%): m.p. >250 °C; IR (KBr) 3412, 3027, 1617, 1491, 1275, 812 and 748 cm⁻¹; ¹H NMR (300 MHz, CDCl₃) δ 6.98-7.03 (8H, m), 7.11 (8H, d, J = 7.80 Hz), 7.22-7.28 (10H, m), 7.34 (4H, t, J = 7.20 Hz), 7.48-7.54 (8H, m), 7.72-7.82 (16H, m), 7.87–7.93 (8H, m) and 8.19 (4H, d, J = 7.80 Hz) ppm; ¹³C NMR (75 MHz, CDCl₃) δ 62.80, 109.87, 120.02, 120.35, 120.64, 122.88, 123.05, 123.46, 124.54, 124.88, 125.99, 126.68, 127.41, 127.52, 127.75, 128.38, 128.98, 129.21, 137.00, 139.19, 139.39, 139.72, 140.09, 140.64, 140.86, 147.66 and 152.74 ppm; HRMS calcd for $C_{97}H_{66}N_4$: m/z 1287.5321; found: 1287.2800 [M⁺]; Anal. calcd for $C_{97}H_{66}N_4$: C 90.48, H 5.17, N 4.35; found: C 90.62, H 5.00, N 4.35.

2,7-Bis(4-(carbazol-9-yl)⁻²-methylbiphenyl-4-yl)-9,9-bis(4-diphenylaminophenyl)fluorene (**CMBPTF**)

CMBPTF was synthesized from **2** (0.5 g, 0.62 mmol), **4** (0.62 g, 1.35 mmol) in similar manner to **BPTF**, and obtained as a white solid (0.67 g, 82%). m.p. 216 °C; IR (KBr) 3410, 3032, 1590, 1500, 1464, 1275, 814 and 748 cm⁻¹; ¹H NMR (300 MHz, CDCl₃) δ 2.51 (4H, s), 6.98-7.03 (8H, m), 7.11 (8H, d, J = 7.80 Hz), 7.23 (10H, d, J = 8.10 Hz), 7.34 (4H, t, J = 7.20 Hz), 7.47 (8H, t, J = 7.80 Hz), 7.53–7.768 (16H, m) 7.71-7.76 (4H, m) 7.91 (2H, d, J = 7.80 Hz) and 8.19 (4H, d, J = 7.80 Hz) ppm; ¹³C NMR (75 MHz, CDCl₃) δ 20.87, 60.05, 109.87, 120.02, 120.35, 120.64, 122.88, 123.05, 123.46, 124.54, 124.88, 125.99, 126.68, 127.41, 127.52, 127.75, 128.38, 128.98, 129.21, 137.00, 139.19, 139.39, 139.72, 140.09, 140.64, 140.86, 147.66 and 152.74 ppm; HRMS calcd for $C_{99}H_{70}N_4$: m/z 1315.5634; found: 1315.8442 [M⁺]; Anal. calcd for $C_{99}H_{70}N_4$: C 90.38, H 5.36, N 4.26; found: C 89.75, H 5.09, N 4.67.

2,7-Bis(4-(biphenyl-4-yl)vinyl)-9,9-bis(4-diphenylaminophenyl)fluorene) (BPVTF)

BPVTF was synthesized from **2** (0.5 g, 0.62 mmol), *trans*-2-(4-biphenyl)vinylboronic acid (0.29 g, 1.30 mmol) in similar manner to **BPTF**, and obtained as a yellow solid (0.40 g, 71%). m.p. >250 °C; IR (KBr) 3410, 3026, 1590, 1470, 1325, 1275, 827 and 760 cm⁻¹; ¹H NMR (300 MHz, CDCl₃) δ 6.96-7.03 (9H, m) 7.10 (9H, d, J = 8.10 Hz), 7.15-7.26 (15H, m), 7.34-7.39 (2H, m), 7.47 (4H, t, J = 7.80 Hz) 7.58-7.67 (15H, m) and 7.76 (2H, d, J = 7.80 Hz H) ppm; ¹³C NMR (75 MHz, CDCl₃) δ 64.10, 120.40, 122.84, 123.00, 124.52, 125.94, 126.90, 127.34, 127.86, 128.80, 128.97, 129.11, 129.19, 136.43, 136.93, 139.27, 139.49, 140.26, 140.65, 146.33, 147.67 and 152.58 ppm; HRMS calcd for $C_{77}H_{56}N_2$: m/z 1008.4443; found: 1009.6281 [M⁺]; Anal. calcd for $C_{77}H_{56}N_2$: C 91.63, H 5.59, N 2.78; found: C 91.23, H 5.40, N 2.90. 9.9-Bis(4-diphenylaminophenyl)-2,7-dibromofluorene (2)

A mixture of 2,7-dibromofluorenone (1) (2.57 g, 6.79 mmol), triphenylamine (16.67 g, 67.99 mmol), and methanesulfonic acid (0.45 ml) was heated at 190 °C for 6 h. The cooled mixture was poured into water. The greenish precipitate was filtered, washed with water and dried to afford crude product. Purification by column chromatography using silica gel eluting with a mixture of CH_2Cl_2 and hexane followed by recrystallized from methanol/ CH_2Cl_2 afforded a light white solid (3.72 g, 61%). ¹H NMR (300 MHz, CDCl₃) δ 6.99 ppm (4H, d, J = 9.0 Hz), 7.00 (8H, t, J = 9.0 Hz), 7.09 (8H, d, J = 9.0 Hz), 7.26 (8H, t, J = 9.0 Hz), 7.55 (4H, t, J = 9.0 Hz), 7.58 (2H, d, J = 9.0 Hz); ¹³C NMR (75 MHz, CDCl₃) δ 64.65 ppm, 121.55, 121.76, 122.77, 123.06, 124.5, 124.68, 128.69, 129.27, 129.38, 130.82, 137.66, 137.98, 146.74, 147.52 and 153.47; HRMS m/z calcd for $C_{49}H_{34}Br_2N_2$, 808.1089; found, 809.1169 [MH $^+$].

4-Bromo-4'-(carbazol-9-yl)biphenyl (8)

A mixture of carbazole (3.35 g, 20.03 mmol), 4,4'-dibromobiphenyl (7) (25.00 g, 80.13 mmol), potassium carbonate (5.53 g, 40.06 mmol), copper powder (1.27 g, 20.03 mmol) and 18-crown-6 (0.79 g, 3.04 mmol) in o-dichlorobenzene (90 ml) was stirred at reflux under N_2 atmosphere for 44 hr at which TLC showed all carbazole completely consumed. The solvent was completely removed under vacuum to

give a brown residue which was then dissolved in CH_2Cl_2 and water. The organic phase was separated and washed with water, brine solution and dried over anhydrous sodium sulphate. Purification by column chromatography over silica get eluting with a mixture of CH_2Cl_2 and hexane gave a white powder (5.10 g, 64%). IR (KBr) 3413, 1604, 1526, 1450, 1335, 1231, 1077 and 1002 cm⁻¹; ¹H NMR (300 MHz, CDCl₃) δ 7.31 (2H, t, J = 7.50 Hz), 7.41-7.49 (4H, m), 7.56 (2H, d, J = 8.70 Hz), 7.62-7.67 (4H, m), 7.79 (2H, d, J = 8.40 Hz) and 8.17 (2H, d, J = 7.50 Hz) ppm; ¹³C NMR (75 MHz, CDCl₃) δ 109.79, 120.08, 120.37, 121.98, 123.49, 126.01, 127.46, 127.51, 128.08, 128.34, 128.53, 128.72, 132.03, 132.10, 137.29, 139.04, 139.20, 139.31 and 140.80 ppm.

4-Bromo-4'-(Carbazol-9-yl)-2-methylbiphenyl (11)

A mixture of 2-(4-(carbazol-9-yl)benzene)-4,4,5,5-tetramethyl-1,3,2-dioxaborolane (9) (3.65 g, 9.88 mmol), 5-bromo-2-iodotoluene (10) (3.50 g, 11.86 mmol), potassium carbonate (8.19 g, 59.30 mmol) in a mixture of tetrahydrofuran (60 ml) and water (20 ml) was stirred and degassed with N_2 for 5 min and then $Pd(Ph_3P)_4$ (0.57 g, 0.49 mmol) was added. The reaction mixture was heated with reflux under N_2 atmosphere for 18 hr. Water and CH_2Cl_2 were added. The organic phase was separated, washed with water, brine solution and dried over magnesium sulphat. A crude residue was purified by column chromatography over silica gel eluting with a mixture of CH_2Cl_2 and hexane (1:6) to give a white solid (3.15 g, 77%). IR (KBr) 3412, 1605, 1528, 1490, 1453, 1336, 1232, 1077 and 1003 cm⁻¹; ¹H NMR (300 MHz, CDCl₃) δ 2.4 (3H, s), 7.23-7.36 (1H, m), 7.44-7.56 (10H, m), 7.66 (2H, d, J = 9.00 Hz) and 8.20 (2H, d, J = 9.00 Hz.) ppm; ¹³C NMR (75 MHz, CDCl₃) δ 20.35, 109.79, 120.08, 120.37, 121.98, 123.49, 126.01, 127.46, 127.51, 128.08, 128.34, 128.53, 128.72, 132.03, 132.10, 137.29, 139.04, 139.20, 139.31 and 142.81 ppm.

2-(4-(Carbazol-9-yl)-biphenyl)-4,4,5,5-tetramethyl-1,3,2-dioxaborolane (3)

A solution of **8** (3.00 g, 7.53 mmol) in tetrahydrofuran (150 ml) was degassed with N₂ and cooled to -78 $^{\circ}$ C in a dry ice-acetone bath. *n*-Butyl lithium solution (1.6 M in hexane, 9.41 ml, 15.06 mmol) was added via syringe and a mixture was stirred at room temperature for 20 min. The mixture was cooled to -78 $^{\circ}$ C in an dry ice-acetone bath and 2-isopropoxy-4,4,5,5-tetramethyl-1,3,2-dioxaborolane (1.68 g, 9.03 mmol) was added. The reaction mixture was allowed to warm to room temperature and stirred for overnight. Water was added and a mixture was extracted with CH₂Cl₂ (50 ml x 3). The combined organic phased was washed with water, brine solution and dried over anhydrous sodium sulphate. Recrystallisation from CH₂Cl₂/hexane gave a white solid (2.85 g, 85%). IR (KBr) 3415, 1610, 1529, 1452, 1360, 1255, 1142, 1091 and 1007 cm⁻¹; 1 H NMR (300 MHz, CDCl₃) δ 2.42 (12H, s), 7.31 (2H, t, J = 7.5 Hz), 7.41-7.50 (4H, m), 7.66 (2H, d, J = 7.8 Hz), 7.72 (2H, d, J = 7.5 Hz) 7.86 (2H, d, J = 7.8 Hz), 7.97 (2H, d, J = 7.5 Hz) and 8.17 (2H, d, J = 7.5 Hz) ppm; 13 C NMR (75 MHz, CDCl₃) δ 24.92, 83.93, 109.85,120.00, 120.33, 123.46, 125.98, 126.43, 127.34, 128.61, 135.44, 137.17, 140.09, 140.85 and 142.88 ppm.

4-(4'-(Carbazol-9-yl)-2-methylbiphenyl)-4,4,5,5-tetramethyl-1,3,2-dioxaborolane (4)

4 was synthesized from **11** (2.80 g, 6.79 mmol) in similar manner to **3**, and obtained as a white solid (2.21 g, 71%). IR (KBr) 3414, 1611, 1521, 1425, 1359, 1316, 1099 and 852 cm⁻¹; ¹H NMR (300 MHz, CDCl₃) δ 1.43 (12H, s), 2.42 (3H,s), 7.29-7.47 (4H, m), 7.50-7.64 (7H, m), 7.77 (1H, d, J = 7.5 Hz), 7.81 (1H, s) 8.17 (2H, d, J = 7.5 Hz) ppm; ¹³C NMR (75 MHz, CDCl₃) δ 20.35, 24.90, 83.88, 109.87, 119.97, 120.32, 123.43, 125.95, 126.65, 129.33, 130.53, 132.39, 134.71, 136.52, 136.98, 140.88, 140.97 and 143.00 ppm.

Quantum chemical calculation

The ground state geometries of all molecules were fully optimized using density functional theory (DFT) at the B3LYP/6-31G (d,p) level, as implemented in Gaussian 03. TDDFT/B3LYP calculation of lowest excitation energies were performed at the optimized geometries of the ground states.

Fabrication and characterization of OLEDs

OLED devices using BPTF, CBPTF, CMBPTF and BPVTF as EML with configuration of ITO/PEDOT:PSS/EML(50 nm)/BCP(40 nm)/LiF(0.5 nm):Al(150 nm) and double-layer green OLED devices using BPTF, CBPTF, CMBPTF and BPVTF as HTL with configuration of ITO/PEDOT:PSS/HTL(40 nm)/Alq3(50 nm)/LiF(0.5 nm):Al(150 nm) were fabricated and characterized as followed. The patterned indium tin oxide (ITO) glass substrate with a sheet resistance 14 Ω \square (purchased from Kintec company) was thoroughly cleaned by successive ultrasonic treatment in detergent, deionised water, isopropanol, and acetone, and then dried at 60 °C in a vacuum oven. A 50 nm thick PEDOT:PSS hole injection layer was spin-coated on top of ITO from a 0.75 wt.% dispersion in water at a spin speed of 3000 rpm for 20 s and dried at 200 °C for 15 min under vacuum. Thin films of each organic EML or HTL were deposited on top of PEDOT:PSS layer by evaporation from resistively heated alumina crucibles at evaporation rate of 0.5-1.0 nm s⁻¹ in vacuum evaporator deposition (ES280, ANS Technology) under a base pressure of $\sim 10^{-5}$ mbar. The film thickness was monitored and recorded by quartz oscillator thickness meter (TM-350, MAXTEK). A 40 nm thick hole-blocking layer of BCP or a 50 nm thick greenemitting layer of Alq3 was then deposited on the organic EML or HTL, respectively, without breaking the vacuum chamber. The chamber was vented with dry air to load the cathode materials and pumped back; a 0.5 nm thick LiF and a 150 nm thick aluminum layers were the subsequently deposited through a shadow mask on the top of EML/HTL film without braking vacuum to from an active diode areas of 4 mm². The measurement of device efficiency was performed according to M.E. Thomson's protocol and the device external quantum efficiencies were calculated using procedure reported previously. Current densityvoltage-luminescence (I-V-L) characteristics were measured simultaneous by the use of a Keithley 2400 source meter and a Newport 1835C power meter equipped with a Newport 818-UV/CM calibrated silicon photodiode. The EL spectra were acquired by an Ocean Optics USB4000 multichannel spectrometer. All the measurements were performed under ambient atmosphere at room temperature.



PART IV

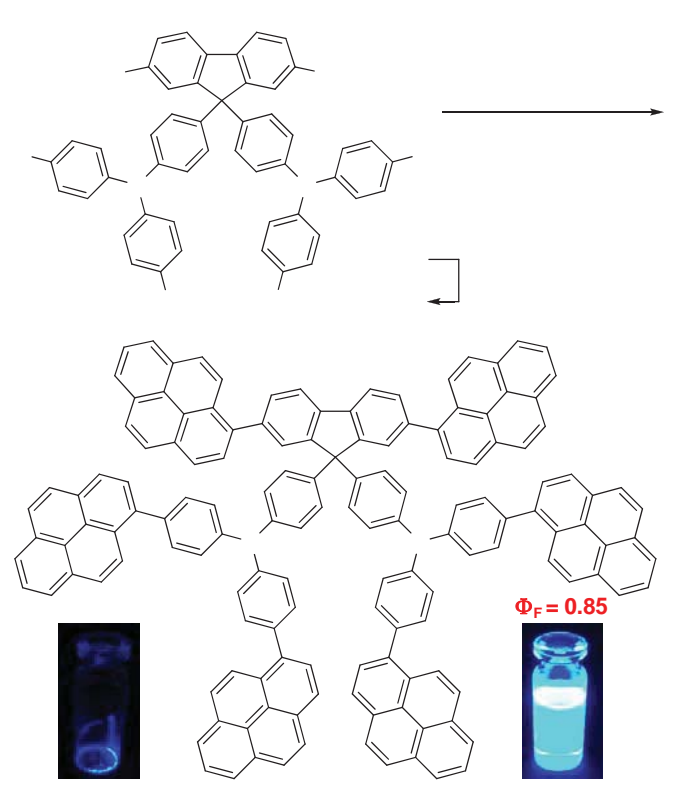
Pyrene-Functionalized 9,9-Bis(4-diphenylaminophenyl)fluorene as Solution-Processed Blue Emitting and Hole-Transporting Materials for Efficient Electroluminescent Devices

1. Introduction

Organic light-emitting diodes (OLEDs) have attracted a great deal of attention due to their applications as next-generation flat-screen displays and general illumination. In the past decade, we have seen great progress in both materials development and device fabrication techniques. One area of on-going research is the pursuit of a stable-blue emitting material. Although, many kinds of blue light-emitting materials have been investigated, such as derivatives of anthracene, fluorene, and polycyclic aromatic hydrocarbons, further improvement for blue OLED compared to red and green devices is still required. Pyrene has also been widely used as a building block to form many emissive materials due to its high photoluminescence efficiency in blue, high carrier mobility, and improved the hole-injection ability than other blue chromophores. Though, many pyrene-functionalized materials were proven to be promising blue emitters for OLEDs, solution-processed analogues remain rare and largely unexplored in OLEDs. To enhance the colour purity of pyrene-based materials, it is essential to integrate either large bulky groups or excimers. multisubstituted rigid moieties to suppress the aggregates and 9.9-Bis(4diphenylaminophenyl)fluorene possesses a highly steric framework and has been successfully used as a building block to form many blue emitting molecules and polymers with improving hole-injection and suppressing aggregation Therefore, we herein implemented all required aspects in the synthesized molecule (Scheme 1). Incorporation of pyrene units into a cruciform of 9,9-bis(4-diphenylaminophenyl) fluorene would offer an effective way to control the π - π stacking interactions and the associated red shift in emission, and maintain the high blue emissive ability of pyrene in the solid state. Moreover, triphenylamine units also improve hole injection and transport ability with high thermal stability. Owning to its supramolecular steric hindrance, the material would possess good solubility and thereby thermally stable amorphous thin film could be deposited by a cheap solution process. Accordingly, this would result in new solution-processable molecular material with combined blue emitting and hole-transporting properties for OLEDs. An investigation of its physical and photophysical properties, and blue OLED fabrication and characterization are also reported.

2. Results and Discussion

PTF was synthesized in two steps from 1 as illustrated in Scheme 1. Bromination of 9,9-bis(4diphenylaminophenyl)-2,7-dibromofluorene (1) with NBS followed by Pd catalyzed cross-coupling of the resultant hexabromo compound 2 with 2-pyrene boronic acid gave PTF as a light yellow solid in a good yield. PTF showed good solubility in organic solvents, opening the door to solution processing techniques. Quantum chemical calculation of PTF performed using TDDFT/B3LYP/6-31G(d,p) method revealed that both triphenylamines at the C-9 position of the fluorene ring generated a highly steric hindrance, resulting a bulky molecular structure with high steric repulsion between the aromatic ring and thereby preventing a closed π - π stacking interaction of the molecule and a good ability to dissolve in the solvent. In the HOMO, electrons are delocalized over the pyrene-triphenylamine moiety indicating less π -electron interaction between fluorene and pyrene moieties, while in the LUMO, the excited electrons delocalized over the quinoid-like pyrene-fluorene plane. The HOMO-LUMO energy gap (E_g cal.) was calculated to be 3.01 eV which slightly deviated from that estimated from the optical absorption edge (2.97 eV). There are factors responsible for the errors in the E_g cal. values because the orbital energy difference between HOMO and LUMO is still an approximate estimation to the transition energy since the transition energy also contains significant contributions from some two-electron integrals. The real situation is that an accurate description of the lowest singlet excited state requires a linear combination of a number of excited configurations.



Scheme 1. Synthesis of PTF.

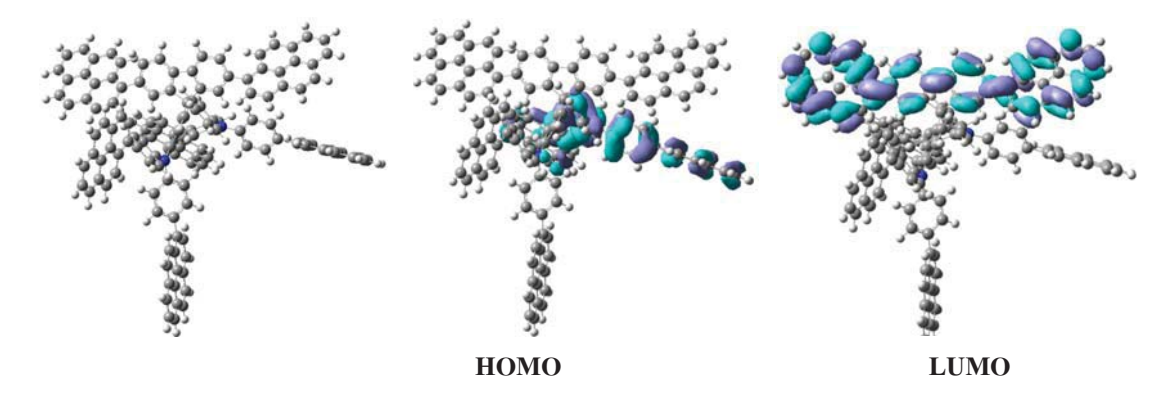


Figure S1 The optimized geometry and HOMO-LUMO orbitals of PTF by TDDFT/B3LYP(3,6)d.

In a CH₂Cl₂ solution, the absorption spectrum of PTF showed absorption bands at 279 and 364 nm, while the photoluminescence spectrum displayed a featureless emission peak at 478 nm (Figure 1a). In solid state, the emission spectrum of the thin film obtained by spin-coating on quart substrate was identical to its solution spectrum. This suggested that the bulky molecular structure of PTF effectively reduced the intermolecular π - π interaction of pyrene units in the solid state. This material exhibited a strong blue fluorescence in both solution and solid state with a high solution fluorescence quantum yield $(\Phi_{\scriptscriptstyle E})$ of 0.85. The thermogravimetric analysis (TGA) revealed that PTF was thermally stable material with a 5% weight loss (T_{5d}) at temperature well over 475 °C (Figure 1b). In a repeated differential scanning calorimetry (DSC) scan, all thermograms displayed only endothermic baseline shifts owing to glass transition (T_o) at 237 °C with no crystallization and melting being observed at higher temperatures, indicating a highly stable amorphous material. Its amorphous feature was further studied by powder X-ray diffraction (XRD) using silicon wafer as a substrate. The XRD pattern of PTF showed broad diffraction peaks between 10.5 and 34.6° with a characteristic peaks ascribed to the π - π stacking of pyrene units being observed (Figure 1c). The morphology of PTF was characterized by an atomic force microscope (AFM). The film spincoated from THF:toluene solution showed a quite smooth surface indicating its good film formation ability (Figure 1d). These results proved that the use of 9,9-bis(4-diphenylaminophenyl)fluorene as a molecular platform could reduce the crystallization of pyrene and improve the amorphous stability of the material, which in turn could increase the service time in device operation and enhance the morphological stability to the thin film. Moreover, the ability of PTF to good thin film by solution casting techniques is highly desirable for fabrication of cheap OLED device.

A cyclic voltammetry (CV) study on PTF revealed a quasi-reversible oxidation wave at 0.86 V with no distinct reduction process being detected (see ESI). The oxidation assigned to the removal of electrons from the triphenylamine-pyrene resulting radical cations occurred at lower potential value than that of other triphenylamine derivatives having the phenyl rings being p-unsubstituted ($E_{1/2} = 0.93$ V), supporting

the existence of the π -electron interaction between the triphenylamine and substituted pyrene as observed in the calculation. Multiple CV scans displayed identical CV curves indicating electrochemically stable molecule. The HOMO and LUMO levels of **PTF** were calculated to be 5.21 and 2.24 eV, respectively.

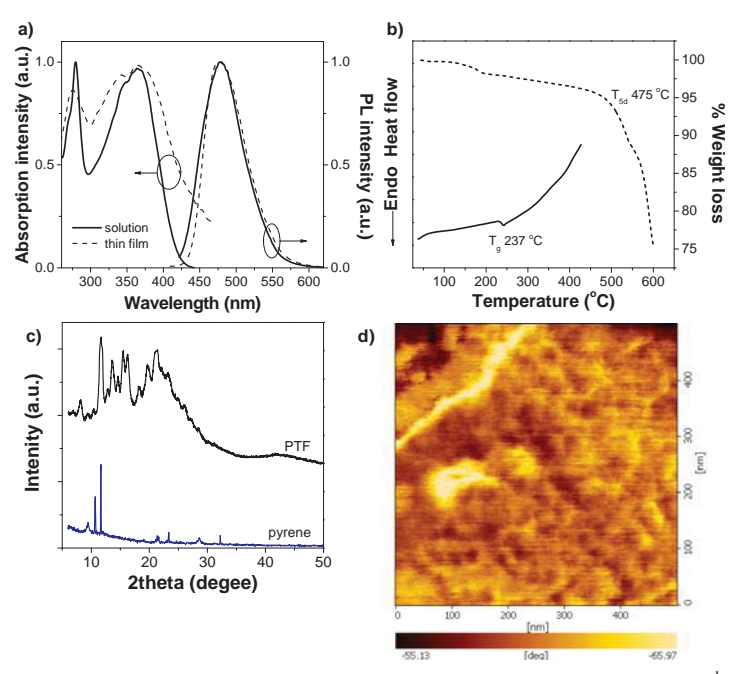


Figure 1. a) UV-Vis absorption and PL spectra in solution and thin film. b) DSC (2nd heating scan) and TGA curves measured at 10 °C/min under N₂. c) Powder X-ray diffraction patterns. d) Tapping mode AFM image of spin-coated film.

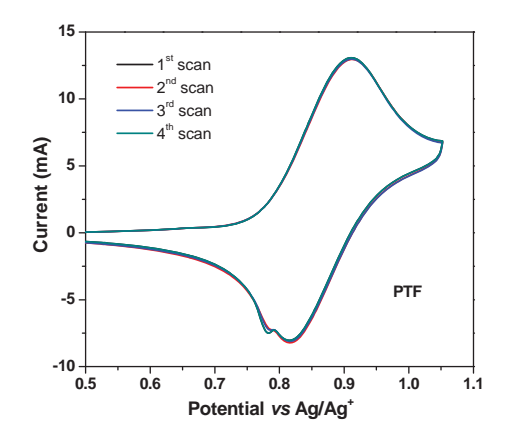


Figure S2 (a) Multiple CV scan curves of **PTF** measured in CH₂Cl₂ at a scan rate of 50 mV/s.

Owning to its high blue fluorescence ($\Phi_F = 0.85$) and its HOMO level (5.21 eV) lying between those of indium tin oxide (ITO) (4.80 eV) and tris(8-hydroxyquinoline)aluminum (Alq3) (5.80 eV), **PTF** can act as bifunctional material, namely blue light-emitting and hole-transporting materials, respectively. The blue and green OLEDs with the structures of ITO/PEDOT:PSS /**PTF**(40 nm)/BCP(40 nm)/LiF(0.5 nm):Al(150 nm) and ITO/PEDOT:PSS/**PTF**(40 nm)/Alq3(50 nm)/LiF(0.5 nm):Al(150 nm) were fabricated,

respectively. The **PTF** layer in both devices was spin-coated from THF:toluene (1:1) solution with controlled thickness. To compare a bifunctional ability of **PTF**, commercially available *N,N'*-diphenyl-*N,N'*-bis(1-naphthyl)-(1,1'-biphenyl)-4,4'-diamine (NPB) was employed as reference EML and HTL materials. From our study, it was found that the incorporation of poly(3,4-ethylenedioxythiophene):poly(4-styrenesulfonate) (PEDOT:PSS), as hole injection layer in the device not only increased the maximum luminance from 2097 cd m⁻² in device VI to 19560 cd m⁻² in device III, but also notably decreased the turn-on voltage from 4.8 V to 3.0 V (Table 1) with unchanged electroluminescence (EL) properties. This is due to a rough and porous surface of spin-coated PEDOT:PSS layer which increases the contact area to enhance hole injection and lowers barrier at the organic-organic interface by relocating the barrier to the more conductive PEDOT:PSS layer.

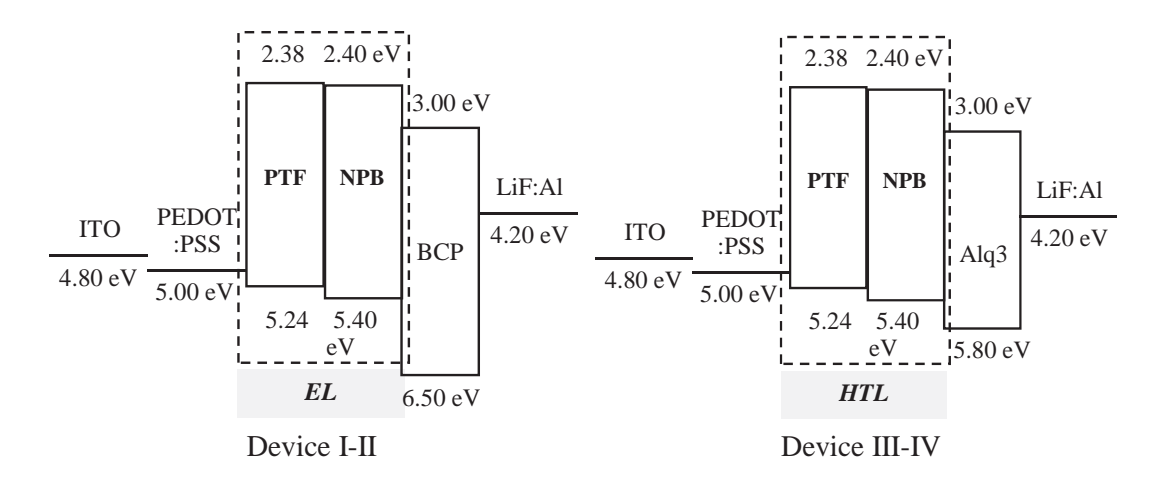


Figure S3 A schematic of the energy band diagrams of each layer of the fabricated OLED devices.

As blue emitter, the PTF-based device (I) exhibited a high maximum brightness of 5997 cd m⁻² for blue OLED at 10.2 V, a low turn-on voltage of 3.2 V and a maximum luminance efficiency of 1.13 cd A⁻¹ (Figure 2, Table 1). The operating voltage at 100 cd m⁻² was 4.8 V indicating good performance was achieved. The device characteristics in terms of maximum brightness, turn-on voltage and maximum luminous efficiency clearly demonstrated that the solution-processed blue-emitting ability of PTF was greater than the NPB-based device (II). Under applied voltage, device I emitted a bright sky blue luminescence with peaks centered at 474 nm and CIE coordinate of 0.15, 0.24. The EL spectrum of the diode matched with the PL spectrum of PTF. No emission shoulder at the longer wavelength owing to excimer and exciplex species formed at the interface of EML and BCP layers, which often occurs in the devices fabricated from EML with planar molecular structure, was detected. This shoulder emission (at 463 nm) was observed in the NPB-based blue OLED (device II). In our case, the formation of these species could be prevented by a bulky nature of the 9,9-bis(4-diphenylaminophenyl)fluorine used as a molecular platform of PTF. Moreover, stable emission was obtained from the device I with the EL spectra

did not change over the entire driven voltages.

As HTL, the PTF-based device (III) exhibited good performance with a high maximum brightness of 19560 cd m⁻² for green OLED at 10.8 V, a low turn-on voltage of 3.0 V and a maximum luminous efficiency of 4.08 cd A⁻¹ (Figure 2, Table 1). The operating voltage at 100 cd m⁻² was 4.2 V indicating good performance is achieved. By comparison with the reference device V, it was found that the incorporation of PTF in the device as HTL not only increased the maximum luminance from 4961 cd m⁻² (η of 0.91 cd A⁻¹) in device V to 19560 cd m⁻² (η of 4.08 cd A⁻¹) in device III, but also significantly decreased the turnon voltage from 4.2 V to 3.0 V. Besides, their EL spectra were nearly identical. Moreover, the device characteristics in terms of luminous efficiency clearly verified that the solution-processed HTM ability of PTF was greater than the NPB-based device (IV). The device III emitted a bright green luminescence with EL spectra matching with the PL spectrum of Alq3, and the EL of the reference devices and other reported devices. No emission at the longer wavelength owing to exciplex species formed at the interface of HTL and ETL materials, which often occurs in the devices fabricated from HTL with planar molecular structures, was detected. More importantly, a stable emission was obtained from this diode with the EL spectra and CIE coordinates did not change over the entire applied voltages (see ESI). Although, many blue emitting and hole-transporting materials have been reported, in terms of the amorphous morphology, significantly high T_g, solution processability and device efficiency, PTF is among the good bifunctional materials reported.

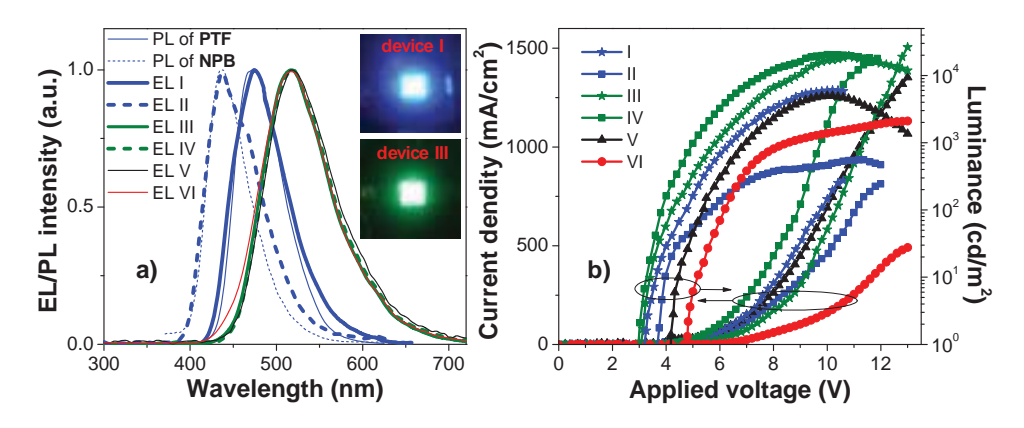


Figure 2. a) EL spectra and b) *I-V-L* characteristics of the fabricated OLED devices.

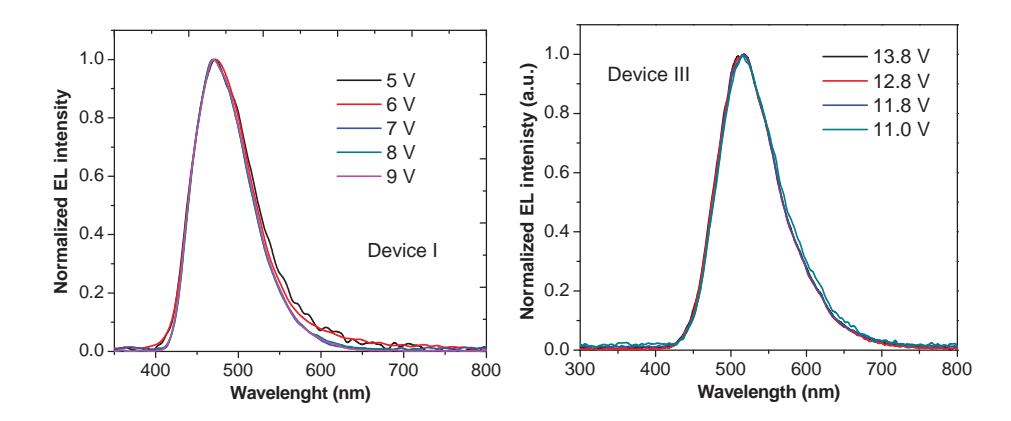


Figure S4 Normalized EL spectra of the OLED devices I and III under different applied voltages.

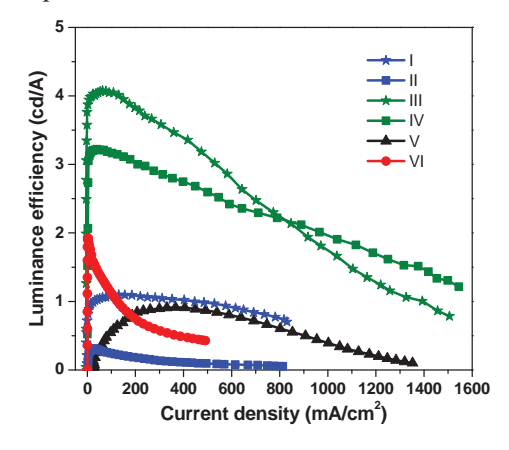


Figure S5 Variation of luminance efficiency with current density of the fabricated OLED devices.

Table 1. Device characteristics of OLEDs fabricated with PTF as EML or HTL.

device	structure	turn-on	emission	maximum	luminance efficiency	CIE coordinates	
		voltage	maxima	luminance	$(\eta,\operatorname{cd} \operatorname{A}^{\text{-1}})$	(x, y)	
		$(V)^a$	(nm)	(cd m ⁻²)			
I	ITO/PEDOT:PSS/PTF/BCP/LiF:Al	3.2	474	5997	1.13	0.15, 0.24	
II	ITO/PEDOT:PSS/NPB/BCP/LiF:Al	3.7	438	558	0.31	0.16, 0.10	
III	ITO/PEDOT:PSS/ PTF /Alq3/LiF:Al	3.0	518	19560	4.08	0.29, 0.53	
IV	ITO/PEDOT:PSS/NPB/Alq3/LiF:Al	3.0	518	20373	3.22	0.29, 0.53	
V	ITO/PEDOT:PSS/Alq3/LiF:Al	4.2	518	4961	0.91	0.30, 0.54	
VI	ITO/ PTF /Alq3/LiF:Al	4.8	516	2097	1.92	0.28, 0.50	

[[]a] At luminance of 1 cd m⁻².

3. Conclusions

In conclusion, we have developed an efficient solution-processable small molecule for OLEDs. By the use of 9,9-bis(4-diphenylaminophenyl)fluorene as a molecular platform, we were able to reduce the crystallization and maintained the high blue emissive ability of pyrene in the solid state, and improve the amorphous stability of the material. **PTF** was an amorphous molecular glass with largely high T_g ,

electrochemically stable, and a strong blue emission both in solution and solid state. Its ability as both blue light-emitter for blue OLEDs and hole-transporter for green OLEDs in terms of device performance and thermal properties was greater than a commonly used NPB. Non-doped sky blue and green OLEDs with luminance efficiencies of 1.13 and 4.08 cd/A were achieved, respectively.

4. Experimental section

4.1 Materials and instruments. All reagents were purchased from Aldrich, Acros or Fluka and used without further purification. All solvents were supplied by Thai companies and used without further distillation. Tetrahydrofuran (THF) was refluxed with sodium and benzophenone, and distilled. Dichloromethane for cyclic voltammetry (CV) measurements was washed with conc. H₂SO₄ and distilled twice from calcium hydride. Chromatographic separations were carried out on silica gel Merk Silica gel 60 (0.0630-0.200 mm).

¹H and ¹³C nuclear magnetic resonance (NMR) spectra were recorded on a Brüker AVANCE 300 MHz spectrometer with tetramethylsilane as the internal reference using CDCl, as solvent in all cases. Infrared (IR) spectra were measured on a Perkin-Elmer FTIR spectroscopy spectrum RXI spectrometer as KBr disc. Ultraviolet-visible (UV-Vis) spectra were recorded as a diluted solution in spectroscopic grade dichloromethane on a Perkin-Elmer UV Lambda 25 spectrometer. Photoluminescence spectra and the fluorescence quantum yields $(\Phi_{\rm p})$ were recorded with a Perkin-Elmer LS 50B Luminescence Spectrometer as a dilute solution in spectroscopic grade dichloromethane and thin film obtained by spin casting. The fluorescence quantum yields $(\Phi_{\scriptscriptstyle E})$ were determined by comparison with a fluorescence standard of quinine sulfate solution in 0.01 M H_2SO_4 ($\Phi_F = 0.54$). Differential scanning carolimetry (DSC) analysis and thermogravimetry analysis (TGA) were performed on a METTLER DSC823e thermal analyzer and a Rigaku TG-DTA 8120 thermal analyzer, respectively, with heating rate of 10 °C/min under nitrogen atmosphere. Cyclic voltammetry (CV) measurements were carried out on an Autolab potentiostat PGSTAT 12 with a three electrode system (platinum counter electrode, glassy carbon working electrode and Ag/Ag⁺ reference electrode) at scan rate of 50 mV/s in dichloromethane under argon atmosphere. The concentration of analytical materials and tetrabutyl ammonium hexafluorophosphate (n-Bu,NPF_c) were 10 ³ M and 0.1 M, respectively. Melting points were measured using an Electrothermal IA 9100 series of digital melting point instrument and are uncorrected.

MALDI-TOF mass spectra were recorded on Bruker Daltonics (Bremen, Germany) Autoflex II Matrix-Assisted Laser Desoprtion/Ionization-Time of Flight Mass Spectrometer (BIFEX) using α -cyano-4-hydroxycinnamic acid as matrix at Chlalongkorn University. The atomic force microscopy (AFM) analysis was performed on SPA 4000 STM/AFM system using standard tipping mode with resonance of 222.223 KHz, force constant of 6.1 (+-20%), cantilever length of 87 (+-5 μ m), cantilever width of 32 (+-5 μ m), scan area of 3-5 μ m and scan speed of 1Hz. Powder X-ray diffraction (XRD) was analyzed by a PHILIPS

X Pert-MDP X-ray diffractometer using Cu K_{α} radiation (λ = 1.5418 Å) at 1,400 W, 40 kV and 35 mA in the scanning angle (2 theta) of 5-50° with resolution of 0.04° at counting step of 1 s/step. The samples were placed on silicon wafer substrate.

4. 2 Synthesis

9,9-Bis(4-di(4-bromophenyl)aminophenyl)-2,7-dibromofluorene (2)

9,9-Bis(4-diphenylaminophenyl)-2,7-dibromofluorene (1) (0.5 g, 0.61 mmol) was dissolved in 40 ml THF in a two-necked flask, (0.44 g, 2.49 mmol). NBS was added with stirring monitoring. The water was added, extracted with CH_2Cl_2 , dried with anhydrous sodium sulfate evaporated solvent gave a white solid of compound **2**. Yield was 0.66 g (90%). m.p. >250 °C; ¹H NMR (300 MHz, CDCl₃) δ 6.93 ppm (12H, t, J = 9.01 Hz), 7.02 (4H, d, J = 8.40 Hz), 7.36 (8H, d, J = 8.70 Hz), 7.51 (4H, d, J = 6.90 Hz) and 7.61 (2 H, d, J = 8.40 Hz); ¹³C NMR (75 MHz, CDCl₃) δ 115.95 ppm, 121.68, 121.85, 123.33, 125.92, 128.92, 129.28, 131.03, 132.43, 137.98 and 146.18; microTOF calcd for $C_{49}H_{30}Br_6N_2$: m/z 1126.1999; found: m/z 1126.7604 [M $^+$].

9,9-Bis(4-di(4-(pyren-2-yl)phenyl)aminophenyl)-2,7-di(pyren-2-yl)fluorene (PTF)

A mixture of 9,9-bis(4-di(4-bromophenyl)aminophenyl)-2,7-dibromofluorene (**2**) (0.6 g, 0.53 mmol), pyrene-1-boronic acid (0.85 g, 3.46 mmol), Pd(PPh₃)₄ (61 mg, 0.05mmol) and an aqueous Na₂CO₃ solution (2 M, 10 ml) in THF (15 ml) was degassed with N₂ for 5 min. The mixture was heated at reflux under N₂ atmosphere for 20 h. After the mixture was cooled to room temperature water (50 ml) was added. The mixture was extracted with CH₂Cl₂ (50 ml x 2). The combined organic phase was washed with water (50 ml), brine solution (50 ml), dried over anhydrous Na₂SO₄, filtered, and the solvents were removed to dryness. Purification by column chromatography using silica gel eluting with a mixture of CH₂Cl₂ and hexane afforded a light yellow solid of **PTF**. Yield was 0.73 g (75%): m.p. >250 °C; ¹H NMR (300 MHz, CDCl₃) δ 7.33 ppm (5H, d, J = 8.40 Hz), 7.42 (8H, d, J = 8.40 Hz), 7.50-7.58 (11H, m), 7.71 (3H, t, J = 7.50 Hz), 7.79 (3H, d, J = 7.50 Hz), 7.97 (15H, t, J = 7.50 Hz), 8.04-8.12 (20H, m), 8.17 (10H, t, J = 7.50 Hz) and 8.24-8.30 (9H, m); ¹³C NMR (75 MHz, CDCl₃) δ 120.58 ppm, 123.96, 124.43, 124.69, 124.75, 124.87, 124.96, 125.01, 125.05, 125.14, 125.23, 125.35, 125.95, 127.30, 127.41, 127.56, 127.64, 128.46, 128.53, 128.94, 129.42, 130.20, 130.42, 130.67, 130.83, 131.00, 131.43, 131.51 and 131.54; microTOF calcd for C₁₄; H₈₄N₂: m/z 1854.2319; found: m/z 1853.5410 [M⁺].

- **4.3 Chemical quantum calculation.** The ground state geometry of **PTF** was fully optimized using density functional theory (DFT) at the B3LYP/6-31G (d,p) level, as implemented in Gaussian 03. TDDFT/B3LYP calculation of lowest excitation energy was performed at the optimized geometry of the ground state.
- **4.4 Device fabrication and testing.** OLED devices using **PTF** and NPB as EML with configuration of ITO/PEDOT:PSS/EML(40 nm)/BCP(40 nm)/LiF(0.5 nm):Al(150 nm) and double-layer green OLED devices using **PTF** and NPB as HTL with configuration ITO/PEDOT:PSS/HTL(40 nm)/Alq3(50

nm)/LiF(0.5 nm):Al(150 nm) were fabricated and characterized as followed. The patterned indium tin oxide (ITO) glass substrate with a sheet resistance 14 Ω/\Box (purchased from Kintec Company) was thoroughly cleaned by successive ultrasonic treatment in detergent, deionised water, isopropanol, and acetone, and then dried at 60 °C in a vacuum oven. A 50 nm thick PEDOT:PSS hole injection layer was spin-coated on top of ITO from a 0.75 wt.% dispersion in water at a spin speed of 3000 rpm for 20 s and dried at 200 °C for 15 min under vacuum. Thin films of each organic EML or HTL were deposited on top of PEDOT:PSS layer by spin-coating chloroform:toluene solution of PTF and NPB (3-1.5% w/v) on an ITO glass substrate at a spin speed of 3000 rpm for 30 second to get a 40 nm thick of EML or HTL layers. The film thickness was measured by using a Tencor α-Step 500 surface profiler. A 40 nm thick holeblocking layer of BCP or a 50 nm thick green-emitting layer of Alq3 was then deposited on the organic EML or HTL, respectively, by evaporation from resistively heated alumina crucibles at evaporation rate of 0.5-1.0 nm/s in vacuum evaporator deposition (ES280, ANS Technology) under a base pressure of ~10⁻⁵ mbar. The film thickness was monitored and recorded by quartz oscillator thickness meter (TM-350, MAXTEK). The chamber was vented with dry air to load the cathode materials and pumped back; a 0.5 nm thick LiF and a 150 nm thick aluminium layers were the subsequently deposited through a shadow mask on the top of EML/BCP films without braking vacuum to from an active diode areas of 4 mm². The measurement of device efficiency was performed according to M.E. Thomson's protocol and the device external quantum efficiencies were calculated using procedure reported previously. After breaking the chamber the device was characterized immediately in an ambient atmosphere (unsealed device). Current density-voltage-luminescence (J-V-L) characteristics were measured simultaneous by the use of a Keithley 2400 source meter and a Newport 1835C power meter equipped with a Newport 818-UV/CM calibrated silicon photodiode. The EL spectra were acquired by an Ocean Optics USB4000 multichannel spectrometer. All the measurements were performed under ambient atmosphere at room temperature.

PART V

Bis(4-diphenylaminophenyl)carbazole end-capped fluorene as solution-processed deep blue light-emitting and hole-transporting materials for electroluminescent devices

1. Introduction

Organic light-emitting diodes (OLEDs) have attracted a great deal of attention due to their applications as next-generation flat-screen displays and general illumination. In the past decade, we have seen great progress in both materials development and device fabrication techniques. One area of on-going research is the pursuit of a stable-blue emitting material. Although, many kinds of blue light-emitting materials have been investigated, such as derivatives of anthracene, pyrene, and polycyclic aromatic hydrocarbons, further improvement for blue OLED compared to red and green devices is still required. Fluorene has also been widely used as a building block to form many emissive materials due to its high photoluminescence efficiency in blue, high carrier mobility, and improved the hole-injection ability than other blue chromophores. Though, many fluorene based materials were proven to be promising blue emitters for OLEDs, solution-processed analogues remain rare and largely unexplored in OLEDs. To enhance the colour purity of fluorene-based materials, it is essential to integrate either large bulky groups or multisubstituted rigid moieties suppress the aggregates and excimers. Bis(4diphenylaminophenyl)carbazole possesses a highly steric structure with hole-transporting property. Therefore, we herein implemented the required aspects in the synthesized molecule (Scheme 1). Endcapping of fluorene with bis(4-diphenylaminophenyl)carbazole would offer an effective way to control the π - π stacking interactions and the associated red shift in emission, and maintain the high blue emissive ability of fluorene in the solid state. Owning to its supramolecular steric hindrance and alkyl chains, the designed compound would possess good solubility and thereby thermally stable amorphous thin film could be deposited by a cheap solution process. Accordingly, this would result in new solution-processable molecular material with combined blue emitting and hole-transporting properties for OLEDs. An investigation of its physical and photophysical properties, and blue OLED fabrication and characterization are also reported.

2. Results and discussion

TCF was synthesized in two steps as illustrated in Scheme 1. Treatment of available 2,7-bis(carbazol-9-yl)-9,9-bis-*n*-hexylfluorene (1) with NBS in THF followed by coupling of the resultant 2 with an excess of

4-(diphenylamino)phenylboronic acid in the presence of Pd(PPh₃)₄ as catalyst and aqueous Na₂CO₃ as base in THF afforded the target **TCF** as white solid in good yield. This compound showed high solubility in common organic solvents at room temperature.

Scheme 1 Synthesis of TCF.

In a CH₂Cl₂ solution, the absorption spectrum of **TCF** showed main absorption band at 345 nm, while the photoluminescence spectrum displayed a featureless emission peak at 408 nm (Fig. 1a). In solid state, the emission spectrum of the thin film obtained by spin-coating on quart substrate was identical to its solution spectrum. This suggested that the bulky molecular structure of **TCF** effectively reduced the intermolecular π - π interaction of the fluorene core in the solid state. This material exhibited a strong blue fluorescence in both solution and solid state with a high solution fluorescence quantum yield (Φ) of 0.75. The HOMO-LUMO energy gap (E_{σ}) was estimated from the optical absorption edge to be 3.23 eV.

The thermogravimetric analysis (TGA) revealed that TCF was thermally stable material with a 5% weight loss (T_{sd}) at temperature well over 417 °C (Fig. 1b). In a repeated differential scanning calorimetry $^{\circ}6H_{13}$ (DSC) scan, all thermograms displayed only endothermic baseline shifts owing to glass transition (T_g) at 169 °C with no crystallization and melting being observed at higher temperatures, indicating a highly stable amorphous material. The morphology of TCF was characterized by an atomic force microscope $^{\circ}K = H$ (AFM). The film spin-coated from THF:toluene solution showed a quite smooth surface indicating its good film formation ability (Fig. 1c). These results proved that the use of bis $^{\circ}K = H$ diphenylaminophenyl)carbazole as a terminal substituent could reduce the crystallization of the conjugated backbone and improve the amorphous stability of the material, which in turn could increase the service time in device operation and enhance the morphological stability to the thin film. Moreover, the ability of

TCF to good thin film by solution casting techniques is highly desirable for fabrication of cheap OLED device.

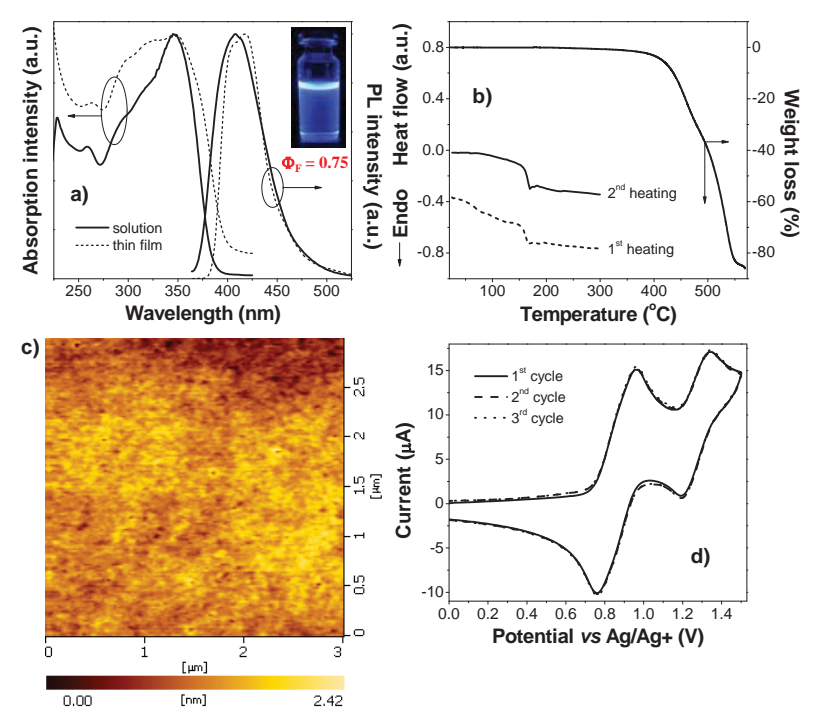


Fig. 1 a) UV-vis absorption and photoluminescence (PL) spectra in CH₂Cl₂ solution and solid film. b) DSC and TGA curves with a heating rate of 10 °C/min under N₂. c) Tapping mode AFM image of spin-coated film. d) CV curves measured in CH₂Cl₂ at a scan rate of 50 mV/s.

A cyclic voltammetry (CV) study on TCF revealed two quasi-reversible oxidation waves at 0.86 and 1.27 V with no distinct reduction process being detected (Fig. 1d). The first oxidation can be assigned to the simultaneous multielectron oxidation process of the peripheral triphenylamine groups, resulting radical cations which occurred at lower potential value than that of other triphenylamine derivatives having the phenyl rings being p-unsubstituted ($E_{1/2} = 0.93 \text{ V}$), supporting the existence of the π -electron interaction between the triphenylamine and carbazole. The second oxidation corresponds to the removal of electrons from the interior moieties. Multiple CV scans displayed identical CV curves indicating electrochemically stable molecule. The HOMO and LUMO levels of TCF were calculated to be 5.19 and 1.96 eV, respectively.

Owning to its high blue fluorescence ($\Phi_F = 0.75$) and its HOMO level lying between those of indium tin oxide (ITO) (4.80 eV) and tris(8-hydroxyquinoline)aluminum (Alq3) (5.80 eV) (Fig. 2a), **TCF** can act as bifunctional material, namely blue light-emitting (EML) and hole-transporting (HTL) materials, respectively. The blue and green OLEDs with the structures of ITO/PEDOT:PSS /EML(40 nm)/BCP(40 nm)/LiF(0.5 nm):Al(150 nm) and ITO/PEDOT:PSS/HTL(40 nm)/Alq3(50 nm)/LiF(0.5 nm):Al(150 nm) were fabricated, respectively. The **TCF** layer in both devices was spin-coated from THF:toluene (1:1) solution with controlled thickness. The reference devices with the same structure based on commonly used

l *N,N'*-diphenyl-*N,N'*-bis(1-naphthyl)-(1,1'-biphenyl)-4,4'-diamine (NPB) were made for comparison. As blue emitter, the **TCF**-based device (I) exhibited a high maximum brightness of 6130 cd m⁻² for blue OLED at 11.6 V, a low turn-on voltage of 3.6 V and a maximum luminance efficiency of 0.93 cd A⁻¹ (Fig. 2, Table 1). The operating voltage at 100 cd m⁻² was 6.2 V indicating good performance was achieved. The device characteristics in terms of maximum brightness, turn-on voltage and maximum luminous efficiency clearly demonstrated that the solution-processed blue-emitting ability of **TCF** was greater than the NPB-based blue device (II). Under applied voltage, device I emitted a bright deep blue luminescence with peak centered at 411 nm and *CIE* coordinate of (0.16, 0.09), which is close to the National Television System Committee (NTSC) deep blue (0.14, 0.10) standard. The EL spectrum of the diode matched with the PL spectrum of **TCF**. No emission shoulder at the longer wavelength owing to excimer and exciplex species formed at the interface of EML and BCP layers, which often occurs in the devices fabricated from EML with planar molecular structure, was detected. This shoulder emission (at 463 nm) was observed in the NPB-based blue OLED (device II). In our case, the formation of these species could be prevented by a bulky nature of the terminal bis(4-diphenylaminophenyl)carbazole. Moreover, stable emission was obtained from the device I with the EL spectra did not change over the entire driven voltages.

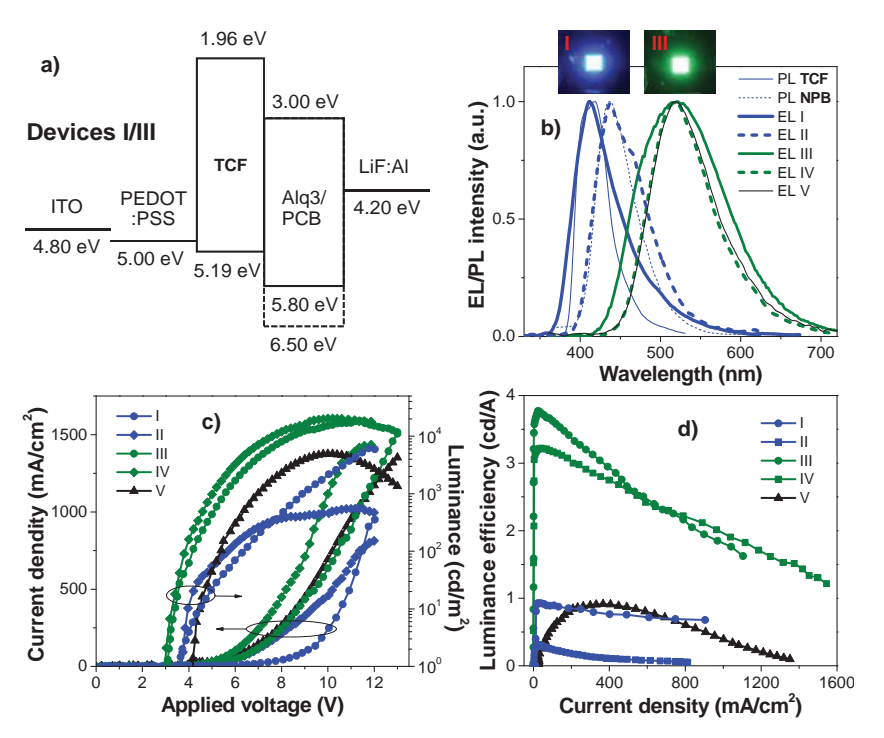


Fig. 2 a) Energy diagrams, b) EL spectra, c) J-V-L characteristics, d) η -J characteristics of the OLED devices.

As HTL, the **TCF**-based device (III) exhibited good performance with a high maximum brightness of 18350 cd m⁻² for green OLED at 11.4 V, a low turn-on voltage of 3.1 V and a maximum luminous efficiency of 3.78 cd A⁻¹ (Fig 2, Table 1). The operating voltage at 100 cd m⁻² was 4.2 V indicating good

performance is achieved. By comparison with the reference device V, it was found that the incorporation of **TCF** in the device as HTL not only increased the maximum luminance from 4961 cd m⁻² (η of 0.91 cd A⁻¹) in device V to 18350 cd m⁻² (η of 3.78 cd A⁻¹) in device III, but also significantly decreased the turn-on voltage from 4.2 V to 3.1 V. Besides, their EL spectra were nearly identical. Moreover, the device characteristics in terms of luminous efficiency clearly verified that the solution-processed HTL ability of **TCF** was greater than the NPB-based device (IV). The device III emitted a bright green luminescence with EL spectra matching with the PL spectrum of Alq3, and the EL of the reference devices and other reported devices. No emission at the longer wavelength owing to exciplex species formed at the interface, which often occurs in the devices fabricated from HTL with planar molecular structures, was detected. More importantly, a stable emission was obtained from this diode with the EL spectra and *CIE* coordinates did not change over the entire applied voltages. Although, many blue emitting and hole-transporting materials have been reported, in terms of the amorphous morphology, high T_g, solution processability and device efficiency, **TCF** is among the good bifunctional materials reported.

Table 1 Device characteristics of OLEDs with TCF as either EML or HTL.

device	EML/HTL	$V_{ m on}^{\ \ c}$	$\lambda_{\rm em}^{d}$	$L_{\mathrm{max}}^{}\mathrm{e}}$	$\it J^{^{ m f}}$	$\eta^{\mathfrak{g}}$	CIE ^h
Iª	TCF	3.6	411	6130	905	0.93	0.16, 0.09
Π^a	NPB	3.7	438	558	748	0.31	0.16, 0.10
III_p	TCF	3.1	518	18350	1041	3.78	0.29, 0.46
IV^b	NBP	3.0	518	20373	1361	3.22	0.29, 0.53
\boldsymbol{V}^{b}	-	4.2	518	4961	693	0.91	0.30, 0.54

^aITO/PEDOT:PSS/**EML**/BCP/LiF:Al. ^bITO/PEDOT:PSS/**HTL**/Alq3/LiF :Al. ^cTurn-on voltage (V) at luminance of 1 cd/m². ^dEmission maximum. ^eMaximum luminance (cd/m²). ^fCurrent density (mA/cm²) at a maximum luminance. ^g Luminance efficiency (cd/A). ^h *CIE* coordinates (x, y)

3. Conclusion

In conclusion, novel highly fluorescent bis(4-diphenylaminophenyl)carbazole end-capped fluorene was synthesized and characterized. This material showed a greater ability as solution processed blue emitter and hole-transporter for OLEDs than a commonly used NPB. High-efficiency deep blue and Alq3-based green devices with luminance efficiencies and *CIE* coordinates of 0.93 cd/A, (0.16, 0.09), and 3.78 cd/A and (0.29, 0.45) were achieved, respectively. The use of triphenylamine-carbazole substituent might be an effective way to prepare amorphous molecules with excellent electrochemical, thermal and morphological stabilities for OLEDs by forming dendritric structures with other fluorescent or non-fluorescent core units.

4. Experimental

2,7-bis(3,6-dibromocarbazol-9-yl)-9,9-bis-n-hexylfluorene (2)

N-Bromosuccinimide (2.97 g, 16.71 mmol) was added in small portions to a solution of 2,7-bis(carbazol-9-yl)-9,9-bis-*n*-hexylfluorene (1) (2.74 g, 4.12 mmol) in tetrahydrofuran (80 ml). The reaction mixture was stirred at room temperature under N_2 atmosphere for 30 min. The mixture was extracted with dichloromethane (200 ml). The organic phase was separated, washed with water (200 ml x 2), brine solution (100 ml), dried over anhydrous sodium sulfate, filtered and the solvents were removed to dryness. Purification by recrystallization from a mixture of dichloromethane and methanol gave light brown solid. Yield was 3.77 g (95%); IR (KBr): 3056, 2924, 1609, 1467, 1282 and 1057 (Ar-Br) cm⁻¹; ¹H-NMR (300 MHz, CDCl₃) δ 0.82-0.89 (10 H, m), 1.15-1.31 (12 H, m), 2.02-2.08 (4 H, m), 7.30 (4 H, d, *J* = 9.0 Hz), 7.53-7.58 (8 H, m), 8.00 (2 H, d, J = 7.8 Hz) and 8.28 (4 H, d, *J* = 1.8 Hz); ¹³C-NMR (75 MHz, CDCl₃) δ 14.00, 22.49, 24.05, 29.53, 31.51, 40.11, 50.90, 55.86, 111.45, 113.16, 121.40, 121.71, 123.35, 124.03, 125.98, 129.48, 136.01, 139.91, 140.00 and 153.15; HRMS-ESI (*m/z*): [MH⁺] calcd. for $C_{49}H_{45}Br_4N_2$, 977.0311; found, 977.0308.

2,7-Bis[3,6-bis(4-diphenylaminophenyl)carbazol-9-yl]-9,9-bis-n-hexylfluorene (PCF)

A mixture of 2 (1.03 g, 1.05 mmol), 4-(diphenylamino)phenylboronic acid (1.24 g, 4.30 mmol) and Pd(PPh₃)₄ (0.02 g, 0.021 mmol) and 2 M Na₂CO₃ (10 ml, 20 mmol) in THF (15 ml) was degassed with N₂ for 5 min. The mixture was stirred at reflux under N₂ atmosphere for 20 h. After cooling, water (50 ml) was added and the mixture was extracted with dichloromethane (50 ml x 2). The combined organic phase was washed with water (100 ml), brine solution (50 ml), dried over anhydrous sodium sulfate, filtered and the solvents were removed to dryness. Purification by column chromatography over silica gel eluting with a mixture of dichloromethane and hexane followed by recrystallization with a mixture of dichloromethane and methanol to give light brown solids. Yield was 1.26 g (73%); IR (KBr) 3025, 2915, 1583, 1476, 1454, 1270, 1023, 805 and 750 cm⁻¹; ¹H NMR (300 MHz, CDCl₃) δ 0.85 (6 H, t, J = 6.6 Hz), 0.95 (4 H, bs), 1.21-1.28 (12 H, m), 2.09-2.12 (4 H, m), 7.07 (8 H, t, J = 7.2 Hz), 7.19-7.25 (24 H, m), 7.31 (16 H, t, J = 7.2 Hz) 7.3 Hz), 7.55 (4 H, d, J = 8.7 Hz), 7.65 (12 H, d, J = 8.4 Hz), 7.08 (4 H, d, J = 9.0 Hz), 8.03 (2 H, d, J = 9.0 Hz) 8.4 Hz) and 8.44 (4 H, s); 13 C NMR (75 MHz, CDCl₃) δ 14.09, 22.56, 24.11, 29.65, 31.58, 40.28, 55.82, 110.17, 118.51, 121.68, 121.78, 122.78, 124.16, 124.28, 124.41, 125.34, 125.85, 127.94, 129.27, 133.25, 136.14, 136.77, 139.60, 140.68, 146.64, 147.84 and 152.99; HRMS-ESI (m/z): $[MH^{\dagger}]$ calcd. for $C_{121}H_{101}N_6$, 1637.8082; found, 1637.8078; Elemental analysis calcd. for $C_{121}H_{100}N_6$, C, 88.72; H, 6.15; N, 5.13; found, C, 88.77; H, 6.20; N, 5.11.

Device fabrication and testing

OLED devices using **TCF** and NPB as EML with configuration of ITO/PEDOT:PSS/EML(40 nm)/BCP(40 nm)/LiF(0.5 nm):Al(150 nm) and double-layer green OLED devices using **TCF** and NPB as HTL with configuration ITO/PEDOT:PSS/HTL(40 nm)/Alq3(50 nm)/LiF(0.5 nm):Al(150 nm) were

fabricated and characterized as followed. The patterned indium tin oxide (ITO) glass substrate with a sheet resistance 14 Ω/□ (purchased from Kintec Company) was thoroughly cleaned by successive ultrasonic treatment in detergent, deionised water, isopropanol, and acetone, and then dried at 60 °C in a vacuum oven. A 50 nm thick PEDOT:PSS hole injection layer was spin-coated on top of ITO from a 0.75 wt.% dispersion in water at a spin speed of 3000 rpm for 20 s and dried at 200 °C for 15 min under vacuum. Thin films of each organic EML or HTL were deposited on top of PEDOT:PSS layer by spin-coating THF:toluene solution of TCF and NPB (3-1.5% w/v) on an ITO glass substrate at a spin speed of 3000 rpm for 30 second to get a 40 nm thick of EML or HTL layers. The film thickness was measured by using a Tencor α-Step 500 surface profiler. A 40 nm thick hole-blocking layer of BCP or a 50 nm thick greenemitting layer of Alq3 was then deposited on the organic EML or HTL, respectively, by evaporation from resistively heated alumina crucibles at evaporation rate of 0.5-1.0 nm/s in vacuum evaporator deposition (ES280, ANS Technology) under a base pressure of $\sim 10^{-5}$ mbar. The film thickness was monitored and recorded by quartz oscillator thickness meter (TM-350, MAXTEK). The chamber was vented with dry air to load the cathode materials and pumped back; a 0.5 nm thick LiF and a 150 nm thick aluminium layers were the subsequently deposited through a shadow mask on the top of EML/BCP films without braking vacuum to from an active diode areas of 4 mm². The measurement of device efficiency was performed according to M.E. Thomson's protocol and the device external quantum efficiencies were calculated using procedure reported previously. After breaking the chamber the device was characterized immediately in an ambient atmosphere (unsealed device). Current density-voltage-luminescence (J-V-L) characteristics were measured simultaneous by the use of a Keithley 2400 source meter and a Newport 1835C power meter equipped with a Newport 818-UV/CM calibrated silicon photodiode. The EL spectra were acquired by an Ocean Optics USB4000 multichannel spectrometer. All the measurements were performed under ambient atmosphere at room temperature.

PART VI

Synthesis and Properties of Oligofluorene-thiophenes as Emissive Materials for Organic Electroluminescent Devices

1 Introduction

Organic light-emitting diodes (OLEDs) have attracted a great deal of attention due to their applications, such as full-color flat panel displays and general illumination. To achieve a full-color display, the efficient tunability of the emission spectrum to a desired color is an important consideration when designing materials. One way of tuning color is to change the molecular structure. Color tuning via fluorescence and phosphorescence has been studied for many years. By means of the modification of the core and peripheral units of organic molecules and the substitution of various groups at the ligands of iridium or other heavy metal complexes emission colors of these materials can be tuned. Polythiophenes (PTs) and derivatives represent an important class of color tunable light-emitting polymers for OLEDs. Through variation in substituent pattern and concomitant change of the backbone distortion, their emission color can be tuned in a wide range, from blue to deep red and into the NIR. However, there are few reports for color tuning using a series of oligothiophenes for OLEDs. A strong aggregation tendency decreases the PL and EL emission efficiency of these materials. In this study, we have designed simple color tunable electroluminescent materials based on oligofluorene-thiophenes. In this case, molecular aggregation of the oligothiophenes will be effectively suppressed by both 3,6-di-tert-butylcarbazole substituent, which significantly impact the emission behaviour of devices. Owing to its high photoluminescence efficiency in blue and high carrier mobility, pyrene would boost the emissive ability of these materials. Moreover, carbazole could improve hole injection and transport properties, and thermal stability, while the fluorene also has a number of advantages. Herein, we report a detailed synthesis, physical and photophysical properties of oligofluorene-thiophenes end-capped with 3,6-di-tert-butylcarbazole and pyrene, namely **CFTnP** (n = 0-4). Investigation and results on their successful use as colour tunable emitting materials for OLED devices are also reported.

2 Results and discussion

Synthesis

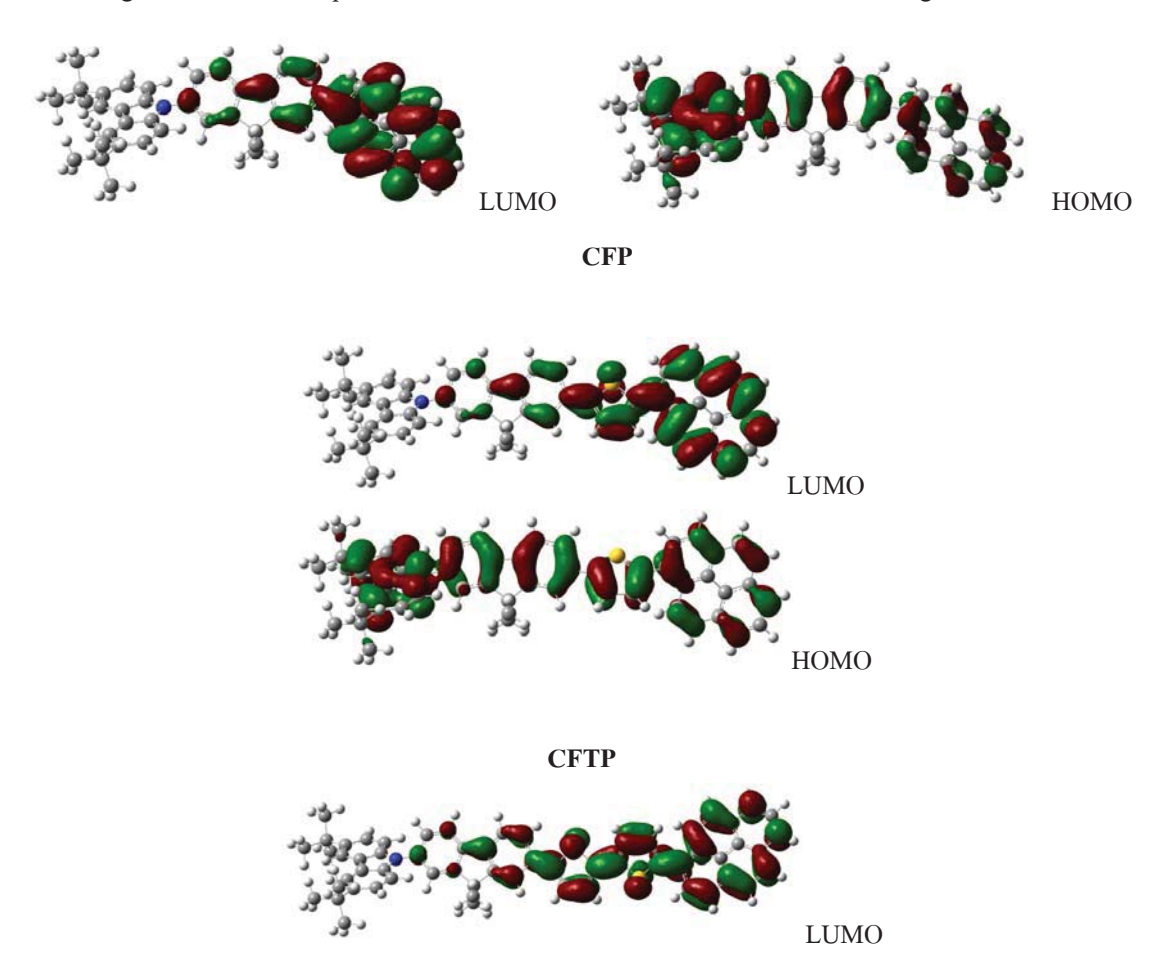
The synthesis of the target molecules **CFTnP** (n = 0-4) is outlined in Scheme 1. A key intermediate **2** was synthesized by Ullmann coupling of available 2,7-dibromo-9,9-bishexylfluorene (1) with 3,6-di-*tert*-butylcarbazole catalyzed by CuI and *trans*-1,2-diaminocyclohexane in the present of K_3PO_4 as base in

refluxing toluene and obtained as white solid in 73% yield. A series of bromo intermediates 4, 6, 8 and 10 were subsequently prepared from 2 in good yields using a combination of Pd catalyzed cross-coupling and bromination reactions in an iterative manner. The former reaction with 2-thiopheneboronic acid catalyzed by Pd(PPh₃)₄ in the presence of Na₂CO₃ was employed to complete a growth of the oligothiophene fragment, and a series of α -substituted oligothiophenes up to the tetramer 3, 5, 7 and 9 were obtained in good yields of 70-81%. The latter bromination with NBS in THF selectively introduced a bromo function to the α -position of the terminal thiophene ring, allowing further cross-coupling reaction to be performed. The bromo intermediates 4, 6, 8 and 10 were prepared in excellent yields. Cross-coupling of these bromo intermediates 4, 6, 8 and 10 with pyrene boronic acid gave the corresponding CFTnP (n = 0-4) in good yields of 65-81% (Scheme 1). Colors of the solid products tainted from colorless to orange solid as a number thiophene units in the molecule increased. Their chemical structures were fully characterized by standard methods. These synthesized materials present good solubility in most organic solvents at room temperature, resulting from the presence of *n*-hexyl groups at the C-9 of fluorene ring. As a result, a uniform, stable and no crystallization thin film should be obtained from a cheap solution casting technique.

Scheme 1 Synthetic route to **CFTnP**. Reagents and conditions: i) 3,6-di-*tert*-butylcarbazole, CuI, K₃PO₄, *trans*-1,2-diaminocyclohexane, toluene, reflux; ii) Pd(PPh₃)₄, 2M Na₂CO₃, THF, reflux; iii) NBS, THF, rt.

Quantum calculation and physical properties

To understand the electronic properties and the geometries of 1-4, quantum chemical calculations were performed using TDDFT/B3LYP/6-31G (d,p) method.⁷ The optimized structures of these compounds revealed that the carbazole moiety attached to the end of the molecules is nearly perpendicular to oligofluorene-thiophene-pyrene plane. However, π -electrons in the HOMO orbitals are able to delocalize over the entire oligofluorene-thiophene-pyrene backbone and carbazole through the lone electron pair of the nitrogen of the carbazole (Fig. 1 and see Supplementary material). In the LUMO orbitals, the excited electrons delocalized over the quinoid-like pyrene-oligothiophene plane, creating a donor- π -acceptor feature. This is due to the electron-acceptor nature of pyrene moieties and the electron-donor property of carbazole uints. The HOMO-LUMO energy gaps (E_g cal.) were calculated to be decreased from 3.12 eV to 2.39 eV with an increase in the π -conjugation length of the oligothiophene units, and these values are in perfect accordance with those estimated from the optical absorption edge (Table 1). However, a slight derivation between the calculated and experimental results was observed. There are factors responsible for the errors in the E_g cal. values because the orbital energy difference between HOMO and LUMO is still an approximate estimation to the transition energy since the transition energy also contains significant contributions from some two-electron integrals. The real situation is that an accurate description of the lowest singlet excited state requires a linear combination of a number of excited configurations.



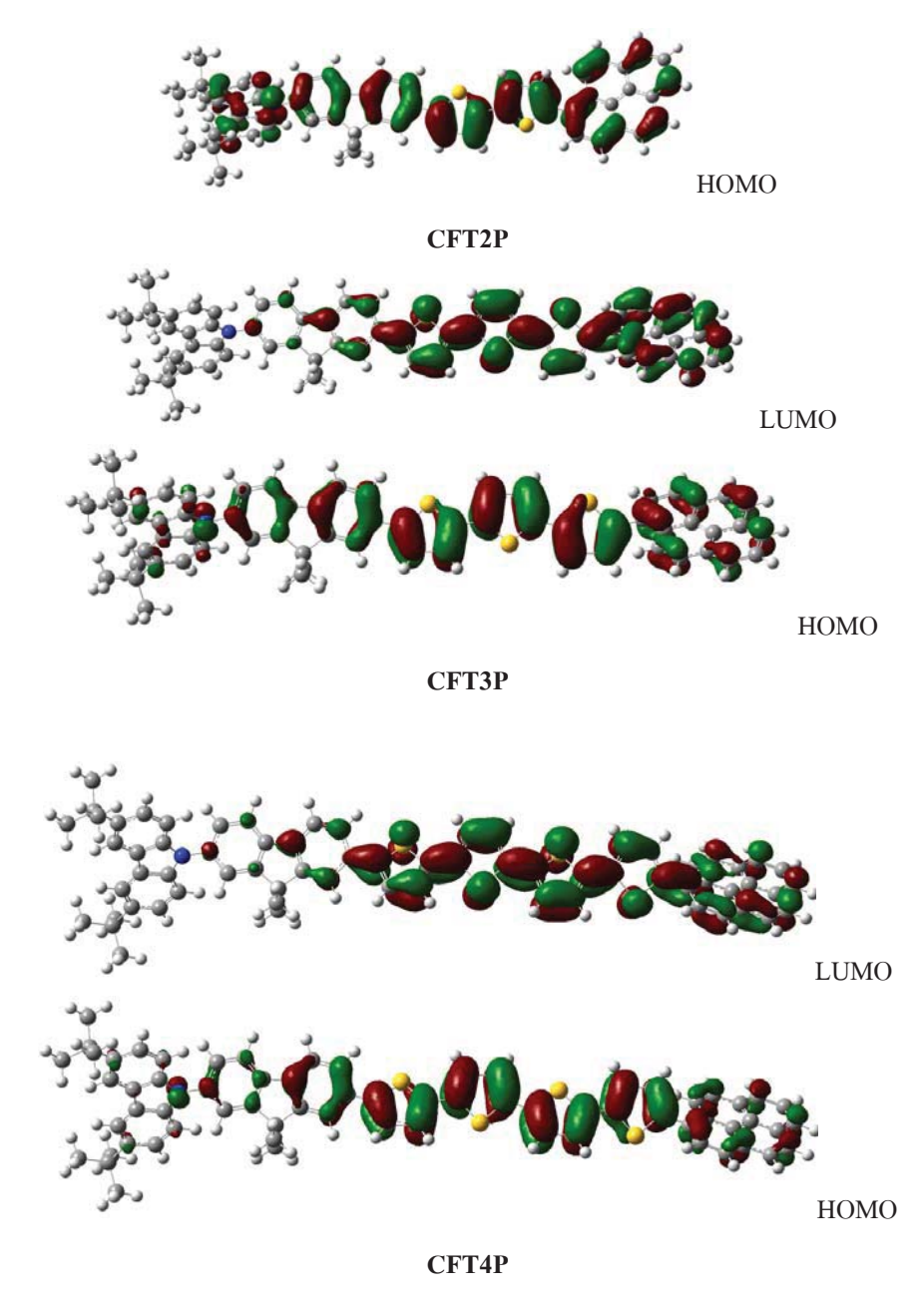


Figure S1 Isodensity surface plots of the molecular orbitals of CFTnP obtained by B3LYP/SVP level of theory. (Isovalue = 0.02).

Photophysical properties of **CFTnP** were investigated in dilute CH_2Cl_2 solution and thin film obtained by thermal evaporation on quart substrate. The pertinent data are presented Fig. 2 and summarized in Table 1. The solution UV-Vis absorption spectra of **CFTnP** showed two major absorption bands. The strong absorption band at longer wavelengths (350-440 nm) corresponding to the π - π * electron transition of the π -conjugated backbone gradually red shifted with the increasing number of thiophene rings because the extent of π -conjugation system in the molecule increased, as expected. The absorption band at 298 nm assigned to the π - π * electron transition of the end-capping carbazole. All compounds in solution were strongly fluorescence with color tuning from deep blue to bright orange as the number of thiophene unit

increased. Fluorescence quantum yields (Φ_F) of these materials ranged from 0.84 to 0.08 (Table 1). The values were found to decrease with the increasing number of thiophene units, which is commonly observed in most cases of oligothiophenes. This is due to with long oligomers the molecules will become extended planar structures and prone to fluorescence quenching brought about by π - π stacking interactions. Their solution fluorescence spectra showed featureless pattern and red shifted as the number of thiophene rings was increased. Upon excitation, either at 298 nm attributed to the absorption of the carbazole moiety or at the absorption of the oligofluorene-thiophene cores (λ_{max}), identical emission spectra were observed, indicating energy or electrons can efficiently transfer from the peripheral carbazole to the inner backbone as observed in the quantum calculation. These materials showed slight stoke Shifts (55-93 nm) suggesting less energy loss during the relaxation process.

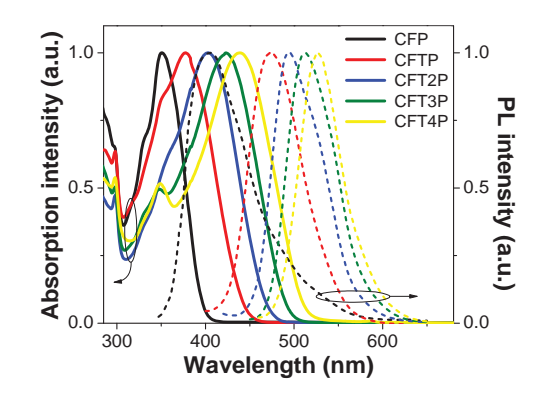


Fig. 2 UV-Vis absorption and PL spectra of CFTnP measured in dilute CH₂Cl₂ solution.

Electrochemical behaviors of all compounds were investigated by cyclic voltammetry (CV), and the resulting data are shown in Fig. 3 and summarized in Table 1. The experiment was carried out in degassed CH_2Cl_2 containing 0.1 M n-Bu₄NPF₆ as a supporting electrolyte under argon atmosphere. CV curves of CFTnP exhibited two quasireversible oxidation processes. The first oxidation wave assigned to the removal of electrons from the terminal carbazole resulting radical cations. Their multiple CV scans revealed identical CV curves with no additional peak at lower potential on the cathodic scan (E_{pc}) being observed suggesting no electrochemical coupling at the 3,6 positions of the peripheral carbazole as they were protected by *tert*-butyl groups and CFTnP are electrochemically stable molecules, as expected. It was found that the oxidation potentials gradually shifted to lower potentials with increasing of the π -conjugation system agreeing to the photophysical results. Similar behaviour has been observed in other end-capped oligothiophenes. The HOMO and LUMO energy levels of CFTnP were calculated from the oxidation onset potentials (E_{onset}) and energy gaps (E_g) and the results are summarized in Table 1. The HOMO energy levels of these materials were in the range of -5.49 to -5.21 eV, matching well with the work function of indium tin oxide (ITO) electrode and favoring the injection and transport of holes. Their LUMO energy levels were in the range of -2.35 to -2.77 eV.

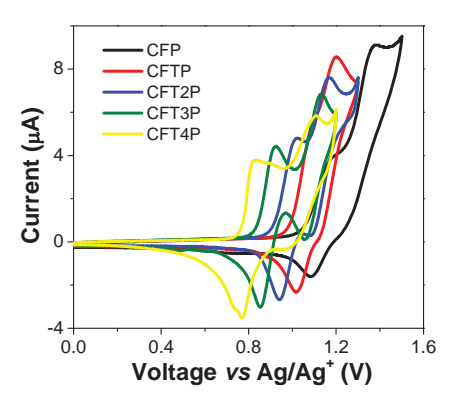


Fig. 3 CV curves of CFTnP measured in CH_2Cl_2/n - Bu_4NPF_6 at scan rate of 50 mV/s.

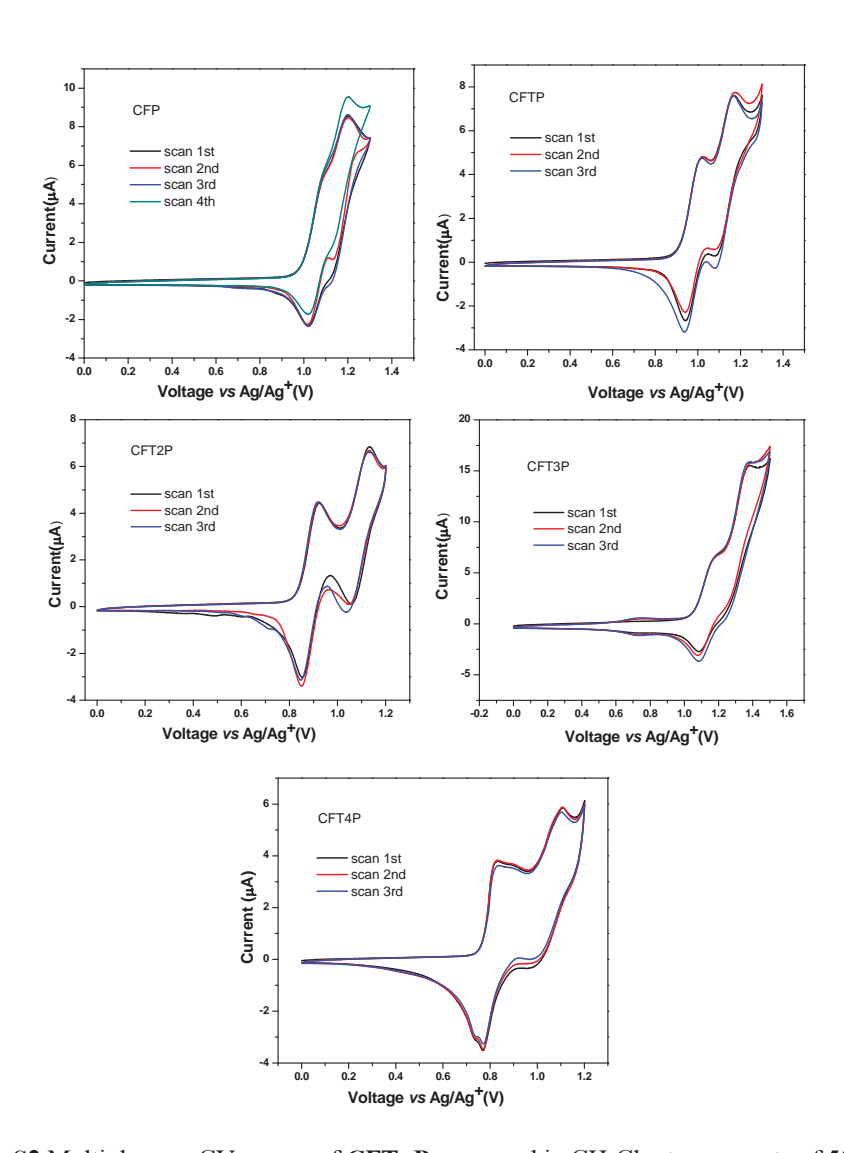


Figure S2 Multiple scan CV curves of CFTnP measured in CH₂Cl₂ at a scan rate of 50 mV/s.

The thermal properties of **CFTnP** were investigated by the thermogravimetric analysis (TGA) and differential scanning calorimetry (DSC), and the results are shown in Fig. 4 and summarized in Table 1. Those results suggested that **CFTnP** were thermally stable materials with temperature at 5% weight loss (T_{5d}) well over 390 °C. In differential scanning calorimetry (DSC) analysis, their thermograms displayed

only endothermic baseline shift owing to glass transition (T_g) ranging from 95 to 118 $^{\circ}$ C with no crystallization and melting peaks at higher temperature being observed. The T_g s were found to steadily increase with the increasing number of thiophene units. The ability of these materials to form a molecular glass with the possibility to prepare thin films from these materials both by evaporation and by solution casting is highly desirable for applications in electroluminescent devices.

Table 1 Physical and photophysical data of CFTnP.

comp	$\lambda_{abs} (nm)^a$	$\boldsymbol{\lambda}_{_{em}}$	$\boldsymbol{\lambda}_{_{em}}$	stokes	$\Phi_{\scriptscriptstyle F}^{^{d}}$	T_g/T_{5d}	E_g	E _g cal.	$E_{1/2}(V)^h$	E _{onset}	HOMO/LU
		$(nm)^a$	(nm)	Shift		(°C) ^e	$(eV)^{f}$	$(eV)^g$		$(V)^h$	MO (eV) ⁱ
			b	(nm) ^c							
CFP	289, 350	406	445	55	0.84	95/390	3.14	3.12	1.13, 1.30	1.05	-5.49/-2.35
CFTP	289, 378	478	483	93	0.36	98/408	2.82	2.88	1.06, 1.16	0.99	-5.43/-2.61
CFT2P	289, 404	495	518	91	0.34	102/416	2.67	2.68	0.98, 1.12	0.92	-5.36/-2.69
CFT3P	289, 424	512	535	90	0.10	116/420	2.54	2.50	0.87, 1.09	0.84	-5.28/-2.74
CFT4P	289, 440	528	553	88	0.08	118/445	2.44	2.39	0.80, 1.04	0.77	-5.21/-2.77

^a Measured in a dilute CH₂Cl₂ solution.

^b Measured on a vapor deposition thin film and excited at the absorption maxima.

 $^{^{\}text{c}}$ Stokes shift calculated from the difference between λ_{max} of the absorption and emission spectra.

^d Determined in CH_2Cl_2 solutions (A < 0.1) at room temperature using quinine sulfate solution in 0.01 M H_2SO_4 ($\Phi_F = 0.54$) as a standard.

 $^{^{\}circ}$ Obtained from DSC on the 2 $^{\rm nd}$ heating cycle and TGA measurements under N_2 at a heating rate of 10 $^{\circ}$ C/min.

^fEstimated from the onset of the absorption spectra ($E_g = 1240/\lambda_{onset}$).

^g Obtained from quantum chemical calculation using TDDFT/ B3LYP/6-31G (d,p).

^h Measured using a three electrode system fitted with a glassy carbon working electrode, a platinum rod counter electrode and SCE reference electrode in degassed CH₂Cl₂ containing 0.1 M *n*-Bu₄NPF₆ as a supporting electrolyte at a scan rate of 50 mV/s.

ⁱ Calculated using the empirical equation: $HOMO = -(4.44 + E_{onset})$ and $LUMO = HOMO + E_{g}$.

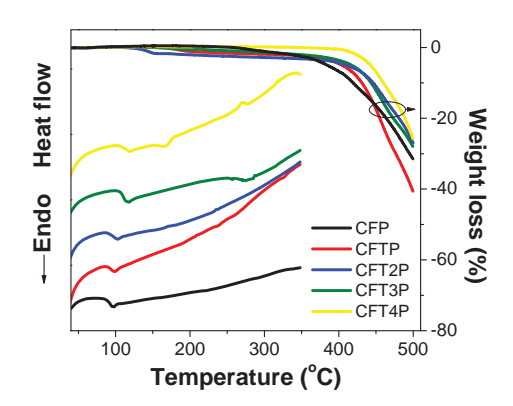


Fig. 4 DSC (2nd heating) and TAG thermograms of **CFTnP** measured under N₂ at heating rate of 10 °C/min.

Electroluminescence properties

To investigate the electroluminescence properties of CFTnP (n = 0-4), OLEDs (devices I-V) were fabricated using these materials as emitting layers (EML) with the device configuration of ITO/PEDOT:PSS/EML(50 nm) /BCP(40 nm)/LiF(0.5 nm):Al(150 nm). Conductive polymer poly(3,4ethylenedioxythiophene):poly(4-styrenesulfonate) (PEDOT:PSS) as hole injection layer and 2,9-dimethyl-4,7-diphenyl-1,10-phenanthroline (BCP) as hole blocking layer were also used to enable high-performance devices (Fig. 5). The electroluminescent (EL) spectra and voltage-luminance and voltage-current density (J-V-L) characteristics of the devices are shown in Fig. 6 and 7, and their electrical parameters are summarized in Table 2. The results revealed that these devices emitted a bright light of various colors including deep blue, sky blue, green, yellow green and orange. The EL spectra of the devices gradually changed from deep blue (434 nm) to orange (552 nm) with the increasing number of thiophene units in the EML molecules (Fig. 6). The spectra were analogous to their corresponding thin film PL spectra indicating that the EL emission originates from the singlet-excited states of the EML materials. Weak emission shoulder corresponding to excimer and exciplex emissions was observed in all diodes. The former might arise from the attached pyrene unit, which is well known for its excimer formation. The latter is often observed at the interface of organic/organic layers in an OLED and can be tuned by adjusting the thickness of those layers. More importantly, a stable emission was obtained from all diodes with the EL spectra and CIE coordinates did not change over the entire applied voltages (see Supplementary material). Device I and devices (III, VI) emitted deep blue (434 nm) and green (512 nm) light with CIE coordinates of (0.16, 0.14) and (0.28, 0.62), receptively, which are close to the National Television System Committee (NTSC) deep blue (0.14, 0.10) and green (0.26, 0.65) standards.

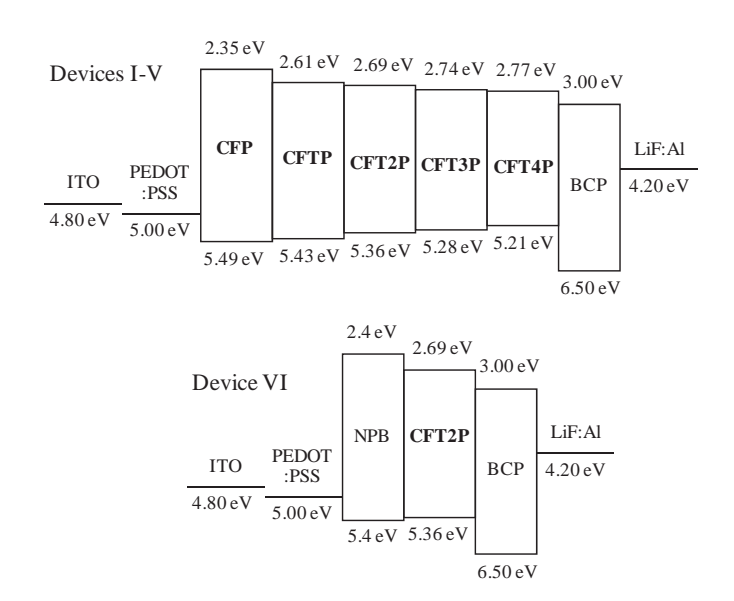


Fig. 5 Schemetic energy digrams of the fabricated OLED devices.

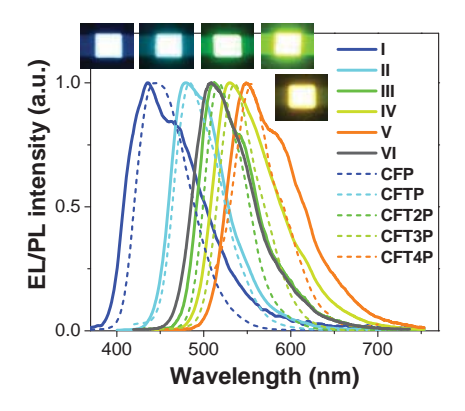


Fig. 6 EL spectra of OLED devices.

The light turn-on voltage at 1 cd/m² for all devices was in the range of 2.2-4.1 V and the operating voltage at 100 cd/m² was in the range of 2.7-5.3 V, indicating good performance is achieved for all the devices (Fig. 7 and 8, Table 2). Device III having CFT2P as EML showed the best performance with a high maximum brightness of 31760 cd/m² at 9.8 V, a low turn-on voltage of 3.1 V and a maximum luminous efficiency of 3.73 cd/A. A comparable device performance was observed from devices IV (CFT3P as EML) and V (CFT4P as EML). However, the devices (I, II) using CFT and CFTP as EML showed lower performance in terms of maximum brightness, turn-on voltage and maximum luminous efficiency. In a view point of simple molecular structure, color quality and device efficiency these materials are among good non doped deep emitters reported. In order to explain the different efficiencies of the OLED devices, analysis of band energy diagrams of all devices revealed that the HOMO levels of all EML materials (5.21-5.49 eV) lied between those of PEDOT:PSS (5.00 eV) and BCP (6.50 eV) (Fig. 5). The injection barriers for holes to migrate from the PEDOT:PSS to EML range from 0.21 eV to 0.49 eV, while the injection barriers for electrons to migrate from BCP to EML range from 0.23 eV to 0.65 eV.

Such energy barriers are progressively narrower from device I (CFP as EML) to device V (CFT4P as EML). This suggests that a migration of holes from the PEDOT:PSS to EML layer and injection of electrons from BCP to ELM are more effective in devices III, IV and V compared to devices I and II, resulting the charge efficiently recombine in the emitting layer and better device performance. It has been demonstrated that the efficiency of an OLED depends both on the balance of electrons and holes and the Φ_F of the emitter.

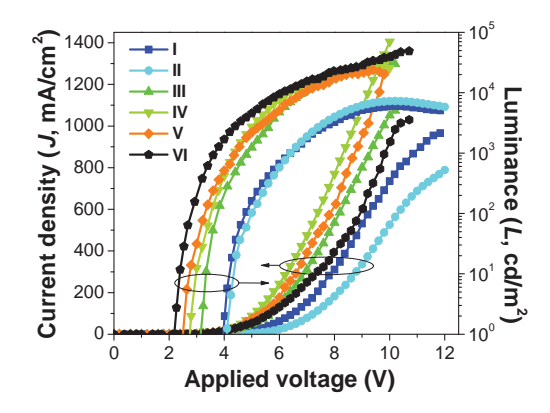


Fig. 7 J-V-L characteristics of OLED devices.

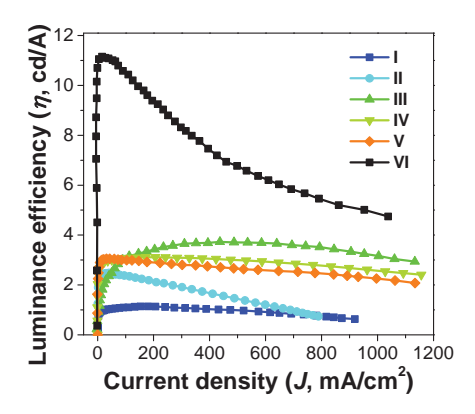


Fig. 8 Variation in luminance efficiency with current density of OLED devices.

As the most-promising result was obtained from device VI, which incorporated N,N'-diphenyl-N,N'-bis(1-naphthyl)-(1,1'-biphenyl)-4,4'-diamine (NPB) as electron blocking layer (EBL). Since the LUMO energy level of NPB (2.40 eV) was higher than that of **CFT2P** (2.69 eV), the NPB layer can block an injected electron from BCP to trap in EML layer which eventually recombines with the captured hole. We found that the incorporation of NPB between PEDOT:PSS and **CFT2P** (as EML) layers not only increased the maximum luminance to 48800 cd/m² (η of 11.15 cd/A), but also decreased the turn-on voltage from 3.1 V to 2.2 V, which is considered to be one of the lowest turn-on voltages for a green OLED (device VI). Moreover, the EL spectrum of this diode was identical to the EL of device III and solid state PL of **CFT2P**.

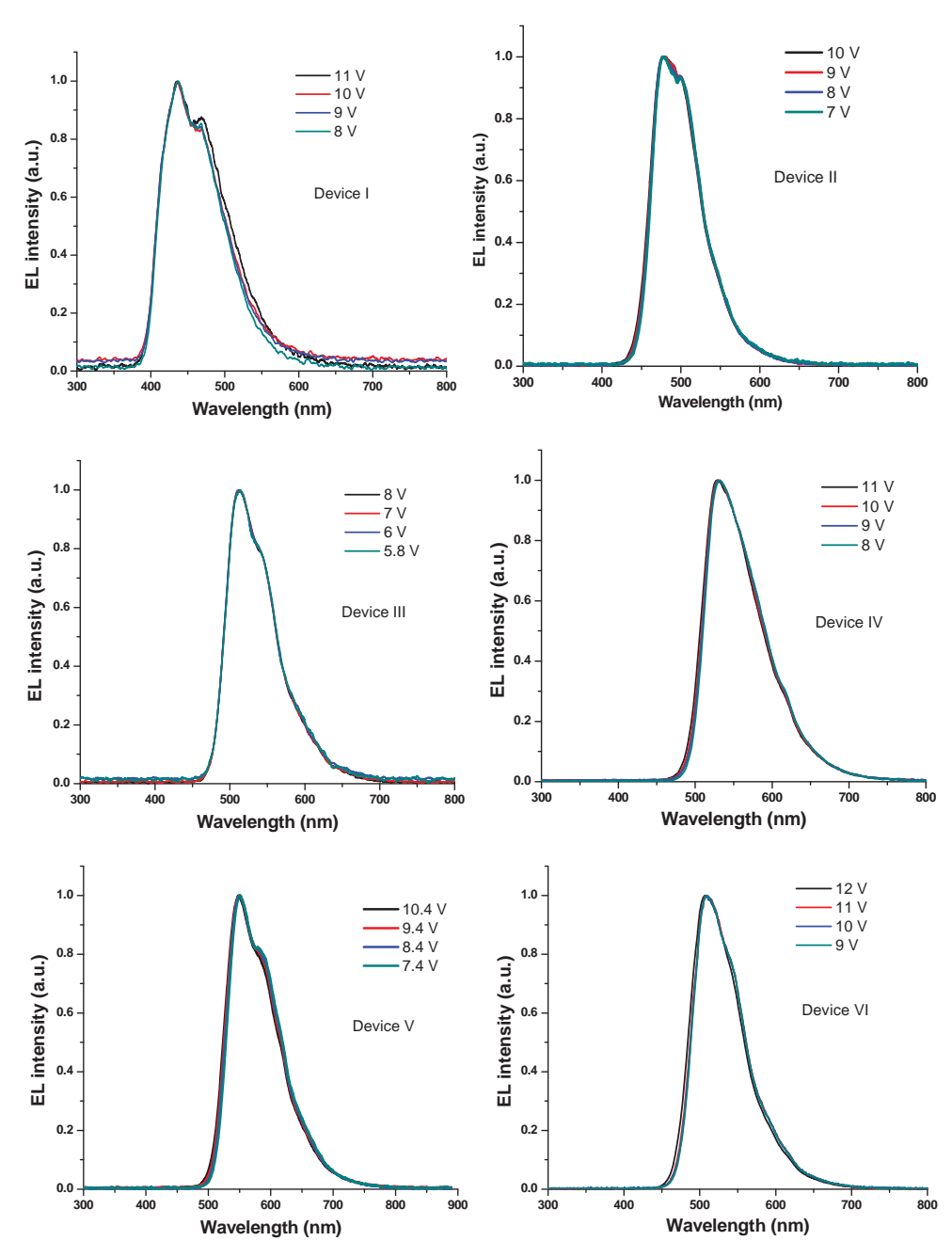


Figure S5 Normalized EL spectra of OLED devices I-VI under different applied voltages.

Table 2 Device characteristics of OLEDs with CFTnP as either EML.

device	structure	$V_{ m on}^{a}$	$\lambda_{\rm em}^{}$	$L_{\mathrm{max}}^{}\mathrm{c}}$	${\it J}^{ m d}$	$\eta^{^{e}}$	EQE	CIE ^g
I	ITO/PEDOT:PSS/CFP/BCP/LiF:Al	4.0	434	6033	767	1.14	0.12	0.16, 0.14
II	ITO/PEDOT:PSS/CFTP/BCP/LiF:Al	4.1	480	7277	563	2.48	0.16	0.16, 0.36
III	ITO/PEDOT:PSS/CFT2P/BCP/LiF:Al	3.1	512	31760	1004	3.73	0.16	0.28, 0.62
IV	ITO/PEDOT:PSS/CFT3P/BCP/LiF:Al	2.8	531	28722	1284	3.11	0.13	0.37, 0.59
V	ITO/PEDOT:PSS/CFT4P/BCP/LiF:Al	2.5	552	24096	1089	3.06	0.13	0.45, 0.51
VI	ITO/PEDOT:PSS/NPB/ CFT2P /BCP/LiF:Al	2.2	509	48800	1029	11.15	0.46	0.27, 0.61

^a Turn-on voltage (V) at luminance of 1 cd/m².

^b Emission maximum.

^c Maximum luminance (cd/m²).

^d Current density (mA/cm²) at maximum luminance.

^e Luminance efficiency (cd/A).

^f External quantum efficiency (%).

^g CIE coordinates (x, y)

3. Conclusions

In conclusion, we have demonstrated a simple and efficient way for tuning color of emissive materials using simple structure oligofluorene-thiophenes end-capped with 3,6-di-*tert*-butylcarbazole and pyrene. The theoretical calculation revealed that the carbazole moiety attached to the end of the molecules is nearly perpendicular to oligofluorene-thiophene-pyrene plane and π -electrons in the ground state delocalize over the entire molecule. The synthesized materials **CPTnF** showed stable electrochemical and thermal properties. OLED devices of these materials emitted brightly in various colors from deep blue to orange. Particularly, deep blue (*CIE* coordinates of 0.16, 0.14) and green (*CIE* coordinates of 0.27, 0.61) devices showed high color quality closed to the NTSC standardswith high luminance efficiencies of 1.14 and 11.15 cd/A, respectively. High EL efficiencies and good color qualities made these materials very promising for display applications.

4. Experimental

General procedure

All reagents were purchased from Aldrich, Acros or Fluka and used without further purification. All solvents were supplied by Thai companies and used without further distillation. Tetrahydrofuran (THF) was refluxed with sodium and benzophenone, and freshly distilled prior to use. Dichloromethane for cyclic voltammetry (CV) measurements was washed with conc. H₂SO₄ and distilled twice from calcium hydride.

 1 H and 13 C nuclear magnetic resonance (NMR) spectra were recorded on a Brüker AVANCE 300 MHz spectrometer with tetramethylsilane as the internal reference using CDCl₃ as solvent in all cases. Infrared (IR) spectra were measured on a Perkin-Elmer FTIR spectroscopy spectrum RXI spectrometer as potassium bromide (KBr) disc. Ultraviolet-visible (UV-Vis) spectra were recorded as a diluted solution in spectroscopic grade dichloromethane on a Perkin-Elmer UV Lambda 25 spectrometer. Photoluminescence spectra and the fluorescence quantum yields ($\Phi_{\rm F}$) were recorded with a Perkin-Elmer LS 50B Luminescence Spectrometer as a dilute solution in spectroscopic grade dichloromethane and thin film obtained by thermal deposition. The fluorescence quantum yields ($\Phi_{\rm F}$) were determined by comparison with a fluorescence standard of known fluorescence quantum yield value according to the following equation:

$$\Phi_{x} = \Phi_{ST} \left(\frac{Slope_{x}}{Slope_{ST}} \right) \left(\frac{\eta_{x}^{2}}{\eta_{ST}^{2}} \right) \tag{1}$$

Where the subscripts x refer to the unknown samples and ST refers to the standard quinine sulfate solution in 0.01 M $\rm H_2SO_4$, whose fluorescence quantum yield is known to be 0.54. Φ is the fluorescence quantum yield, Slope is the slope from the plot of integrated fluorescence intensity vs absorbance, and η is the refractive index of the solvent. The refractive indexes of the solvents were taken as 1.424 and 1.333 for $\rm CH_2Cl_2$ and 0.01 M $\rm H_2SO_4$, respectively.

Differential scanning carolimetry (DSC) analysis and thermogravimetry analysis (TGA) were performed on a METTLER DSC823e thermal analyzer and a Rigaku TG-DTA 8120 thermal analyzer, respectively, with heating rate of 10 °C/min under nitrogen atmosphere. Cyclic voltammetry (CV) measurements were carried out on an Autolab Potentiostat PGSTAT 12 with a three electrode system (platinum counter electrode, glassy carbon working electrode and Ag/Ag⁺ reference electrode) at scan rate of 50 mV/s in dichloromethane under argon atmosphere. The concentrations of an analytical material and supporting electrolyte tetrabutyl ammonium hexafluorophosphate (*n*-Bu₄NPF₆) were 10⁻³ M and 0.1 M, respectively. Melting points were measured using an Electrothermal IA 9100 series of digital melting point instrument and are uncorrected. High resolution mass spectrometry (HRMS) analysis was performed by Mass Spectrometry Unit, Mahidol University, Thailand using a Bruker Daltonics (Bremen, Germany) Autoflex II Matrix-Assisted Laser Desoprtion/Ionization-Time of Flight Mass Spectrometer.

The ground state geometries were fully optimized using density functional theory (DFT) at the B3LYP/6-31G (d,p) level, as implemented in Gaussian 03. TDDFT/B3LYP calculation of lowest excitation energies were performed at the optimized geometries of the ground states.

Fabrication and characterization of OLEDs

OLED devices using CFTP as EML with configuration of ITO/PEDOT:PSS/EML(50 nm)/BCP(40 nm)/LiF(0.5 nm):Al(150 nm) were fabricated and characterized as followed. The patterned indium tin oxide (ITO) glass substrate with a sheet resistance $14~\Omega/\Box$ (purchased from Kintec Company) was thoroughly cleaned by successive ultrasonic treatment in detergent, deionized water, isopropanol, and acetone, and then dried at 60 °C in a vacuum oven. A 50 nm thick PEDOT:PSS hole injection layer was spin-coated on top of ITO from a 0.75 wt.% dispersion in water at a spin speed of 3000 rpm for 20 s and dried at 200 °C for 15 min under vacuum. Thin films of each organic EML or HTL were deposited on top of PEDOT:PSS layer by evaporation from resistively heated alumina crucibles at evaporation rate of 0.5-1.0 nm/s in vacuum evaporator deposition (ES280, ANS Technology) under a base pressure of ~ 10^{-5} mbar. The film thickness was monitored and recorded by quartz oscillator thickness meter (TM-350, MAXTEK). A 40 nm thick hole-blocking layer of BCP or a 50 nm thick green-emitting layer of Alq3 was then deposited on the organic EML or HTL, respectively, without breaking the vacuum chamber. The chamber was vented with dry air to load the cathode materials and pumped back; a 0.5 nm thick LiF and a 150 nm

thick aluminum layers were the subsequently deposited through a shadow mask on the top of EML/HTL film without braking vacuum to from an active diode areas of 4 mm². The measurement of device efficiency was performed according to M.E. Thomson's protocol and the device external quantum efficiencies were calculated using procedure reported previously. Current density-voltage-luminescence (*J-V-L*) characteristics were measured simultaneous by the use of a Keithley 2400 source meter and a Newport 1835C power meter equipped with a Newport 818-UV/CM calibrated silicon photodiode. The EL spectra were acquired by an Ocean Optics USB4000 multichannel spectrometer. All the measurements were performed under ambient atmosphere at room temperature.

Synthesis and characterization

2-(3,6-Di-tert-butylcarbazol-N-yl)-7-bromo-9,9-dihexylfluorene (2)

A stirred mixture of 2,7-dibromo-9,9-dihexylfluorene (1) (7.5 g, 23.18 mmol), 3,6-di-*tert*-butylcarbazole (2.16 g, 7.33 mmol), CuI (0.74 g, 3.86 mmol), K_3PO_4 (4.1 g, 19.3 mmol) and *trans*-1,2-diaminocyclohexane in toluene (70 ml) was refluxed for 24 h under N_2 atmosphere. After cooling, the reaction mixture was extracted with dichloromethane (100 ml x 3). The combined organic phase was washed with water (100 ml), brine solution (100 ml), dried over sodium sulfate anhydrous, filtered and the solvent was remove in vacuum. Purification by column chromatography using silica gel eluting with hexane afforded viscous oil (3.69 g, 73%). FT-IR (KBr) 3028, 2954, 2926, 2853, 1617, 1560, 1489, 1474, 1364, 876, 811, and 614 cm⁻¹; 1 H-NMR (300 MHz, CDCl₃) δ 8.18 (2H, s), 7.86 (1H, d, J = 7.7 Hz), 7.63 (1H, d, J = 8.5 Hz), 7.51 (6H, m), 7.39 (2H, d, J = 8.6 Hz), 1.98 (4H, m), 1.53 (16H, m) and 0.95 (6H, m) ppm; 13 C-NMR (75 MHz, CDCl₃) δ 153.24, 152.14, 142.91, 139.51, 137.35, 130.22, 126.29, 125.52, 123.62, 123.62, 121.42, 121.16, 120.87, 116.36, 109.19, 55.71, 40.36, 40.25, 32.06, 31.86, 29.96, 29.74, 29.27, 23.91, 22.64 and 14.10 ppm; HRMS-ESI calcd for $C_{45}H_{56}BrN$: m/z 689.3596 found 689.3371 [M $^{+}$]. 2-(3, 6-Di-tert-butylcarbazol-N-yl)-7-(thiophen-2-yl)-9,9-dihexylfluorene (3)

A mixture of **2** (3.5 g, 5.16 mmol), 2-thiopheneboronic acid (0.77 g, 5.92 mmol), $Pd(PPh_3)_4$ (0.042 g, 0.036 mmol) and an aqueous Na_2CO_3 solution (2 M, 25.8 ml) in THF (30 ml) was degas in with N_2 at 2 min. The mixture was heated at reflux under N_2 atmosphere for 24 h. After the mixture cooled to room temperature water (50 ml) was added. The mixture was extracted with dichloromethane (50 ml x 3). The combined organic phase was washed with water (50 ml), brine solution (50 ml) dried over anhydrous sodium sulfate, filtered and the organic solvent was removed in vacuum. Purification by column chromatography using silica gel eluting with hexane afforded viscous oil, which then solidified to light yellow solids (2.68 g, 75%). m.p. 56-58 °C; FT-IR (KBr) 2950, 2925, 2854, 1608, 1583, 1488, 1473, 1453, 1390, 1376, 1358, 1294, 1259, 1229, 1172, 1148, 1103, 1078, 1030, 922, 875, 854, 837, 808, 757,691, 672, 652 and 614 cm⁻¹; ¹H-NMR (300 MHz, CDCl₃) δ 8.26 (2H, s), 8.10 (1H, d, J = 8.7 Hz), 7.81 (1H, d, J = 7.8 Hz), 7.73-7.69 (2H, m), 7.62-7.55 (4H, m), 7.49-7.46 (3H, m), 7.37-7.36 (1H, m), 7.19-7.17 (1H, m),

2.13-2.07 (4H, m), 1.56-1.50 (18H, m),1.89 (12H, m) and 0.96-0.84 (10H, m) ppm; 13 C-NMR (75 MHz, CDCl₃) δ 152.67, 151.84, 145.10, 142.85, 140.02, 139.48, 139.39, 136.97, 133.48, 128.15, 125.43, 125.16, 124.69, 123.63, 123.42, 123.05, 121.43, 120.79, 120.25, 116.37, 109.29, 55.52, 40.43, 34.81, 32.10, 31.60, 29.72, 23.94, 22.66 and 14.12 ppm; HRMS-ESI calcd for $C_{49}H_{59}NS$: m/z 693.4368 found 693.3612 [M †]. 2-(3,6-Di-tert-butylcarbazol-N-yl)-7-(2,2'-bithiophen-5-yl)-9,9-dihexylfluorene (5)

5 was synthesized from 4 in similar manner to 3 and obtained as light yellow solids (4.31 g, 74%). m.p $70\text{-}72~^\circ\text{C}$; FT-IR (KBr) 3044, 2952, 2925, 2855, 1612, 1480, 1362, 1324, 1290, 1261, 1233, 1033, 877, 837, 794, 691 and 613 cm $^{-1}$; $^{1}\text{H-NMR}$ (300 MHz, CDCl $_{3}$) δ 8.28 (2H, s), 7.93 (1H, d, J = 7.5 Hz), 7.80 (1H, d, J = 7.5 Hz), 7.70 (2H, d, J = 7.2 Hz), 7.63-7.57 (4H, m) 7.50 (2H, d, J = 8.4 Hz), 7.38 (1H, s), 7.26 (3H, d, J = 9 Hz, J = 6 Hz), 7.11-7.08 (1H, m), 2.12 (4H, m), 1.58 (18H, m), 1.12 (12H, m) and 0.87 (10H, m) ppm; $^{13}\text{C-NMR}$ (75 MHz, CDCl $_{3}$) δ 152.73, 151.96, 143.82, 142.91, 140.20, 139.45, 137.59, 137.09, 136.62, 133.17, 127.96, 125.50, 124.86, 124.73, 124.42, 123.71, 123.66, 123.50, 121.49, 120.84, 120.34, 119.93, 116.40, 109.34, 55.57, 40.45, 34.84, 32.13, 31.63, 29.76, 27.02, 24.00, 22.68 and 14.22 ppm; HRMS-ESI calcd for $\text{C}_{53}\text{H}_{61}\text{NS}_{2}$: m/z 775.4245 found 774.8981 [M $^{+}$].

2-(3,6-Di-tert-butylcarbazol-N-yl)-7-(2,2':5',2''-terthiophen-5-yl)-9,9-dihexylfluorene (7)

7 was synthesized from **6** in similar manner to **3** and obtained as yellow solids (1.10 g, 70%). m.p. 92-94 °C; FT-IR (KBr) 3042, 2952, 2925, 2855, 1609, 1477, 1362, 1324, 1294, 1262, 1233, 1033, 877, 837, 791, 690 and 614 cm⁻¹; 1 H-NMR (300 MHz, CDCl₃) δ 8.22 (2H, s), 7.90 (1H, d, J=8.7 Hz), 7.77 (1H, d, J = 7.8 Hz), 7.67-7.63 (2H, m), 7.58-7.51 (4H, m), 7.44 (2H, d, J = 8.4 Hz), 7.35 (1H, d, J = 3.6 Hz), 7.26-7.22 (3H, m), 7.16-7.13 (2H, m), 7.07-7.04 (1H, m), 2.09-2.04 (4H, m), 1.54 (18H, m),1.15(12H, m) and 0.85-0.81 (10H, m) ppm; 13 C-NMR (75 MHz, CDCl₃) δ 152.68, 151.93, 143.91, 142.87, 140.22, 139.38, 137.17, 137.06, 136.30, 136.24, 133.03, 127.95, 125.45, 124.81, 124.64, 124.56, 124.46, 124.18, 123.75, 123.62, 123.43, 121.43, 120.81, 120.31, 119.88, 116.36, 109.28, 55.53, 40.40, 34.79, 32.08, 31.59, 29.27, 23.95, 22.64 and 14.10 ppm; HRMS-ESI calcd for $C_{57}H_{63}NS_3$: m/z 857.4123 found 857.5636 [M $^+$]. 2-(3,6-Di-tert-butylcarbazol-N-yl)-7-(2,2':5',2'':5'',2'''-quaterthiophen-5-yl)-9,9-dihexylfluorene (9)

9 was synthesized from **8** in similar manner to **3** and obtained as pale orange solids (1.38 g, 81%). m.p. 119-120 °C; FT-IR (KBr) 3064, 2951, 2924, 2854, 2361, 1608, 1475, 1362, 1323, 1293, 1261, 1231, 1033, 876, 834, 808, 790, 741, 688, 614 cm⁻¹; ¹H-NMR (300 MHz, CDCl₃) δ 8.17 (2H, s), 7.88 (1H, d, J = 8.4 Hz), 7.76 (1H, d, J = 7.8 Hz), 7.66-7.47 (6H, m), 7.42-7.34 (3H, m), 7.26-7.20 (3H, m), 7.16-7.03 (5H, m), 2.06-2.00 (4H, m), 1.51-1.49 (18H, m), 1.12 (12H, m) and 0.82-0.78 (10H, m) ppm; ¹³C-NMR (75 MHz, CDCl₃) δ 152.65, 151.90, 144.01, 142.83, 140.23, 139.33, 137.03, 136.40, 136.12, 135.88, 132.96, 135.88, 132.96, 127.93, 125.42, 124.78, 124.69, 124.61, 124.44, 124.38, 124.29, 124.23, 123.79, 123.57,

 $123.38,\ 121.39,\ 120.77,\ 120.26,\ 119.86,\ 116.31,\ 109.22,\ 55.50,\ 40.36,\ 34.76,\ 32.03,\ 31.54,\ 29.66,\ 26.92,$ $23.90,\ 22.59\ \text{and}\ 14.04\ \text{ppm};\ \text{HRMS-ESI}\ \text{calcd}\ \text{for}\ \text{C}_{61}\text{H}_{65}\text{NS}_4;\ \text{m/z}\ 939.4000\ \text{found}\ 940.4363\ [\text{MH}^{^{\dag}}].$

2-(3,6-Di-tert-butylcarbazol-N-yl)-7-(5-bromothiophen-2-yl)-9,9-dihexylfluorene (4)

N-bromosuccinamide (0.165 g, 0.927 mmol) was added in small portions to a stirred solution of **3** (0.63 g, 0.929 mmol) in THF (20 ml). After being stirred at room temperature for 30 min, water was added. The mixture was extracted with DCM (30 ml x 3). The combined organic phase was washed with water (50 ml), brine solution (50 ml), dried over anhydrous sodium sulfate, filtered and the solvent was remove in vacuum. Purification by short column chromatography using silica gel eluting with dichloromethane:hexane (5:95) gave light yellow solids (0.68 g, 95%). m.p. 77-80 °C; FT-IR (KBr) 3042, 2954, 2926, 2855, 1610, 1584, 1490, 1474, 1362, 1324, 1294, 1262, 1233, 1201, 877, 809, 790, 714 and 614 cm⁻¹; ¹H-NMR (300 MHz, CDCl₃) δ 8.18 (2H, s), 7.87 (1H, d, J = 8.7 Hz), 7.74 (1H, d, J = 7.8 Hz), 7.56-7.47 (6H, m), 7.39 (2H, d, J = 8.7 Hz), 7.15 (1H, d, J = 3.6 Hz), 7.07 (1H, d, J = 3.9 Hz), 2.04-21.98 (4H, m), 1.52 (18H, m),1.19-1.11 (12H, m) and 0.82-0.77 (10H, m) ppm; ¹³C-NMR (75 MHz, CDCl₃) δ 152.64, 151.94, 146.54, 142.85, 140.41, 139.33, 139.22, 137.14, 132.63, 130.88, 125.44, 124.79, 123.56, 123.40, 123.09, 121.41, 120.81, 120.28, 119.91, 116.31, 111.14, 109.20, 55.50, 40.32, 34.75, 32.03, 31.51, 29.63, 23.88, 22.56 and 14.00 ppm; HRMS-ESI calcd for $C_{49}H_{58}BrNS$: m/z 771.3473 found 772.3613 [MH⁺].

2-(3,6-Di-tert-butylcarbazol-N-yl)-7-(5'-bromo-2,2'-bithiophen-5-yl)-9,9-dihexylfluorene (6)

6 was synthesized from **5** in similar manner to **4** and obtained as light yellow solids (3.24 g, 98). m.p. 87-89 °C; FT-IR (KBr) 3042, 2953, 2925, 2855, 2360, 1609, 1475, 1362, 1323, 1294, 1261, 1233, 968, 876, 809, 788 and 614 cm⁻¹; ¹H-NMR (300 MHz, CDCl₃) δ 8.17 (2H, s), 7.88 (1H, d, J = 8.4 Hz), 7.75 (1H, d, J = 8.4 Hz), 7.64-7.58 (6H, m), 7.39 (2H, d, J = 8.7 Hz), 7.30 (1H, d, J = 3.9 Hz), 7.13 (1H, d, J = 3.6 Hz), 7.02-6.97 (2H, m), 2.06-2.04 (4H, m), 1.49 (18H, m), 1.27-1.12 (12H, m) and 0.82-0.77 (10H, m) ppm; ¹³C-NMR (75 MHz, CDCl₃) δ 152.65, 151.91, 144.33, 142.84, 140.33, 139.33, 139.29, 139.00, 137.09, 135.39, 132.83, 130.71, 125.43, 124.92, 124.84, 123.65, 123.62, 123.56, 123.40, 121.41, 120.78, 120.26, 119.92, 116.31, 110.92, 109.22, 55.50, 40.35, 34.75, 31.93, 31.53, 29.65, 23.89, 22.57 and 14.02 ppm; HRMS-ESI calcd for C₅₃H₆₀BrNS₂: m/z 853.3351 found 854.3693 [MH⁺].

2-(3,6-Di-tert-butylcarbazol-N-yl)-7-(5"-bromo-2,2':5',2"-terthiophen-5-yl)-9,9-dihexylfluorene (8)

8 was synthesized from **7** in similar manner to **4** and obtained as yellow solids (3.12 g, 99%). m.p. 104-106 °C; FT-IR (KBr) 3042, 2926, 2953, 2855, 2361, 1609, 1476, 1362, 1324, 1294,1261, 1233, 968, 877, 809, 789 and 614 cm⁻¹; ¹H-NMR (300 MHz, CDCl₃) δ 8.19 (2H, s), 7.89 (1H, d, J = 8.4 Hz), 7.76 (1H, d, J = 7.8 Hz), 7.66-7.48 (6H, m), 7.40 (2H, d, J = 8.4 Hz), 7.34 (1H, d, J = 3.6 Hz), 7.20 (1H, d, J = 3.9 Hz),

7.13 (1H, d, J = 3.6 Hz), 7.05 (1H, d, J = 3.9 Hz), 6.99 (1H, d, J = 3.6 Hz), 6.94 (1H, d, J = 3.9 Hz), 2.06-2.01 (4H, m), 1.49-1.44 (18H, m), 1.12 (12H, m) and 0.82-0.78 (10H, m) ppm; ¹³C-NMR (75 MHz, CDCl₃) δ 152.65, 151.91, 144.21, 142.84, 140.29, 139.33, 138.62, 137.07, 136.80, 135.89, 135.05, 132.90, 130.73, 125.43, 124.83, 124.70, 124.13, 123.75,123.56, 123.40, 121.40, 120.77, 120.26, 119.88, 116.31, 111.11, 109.22, 55.05, 40.36, 34.75, 32.03, 31.53, 29.65, 23.90, 22.58 and 14.02 ppm; HRMS-ESI calcd for $C_{57}H_{62}BrNS_3$: m/z 935.3228 found 935.7048 [M $^{+}$].

2-(3,6-Di-tert-butylcarbazol-N-yl)-7-(5'''-bromo-2,2':5',2'':5'',2'''-quaterthiophen-5-yl)-9,9-dihexylfluorene (10)

10 was synthesized from **9** in similar manner to **4** and obtained as deep yellow solids (0.23 g, 95%). m.p. 112-116 °C; FT-IR (KBr) 3064, 2952, 2924, 2854, 2361, 1609, 1476, 1362, 1323, 1294, 1261, 1232, 969, 876, 809, 788, 693 and 614 cm⁻¹; ¹H-NMR (300 MHz, CDCl₃) δ 8.18 (2H, s), 7.88 (1H, d, J = 8.7 Hz), 7.76 (1H, d, J = 7.8 Hz), 7.66-7.48 (6H, m), 7.41-7.33 (3H, m), 7.20 (1H, d, J = 3.6 Hz), 7.16-7.08 (3H, m), 7.04 (1H, d, J = 3.6 Hz), 6.99 (1H, d, J = 3.9 Hz), 6.93 (1H, d, J = 3.6 Hz), 2.06-2.01 (4H, m), 1.56-1.43 (18H, m), 1.12 (12H, m) and 0.82-0.77 (10H, m) ppm; ¹³C-NMR (75 MHz, CDCl₃) δ 152.65, 151.91, 144.13, 142.84, 140.26, 139.32, 137.05, 136.68, 136.01, 135.21, 132.92, 130.74, 125.42, 124.77, 124.70, 124.61, 124.27, 124.24, 123.81, 123.77, 123.57, 123.39, 121.39, 120.77, 120.26, 119.88, 116.31, 111.18, 109.22, 55.50, 40.36, 34.75, 32.03, 31.54, 29.66, 26.92, 23.90, 22.59 and 14.04 ppm; HRMS-ESI calcd for C₆₁H₆₄BrNS₆: m/z 1017.3125 found 1017.1455 [M⁺].

2-(3,6-Di-tert-butylcarbazol-N-yl)-7-pyrenyl-9,9-dihexylfluorene (CFP)

A mixture of **2** (1.5 g, 2.2 mmol), pyreneboronic acid (0.584 g, 2.37 mmol), Pd(PPh₃)₄ (0.653 g, 2.656 mmol), Na₂CO₃ solution (2 M, 6.5 ml) in THF (20 ml) was degas in with N₂ at 2 min. The mixture was heated at reflux under N₂ atmosphere for 24 h. After cooled to room temperature, water (50 ml) was added. The reaction mixture was extracted with dichloromethane (50 ml x 3). The combined organic phase was washed with water (50 ml), brine solution (50 ml), dried over sodium sulfate anhydrous, filtered and the solvent was remove in vacuum. The product was obtained by silica gel chromatography eluting with dichloromethane/hexane to afforded light yellow solids (1.25 g, 69%). m.p. 152-154 °C; FT-IR (KBr) 3042, 2951, 2925, 2854, 1613, 1581, 1478, 1365, 1324, 1293, 1260, 1232, 877, 845, 808, 757, 719, 685 and 613 cm⁻¹. ¹H-NMR (300 MHz, CDCl₃) δ 8.30-8.24 (3H, m), 8.20-8.07 (8H, m), 8.04- 7.94 (4H, m), 7.68 (2H, d, J = 8.4 Hz), 7.63-7.59 (2H, m), 7.54-7.49 (2H, m), 2.10-2.05 (4H, m), 1.51 (18H, m), 1.18 (12H, m) and 0.86-0.81 (10H, m) ppm; ¹³C-NMR (75 MHz, CDCl₃) δ 152.83, 151.19, 142.86, 140.17, 139.69, 139.65, 139.42, 138.22, 137.02, 131.58, 131.04, 130.63, 129.61, 128.87, 128.67, 127.73, 127.65, 127.51, 126.10, 125.83, 125.66, 125.43, 125.36, 125.21, 125.01, 124.87, 124.73, 123.65, 123.43, 123.28, 123.19, 121.61, 121.51, 120.90, 119.82, 117.83, 116.38, 109.32, 55.57, 40.37, 34.82, 32.11, 31.6, 29.76, 24.11, 22.68 and 14.16 ppm; HRMS-ESI calcd for C₆₁H₆₈N: m/z 811.5117 found 812.1358 [M⁺].

2-(3,6-Di-tert-butylcarbazol-N-yl)-7-(5-pyrenylthiophen-2-yl)-9,9-dihexylfluorene (CFTP)

CFTP was synthesized from **4** in similar manner to **CFP** and obtained as yellow solids (0.35 g, 81%). m.p. 170-172 °C; FT-IR (KBr) 3040, 2952, 2925, 2854, 1609, 1583, 1478, 1363, 1324, 1294, 1262, 1233, 877, 845, 808, 757, 718, 684 and 614 cm⁻¹; ¹H-NMR (300 MHz, CDCl₃) δ 8.69 (1H, d, J = 9.3 Hz), 8.24-8.05 (10H, m), 7.94 (1H, d, J = 8.1 Hz), 7.86-7.78 (3H, m), 7.61-7.54 (5H, m), 7.47 (1H, d, J = 8.7 Hz), 2.12-2.10 (4H, m), 1.55 (18H, m), 1.19 (12H, m) and 0.88-0.84 (10H, m) ppm; ¹³C-NMR (75 MHz, CDCl₃) δ 152.69, 151.96, 145.82, 142.86, 141.85, 140.18, 139.48, 139.38, 137.01, 133.38, 131.52, 131.08, 131.01, 129.75, 129.08, 129.01, 128.28, 128.07, 127.88, 127.40, 126.23, 125.45, 125.14, 125.01, 124.93, 124.85, 124.73, 123.63, 123.53, 123.42, 121.43, 120.81, 120.36, 119.99, 116.37, 109.29, 55.56, 40.46, 34.81, 32.09, 31.63, 29.74, 23.98, 22.67 and 14.13 ppm; HRMS-ESI calcd for $C_{65}H_{67}NS$: m/z 893.4994 found 893.6961 [M⁺].

2-(3,6-Di-tert-butylcarbazol-N-yl)-7-(5'- pyrenyl-2,2'-bithiophen-5-yl)-9,9-dihexylfluorene (CFT2P)

CFT2P was synthesized from **6** in similar manner to **CFP** and obtained as yellow solids (0.494 g, 72%). m.p. 216-218 °C; FT-IR (KBr) 3042, 2952, 2926, 2855, 1609, 1583, 1477, 1363, 1324, 1294, 1262, 1233, 1033, 876, 845, 808, 756, 719 and 614 cm⁻¹; ¹H-NMR (300 MHz, CDCl³) δ 8.64 (1H, d, J = 9.3 Hz), 8.25-8.18 (9H, m), 8.09-8.04 (1H, m), 7.91 (1H, d, J = 8.4 Hz), 7.79 (1H, d, J = 7.8 Hz), 7.70 (1H, d, J = 7.8 Hz), 7.72-7.65 (2H, m), 7.57-7.50 (4H, m) 7.42 (4H, d, J = 9.3 Hz), 7.34 (2H, d, J = 10.8 Hz), 2.09-2.07 (4H, m), 1.51 (18H, m),1.15 (12H, m) and 0.84-0.80 (10H, m) ppm; ¹³C-NMR (75 MHz, CDCl₃) δ 152.66, 151.92, 143.90, 142.83, 141.55, 140.19, 139.35, 138.35, 137.02, 136.46, 133.08, 131.50, 130.98, 129.33, 129.00, 128.78, 128.21, 128.10, 127.91, 127.35, 126.22, 125.45, 125.14, 124.89, 124.81, 124.69, 124.05, 123.79, 123.57, 123.39, 121.41, 120.77, 120.27, 119.88, 116.32, 109.24, 55.51, 40.38, 34.76, 32.04, 31.55, 30.91, 29.67, 23.92, 22.60 and 14.05 ppm; HRMS-ESI calcd for $C_{69}H_{69}NS_2$: m/z 975.4871 found 975.4896 [M[†]].

2-(3,6-Di-tert-butylcarbazol-N-yl)-7-(5"- pyrenyl-2,2':5',2"-terthiophen-5-yl)-9,9-dihexylfluorene (CFT3P)

CFT3P was synthesized from **8** in similar manner to **CFP** and obtained as pale orange-yellow solids (0.252 g, 65%). m.p. 220-221 °C; FT-IR (KBr) 3041, 2951, 2925, 2855, 1608, 1583, 1476, 1362, 1324, 1294, 1262, 1232, 1034, 876, 844, 792, 756, 718 and 614 cm⁻¹; ¹H-NMR (300 MHz, CDCl₃) δ 8.62 (1H, d, J = 9.0 Hz), 8.24-8.13 (9H, m), 8.08-8.03 (1H, m), 7.90 (1H, d, J = 8.4 Hz), 7.78 (1H, d, J = 7.8 Hz), 7.69-7.63 (2H, m), 7.56-7.49 (4H, m), 7.43-7.34 (5H, m), 7.25-7.22 (3H,m) 2.06 (4H, m), 1.50 (18H, m),1.14 (12H, m) and 0.84-0.80 (10H, m) ppm; ¹³C-NMR (75 MHz, CDCl₃) δ 152.66, 151.92, 143.98, 142.84, 141.74, 140.23, 139.34, 137.95, 137.04, 136.40, 136.23, 136.14, 132.99, 131.49, 131.15, 130.97,

129.24, 129.00, 128.80, 128.20, 128.12, 127.93, 127.35, 126.23, 125.46, 125.16. 124.85, 124.80, 124.69, 124.45, 124.30, 124.17, 123.79, 123.57, 123.39, 121.40, 120.77, 120.28, 119.88, 116.32, 109.23, 55.51, 40.37, 34.76, 32.04, 31.55, 29.67, 23.91, 22.60 and 14.04 ppm; HRMS-ESI calcd for $C_{73}H_{71}NS_3$: m/z 1057.4749 found 1057.8557 [M $^+$].

2-(3,6-Di-tert-butylcarbazol-N-yl)-7-(5'''- pyrenyl-2,2':5',2'':5'',2'''-quaterthiophen-5-yl)-9,9-dihexylfluorene (CFT4P)

CFT4P was synthesized from **10** in similar manner to **CFP** and obtained as orange solids (0.252 g, 30%). m.p. 224-226 °C; FT-IR (KBr) 3039.17, 2923.99, 1601.42, 1582.92, 1474.87, 1361.62, 1323.38, 1293.56, 1261.08, 876.38, 843.43, 789.74, 755.90, 718.17, 681.01 and 613.59 cm⁻¹; ¹H-NMR (300 MHz, CDCl₃) δ 8.59 (1H, d, J = 9.6 Hz), 8.19 (6H, s), 8.18-8.02 (6H, m), 7.88 (1H, d, J = 8.1 Hz), 7.76 (1H, d, J = 7.8 Hz), 7.65-7.61 (2H, m), 7.56-7.48 (5H, m), 7.41 (2H, d, J = 8.4 Hz), 7.37-7.32 (3H, m), 7.16 (4H, d, J = 12.6 Hz), 2.07-2.02 (4H, m), 1.50 (18H, m), 1.18 (12H, m) and 0.83-0.79 (10H, m) ppm; ¹³C-NMR (75 MHz, CDCl₃) δ 152.68, 151.91, 142.85, 140.31, 139.34, 137.06, 136.02, 131.47, 131.17, 130.95, 128.72, 128.14, 127.95, 127.33, 126.22, 125.49, 125.42, 125.18, 124.80, 124.68, 124.45, 124.28, 123.58, 123.40, 121.39, 120.80, 120.26, 119.88, 116.33, 109.24, 55.51, 40.37, 34.77, 32.05, 31.91, 31.56, 29.68, 23.93, 22.61 and 14.06 ppm; HRMS-ESI calcd for C₇₇H₇₅NS₄: m/z 1141.4782 found 1140.4720 [MH⁺].

PART VII

Synthesis and Properties of Fluorene-oligothiophenes Perylenediimide Triads and Their Electropolymerizations

1. Introduction

In recent years, perylene tetracarboxylicdiimides (PDIs) have received considerable interest for use as photoactive materials in a variety of fields ranging from industrial pigments to components of molecular photonic and electronic devices because of their high luminescence efficiency, and excellent thermal and photochemical stability. Driven by such a wide range of applications, the structure of PDIs has been modified by introducing side groups either to the imide nitrogen atoms or at the bay positions with the aim of fine-tuning the chemical and photophysical properties of PDIs. The former modification has been found to improve the solubility of PDIs with unchanged photophysical properties, while the latter approach mostly resulted in a change in photophysical properties of PDIs with significant drop on fluorescence quantum yield in some cases. Covalently linking two electron-rich donor moieties to the imide nitrogens of a central PDI has been found to create donor-acceptor-donor (D-A-D) triads with unique properties for organic light-emitting diodes (OLEDs) and solar cells as well as implications in photo-induced energy and/or electron-transfer processes. Some examples of PDI-based triads have been reported recently in the literature, e.g., those concerning the use of polyphenylene dendrimer, porphyrin, phthalocyanine, oligo(p-phenylenevinylene) and benzothiazole-2-yl-9,9-didecylfluorene as the donors.

The oligothiophene (OT) skeleton is among the most versatile and effective of π -conjugated organic backbones, and together with its great chemical stability, the OT-based system represents a promising class of organic materials. Although many OT-based materials have proven to be promising organic semiconductors for electronic devices, OT functionalized PDIs remain rare and largely unexplored. In this contribution, we synthesize novel PDI-based triads by linking the fluorene-oligothiophenes (FTn) at the *N*-imides of PDI. Their optical and electrochemical properties are investigated with the goal of developing new functional materials.

2. Results and discussion

Synthesis

The **PFTn** (n = 0-4) triads were synthesized according to the procedures outlined in Scheme 1. Starting from 2-nitro-7-iodo-9,9-didodecylfluorene (1) a series of 2-nitro-fluorene-oligothiophene intermediates 2-5 were synthesized using a combination of metal catalyzed cross-coupling and bromination reactions in an iterative manner. Suzuki cross-coupling reaction with 2-thiopheneboronic acid catalyzed by $Pd(PPh_3)_4$ in

the presence of Na_2CO_3 was employed to complete a development of the oligothiophene segment and a series of Ω -substituted oligothiophenes up to the tetramer 2-5 were obtained in good yields of 64-92%, while bromination with NBS in THF selectively introduced a bromo function to the Ω -position of the terminal thiophene ring, allowing further cross-coupling reaction to be performed. The bromo intermediates 7-9 were prepared in excellent yields. The nitro groups of compounds 2-6 were then transformed efficiently to the related amino moiety using $SnCl_2/HCl$ in EtOH/EtOAc. Subsequently, condensation of the resultants with perylene dianhydride in the presence of imidazole gave the **PFTn** triads as deep red solids in moderate to good yields of 52-71%. Their chemical structures were characterized unambiguously with 1 H- and 13 C-NMR, FTIR spectroscopy, and mass spectrometry. These compounds were soluble in most organic solvents.

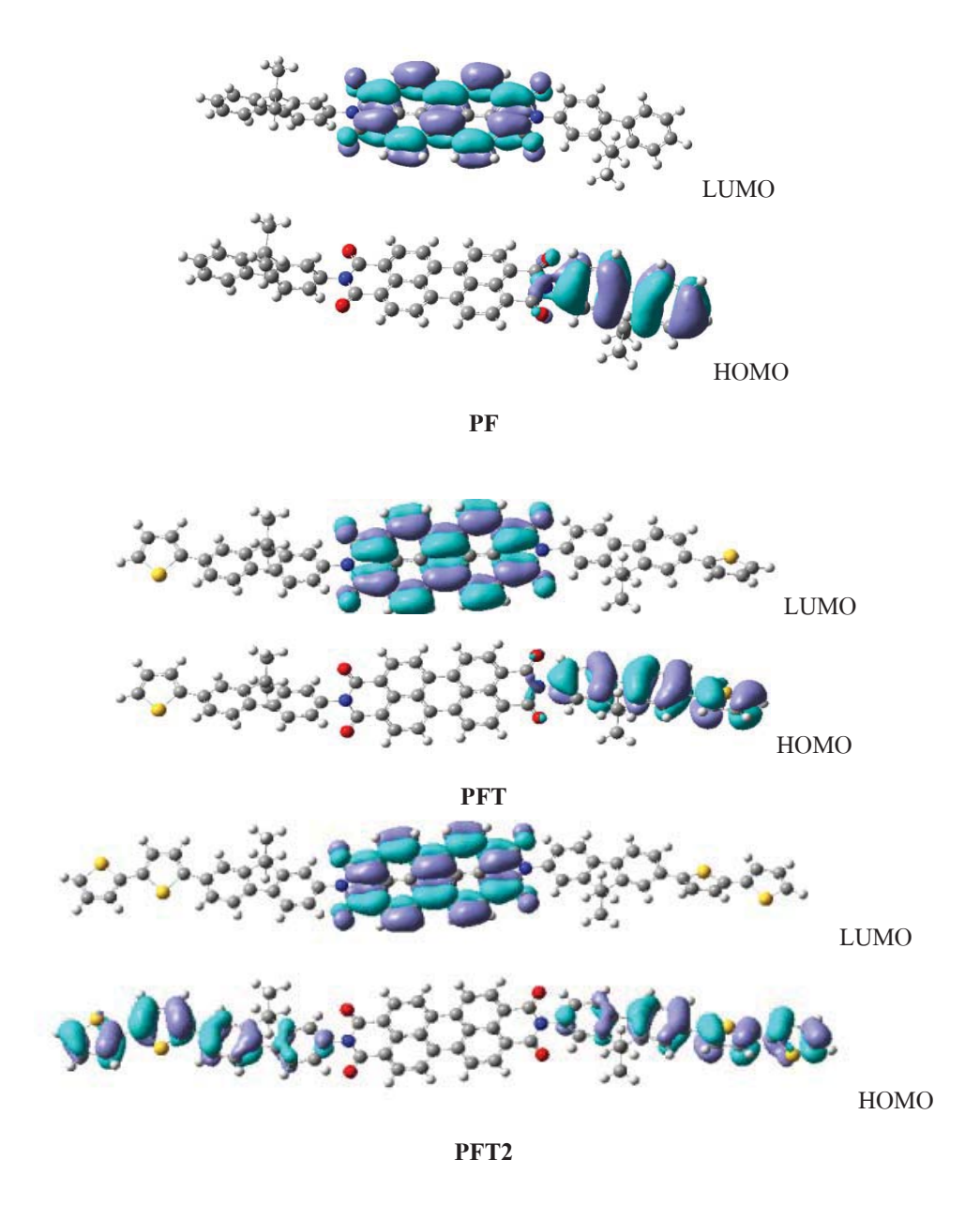
$$\begin{array}{c} O_2N \\ C_{12}H_{25} \\ C_{12}H$$

Scheme 1. Synthesis of the PFTn triads.

Quantum calculation and physical properties

To gain inside the electronic properties and the geometries of the triads, quantum chemical calculations were performed using TDDFT/B3LYP/6-31G (d,p) method. In the optimized geometries of the molecules, the π -conjugated FTn planes were twisted nearly perpendicular to the PDI plane, implying two isolated chemically bonded chromophores. The π -electrons in the HOMO orbitals were delocalized on the conjugated backbone of FTn, while the excited electrons in LUMO orbitals localized over the quinoid-like

perylene plane, creating a D-A-D triad with the FTn acting as donor and PDI acting as acceptor (Fig. 1 and S1, ESI \dagger). The energy band gaps (E $_{\rm g}$ cal.) of the **PFTn** triads were calculated and presented in Tables 1 and S1. These calculated values (from TDDFT calculation and Δ HOMO-LUMO) are in good agreement with those estimated from the optical absorption edge and cyclic voltammetry, respectively. However, a slight derivation between the calculated and experimental results was observed. There are factors responsible for the errors because the orbital energy difference between HOMO and LUMO is still an approximate estimation to the transition energy since the transition energy also contains significant contributions from some two-electron integrals. The real situation is that an accurate description of the lowest singlet excited state requires a linear combination of a number of excited configurations.



หน้าที่ 106

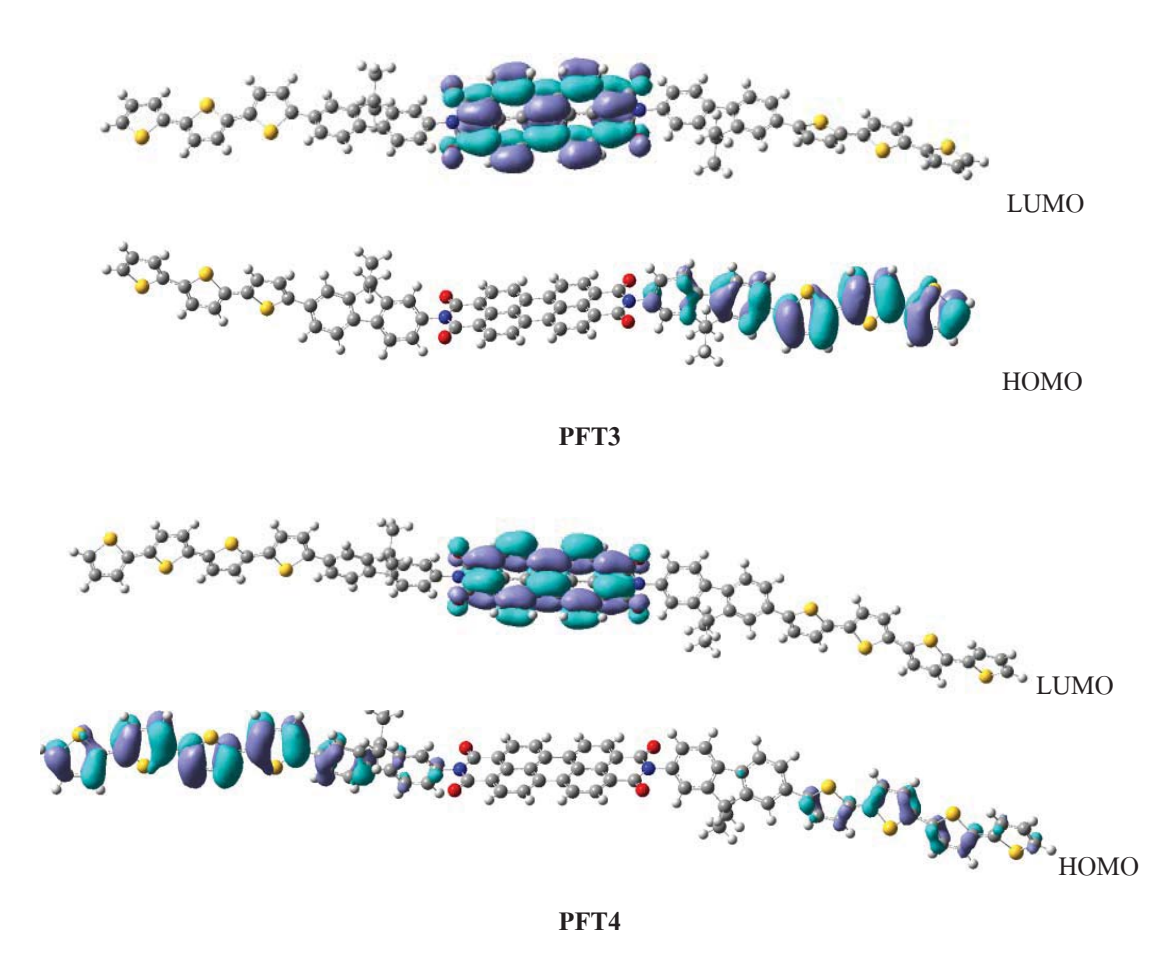


Fig. S1 The optimized geometries and HOMO-LUMO orbitals of PFTn by TDDFT/B3LYP(3,6)d.

Table S1. The calculated HOMO and LUMO energy levels and \boldsymbol{E}_{g} of PFTn.

Commit	НОМО	LUMO	E _g (eV)	E _g (eV)		
Compd	(eV)	(eV)	$\Delta_{ ext{ iny H-L}}$	TDDFT		
PF	-5.8164	-3.4226	2.3938	2.4182		
PFT1	-5.4395	-3.4797	1.9598	2.4120		
PFT2	-5.1715	-3.4648	1.7067	2.4074		
PFT3	-4.9859	-3.4528	1.5331	2.4064		
PFT4	-4.8948	-3.4716	1.4232	2.3913		

All the compounds showed good thermal stability as measured by thermalgravimetric analysis (TGA). The temperatures with 5% weight loss for **PFTn** (n = 0-4) were 356, 355, 390, 410 and 416 °C, respectively (Fig. S2, ESI†). The UV-Vis absorption spectra of the triads in CH_2Cl_2 showed broad absorption bands in the range of 300-420 nm and the bands with a well-resolved vibronic structure at longer wavelengths (Fig. 2a and Table 1). These spectra characterized the summation of the spectra of both donor and acceptor units, indicating the absence of significant interaction in the ground state between FTn and PDI moieties. The former corresponded to the π - π * transition of the FTn and was gradually red-shifted

with the increasing number of thiophene units as the extent of the π -conjugation system in the oligomeric backbone increases, as expected. The latter bands (maxima at 459, 490 and 526 nm) are attributed to the π - π * transition of the PDI skeleton, in which the peak at 459 nm originated from the S_0 - S_2 transition, while the peaks at 526 and 490 nm derived from the transitions from S_0 to 0- and 1-vibronic states of S_1 , respectively. These peaks were identical for all compounds. Their similarity to typical PDI derivatives in terms of both the absorption maxima and molar extinction coefficients indicated that increasing the π -conjugation length of the FTn had little or no effect on the electronic property of the PDI moiety.

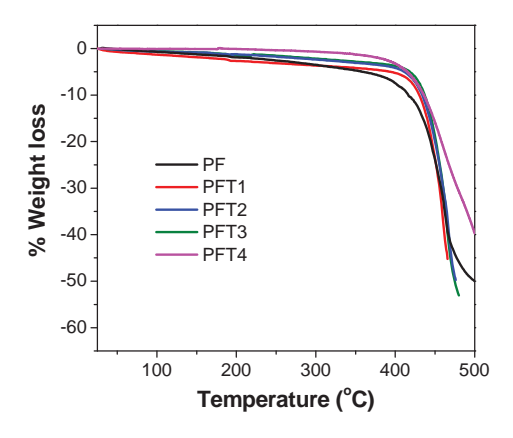


Fig. S2 TGA thermograms of **PFTn** measured at 10 °C/min under N₂.

The fluorescence emission of the PDI unit of all PFTn triads (excited at 470 and 500 nm) in CH₂Cl₂ was quasi quantitatively quenched (99.6% compared to emission of N,N'-bis(2-ethylhexyl)-3,4,9,10perylenetetracarboxylic diimide under the same conditions). This could be explained by an intramolecular photo-induced electron transfer (PET) from the donor FTn to the excited acceptor PDI to form the radical cation FTn and radical anion PDI species, respectively, which undergo non-radiative relaxation processes as represented in Fig. 3. For the same reason, the emission of FTn in PF-PFT2 triads upon excitation at the absorption of the FTn moieties (<410 nm) was also diminished (Fig. 2c) compared with α-(fluoren-2-yl)oligothiophene references. The energy transfer from an excited FTn species to the acceptor moiety gives rise to the excited PDI* which then continues a PET followed by non-radiative multiphonon relaxation processes. In contrast, the PFT3 and PFT4 triads showed strong fluorescence from their FTn moieties, possibly due to a reverse energy transfer from the acceptor PDI to the donor FTn driven by the absorption spectral overlap of both chromophores. The excited PDI* species formed undergoes a reverse energy transfer to give FTn* which then carries on a fluorescence decay process. This emissive decay of the PDI species was slightly gone on as a tiny emission peak at longer wavelength being observed. A significant degree of an absorption spectral overlap in PFTn was reflected in the greater fluorescence quantum yield (Φ_F) of **PFT4** $(\Phi_F = 0.78)$ compared to **PFT3** $(\Phi_F = 0.27)$, while **PF-PFT2** triads showed very low $\Phi_{\rm F}$ s (Table 1). Normalized PL spectra of all **PFTn** triads excited at the absorption

of FTn showed emission peaks (326-495 nm) related to the emission of each FTn and much weaker emission peaks at a longer wavelength (540 nm) agreeing to the emission of PDI (Fig. 2b), supporting the presence of intramolecular energy transfer from the excited FTn * to PDI. The emission maxima of the former bands were steadily red-shifted with increasing π -conjugation lengths of the FTn moieties.

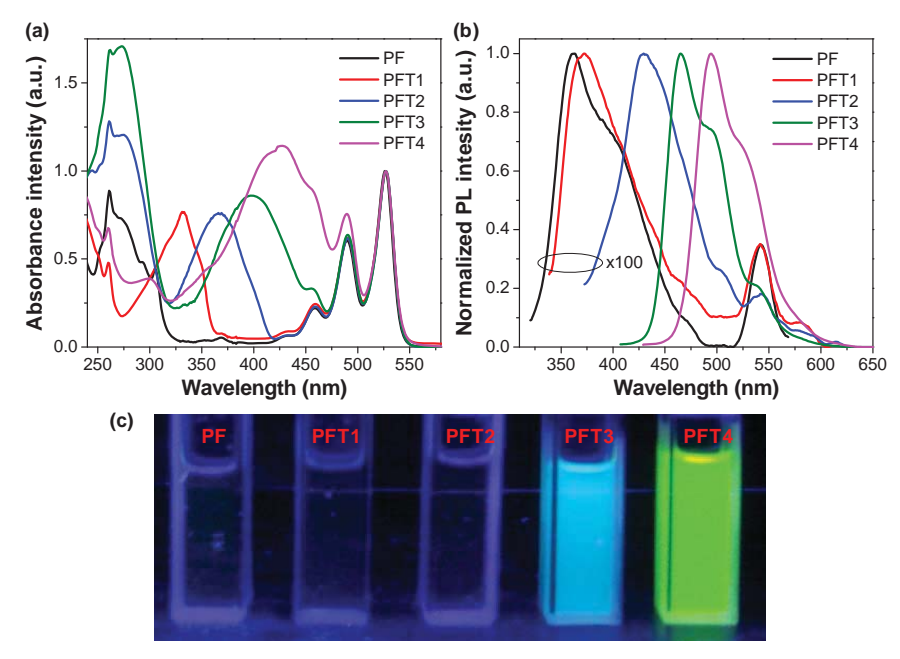


Fig. 2 (a) UV-Vis absorption spectra, (b) PL spectra excited at the absorption of FTn and (c) emission colours of **PFTn** in CH₂Cl₂.

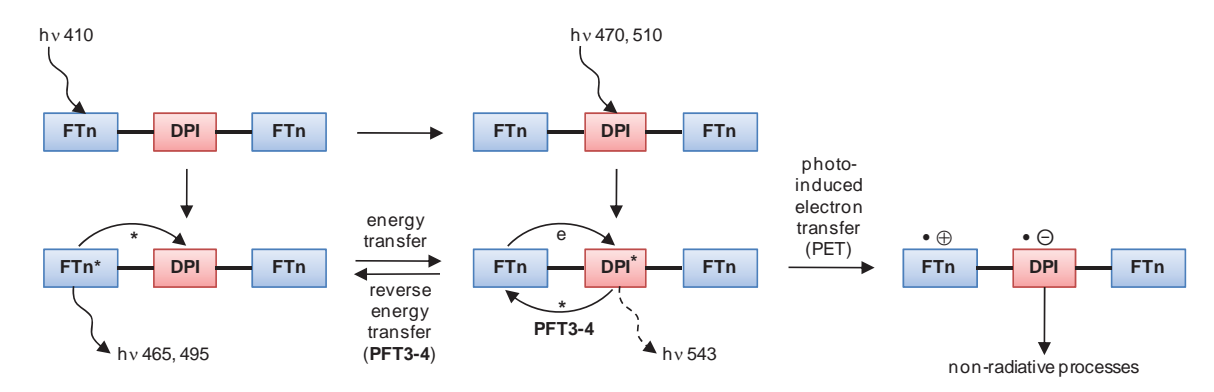


Fig. 3 Proposed photo-induced energy and electron transfer mechanisms in PFTn.

Table 1. Physical data for PFTn.

Com.	λ_{abs}^{a}	λ_{em}^{b}	$\Phi_{\scriptscriptstyle F}^{\ c}$	T_{5d}^{d}	E _{1/2} vs SCE (V) ^e			E _g f	E _g ^h	E _g cal	(eV)	HOMO/LUMO ^j	
	(nm)	(nm)		(°C)	E ^{1r}	E^{2r}	E ¹⁰	E_{pc}	(eV)	(eV)	DFT	$\Delta_{\text{H-L}}$	(eV)
PF	526	362, 543w	0.005	356	-0.58	-0.76	1.38	-	2.28	1.80	2.42	2.39	5.74/3.94
PFT1	526	374, 543w	0.002	355	-0.56	-0.74	1.34	0.99	2.28	1.76	2.41	1.96	5.72/3.95
PFT2	526	430, 542w	0.004	390	-0.56	-0.74	1.10	0.74	2.28	1.51	2.41	1.71	5.48/3.96
PFT3	526	465, 541sh	0.27	410	-0.56	-0.74	0.95	0.64	2.28	1.40	2.41	1.53	5.36/3.96
PFT4	526	495	0.78	416	-0.57	-0.75	0.83	-	2.28	1.29	2.39	1.42	5.23/3.94

^aMeasured in CH_2Cl_2 ; ^bExcited at the absorption of the FTn moiety; ^cMeasured in CH_2Cl_2 with quinine sulfate as a standard; ^dObtained from TGA measured at 10 °C/min under N_2 ; ^eObtained from CV in CH_2Cl_2/n -Bu₄NPF₆ (0.1 M) at scan rate of 50 mV/s; ^fCalculated from the absorption edge; ^hCalculated from the difference between E^{re}_{onset} and E^{ox}_{onset} ; ⁱObtained from quantum chemical calculation: DTF (TDDFT calculation), Δ_{H-L} (Δ HOMO-LUMO); ^jEstimated from HOMO = -(4.44 + E^{ox}_{onset}); LUMO = -(4.44 + E^{re}_{onset}).

Electrochemical property and electropolymerization

Electrochemical behaviors of all compounds were investigated by cyclic and differential pulse voltammetry (CV and DPV), and the resulting data are shown in Fig. 4 and summarized in Table 1. The experiment was carried out in degassed CH2Cl2 containing 0.1 M n-Bu4NPF6 as a supporting electrolyte under argon atmosphere. The results revealed that **PFTn** exhibited amphoteric redox behaviors. As shown in Fig. 4a, two one-electron chemically reversible reduction processes ascribed to the successive formation of the anion radical (FTn-PDI. and dianion (FTn-PDI. of the PDI moiety were observed in the negative side of all CV curves. The half-wave potentials for both reduction waves of all compounds were nearly identical ($E_{1/2}^{1r} = -0.58$, $E_{1/2}^{2r} = -0.74$ V) and comparable to those of N,N'-bis(2,5-di-tertbutylphenyl)-3,4,9,10-perylene tetracarboxylic diimide ($E_{1/2}^{1r} = -0.50$, $E_{1/2}^{2r} = -0.73$ V), emphasizing that these triads are composed of two isolated chromophores, this being confirmed by optical studies. In the positive side, **PFTn** (n = 0-4) exhibited one quasi-reversible oxidation wave at $E_{1/2}^{10} = 1.38$, 1.34, 1.10, 0.95 and 0.83 V, respectively, ascribed to the oxidation of the terminal FTn moieties resulting in radical cations (FTn. +PDI), with the oxidation of the PDI moiety not being observed. As expected, the oxidation potentials of these compounds gradually decreased as the number of thiophene units in the molecules increased due to an increase in π -conjugation length of FTn. During the cathodic sweep (E_{pc}) of PFT1-3, additional peaks at lower potentials were observed at 0.99, 0.74 and 0.64 V, respectively, indicating the radical cation formed undergo oxidative coupling on the surface of the electrode. In contrast, the fluorene radical cation (F.) of **PF** and especially FT4 of **PFT4** were relatively stable. It has been known that the terminal thiophene unit can be easily oxidized by either chemical or electrochemical processes to form a thiophene raical cation. This species is prone to undergo a coupling reaction to form a dimer as it was observed in the cases of **PFT1-PFT3**. As described in Fig. 5a, once an electron is removed from the ring, the radical formed is delocalized over all four carbon and sulfur atoms of the thiophene ring to form radical cations **A**, **B**, **C**, **D** and **E** which can be represented by **F**. The dimerization coupling reaction could occur through a reaction of species **B**, **D** and **E** with the latter is more likely due to due to less crowding. However, as number of thiophene units in the segment increases by more than three units, the radical cation becomes inactive to such reaction as observed in **PFT4** and Ω -(fluoren-2-yl)oligothiophenes. The extended π -electron delocalization systems in FT4 and longer oligothiophenes play an important role in stabilization of the FT4. $^{\oplus}$ species to such electrochemical reaction (Fig. 5b).

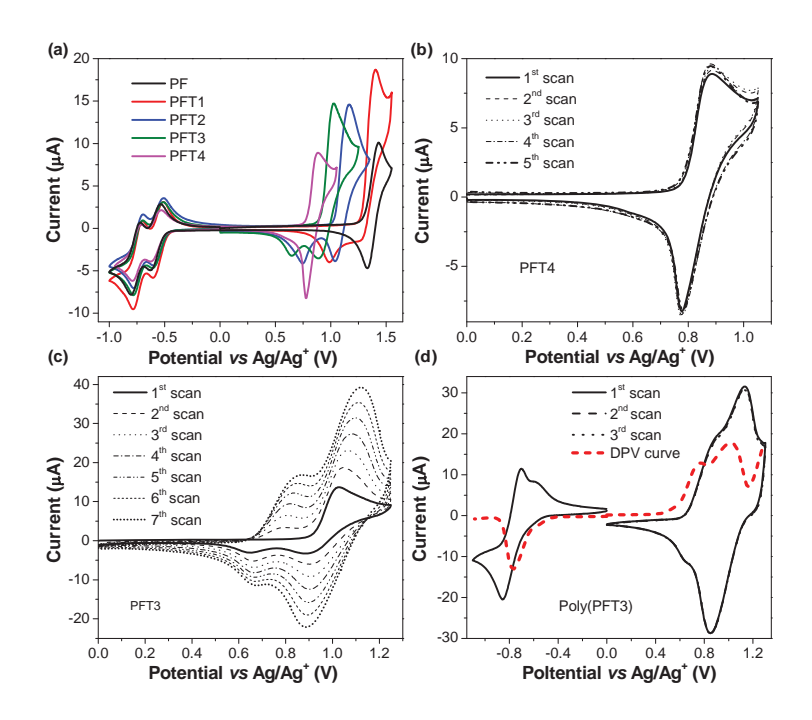


Fig. 4 (a) CV curves of **PFTn**. (b) Repeated CV scans of **PFT4**. (c) Repeated CV scans of **PFT3**. (d) CV and DPV curves of polymer film, **poly(PFT3)**, in CH₂Cl₂/n-Bu₄NPF₆, scan rate of 100 mV/s, glassy carbon disk working electrode.

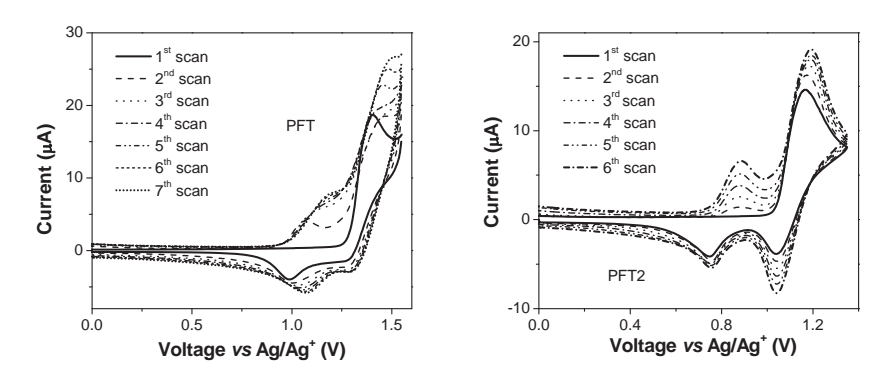


Figure S3 Repeated CV scans of **PFT1-2** in DCM/TBAPF₆ (0.1 M), scan rate of 100 mV/s, glassy carbon disk working electrode.

Fig. 5 (a) π -Electron delocalization in thiophene radical cation and its coupling reaction. (b) Stabilization of FT4^{*+} by the extended π -system.

S

Repeated CV scans of PF and PFT4 revealed unchanged CV curves, while those of PFT1-3 displayed a gradual increase in the current density of the reversible peaks after each successive cycle (Fig. 3b, 3c and S3, ESI†). This clearly indicated that PFT1-3 underwent a series of electrochemical reactions resulting in their corresponding photoactive polymer films, poly(PFT1)-poly(PFT3), being deposited on the working electrode surface (Fig. 3c). The as-prepared polymer films were electrochemically characterized in a monomer-free electrolyte solution. In this way, Fig. 3d and S4 (ESI†) showed the stabilized voltammograms of poly(PFT1)-poly(PFT3), which were cycled between -1.2 V and 1.5 V. The CV and DPV traces of the polymer film of poly(PFT3) for example exhibited two reversible oxidation couples with half-wave potentials at $E_{1/2}^{10} = 0.76$ and $E_{1/2}^{20} = 1.02$ V, and one reversible reduction at half-wave potential ($E_{1/2}^{r}$) of -0.77 V. The reduction potentials of all polymers were nearly identical ($E_{1/2}^{r}$ = -(0.76-0.78) V), while their first oxidation potentials gradually decreased as the number of thiophene units in the monomers increased. The reversible oxidation, concomitant with the cathodic shift in the oxidation potentials of poly(PFT1)-poly(PFT3) relative to their corresponding monomers, confirms the conjugated nature of the polymers. The oxidation and reduction processes exhibited by the polymers proved that they can be both p- and n-doped and further confirms that the polymers can communally transport holes and electrons. The energy band gaps (E_n) and the HOMO/LUMO levels of poly(PFT1)-poly(PFT3) estimated from the onset of the redox waves in the voltammograms are listed in Table 2. The HOMO levels of poly(PFT2) (5.18 eV) and poly(PFT3) (5.10 eV) are compatible with the standard ITO anod Q.9 eV). while their low LUMO levels (3.75-3.78 eV) are comparable with common cathodes such as aluminum (4.1 eV) and magnesium (3.7 eV), that made these polymers good candidates for optoelectronic device applications. The energy compatibility implies a low work function for the injection of charges from the electrodes; thereby a charge injection layer is not required to overcome the barrier height, leading to simpler device construction.

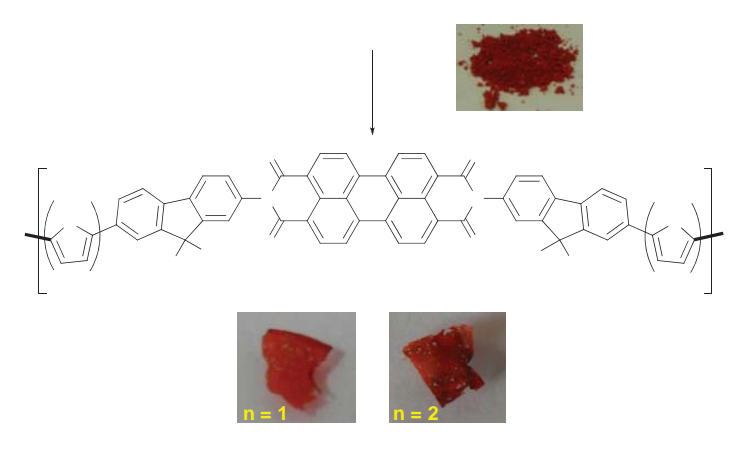


Fig. 6 Electropolymerizations of PFT1-3.

Table 2. Physical data for Poly(PFTn).

Com.	E _{1/2} vs SCE (V) ^a			HOMO/LUMO ^b	E_{g}^{c}
·	E	E ¹⁰	E ^{2O}	(eV)	(eV)
Poly(PFT1)	-0.78	1.10	-	5.51/3.77	1.74
Poly(PFT2)	-0.76	0.78	1.02	5.18/3.75	1.43
Poly(PFT3)	-0.77	0.75	1.02	5.10/3.78	1.32

^aObtained from CV in CH₂Cl₂/n-Bu₄NPF₆ at scan rate of 100 mV/s, glassy carbon disk working electrode;

Electropolymerizations of **PFT1-3** on ITO/glass substrate as a working electrode successfully resulted in polymer films of **poly(PFT1)-poly(PFT3)** coating on top of the ITO film, native transparent conducting anode (Fig. 7a and S5; ESI \dagger). The red to dark red polymer plastic films were obtained and characterized by FTIR and UV-Vis spectroscopy. The absorption spectra of polymer plastic films **poly(PFT1)** and **poly(PFT2)** showed characteristic absorption bands of both oligothiophene and PDI chromophores as observed in the monomers. The absorption band at lower wavelength assigned to an absorption of oligothiophene chromophore was red shifted compared to that absorption band of their corresponding monomers (Fig. 7b), indicating the formaion of more extended π -systems.

n

^bEstimated from HOMO = -(4.44 + E_{onset}^{ox}); LUMO = -(4.44 + E_{onset}^{re}); ^cCalculated from the difference between E_{onset}^{re} and E_{onset}^{ox} .

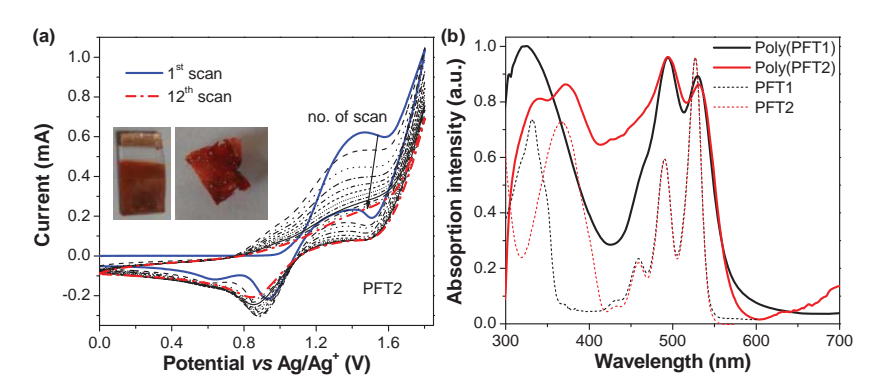


Fig. 7 (a) Repeated scan electropolymerization of **PFT2** in CH₂Cl₂/*n*-Bu₄NPF₆, scan rate of 100 mV/s, ITO/glass as a working electrode. (b) UV-Vis absorption spectra of the polymer films and monomers.

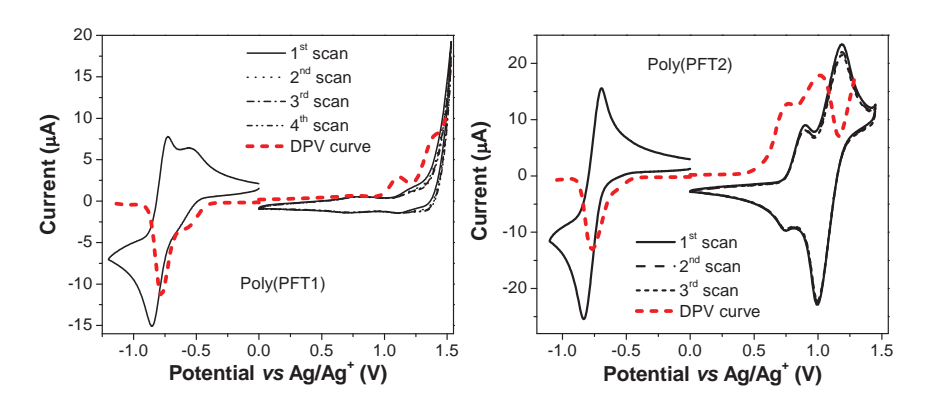


Figure S4 CV and DPV curves of polymer films, poly(PFT1) and poly(PFT2), in DCM/TBAPF $_6$ (0.1 M), scan rate of 100 mV/s, glassy carbon disk working electrode.

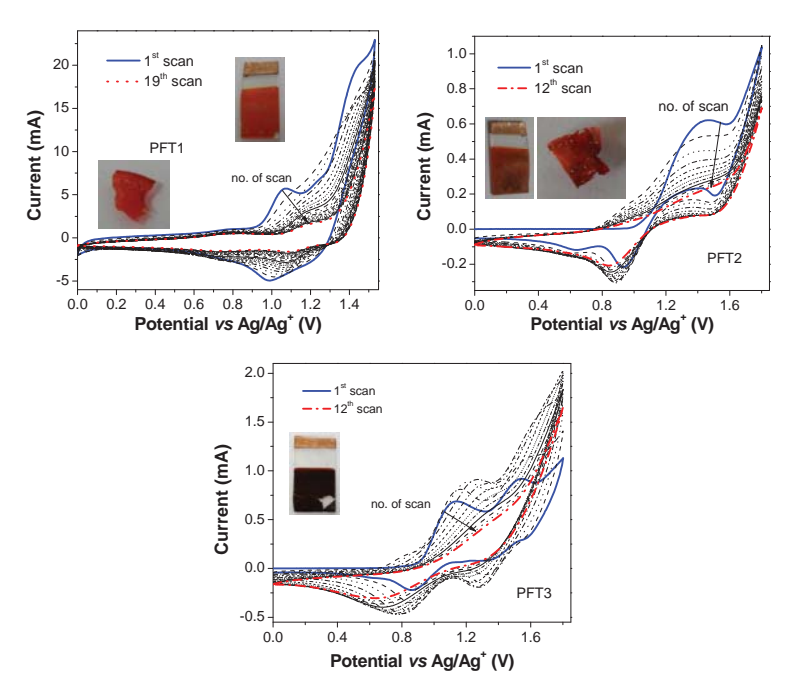


Figure S5 Repeated scan electropolymerization of PFT1-3 in DCM/TBAPF $_6$ (0.1 M), scan rate of 100 mV/s, ITO/glass working electrode.

3. Conclusions

In summary, we have successfully synthesized a series of new D-A-D triads (**PFTn**) consisting of the FTn as donor and PDI as acceptor. Optical and electrochemical studies indicate that the triads comprise two isolated electron donor and acceptor chromophores with good photostability. These triads have a strong intramolecular photo-induced electron transfer (PET) between both chromophores, which gives rise to a quasi-quantitatively fluorescence quenching of both PDI and FTn moieties. However, a reverse energy transfer from the acceptor PDI to the donor FTn induces a strong fluorescence emission from the FTn moieties in the **PFT3** and **PFT4** triads. In the oxidation process, the triads bearing short oligothiophenes (n ≤ 3) undergo an electrochemical oxidative coupling reaction, while the longer oligomers (n > 3) are stable to such electrochemical reaction. Interestingly, polymer plastic films of **poly(PFT1)-poly(PFT3)** could be obtained from **PFT1-3** by electropolymerization on the ITO/glass electrodes. Our results demonstrate that the synthesized perylene-based triads could be used as new organic semiconductor materials for applications in the field of organic optoelectronics.

4. Experimental Section

General procedure

¹H and ¹³C nuclear magnetic resonance (NMR) spectra were recorded on a Brüker AVANCE 300 MHz spectrometer with tetramethylsilane as the internal reference using CDCl, as solvent in all cases. Infrared (IR) spectra were measured on a Perkin-Elmer FTIR spectroscopy spectrum RXI spectrometer as KBr disc or thin film obtained from electropolymerization, Ultraviolet-visible (UV-Vis) spectra were recorded as a dilute solution in spectroscopic grade dichloromethane or thin film obtained from electropolymerization on a Perkin-Elmer UV Lambda 25 spectrometer. Photoluminescence spectra and the fluorescence quantum yields (Φ_r) were recorded with a Perkin-Elmer LS 50B Luminescence Spectrometer as a dilute solution in spectroscopic grade dichloromethane. The quantum yields $(\Phi_{\scriptscriptstyle E})$ were determined by comparison with a fluorescence standard of quinine sulfate solution in 0.01 M H_2SO_4 ($\Phi_F = 0.54$). Thermalgravimetric analysis (TGA) were performed on a Rigaku TG-DTA 8120 thermal analyzer, respectively, with heating rate of 10 °C/min under nitrogen atmosphere. All cyclic voltammetry (CV) measurements were carried out on an Autolab potentiostat PGSTAT 12 with a three electrode system (glassy carbon/ITO glass working electrodes, platinum counter electrode and Ag/Ag⁺ reference electrode) at scan rate of 50 or 100 mV/s in dichloromethane under argon atmosphere. The concentration of analytical materials and tetrabutyl ammonium hexafluorophosphate (n-Bu₄NPF₆) were 10⁻³ M and 0.1 M, respectively. Melting points were measured using an Electrothermal IA 9100 series of digital melting point instrument and are uncorrected. MALDI-TOF mass spectra were recorded on Bruker Daltonics (Bremen, Germany) Autoflex II Matrix-Assisted Laser Desorption/Ionization-Time of Flight Mass Spectrometer (BIFEX) using Oc-cyano-4hydroxycinnamic acid as matrix at Mahidol University.

Synthesis

2-Nitro-7-(5-bromothiophen-2-yl)-9,9-didodecylfluorene (7)

To a solution of **2** (0.83 g, 1.39 mmol) in THF (26 ml) under N_2 atmosphere, NBS (0.35 g, 1.98 mmol) was added in small portions. Water (100 ml) was added, the mixture was extracted with CH_2Cl_2 (2 x 50 ml). The combined organic layer was washed with water (100 ml), brine solution (100 ml), dried over anhydrous sodium sulfate, filtered and evaporated to dryness. Purification with column chromatography over silica gel eluting with CH_2Cl_2 :hexane gave a light yellow viscous oil (0.86 g, 92%). IR (KBr): v 727 cm⁻¹, 738, 797, 822, 886, 900, 990, 1006, 1079, 1127, 1208, 1339, 1443, 1460, 1521, 1588, 1611, 2851 and 2924; ¹H-NMR (300 MHz): δ 0.59 ppm (d, 4 H, J = 4.20 Hz), 0.86 (t, 7 H, J = 6.90 Hz), 1.20 (m, 35 H), 2.04 (t, 4 H, J = 7.50Hz), 7.07 (d, 1 H, J = 3.90 Hz), 7.17 (d, 1 H, J = 3.60 Hz), 7.51 (s, 1H), 7.55 (d, 1 H, J = 6.60 Hz), 7.77 (d, 1 H, J = 5.10 Hz), 8.19 (s, 1 H) and 8.25 (d, 1 H, J = 6.30 Hz); ¹³C-NMR (75 MHz): δ 14.10 ppm, 22.67, 23.74, 29.16, 29.30, 29.47, 29.52, 29.58, 29.80, 31.89, 40.02, 55.84, 112.08, 118.26, 119.84, 119.92, 121.78, 123.42, 123.81, 125.05, 131.03, 134.55, 138.50, 145.74, 146.89, 147.20, 152.09 and 153.34; HRMS-ESI calcd for $C_{41}H_{58}BrNO_2S$: m/z 707.3372; found: m/z 707.7010 [M⁺].

2-Nitro-7-(5'-bromo-2,2'-bithiophen-5-yl)-9,9-didodecylfluorene (8)

Compound **8** was synthesized from **3** in similar manner to **7** and obtained as a yellow solid (1.65 g, 97%). m.p. 48 °C; IR (KBr): ν 738 cm⁻¹, 788, 822, 881, 970, 1076, 1141, 1272, 1334, 1465, 1518, 1611, 2851 and 2929; ¹H-NMR (300 MHz): δ 0.62 ppm (s, 4 H), 0.85 (t, 6 H, J = 6.90 Hz), 1.15 (m, 36 H), 2.05 (t, 4 H, J = 7.89 Hz), 6.97 (dd, 2 H, J = 4.98 Hz), 7.11 (d, 1 H, J = 3.7 Hz), 7.20 (m, 1 H), 7.32 (d, 1 H, J = 3.80 Hz), 7.44 (m, 1 H), 7.57 (s, 1 H), 7.62 (dd, 1 H, J = 6.8 Hz), 7.76 (d, 2 H, J = 8.8 Hz), 8.20 (s, 1 H) and 8.30 (d, 1 H, J = 8.10 Hz); ¹³C-NMR (75 MHz): δ 14.09 ppm, 22.66, 23.74, 29.17, 29.30, 29.47, 29.52, 29.58, 29.80,31.88, 40.04, 55.83, 111.27, 118.26, 119.79, 119.93, 121.74, 123.43, 123.85, 124.39, 124.95, 125.09, 130.76, 134.80, 136.21, 138.39, 138.71, 143.43, 146.98, 147.15, 152.08 and 153.31; HRMS-ESI calcd for $C_{45}H_{60}BrNO_{2}S_{2}$: m/z 789.3249; found: m/z 789.4159 [M⁺].

2-Nitro-7-(5"-bromo-2,2':5',2"-terthiophen-5-yl)-9,9-didodecylfluorene (9)

Compound **9** was synthesized from **4** in similar manner to **7** and obtained as an orange solid (1.20 g, 91%). m.p. 80 °C; IR (KBr): ν 668 cm⁻¹, 738, 783, 794, 819, 967, 1074, 1138, 1219, 1328, 1462, 1518, 1588, 1608, 2341, 2364, 2851 and 2924; ¹H-NMR (300 MHz): δ 0.62 ppm (s, 4H), 0.84 (d, 12H, J=6.30 Hz), 1.17 (m, 30H), 2.08 (t, 4H, J = 7.50 Hz), 7.01 (t, 3H, J = 16.02 Hz), 7.14 (d, 2H, J = 19.21 Hz), 7.37 (s, 1H), 7.60 (t, 2H, J = 14.41 Hz), 7.79 (d, 2H, J = 8.1 Hz), 8.22 (s, 1H) and 8.28 (d, 1H, J = 8.10 Hz); ¹³C-NMR (75 MHz): δ 14.11 ppm, 22.67, 23.74, 29.19, 29.32, 29.49; 29.54, 29.60, 29.82, 31.89, 40.07, 55.83, 118.25, 119.79, 119.87, 121.76, 123.45, 123.84, 124.38, 124.50, 124.70, 125.04, 130.76, 134.87, 138.20, 147.01, 147.10, 152.07, 153.31 and 155.12; HRMS-ESI calcd for $C_{49}H_{62}BrNO_2S_3$: m/z 871.3126; found: m/z 872.0018 [M †].

7-(Thiophene-2yl)-2-nitro-9,9-didodecylfluorene (2)

A mixture of 7-iodo-2-nitro-9,9-didodecylfluorene (1) (3.95 g, 5.86 mmol), 2-thiophene boronic acid (0.82 g, 6.45 mmol), 2M Na₂CO₃ (56.37 ml), (Ph₃P)₄Pd (0.33 g, 0.29 mmol) in THF (88 ml) was degassed with N₂ for 10 min. The reaction mixture was stirred at reflux under N₂ atmosphere for 22 h. Water (100 ml) was added, the mixture was extracted with CH₂Cl₂ (2 x 100 ml). The combined organic layer was washed with water (100 ml), brine solution (100 ml), dried over anhydrous sodium sulfate, filtered and evaporated to dryness. Purification with column chromatography over silica gel eluting with hexane gave a light yellow viscous oil (3.44 g, 92%); IR (KBr): v 737 cm⁻¹, 795, 823, 839, 886, 1011, 1075, 1125, 1221, 1276, 1332, 1463, 1523, 1605, 2852, 2918 and 3073; ¹H-NMR (300 MHz): δ 0.64 ppm (t, 4 H, J = 8.40 Hz), 0.89 (m, 6 H), 1.22 (m, 36 H), 2.07 (t, 4 H, J = 8.40 Hz), 7.15 (t, 1 H, J = 3.60 Hz), 7.36 (d, 1 H, J = 5.10 Hz), 7.45 (d, 1 H, J = 3.6 Hz), 7.63 (s, 1 H), 7.68 (d, 1 H, J = 6.30 Hz), 7.78 (d, 2 H, J = 8.7 Hz), 8.22 (d, 1 H, J = 2.10 Hz) and 8.27 (d, 1 H, J = 6.30 Hz); HRMS-ESI calcd for C₄₁H₅₉NO₂S: m/z 629.4267; found: m/z 629.7867 [M⁺].

2-Nitro-7-(2,2'-bithiophen-5-yl)-9,9-didodecylfluorene (3)

Compound **3** was synthesized from **7** in similar manner to **2** and obtained as a yellow solid (0.88 g, 97%). m.p. 52 °C; UV-Vis: λ_{max} 262 nm (log ε = 4.35), 402 (4.68); IR (KBr): ν 737 cm⁻¹, 796, 823, 838, 886, 1011, 1077, 1125, 1221, 1276, 1333, 1463, 1522, 1607, 2852, 2918 and 3072; ¹H-NMR (300 MHz): δ 0.85 ppm (t, 6 H, J = 6.97 Hz), 1.19 (m, 40 H), 2.05 (t, 4 H, J = 8.16 Hz), 7.06 (t, 1 H, J = 4.02 Hz), 7.19 (d, 1 H, J = 3.76 Hz), 7.24 (d, 2 H, J = 2.56 Hz), 7.35 (d, 1 H, J = 3.77Hz), 7.59 (s, 1 H), 7.64 (d, 1 H, J = 8.03 Hz), 7.76 (d, 2 H, J = 8.28 Hz), 8.20 (s, 1 H) and 8.26 (d, 1 H, J = 6.45 Hz); ¹³C-NMR (75 MHz): δ 14.08 ppm, 22.65, 23.75, 29.18, 29.29, 29.48, 29.52, 29.58, 29.82, 31.88, 40.06, 55.82, 118.25, 119.73, 119.87, 121.70, 123.42, 123.83, 124.37, 124.66, 124.70, 125.03, 127.94, 135.06, 137.24, 137.38, 138.20, 142.90, 147.09, 152.07 and 153.29; HRMS-ESI calcd for $C_{45}H_{51}NO_{5}S_{5}$: m/z 711.4144; found: m/z 711.5162 [M⁺].

2-Nitro-7-(2,2':5',2"-terthiophen-5-yl)-9,9-didodecylfluorene (4)

Compound **4** was synthesized from **8** in similar manner to **2** and obtained as a yellow solid (1.51 g, 84%). m.p. 82 °C; UV-Vis: λ_{max} 259 nm (log ϵ = 4.32) and 422 (4.68); IR (KBr): v 735 cm⁻¹, 792, 833, 901, 1018, 1075, 1140, 1219, 1267, 1329, 1463, 1517, 1616, 1638, 2848 and 2918; ¹H-NMR (300 MHz): δ 0.84 ppm (d, 6 H, J = 6.60 Hz), 1.16 (m, 40 H), 2.07 (t, 4 H, J = 7.50 Hz), 7.06 (s, 1 H), 7.14 (m, 6 H), 7.37 (s, 1 H), 7.61 (s, 2 H), 7.78 (d, 2 H, J = 8.10 Hz), 8.22 (s, 1 H) and 8.27 (d, 2 H, J = 8.4 Hz); ¹³C-NMR (75 MHz): δ 14.09 ppm, 22.66, 23.75, 29.18, 29.31, 29.48, 29.53, 29.59, 29.82, 31.88, 40.06, 55.83, 118.25, 119.75, 119.87, 121.73, 123.43, 123.82, 124.40, 124.44, 124.48, 124.63, 124.66, 125.02, 127.94, 134.97, 135.96, 136.56, 137.05, 138.25, 143.00, 147.05, 147.11, 152.08 and 153.51; HRMS-ESI calcd for $C_{49}H_{63}NO_2S_3$: m/z 793.4021; found: m/z 793.5124 [M⁺].

2-Nitro-7-(2,2':5',2'':5'',2'''-quaterthiophen-5-yl)-9,9-didodecylfluorene (5)

Compound **5** was synthesized from **9** in similar manner to **2** and obtained as an orange solid (0.76 g, 64%). m.p. 102 °C; UV-Vis: λ_{max} 249 nm (log ε = 4.53) and 437 (4.99); IR (KBr): ν 682 cm⁻¹, 738, 788, 827, 883, 1079, 1130, 1331, 1460, 1518, 1588, 1602, 2341, 2369, 2862 and 2929; ¹H-NMR (300 MHz): δ 0.63 ppm (s, 4 H), 0.84 (d, 6 H, J = 6.90 Hz), 1.17 (m, 36 H), 2.08 (t, 4 H, J = 7.80 Hz), 7.16 (m, 8 H), 7.38 (s, 1 H), 7.61 (s, 1 H), 7.65 (d, 1 H, J = 8.10 Hz), 7.78 (d, 2 H, J = 8.10 Hz), 8.22 (s, 1 H) and 8.28 (d, 1 H, J = 8.40 Hz); ¹³C-NMR (75 MHz): δ 14.09 ppm, 22.66, 23.75, 29.18, 29.31, 29.48, 29.53, 29.59, 29.82, 31.89, 40.06, 55.83, 118.25, 119.76, 119.86, 121.74, 123.43, 123.83, 124.37, 124.43, 124.48, 124.51, 124.66, 124.70, 125.03, 125.57, 127.28, 127.84, 127.93, 128.07, 134.94, 135.74, 136.06, 136.21, 136.54, 136.97, 137.00, 138.28, 143.09, 147.04, 147.11, 152.08 and 153.31; HRMS-ESI calcd for $C_{53}H_{65}NO_2S_4$: m/z 875.3898; found: m/z 875.7712 [M⁺].

N,N-Bis(7-(thiophen-2-yl)-9,9-didodecylfluoren-2-yl)-3,4,9,10-perylenetetracarboxylic diimide (PFT1)

A mixture of 2 (1.41 g, 2.23 mmol), tin (II) chloride (5.04 g, 22.33 mmol), ethanol (37 ml), ethyl acetate (13 ml) and conc. HCl (5 drops) was heated under reflux under N₂ atmosphere for 24 h and then cooled to room temperature. The solution was reduced on a rotary evaporator to give pale yellow oil. Ethyl acetate (50 ml) was added followed by sodium hydrogen carbonate (50 ml). The crude mixture was extracted with ethyl acetate (3 x 50 ml). The combined organic layer was washed with water (100 ml), brine solution (100 ml), dried over anhydrous sodium sulfate, filtered and evaporated to dryness to give the crude product which was used without purification. To a round bottom flask containing the obtained crude product (1.24 g, 2.22 mmol), perylene-3,4,9,10-tetacarboxylic acid dianhydride (0.41 g, 1.06 mmol) and imidazole (6.20 g) were added. The mixture was heated at 140 °C under N, atmosphere for 20 h and allowed to cool to room temperature. Water (100 ml) was added, the mixture was extracted with CH,Cl, (2 x 50 ml). The combined organic layer was washed with water (100 ml), 2M HCl (70 ml), brine solution (100 ml), dried over anhydrous sodium sulfate, filtered and evaporated to dryness. Purification with column chromatography over silica gel eluting with CH,Cl,:hexane followed by recrystallisation with a mixture of CH₂Cl₂ and CH₃OH gave a red solid (1.05 g, 63%). m.p. 176 °C; UV-Vis: λ_{max} 217 nm (log ϵ = 5.01), 260 (4.65), 331 (4.86), 459 (4.36), 490 (4.79) and 527 (4.98); IR (KBr): v 741 cm⁻¹, 796, 809, 849, 963, 1116, 1173, 1248, 1349, 1401,1465, 1592, 1664, 1704, 2848, 2918 and 3410; ¹H-NMR (300 MHz): δ 0.85 ppm (m, 21 H), 1.11 (d, 71 H, J = 28.38 Hz), 2.02 (t, 8 H, J = 7.79 Hz), 7.13 (t, 2 H, J = 5.49 Hz), 7.35 (m, 8 H), 7.63 (t, 4 H, J = 4.78 Hz), 7.74 (d, 2 H, J = 7.86 Hz), 7.86 (d, 2 H, J = 8.48 Hz), 8.16 (d, 4 H, J = 8.09Hz) and 8.74 (d, 4 H, J = 7.89 Hz); ¹³C-NMR (75 MHz): δ 14.11 ppm, 22.69, 23.86, 29.25, 29.36, 29.61, 29.60, 30.05, 31.93, 40.16, 55.47, 120.37, 120.44, 123.00, 123.23, 123.58, 123.70, 124.60, 125.08, 126.60, 127.34, 128.05, 129.72, 131.68, 133.57, 133.77, 134.79, 139.95, 141.03, 145.12, 151.94, 152.09 and 163.49; HRMS-ESI calcd for $C_{106}H_{126}N_2O_4S_2$: m/z 1555.9193; found: m/z 1555.0088 [M⁺].

N,N-Bis(7-(2,2'-bithiophen-5-yl)-9,9-didodecylfluoren-2-yl)-3,4,9,10-perylenetetracarboxylic diimide (PFT2)

PFT2 was synthesized from **3** in similar manner to **PFT** and obtained as a red solid (0.89, 65%). m.p. 184 $^{\circ}$ C; UV-Vis: λ_{max} 261 nm (log ε = 5.27), 274 (5.24), 369 (5.04), 459 (4.32), 490 (4.82) and 527 (5.01); IR (KBr): ν 746 cm⁻¹, 794, 963, 1121, 1175, 1252, 1342, 1401, 1467, 1592, 1669, 1701, 2848, 2918 and 3415; ¹H-NMR (300 MHz): δ 0.84 ppm (t, 12 H, J = 6.94 Hz), 1.19 (t, 80 H, J = 24.52 Hz), 2.03 (t, 8 H, J = 7.96 Hz), 7.05 (t, 2 H, J = 4.31 Hz), 7.19 (d, 2 H, J = 3.69 Hz), 7.25 (t, 4 H, J = 4.56 Hz), 7.34 (m, 6 H), 7.62 (t, 4 H, J = 7.22 Hz), 7.75 (d, 2 H, J = 7.91 Hz), 7.86 (d, 2 H, J = 8.45 Hz), 8.68 (d, 4 H, J = 8.19 Hz) and 8.77 (d, 4 H, J = 7.95 Hz); ¹³C-NMR (75 MHz): δ 14.11 ppm, 22.69, 23.84, 29.23, 29.36, 29.60, 29.67,30.03, 31.93, 40.17, 55.50, 119.97, 120.40, 120.49, 123.30, 123.58, 123.64, 123.72, 124.34, 124.64, 124.74, 126.74, 127.33, 127.87, 129.83, 131.81, 133.23, 133.86, 134.93, 136.54, 137.54, 140.08, 140.99, 143.82, 151.97, 153.16 and 163.57; HRMS-ESI calcd for $C_{114}H_{130}N_2O_4S_4$: m/z 1719.8947; found: m/z 1720.6263 [M⁺].

N,N-Bis(7-(2,2':5',2"-terthiophen-5-yl)-9,9-didodecylfluoren-2-yl)-3,4,9,10-perylenetetracarboxylic diimide (PFT3)

PFT3 was synthesized from **4** in similar manner to **PFT** and obtained as a deep red solid (1.03 g, 49%). m.p. 169 °C; UV-Vis: λ_{max} 262 nm (log ε = 5.26), 273 (5.27), 397.5 (4.97), 458 (4.79), 490 (4.81) and 527 (5.03); IR (KBr): v 744 cm⁻¹, 790, 963, 1116, 1173, 1250, 1342, 1401, 1463, 1592, 1666, 1704, 2848, 2918 and 3410; ¹H-NMR (300 MHz): δ 0.85 ppm (t, 12H, J = 6.92 Hz), 1.19 (m, 80 H), 2.04 (t, 8 H, J = 7.65 Hz), 7.03 (d, 2 H, J = 3.73 Hz), 7.08 (m, 4H), 7.18 (s, 4 H), 7.22 (d, 2 H, J = 5.4 Hz), 7.35 (m, 6 H), 7.61 (t, 4 H, J = 5.63 Hz), 7.74 (d, 2 H, J = 7.9 Hz), 7.85 (d, 2 H, J = 8.45 Hz), 8.61 (d, 4 H, J = 8.22 Hz) and 8.74 (d, 4 H, J = 7.91 Hz); ¹³C-NMR (75 MHz): δ 14.14 ppm, 22.72, 23.86, 29.26, 29.40, 29.63, 29.71, 30.04, 31.95, 40.16, 55.51, 119.95, 120.45, 120.55, 123.25, 123.66, 123.69, 123.75, 124.21, 124.41, 124.53, 124.58, 124.75, 126.61, 127.40, 127.93, 131.72, 133.12, 133.85, 134.82, 136.17, 136.30, 137.25, 140.16, 140.96, 143.94, 151.18 and 163.53; HRMS-ESI calcd for $C_{122}H_{134}N_2O_4S_6$: m/z 1883.8701; found: m/z 1884.4571 [M⁺].

N,N-Bis(7-(2,2':5',2'':5'',2'''-quaterthiophen-5-yl)-9,9-didodecylfluoren-2-yl)-3,4,9,10-perylenetetracarboxylic diimide (PFT4)

PFT4 was synthesized from **5** in similar manner to **PFT** and obtained as a red solid (0.43 g, 52%). m.p. 170 °C; UV-Vis: λ_{max} 227 nm (log ϵ = 4.98), 260 (4.78), 298 (4.54), 427 (5.01), 490 (4.89) and 527 (4.99); IR (KBr): v 744 cm⁻¹, 790, 963, 1175, 1250, 1342, 1401, 1463, 1594, 1666, 1704, 2848, 2918 and 3410; ¹H-NMR (300 MHz): δ 0.68 ppm (s, 4 H), 0.87 (s, 26 H), 1.14 (d, 62 H, J = 21.90 Hz), 2.05 (s, 8 H), 7.20 (m, 18 H), 7.62 (d, 8 H, J = 10.20 Hz), 7.75 (d, 2 H, J = 7.20 Hz), 7.86 (d, 2 H, J = 7.20 Hz), 8.66 (d, 4 H, J = 7.20 Hz) and 8.77 (d, 4 H, J = 6.9 Hz); ¹³C-NMR (75 MHz): δ 14.11 ppm, 22.69, 23.86, 29.24, 29.37,

29.61, 29.68, 30.03, 31.94, 40.16, 40.38, 55.51, 119.77, 119.95, 120.42, 120.54, 123.27, 123.69, 123.77, 124.23, 124.35, 124.41, 124.58, 126.69, 127.40, 127.92, 128.05, 129.79, 131.76, 133.11, 133.89, 134.89, 135.82, 135.89, 136.11, 136.36, 136.43, 137.06, 140.18, 140.94, 144.07, 151.96, 152.20 and 163.54; HRMS-ESI calcd for $C_{130}H_{138}N_2O_4S_8$: m/z 2047.8456; found: m/z 2049.836 [MH₂⁺].

N,N-Bis(9,9-didodecylfluoren-2-yl)-3,4,9,10-perylenetetra carboxylic diimide (PF)

PF was synthesized from 9,9-didodecylfluorene (**6**) in similar manner to **PFT** and obtained as a red solid (1.80 g, 66%). m.p. 192 °C; UV-vis (CH₂Cl₂): λ_{max} 226 nm (log ε = 5.21), 261 (4.95), 305 (4.65), 368 (3.73), 458 (4.35), 489 (4.79) and 526 (5.00); IR (KBr) v 739 cm⁻¹, 1174, 1354, 1450, 1590, 1660, 1701, 2848, 2992, 3409 and 3549; ¹H NMR (300 MHz, CDCl₃): δ 0.92 ppm (t, 12 H, J = 6.98 Hz), 1.24 (m, 80 H), 2.01 (t, 8 H, J = 8.10 Hz), 7.39 (m, 10 H), 7.79 (d, 2 H, J = 8.1 Hz), 7.88 (d, 2 H, J = 8.40 Hz), 8.67 (d, 4 H, J = 8.10 Hz) and 8.79 (d, 4 H, J = 7.8 Hz); ¹³C-NMR (75 MHz): δ 14.11 ppm, 22.69, 23.87, 29.24, 29.37, 29.61, 19.69, 30.03, 31.94, 40.16, 55.51, 119.78, 119.96, 120.41, 120.54, 123.26, 123.69, 123.76, 124.23, 124.34, 124.40, 124.58, 124.66, 124.79, 126.68, 127.40, 127.91, 129.78, 131.74, 133.11, 133.89, 134.87, 135.82, 135.89, 136.11, 136.36, 136.44, 137.06, 140.18, 140.94, 144.07, 151.96, 152.20 and 163.53; HRMS-ESI calcd for $C_{98}H_{123}N_2O_4$: m/z 1391.9438; found: m/z 1392.9507. [MH⁺].

Electropolymerization

Electropolymerizations were carried out using ITO/glass working electrode under an argon atmosphere in 0.1 M solutions of $n\text{-Bu}_4\text{NPF}_6$ in CH_2Cl_2 and containing 0.25 mM of **PFT1-3**. Cyclic scanning (100 mV/s) of the working electrode was applied at potentials up to 1.70 V vs SCE, and the solution was continuously maintained under argon. After electrolysis, the working electrode was washed five times with 10 mL of CH_3CN and CH_2Cl_2 to remove traces of the conducting salt and monomer present on the deposited film and was finally dried under argon at room temperature.

Poly(PFT1): red film; UV-Vis (film): λ_{max} 322, 494 and 530; IR: v 556 cm⁻¹, 746, 797, 839, 1051, 1164, 1177, 1253, 1342, 1457, 1600, 1653, 1669, 1700, 2851 and 2924.

Poly(PFT2): deep red film; UV-Vis (film): λ_{max} 339, 371, 494 and 531; IR: ν 559 cm⁻¹, 738, 839, 1034, 1071, 1107, 1169, 1247, 1356, 1384, 1404, 1474, 1594, 1669, 1706, 2879, 2929 and 2969.

Poly(PFT3): dark red film; IR: v 555 cm⁻¹, 739, 842, 1044, 1051, 1117, 1169, 1347, 1366, 1384, 1414, 1464, 1590, 1670, 1705, 2878, 2932 and 2971.

Quantum calculation

The ground state geometries of all molecules were fully optimized using density functional theory (DFT) at the B3LYP/6-31G (d,p) level, as implemented in Gaussian 03. TDDFT/B3LYP calculation of lowest excitation energies were performed at the optimized geometries of the ground states.

PART VIII

$\label{eq:carbazole} Carbazole\ Dendronized\ Triphenylamines\ as\ Solution-Processed\ High\ T_g$ $\ Amorphous\ Hole\ Transporting\ Materials\ for\ Organic\ Electroluminescent\ Devices$

1. Introduction

Organic light-emitting diodes (OLEDs) have attracted a great deal of attention due to their applications, such as full-color or large-area flat panel displays, backlight, and general illumination. The past decade has seen great progress in both device fabrication techniques and materials development. One of the key developments is the use of hole-transporting layers (HTLs) for hole injection from the anode into the emitting layer providing significant improvement in the performance of the device. In general, high glass transition temperature (T_g) amorphous hole-transporting materials (AHTMs) are needed for highly efficient and long lifetime OLED devices. The most commonly used HTMs, N,N'-diphenyl-N,N'-bis(1-naphthyl)-(1,1'-biphenyl)-4,4'-diamine (NPB) and N,N'-bis(3-methylphenyl)-N,N'-bis(phenyl)benzidine (TPD), provide many attractive properties such as high charge carrier mobility and ease of sublimation. However, their low T_g (65 °C for TPD and 100 °C for NPB), ease of crystallization and low morphological stability usually lead to degradation and short lifetime of the devices. Recently, many arylamine- and carbazole-based AHTMs with high T_g such as carbazole end-capped molecules, 9,9-bis(4-[bis-(4-carbazol-9-yl-biphenyl-4-yl)-amino]phenyl)fluorenes, binaphthalene derivatives and triarylamine-based starburst molecules, have been reported.

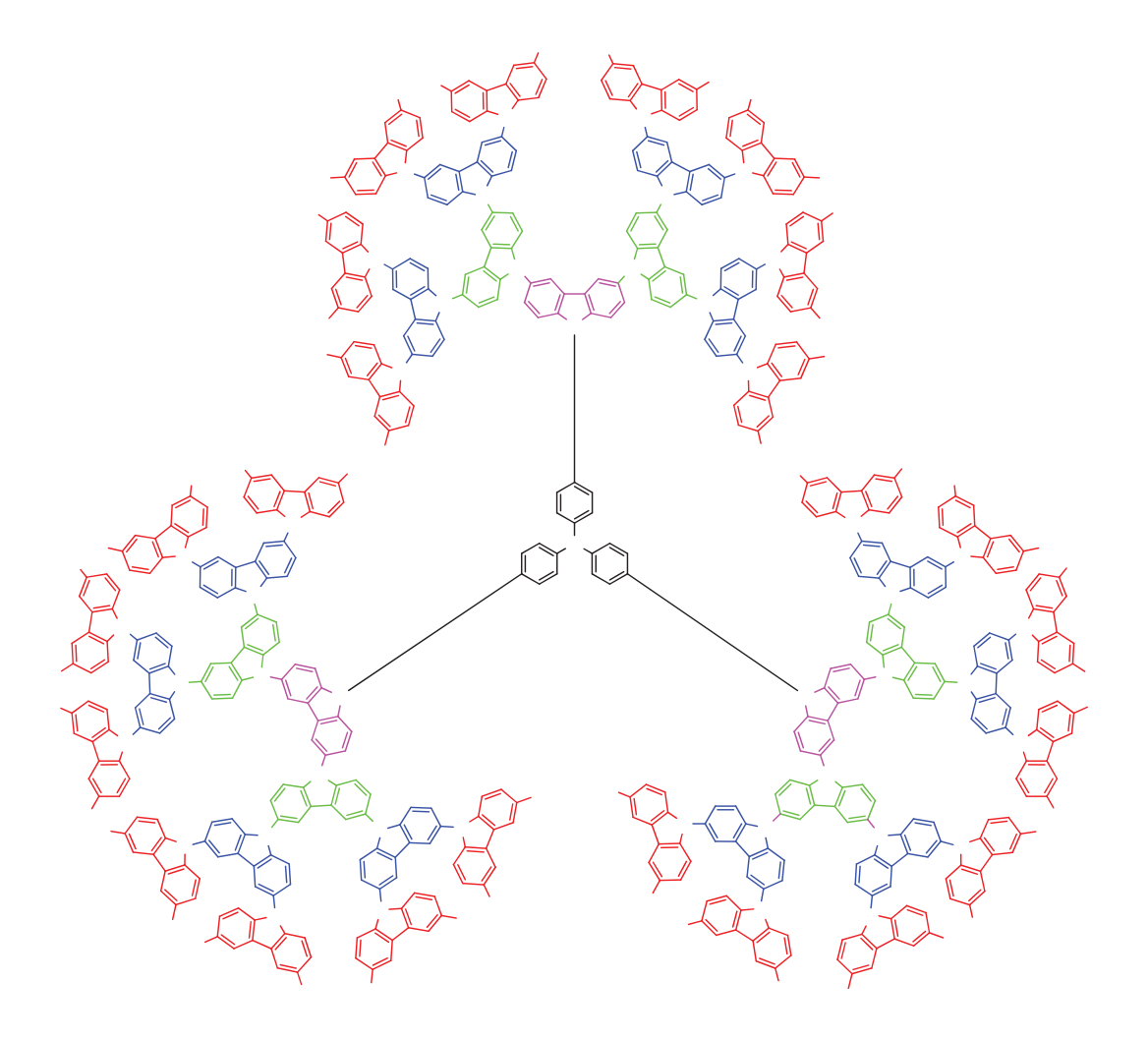
It is known that a suppressing crystallization formation and improving in morphological stability of the molecule can be achieved by forming a bulky structure, in particular a structure of dendrimer. Dendrimers have several unique characteristics that arise from their spherical shape, giving them properties that are very different from both polymers and small molecules. As they are precisely determined structure, they can be characterized like any small molecules. Unlike polymers, they have distribution size that can lead to slight variations their properties. However, as macromolecules, they can form amorphous films, and have high melting (T_m) and glass transition temperature (T_g) and are therefore much less likely to crystalline. Recent progress in organic synthesis provides the buildup of dendritic molecules bearing well-designed building blocks in the core, branching point and on the surface. Many kinds of dendrimers have been synthesized and considered for several applications including electroactive materials for OLEDs such as stilbene and phenylacetylene dendrimers as emitting materials, and aryl amine and oxadiazole dendrimers as hole- and electron transporting layers.

Owing to its excellent hole-transporting ability, high charge carrier mobility, high thermal, morphological and photochemical stability, and the ease of functionality at the 3, 6 or N-positions, carbazole has been used as a building block to form many HTMs. Certainly, it is very attractive to explore and develop high generation carbazole dendrons and their dendrimers that meet the requirements as AHTMs for OLEDs and can be synthesized using simple and low-cost methods. Therefore, we herein implemented all required aspects in the chosen dendrimers (GnCT, Scheme 1). Carbazole as the branching unit and triphenylamine as the core offer a perfect hole-transporting ability with high charge carrier mobility and high glass transition temperature. The strongly twisted carbazole unit in the dendron and the presence of *tert*-butyl groups as the surface offer bulky dendrimer with high solubility, and thereby yield electrochemically and thermally stable amorphous thin film which could be deposited by cheap solution process. An investigation of their physical and photophysical properties, and green OLED fabrication and characterization are also reported.

2. Results and Discussion

Synthesis. The synthetic routes of carbazole dendrons (Gn-H) and their triphenylamine dendrimers (GnCT) are shown in Scheme 2. The dendrons up to 4th generation were synthesized via a convergent approach which begins from the outside of the molecule or the surface groups and then builds inwards through the branching groups towards the core. The synthesis involved the iterative cycle of two orthogonal reactions, Ullmann coupling and detoxylation reactions. The former reaction is a coupling of 9-H-carbazole with aryl iodide to create the next generation dendrons. The latter reaction is a functional group restoration so that a successive coupling reaction can be repeated. tert-Butyl substituents on 3,6position of the carbazole ring were chosen as the surface groups to provide solubility and add to electrochemical stability of the dendrons. Coupling of ready obtained 3,6-di-tert-butylcarbazole (G1-H) and 3,6-diiodo-9-tosylcarbazole (2) in a stoichiometric equivalents of 2.2:1 under mild catalytic system of CuI as catalyst, ±trans-1,2-diaminocyclohexane as co-catalyst, K₃PO₄ as base in toluene at reflux afforded an intermediate G2-Ts in a reasonable good yield of 80%. Deprotection of the tosylate group of the resultant with aqueous KOH in DMSO/THF gave the N-H form of the dendron G2-H in a quantitative yield. By repeating these two reactions in an iterative manner, higher generation carbazole dendrons, G3-H and G4-H, were formed in good yields over two steps of 73% and 71%, respectively. Unfortunately, higher generation dendrons could not be constructed because of the steric hindrance around the focus of a large dendron that can inhibit a complete coupling in this reaction manner. Finally, coupling of three dendrons of each generation (Gn-H) with ready obtained tri(p-iodophenyl)amine (3) under the same Ullmann coupling conditions afforded the corresponding dendrimers (GnCT) as a white solid in reasonable good yields of 75-78%. The structures of all dendrons and dendrimers were characterized unambiguously with FTIR, ¹H-NMR, ¹³C-NMR spectroscopy. The MALDI-TOF mass spectrometry demonstrated that all dendrimers were monodisperse with their molecular weights being identical to the calculated masses. These dendrimers showed good solubility in most organic solvents, opening the door to solution processing techniques with uniform and stable amorphous thin films of these dendrimers can be obtained. This probably results from the presence of *tert*-butyl surface groups and their structural bulkiness.

Scheme 1. Molecular structures of the carbazole dendronized triphenylamine (GnCT)

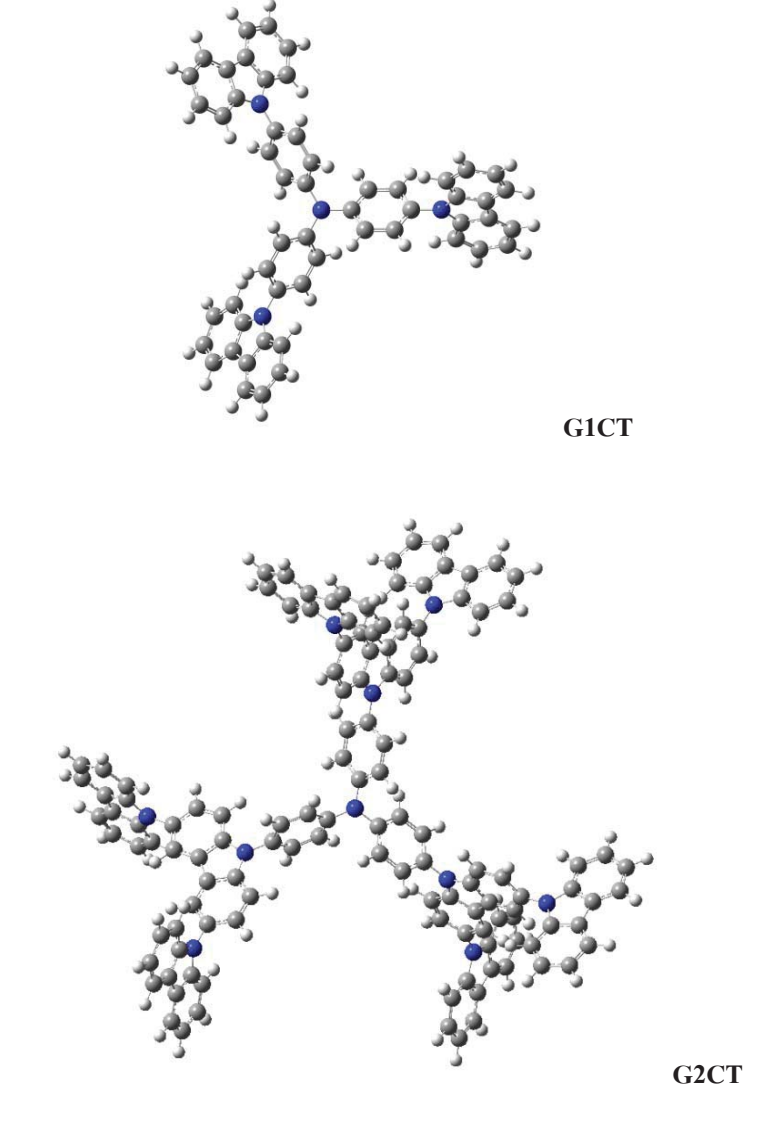


Scheme 1. Synthetic route to carbazole dendrons (Gn-H) and dendrimers (GnCT)

^ai: *tert*-BuCl, ZnCl₂, MeNO₂, ultrasonicate. ii: a) KI, KIO₃, AcOH, b) TsCl, acetone. iii: CuI, K₃PO₄, ±*trans*-1,2-diaminocyclohexane, toluene, heat. iv: KOH, H₂O/THF/DMSO.

Theoretical Calculation and Optical Properties. The geometrical structures of the dendrimers (GnCT) optimized using the HF/6-31G(d.p) method are shown in Figures 2 and S1. The results showed that each new generation of the dendrimers introduced an extra branching group into the structure, and it was these branching groups that made up the bulk of a large dendrimers. As the generation number increased, the number of repeating branching units got exponentially larger, while the volume available increased as the cube of the generation number. The dendrimers therefore find themselves increasingly sterically hindered structures, which are pushed into a sphere with the core at the center and the outer face covered by the surface groups. G4CT had a ball-like structure by means of the triphenylamine core is in the middle and completely surrounded by the carbazole dendrons. Apart from the differences in the size, the conformations of all dendrimers were very similar. Each phenyl unit of the triphenylamine core had a

dihedral angle of $83-85^{\circ}$ to the molecular plane of the attached carbazole ring, while each plane of the carbazole ring in the dendron twisted nearly perpendicular to the other. Such structural characteristics can influence some of their electronic and physical properties such as a suppression of the π -electron conjugation between each aromatic unit.



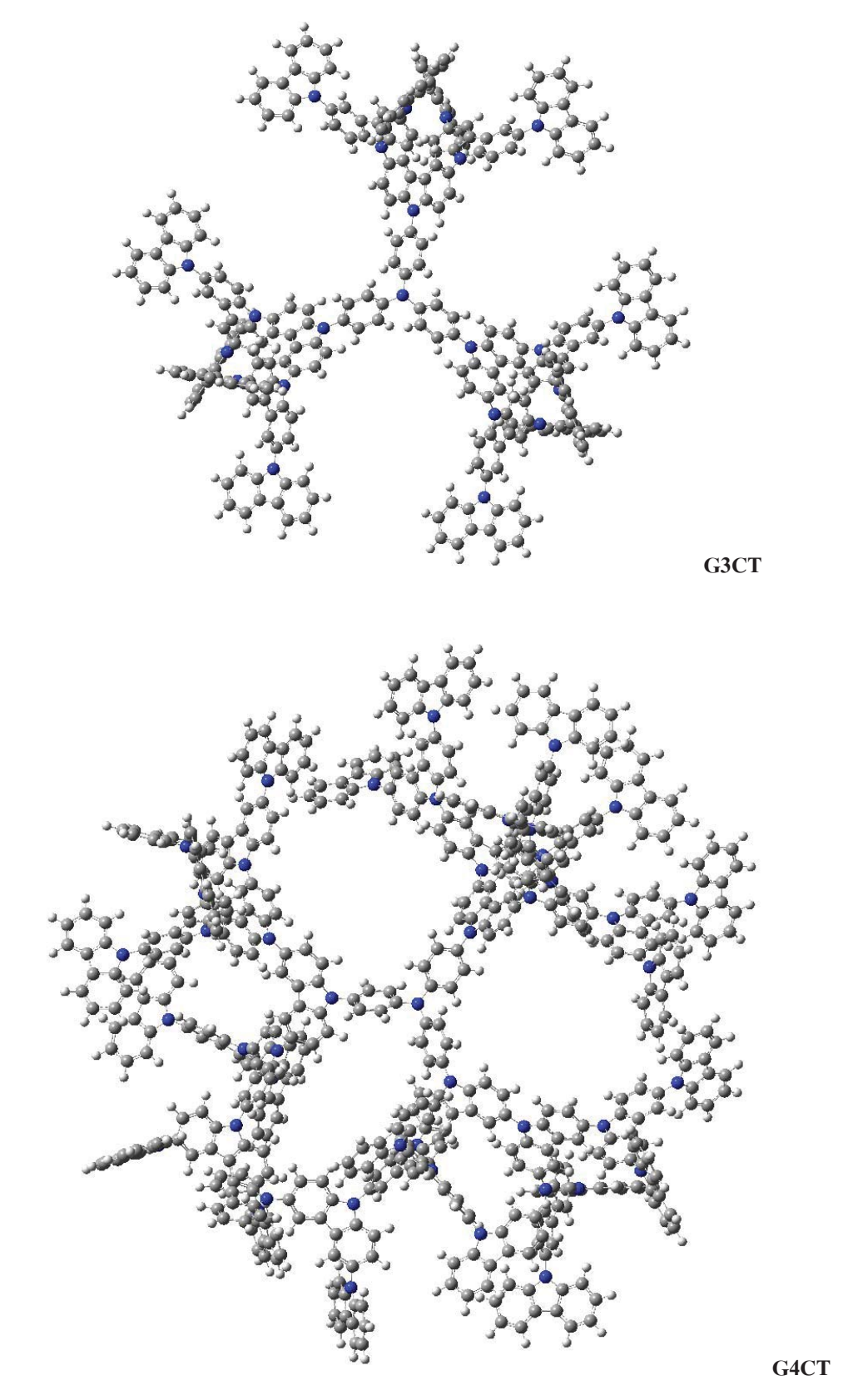


Figure S1. The optimized geometries of **GnCT** by the GIAO (Gauge-Independent Atomic Orbital) method at the HF/6-31G(d,p) level with *tert*-butyl groups are omitted.

The optical properties of the dendrimers GnCT were investigated by UV-Vis and photoluminescence (PL) spectroscopy in both dilute CH_2Cl_2 solution and thin film spin-coated from chloroform:toluene (1:1) solution on quart substrate. The results are shown in Figure 3 and summarized in Table 1. The solution absorption spectra of these dendrimers showed similar absorption features which were characterized by strong absorption bands at around 289 nm assigned to the π - π * local electron transition of each carbazole unit, and less intense absorption bands at longer wavelength (> 320 nm) related to the π - π * electron transition of the conjugated core. The absorption edge slightly red-shifted about 3 nm from G1CT to G2CT-G4CT, suggesting generation of number of the dendrons has little effect on electronic properties of the dendrimers. In the solid state, the absorption spectra of all dendrimers showed similar absorption features to their corresponding solution absorption spectra with the absorption edges of both G1CT and G2CT being slightly red-shifted (4-5 nm) compared to their corresponding solution spectra. The energy band gaps (E_g) of the dendrimers deduced from the absorption edge were nearly identical (3.40-3.37 eV), despite the somewhat different molecular sizes, indicating similar π -conjugation length. This can be explained by an out of plane twisting of each carbazole unit in the dendron limiting π -interaction between the carbazoles.

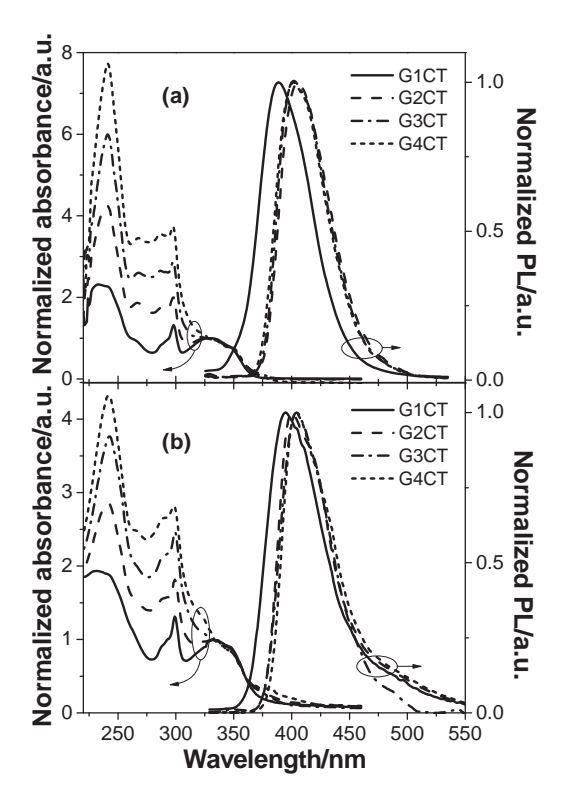


Figure 3. UV-Vis and photoluminescence (PL) spectra of **GnCT** in (a) CH₂Cl₂ solution and (b) thin film obtained from spin coating.

Table 1. Physical and photophysical properties of the dendrimers (GnCT).

material	$\lambda_{abs} (nm)^a$	$\lambda_{em} (nm)^a$	$\Phi_{\scriptscriptstyle F}^{\;\;b}$	$T_g/T_c/T_m/T_{5d}$ (°C) ^c	$\mathbf{E}_{1/2}(\mathbf{V})^d$	$E_g (eV)^f$	HOMO/LUMO
							(eV) ^g
G1CT	298, 331	395	0.37	215/279/398/344	0.80, 1.07, 1.28, 1.51	3.40	-5.21/-1.81
G2CT	298, 331	402	0.30	321/366/516/395	0.97, 1.15, 1.22	3.40	-5.36/-1.96
G3CT	298, 331	404	0.29	368/ - / - /396	0.99, 1.16	3.38	-5.38/-2.00
G4CT	298, 331	404	0.15	401/ - / - /413	1.02, 1.19	3.37	-5.38/-2.01

^aMeasured as thin film obtained by spin casting. ^bDetermined in CH₂Cl₂ solutions with quinine sulfate solution in 0.01 M H₂SO₄ ($\Phi_F = 0.54$) as a standard. ^cObtained from DSC and TGA measurements. ^d Obtained from CV and DPV at a scan rate of 50 mV/s. ^eOxidation onset potential. ^fEstimated from the onset of the absorption spectra ($E_g = 1240/\lambda_{onset}$). ^gCalculated from HOMO = -(4.44 + E_{onset}) and LUMO = HOMO + E_g , where E_{onset} is the onset of the oxidation.

The solution photoluminescence (PL) spectra of GnCT showed an emission band in blue-purple region with a featureless pattern. PL spectra of G2CT-G4CT were nearly the same and red shifted (15 nm) comparing to the PL of G1CT. Fluorescence quantum yields ($\Phi_{\rm F}$) of GnCT determined in CH₂Cl₂ gradually decreased from 0.37 to 0.12 as generation number of the dendrimer increased. In the solid state, a slight red shift (6 nm) in PL spectra of G1CT from its solution PL was observed, while those of G2CT-G4CT were identical to their corresponding solution PL, indicating weak intermolecular electronic interactions in less bulky G1CT dendrimer.

Electrochemical Properties. The electrochemical properties of all dendrimers were investigated by cyclic and differential pulse voltammetry (CV and DPV), and the resulting data are shown in Figure 4a and summarized in Table 1.

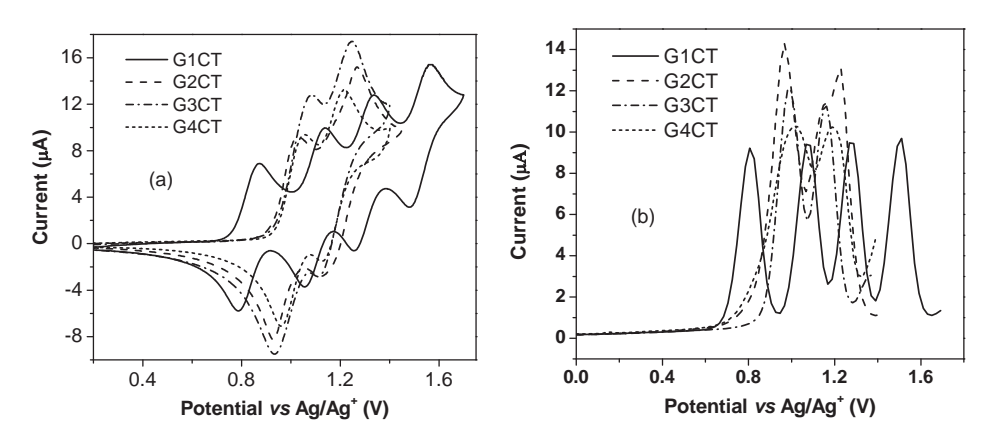


Figure S2 (a) CV and (b) DPV curves of GnCT measured in CH₂Cl₂ at a scan rate of 50 mV s⁻¹.

The experiment was carried out in degassed CH₂Cl₂ containing 0.1 M n-Bu₄NPF₆ as a supporting electrolyte under argon atmosphere. G1CT was found to exhibit well separated four quasi-reversible

oxidation processes, whereas G2CT-G4CT showed two quasi-reversible oxidation processes. The first oxidation wave assigned to the removal of electrons from the carbazoles in the dendron to give radical cation and the rest to the oxidation of the remaining moieties. The potentials of the first oxidation increased from 0.80, 0.97, 0.99 to 1.02 V when the generation of the dendrimers increased. Their multiple CV scans revealed identical CV curves with no additional peak at lower potential on the cathodic scan (E_{nc}) being observed, indicating no oxidative coupling at the 3, 6 positions of the peripheral carbazole led to electro-polymerization (Figure S2). The present of 3,6-di-tert butyl groups could prevent this type of electrochemical coupling reaction which is usually detected in some carbazole derivatives with unsubstituted 3,6-positions. The results suggested that these dendrimers were electrochemically stable molecules. Moreover, under these measurement conditions, no distinct reduction process was detected in all samples. The HOMO energy levels of the dendrimers were calculated from the onset of the oxidation. The HOMO level of G1CT (-5.21 eV) was slightly higher than those of higher generation dendrimers G2CT-G4CT (-5.36- -5.38 eV), Beside, the LUMO energy levels of these materials were calculated to be between -1.81 and -2.01 eV by subtracting the energy band gaps (E_n) from HOMO levels (Table 1). With their HOMO energy levels matching well with the work functions of indium tin oxide (ITO) electrode and stable electrochemical property, these dendrimers have great potential for hole injection and transport in OLED.

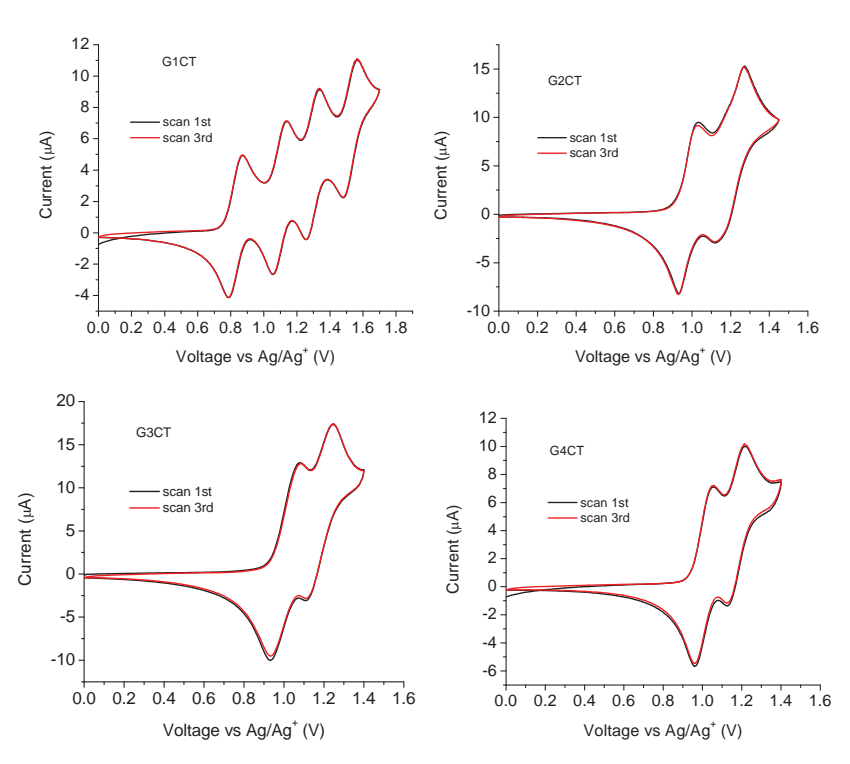


Figure S2.1 Multiple CV scan curves of GnCT measured in CH₂Cl₂ at a scan rate of 50 mV s⁻¹.

Thermal and Morphological Properties. For OLED applications, thermal stability of organic materials is crucial for device stability and lifetime. The thermal instability or low glass transition temperature (T_g) of the amorphous organic layer may result in the degradation of organic devices due to morphological changes. The thermal properties of GnCT were investigated by thermogravimetric analysis (TGA) and differential scanning calorimetry (DSC), and the results are shown in Figure 4b and summarized in Table 1. Those results suggested that all dendrimers were thermally stable materials with the decomposition temperature at 5% weight loss (T_{5d}) over 350 °C in TGA analysis. Their phase transition properties were more interesting. In DSC analysis, G1CT and G2CT had the same phase transition behaviors. In both 1st and 2nd heating scans, the DSC curves of both dendrimers displayed an endothermic baseline shift owing to glass transition (Tg) followed by broad exothermic peak due to the crystallization (T_c) and endothermic melting peak (T_m) at higher temperature. The T_gs of G1CT and G2CT were 215 and 321 °C, respectively. For higher generation dendrimers, different phase transition behaviors were observed. DSC curves of G3CT and G4CT showed only baseline shift due to Tg at 368 and 401 °C, respectively, with no crystallization and melting were detected at higher temperature in both scans. These results indicated that all dendrimers were stable amorphous materials with high T_g which was substantially higher those of the commonly used HTMs such as NPB ($T_g = 100$ °C) and TPD ($T_g = 63$ °C), and many reported carbazole and triphenylamine derivatives. To our knowledge, we believe that G4CT is among one of the highest T_g AHTMs being reported so far. It was noticed that the T_gs of these dendrimers increased as the generation of the dendron increased because of the rigid structure of the carbazole dendron. The results indicate that the new carbazole dendronized triphenylamines can reduce the crystallization of both carbazole and triphenylamine and improve the amorphous stability of the materials, which in turn could increase the service time in device operation and enhance the morphological stability to the thin film. Moreover, the abilities of GnCT to form a molecular glass and dissolve in organic solvents offers the possibility to prepare good thin films by solution casting techniques which are highly desirable for fabrication of OLED device.

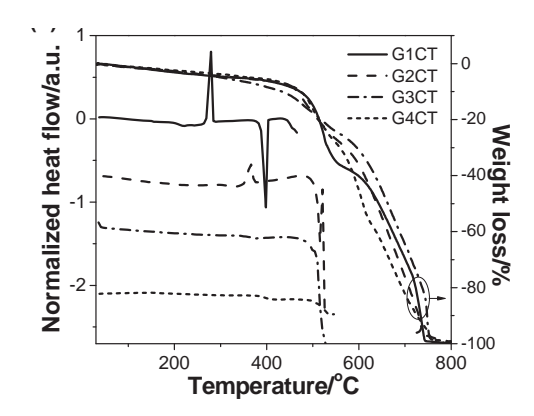


Figure 4. DSC (2nd heating scan) and TGA curves measured at 10 °C min⁻¹ under N₂.

The amorphous characteristics of **GnCT** were further studied by powder X-ray diffraction (XRD) using silicon wafer as a substrate. The XRD patterns are shown in Figure 5. For **G1CT**, a series of sharp peaks were recorded at 2θ of 17, 18 and 21° (the corresponding d values are 5.2, 4.9 and 4.3 Å) which were attributed to the π - π stacking of carbazole segments. In higher generation dendrimers **G2CT-G4CT**, these peaks became broad amorphous peaks at the same positions. The XRD experiment indicated that formation of high generation dendrimers (**G2-G4**) could effectively reduce the crystalline nature of carbazole to develop amorphous materials.

The morphologies of the dendrimers were also characterized by atomic force microscope (AFM) using standard tapping mode. The films were spin-coating from chloroform:toluene solution on glass substrate and then heated at 60 °C for 30 min to remove the solvents. As depicted in Figure 6, the films of all dendrimers showed a quite smooth surface, indicating their good film formation abilities. For G1CT, a few pinholes were observed. The presence of pinholes in the film might cause a large leakage current. We believed that the small molecular size and the crystallization ability of G1CT caused the pinhole formation in the film.

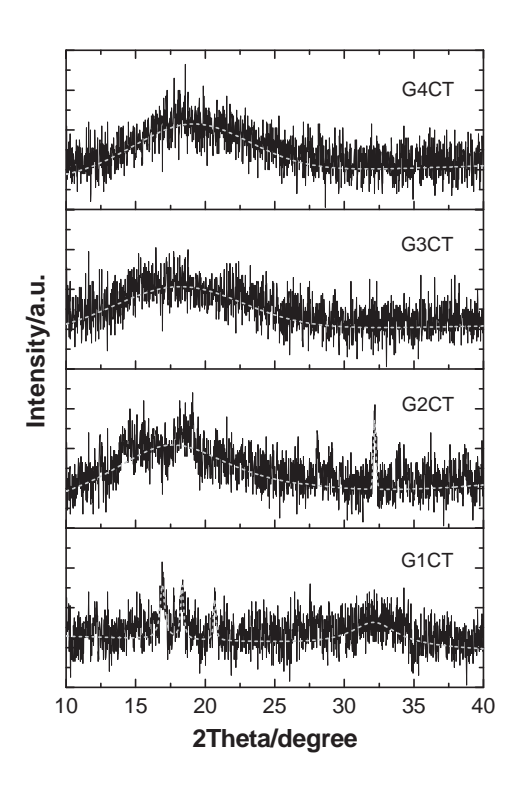


Figure 5. Powder X-ray diffraction patterns of **GnCT** on silicon wafer substrate (dotted line represents Xfit data).

OLED Studies. To investigate HTM abilities of **GnCT**, green OLEDs (V-VIII) were fabricated using these dendrimers as hole-transporting layers (HTL); the devices have the configuration of indium tin oxide (ITO)/PEDOT:PSS/HTL(40 nm)/Alq3(50 nm)/LiF(0.5 nm):Al(150 nm), where tris-(8-

hydroxyquinoline)aluminum (Alq3) as the green light-emitting (EML) and electron-transporting layers (ETL), and ITO and LiF:Al as anode and cathode, respectively (Figure 7a). The HTL was spin-coated from chloroform:toluene (1:1) solution with controlled thickness. To evaluate the effect of the interfacial layer and to compare hole-transporting abilities of the synthesized dendrimers **GnCT**, the reference devices (I-IV) of the same structure with and without a commonly used commercial HTM, *N,N'*-diphenyl-*N,N'*-bis(1-naphthyl)-(1,1'-biphenyl)-4,4'-diamine (NPB) as HTL were made. As the devices were fabricated identically, the differences between them should indicate the improvement achieved with the new material or device structure.

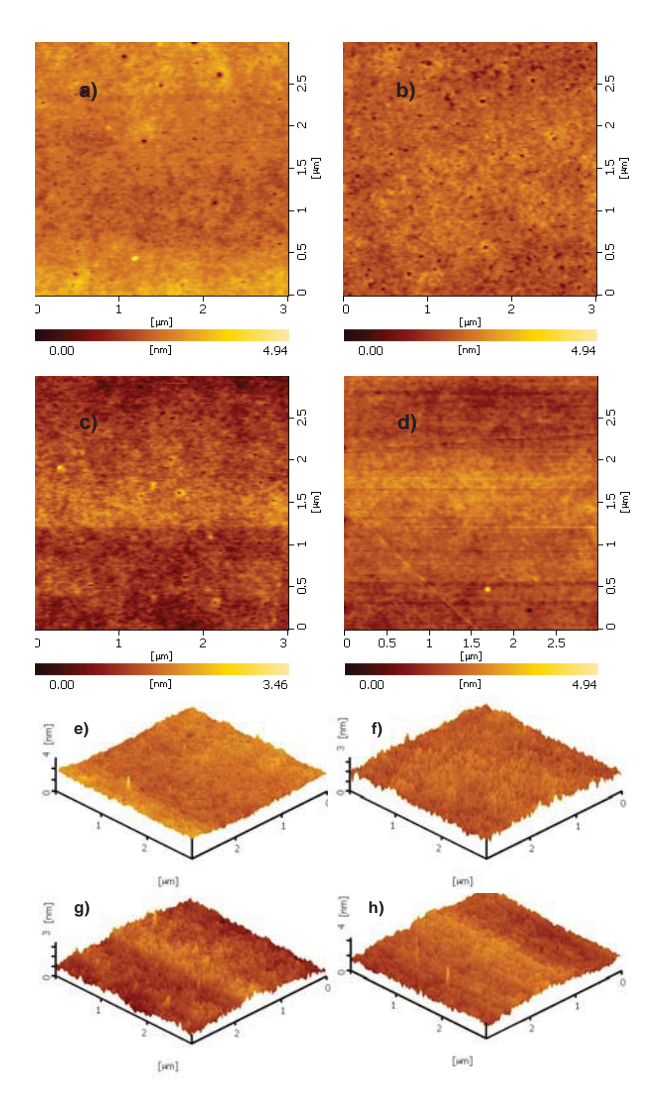


Figure S4 Tapping mode AFM images of spin-coated films: a) and e) G1CT; b) and f) G2CT; c) and g)

G3CT; d) and h) G4CT

The optical and electrical characteristics of all fabricated OLED devices are illustrated in Figures 7a, 8 and all parameters are summarized in Table 2. From our study and other reports, it was found that the incorporation of conductive polymer, poly(3,4-ethylenedioxythiophene):poly(4-styrenesulfonate)

(PEDOT:PSS), in the device as hole injection layer not only increased the maximum luminance from 9243 cd m^{-2} (η of 1.34 cd A^{-1}) in device I to 30044 cd m^{-2} (η of 4.42 cd A^{-1}) in device II, but also significantly decreased the turn-on voltage from 6.0 V to 3.1 V. Moreover, their EL spectra were near identical. It has been pointed out that the lower operating voltage of PEDOT:PSS-based device can be attributed to the rough and porous surface of spin-coated PEDOT:PSS polymer layer, which increases the contact area to enhance hole injection and lowers barrier at the organic-organic interface by relocating the barrier to the more conductive PEDOT:PSS layer. To enable high-performance devices therefore PEDOT:PSS as hole injection layer was integrated into the devices. Under applied voltage, all GnCT-based devices (V-VIII) exhibited a bright green emission with peaks centered at 518 nm and CIE coordinates of (0.29, 0.53) (Figure 7b). The electroluminescence (EL) spectra of these diodes were identical, and matched with the PL spectrum of Alq3, the EL of the reference devices (II-IV) and also other reported EL spectra of Alq3-based devices. No emission at the longer wavelength owing to exciplex species formed at the interface of HTL and ETL materials, which often occurs in the devices fabricated from HTL with planar molecular structure, was detected. In our case, the formation of exciplex species could be prevented by the bulky nature of the carbazole dendron. From these results and in view of the fact that a barrier for electronmigration at the Alq3/HTL interface (~1.00 eV) is nearly five times higher than those for hole-migration at the HTL/Alq3 interface (~0.21 eV). Hence, under the present device configuration of ITO/PEDOT:PSS/GnCT/Alq3/LiF:Al, GnCT would act only as HTM, and Alq3 would act preferably as an electron blocker more than as a hole blocker and charge recombination thus confined to Alq3 layer. More importantly, a stable emission was obtained from all diodes (V-VIII) with the EL spectra and CIE coordinates did not change over the entire applied voltages (Figure S3).

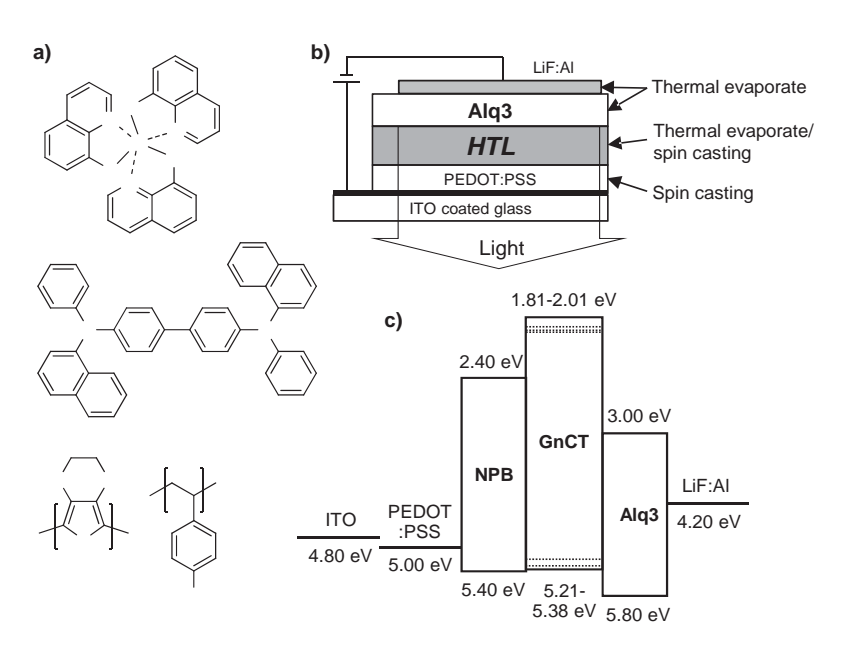


Figure S9 a) Molecular structures of the materials used in this work. b) Typical Alq3-based green OLED devices fabricated in this work. c) A schematic of the energy band diagram of each layer of the devices.

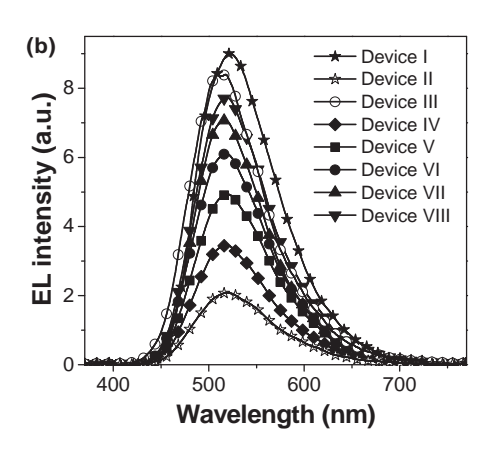


Figure 7. (b) EL spectra of the devices.

The light turn-on voltage 1 cd m⁻² for all devices (V-VIII) was in the range of 3.0-3.1 V and the operating voltage at 100 cd m⁻² was in the range of 3.8-4.4 V, indicating good performance is achieved for all the devices. By comparison with the reference device III, it was found that the incorporation of GnCT in the device as HTL not only increased the maximum luminances from 4631 cd m⁻² to 18350-25397 cd m ², but also significantly decreased the turn-on voltage from 4.2 V to 3.0 V. Besides, their EL spectra were nearly identical. Moreover, the device characteristics in terms of maximum brightness, turn-on voltage and maximum luminous efficiency clearly demonstrated that the hole-transporting abilities of G2CT, G3CT and G4CT were greater than NPB-based device (IV) fabricating by the same spin coating process, and comparable to NPB-based device (II) fabricating by thermal evaporating technique. Device VII having dendrimer G3CT as HTL exhibited the best performance with a high maximum brightness of 25390 cd m⁻² for green OLED at 10.8 V, a low turn-on voltage of 3.0 V, a maximum luminous efficiency of 4.47 cd A⁻¹ and a maximum external quantum efficiency of 0.21%. A comparable device performance was observed from devices VI (G2CT as HTL) and VIII (G4CT as HTL) (Table 2). However, the devices using G1CT as HTL showed lower performance in terms of maximum brightness and maximum luminous efficiency which might be due to the presence of pinholes in the films and its high HOMO level (-5.21 eV) compared to other dendrimers (-5.36- -5.38 eV). In order to further explain the different efficiencies of the OLED devices, analysis of band energy diagrams of all devices (V-VIII) was performed and it revealed that the HOMO levels of all HTL materials (-5.21- -5.38 eV) lie between those of PEDOT:PSS (-5.00 eV) and Alq3 (-5.80 eV) (Figure 7a). When the diodes operate at forward bias, holes are injected from ITO/PEDOT:PSS electrode pass HTL to Alq3 layer and electrons are injected from Al electrode to Alq3 layer, and both holes and electrons are accumulated at the interface between HTL layer and Alq3 layer because of barrier. The injection barriers for the gathered holes to transfer from the HTL to Alq3 are 0.59 eV (device V) and ~0.42 eV (devices VI-VIII). Accordingly, a migration of holes from the HTL to Alq3 layers is more effective in devices VI-VIII compared to device V, resulting in the charge efficiently

recombine in the Alq3 emitting layer and better device performance. It has been demonstrated that the efficiency of an OLED depends both on the balance of electrons and holes and the $\Phi_{\rm F}$ of the emitter. Although, many HTMs have been reported, in terms of the amorphous morphology, significantly high $T_{\rm g}$, solution processability and device efficiency, these dendrimers G2CT-G4CT are among the good HTMs reported.

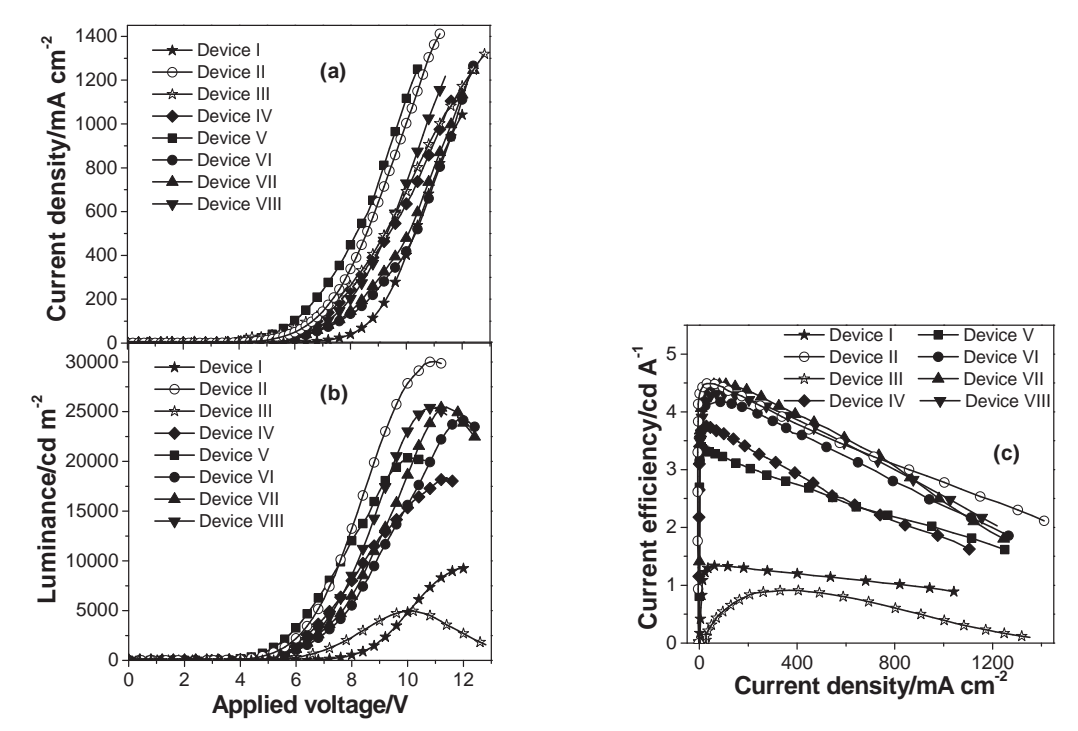


Figure 8. (a) Luminance-applied voltage characteristics, (b) current density-applied voltage characteristics, and (c) variation of luminance efficiency with current density of OLEDs with and without **GnCT** as HTL.

Table 2. Device characteristics of OLEDs with and without GnCT as HTLs.

devic	structure	turn-on	maximum luminance	EL maxima	$\eta_{_{ m max}}$	CIE _{x,y}
e		voltage (V)	$(\operatorname{cd} \operatorname{m}^{-2})$	(nm)	(cd A ⁻¹)	
I	ITO/NPB/ALq3/LiF:Al ^a	6.0	9243	522	1.34	0.31,0.55
II	ITO/PEDOT:PSS/NPB/ALq3/LiF:Al ^a	3.1	30044	515	4.42	0.25,0.48
III	ITO/PEDOT:PSS/ALq3/LiF:Al	4.2	4961	518	0.91	0.30,0.54
IV	ITO/PEDOT:PSS/NPB/ALq3/LiF;Al	3.0	20373	517	3.22	0.29,0.53
V	ITO/PEDOT:PSS/G1CT/ALq3/LiF:A1	3.0	18350	518	3.75	0.29,0.53
VI	ITO/PEDOT:PSS/G2CT/ALq3/LiF:A1	3.0	24165	518	4.20	0.29,0.53
VII	ITO/PEDOT:PSS/G3CT/ALq3/LiF:Al	3.0	25390	518	4.47	0.29,0.53
VIII	ITO/PEDOT:PSS/G4CT/ALq3/LiF:Al	3.0	25397	518	4.32	0.29,0.53

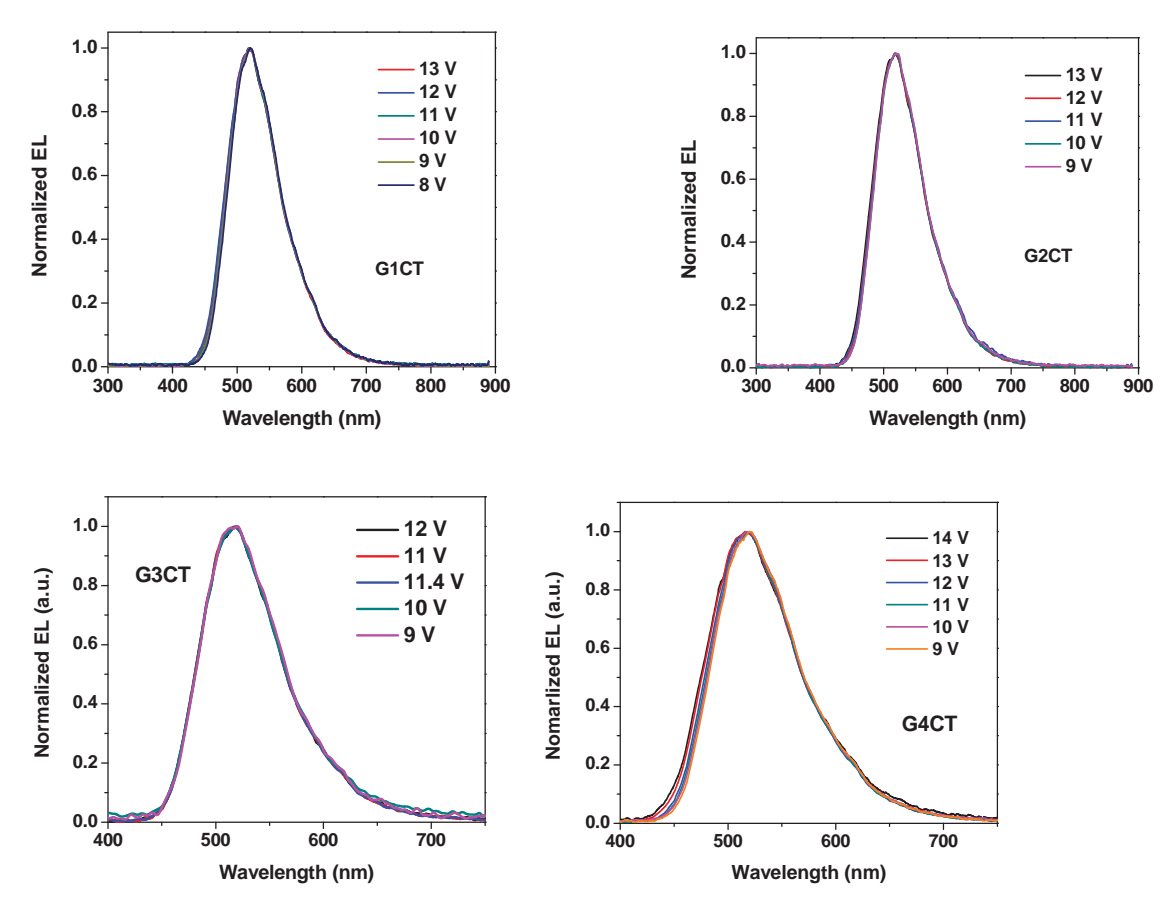


Figure S3 Normalized EL spectra of OLED devices V-VIII under different applied voltages.

3. Conclusions

In conclusion, we have presented a facile and efficient synthesis of rigid carbazole dendrons up to the 4th generation using simple Ullmann coupling and detosylation reactions. Their triphenylamine dendrimers showed chemically-stable redox and thermally stable amorphous properties with substantially high glass transition temperatures (T_g) up to 401 °C. Alq3-based green OLEDs using these materials as the hole-transporting layer (HTL) with the device configuration of ITO/PEDOT:PSS/HTL/Alq3/LiF:Al emit brightly (λ_{em} 518 nm) from the Alq3 layer with a maximum luminance, maximum efficiency and low turn-on voltage of 25,390 cd m⁻², 4.47 cd A⁻¹ and 3.0 V, respectively. The abilities of these dendrimers as solution-processed HTLs for green OLEDs in terms of device performance and thermal property were greater than a common hole-transporter NPB. These dendrimers may also be promising materials for long-lifetime device applications, especially for high-temperature applications in OLEDs or other organic optoelectronic devices. The use of these carbazole dendrons by forming dendritic structures with other fluorescent or non-fluorescent core units might be an effective way to prepare high T_g amorphous materials for various applications.

4. Experimental Section

General. All reagents were purchased from Aldrich, Acros or Fluka and used without further purification. All solvents were supplied by Thai companies and used without further distillation. Tetrahydrofuran (THF) was refluxed with sodium and benzophenone, and distilled. Dichloromethane for cyclic voltammetry (CV) measurements was washed with conc. H₂SO₄ and distilled twice from calcium hydride. Chromatographic separations were carried out on silica gel Merk Silica gel 60 (0.0630-0.200 mm). ¹H and ¹³C nuclear magnetic resonance (NMR) spectra were recorded on a Brüker AVANCE 300 MHz spectrometer with tetramethylsilane as the internal reference using CDCl₃ as solvent in all cases. Infrared (IR) spectra were measured on a Perkin-Elmer FTIR spectroscopy spectrum RXI spectrometer as KBr disc. Ultraviolet-visible (UV-Vis) spectra were recorded as a diluted solution in spectroscopic grade dichloromethane on a Perkin-Elmer UV Lambda 25 spectrometer. Photoluminescence spectra and the fluorescence quantum yields ($\Phi_{\rm p}$) were recorded with a Perkin-Elmer LS 50B Luminescence Spectrometer as a dilute solution in spectroscopic grade dichloromethane and thin film obtained by spin casting. The fluorescence quantum yields (Φ_p) were determined by comparison with a fluorescence standard of quinine sulfate solution in 0.01 M H_2SO_4 ($\Phi_F = 0.54$). Differential scanning carolimetry (DSC) analysis and thermogravimetry analysis (TGA) were performed on a METTLER DSC823e thermal analyzer and a Rigaku TG-DTA 8120 thermal analyzer, respectively, with heating rate of 10 °C/min under nitrogen atmosphere. Cyclic voltammetry (CV) measurements were carried out on an Autolab potentiostat PGSTAT 12 with a three electrode system (platinum counter electrode, glassy carbon working electrode and Ag/Ag⁺ reference electrode) at scan rate of 50 mV/s in dichloromethane under argon atmosphere. The concentration of analytical materials and tetrabutyl ammonium hexafluorophosphate (n-Bu₄NPF₆) were 10 ³ M and 0.1 M, respectively. Melting points were measured using an Electrothermal IA 9100 series of digital melting point instrument and uncorrected.

MALDI-TOF mass spectra were recorded on Bruker Daltonics (Bremen, Germany) Autoflex II Matrix-Assisted Laser Desoprtion/Ionization-Time of Flight Mass Spectrometer (BIFEX) using α -cyano-4-hydroxycinnamic acid as matrix (except G4CT without matrix) at Chulalongkorn University. The atomic force microscopy (AFM) analysis was performed on SPA 4000 STM/AFM system using standard tipping mode with resonance of 222.223 KHz, force constant of 6.1 (+-20%), cantilever length of 87 (+-5 μ m), cantilever width of 32 (+-5 μ m), scan area of 3-5 μ m and scan speed of 1Hz. Powder X-ray diffraction (XRD) was analyzed by a PHILIPS X Pert-MDP X-ray diffractometer using Cu K $_{\alpha}$ radiation (λ = 1.5418 Å) at 1,400 W, 40 kV and 35 mA in the scanning angle (2 theta) of 10-40 $^{\circ}$ with resolution of 0.04 $^{\circ}$ at counting step of 1 s/step. The samples were placed on silicon wafer substrate.

The ground state geometries of **GnCT** were fully optimized using HF/6-31G(d,p) level as implemented in Gaussian 03. ¹⁵

Synthesis.

Synthesis of G1-H: To a stirred solution of carbazole (10.00 g, 59.80 mmol) and zinc chloride (24.45 g, 179.41 mmol) in nitromethane was added *tert*-butylchloride (19.77 ml, 179.41 mmol) under N_2 atmosphere. The solution was sonicated at room temperature for 3h. The mixture was added with water (100 ml) and extracted with dichloromethane (3 x 100 ml). The combined organic layer was washed with water (100 ml), neutralized with sodium carbonate solution, brine solution (100 ml), dried over anhydrous Na_2SO_4 , filtered and removal of the solvent to dryness. Purification by recrystallization from dichloromethane and hexane gave a white powder (15.37 g, 92%). m.p. 217-219 °C; ¹H-NMR (300 MHz, CDCl₃,) δ 1.47 (s, 18H; CH₃), 7.34 (d, J = 8.5 Hz, 2H; ArH), 7.48 (dd, J = 8.5 Hz, J = 1.6 Hz, 2H; ArH), 7.87 (s, 1H; Ar-NH), 8.11 (s, 2H; ArH). ¹³C-NMR (75 MHz, CDCl₃) δ 32.12, 34.56, 110.12, 116.21, 123.32, 123.58, 138.07, 142.27. IR (KBr disc, cm⁻¹), 3419 (s (N-H 2°-amine)), 3045 (s (=C-H aromatic)), 2861-2993 (s (CH₃)), 1493-1651 (s (C=C aromatic)), 1363, 1300, 1296 (vs (C-N aromatic)), 1264, 1202, 1137, 1102, 1034, 922, 880 (w (N-H (2°-amine)), 818 (vs (=C-H aromatic)), 617. MALDI-TOF (m/z) (M⁺) calcd for $C_{20}H_{25}N$: 279.1987, found: 278.167 (M⁺).

Synthesis of 2: To a solution of 3,6-diiodocarbazole (10 g, 59.80 mmol) and KOH (24.45 g, 179.41 mmol) in acetone (150 ml) under N₂ atmosphere was added slowly with *p*-toluenesulfonylchloride (24.45 g, 179.41 mmol). The reaction mixture was heated at reflux for 15 min. The reaction solution was poured into water (100 ml) and extracted with dichloromethane (3 x 100 ml). The combined organic phase was washed with water (100 ml), brine solution (100 ml), dried over anhydrous Na₂SO₄, filtered and removal of the solvent to dryness. Purification by recrystallization with dichloromethane and hexane gave a yellow powder (12.31 g, 90%). m.p. > 250 °C; ¹H-NMR (300 MHz, CDCl₃, δ): 2.30 (s, 3H; CH₃), 7.15 (d, J = 8.4 Hz, 2H; ArH), 7.66 (d, J = 8.4 Hz, 2H; ArH), 7.79 (dd, J = 9 Hz, J = 1.5 Hz, 2H; ArH), 8.09 (d, J = 9 Hz, 2H; ArH), 8.17 (s, 2H; ArH). 13 C-NMR (75 MHz, CDCl₃, δ): 21.55, 32.02, 87.96, 116.97, 126.46, 127.17, 129.15, 129.90, 134.45, 136.54, 137.81, 145.48. IR (KBr disc, cm⁻¹), 3045(s (=C-H aromatic)), 2865-2958 (s (CH₃)), 1493-1594 (s (C=C aromatic)),1465, 1423, 1362 (vs (C-N aromatic)),1207, 1188, 1169 (s (S=O)), 1130, 1090,1020, 967, 819, 711(vs (=C-H aromatic)), 588, 571,533 (s (C-I)). MALDITOF (m/z) (M⁺) calcd for C₁₉H₁₃I₂NO₂S: 572.8756, found: 572.280 (M⁺).

Synthesis of G2-Ts: A mixture of 2 (4 g, 6.98 mmol), G1-H (4.29 g, 15.35 mmol), K₃PO₄ (3.72 g, 17.50 mmol) and CuI (0.57 g, 3.50 mmol) in toluene (60 ml) was degassed with N₂ for 5 min followed by an addition of (±)-trans-1,2-diaminocyclohexane. The reaction mixture was heated at 110 °C for 24 h and the solvent was removed to dryness. The crude was added with and water (100 ml) and extracted with dichloromethane (2 x 100 ml). The combined organic phase was washed with water (100 ml), brine solution (100 ml), dried over anhydrous Na₂SO₄, filtered and removal of the solvent to dryness. Purification by column chromatography over silica gel eluting with a mixture of dichloromethane and hexane (1:4) followed by recrystallization with a mixture of dichloromethane and methanol afforded a

white solid (4.77 g, 78%); m.p. 222-224 °C. ¹H NMR (300 MHz, CDCl₃, δ): 1.48 (s, 36H; CH₃), 2.42 (s, 3H; CH₃), 7.28-7.37 (m, 6H; ArH), 7.47 (dd, J = 9.0 Hz, J = 1.5 Hz, 4H; ArH), 7.76 (dd, J = 9.0 Hz, J = 1.8 Hz, 2H; ArH), 7.94 (d, J = 8.1 Hz, 2H; ArH), 8.07 (d, J = 1.8 Hz, 2H; ArH), 8.16 (s, 2H; ArH), 8.17 (s, 2H; ArH), 8.58 (s, 1H; ArH), 8.61 (s, 1H; ArH). ¹³C-NMR (75 MHz, CDCl₃, δ): 21.70, 32.04, 32.08, 34.77, 109.01, 109.14, 116.20, 116.34, 118.53, 123.43, 123.57, 123.73, 126.79, 127.13, 130.10, 134.58, 135.06, 137.41, 139.55, 145.51. IR (KBr disc, cm⁻¹), 3054 (s (=C-H aromatic)), 2861-2949 (s (CH₃)), 1489-1614 (s (C=C aromatic)), 1453, 1374, 1362 (vs (C-N aromatic)), 1325, 1295, 1261, 1235, 1179, 1169 (s (S=O)), 1132, 1092, 1033, 973, 875, 807, (vs (=C-H aromatic)), 740, 705, 667,585. MALDI-TOF (m/z) (M⁺) calcd for $C_{50}H_{61}N_3O_2S$: 875.4484, found: 874.919 (M⁺).

Synthesis of G2-H: A mixture of G2-Ts (1 g, 1.14 mmol), KOH (0.13 g, 2.32 mmol), dimethylsulphoxide (6 ml), tetrahydrofuran (12 ml) and water (2 ml) was stirred at reflux temperature under N_2 atmosphere for 25 min. After the mixture was cooled to room temperature, 10% HCl (20 ml) was added, followed by water (10 ml) and methanol (5 ml). The precipitate was collected on by filtration and washed with water several times followed by recrystallization with a mixture of dichloromethane and methanol to give a white solid (0.78 g, 95%). m.p 246-248 °C. ¹H NMR (300 MHz, CDCl₃, δ): 1.48 (s, 36H; CH₃), 7.33 (d, J = 8.4 Hz, 4H; ArH), 7.47 (d, J = 8.4 Hz, 4H; ArH), 7.59 (d, J = 6.9 Hz, 4H; ArH), 8.18 (s, 6H; ArH), 8.45 (s, 1H; Ar-NH). 13 C-NMR (75 MHz, CDCl₃, δ) 30.93, 32.06, 34.74, 109.14, 111.89, 116.19, 119.40, 123.09, 123.56, 124.09, 125.93, 130.44, 139.04, 140.22, 142.53. IR (KBr disc, cm⁻¹), 3450 (s (N-H 2°-amine)), 3046 (s (=C-H aromatic)), 2865-2958 (s (CH₃)), 1493-1627 (s (C=C aromatic)), 1363, 1325, 1292 (vs (C-N aromatic)), 1262, 1236, 1168, 1033, 875 (w (N-H (2°-amine)), 809 (vs (=C-H aromatic)), 741, 655, 611, 570. MALDI-TOF (m/z) (M[†]) calcd for $C_{52}H_{55}N_3$: 721.4396, found: 720.876 (M[†]).

Synthesis of G3-Ts: G3-Ts was prepared in similar manner to G2-Ts from G2-H (4.29 g) and 2 (4 g), and obtained as a white solid (9.34 g, 76%). m.p. > 250 °C. ¹H-NMR (300 MHz, CDCl₃, δ): 1.51 (s, 72H; CH₃), 2.46 (s, 3H; CH₃), 7.37-7.42 (m, 10 H; ArH), 7.50 (d, J = 8.4 Hz, 9H; ArH), 7.66 (s, 8H; ArH), 8.01 (d, J = 8.7 Hz, 2H; ArH), 8.07 (d, J = 8.1 Hz, 2H; ArH), 8.20 (s, 8H; ArH), 8.31 (s, 4H; ArH), 8.42 (s, 2H; ArH), 8.81 (d, J = 9.0 Hz, 2H; ArH). ¹³C-NMR (75 MHz, CDCl₃, δ) 21.78, 32.09, 34.78, 76.64, 77.06, 77.48, 109.10, 110.98, 116.29, 116.79, 119.52, 123.19 123.62, 124.07, 126.16, 127.92, 127.16, 127.51, 131.15, 130.30, 133.61, 138.24, 140.18, 140.18, 142.66, 145.90. IR (KBr disc, cm⁻¹), 3046 (s (=C-H aromatic)), 2861-2949 (s (CH₃)), 1489-1629 (s (C=C aromatic)),1379,1362 (vs (C-N aromatic)),1324, 1295, 1281, 1262, 1231, 1187, 1175 (s (S=O)), 1131, 1033, 875, 807, (vs (=C-H aromatic)), 741, 689, 664, 611, 585, 543. MALDI-TOF (m/z) (M[†]) calcd for C₁₂₃H₁₂₁N₇O₂S: 1759.9302, found: 1760.625 (M[†]) (M[†]).

Synthesis of G3-H: G3-H was prepared in similar manner to G2-H from G3-Ts (1 g), and obtained as a white solids (0.65 g, 95%). m.p. >250 °C. ¹H-NMR (300 MHz, CDCl₂, δ): 1.46 (s, 72H; CH₂),

7.35 (d, J = 8.4 Hz, 8H; ArH), 7.46 (dd, J = 9.0 Hz, J = 1.8 Hz, 8H; ArH), 7.61 (s, 8H; ArH), 7.84 (s, 4H; ArH), 8.16 (s, 4H; ArH), 8.17 (s, 4H; ArH), 8.27 (s, 4H; ArH), 8.47 (s, 2H; ArH), 8.65 (s, 1H; Ar-NH).

13 C-NMR (75 MHz, CDCl₃, δ) 32.05, 34.73, 109.12, 111.08, 112.47, 116.20, 123.09, 123.55, 123.74, 124.27, 125.99, 126.35129.60, 130.69, 139.68, 140.21, 142.52. IR (KBr disc, cm⁻¹), 3424 (s (N-H 2°-amine)), 3046 (s (=C-H aromatic)), 2865-2958 (s (CH₃)), 1487-1631 (s (C=C aromatic)),1363, 1325, 1294 (vs (C-N aromatic)), 1280, 1263, 1235, 1034, 875 (w (N-H (2°-amine)), 809 (vs (=C-H aromatic)), 714, 668, 655, 611. MALDI-TOF (m/z) (M⁺) calcd for C₁₁₆H₁₁₅N₇: 1605.9214, found: 1606.277 (M⁺).

Synthesis of G4-Ts: G4-Ts was prepared in similar manner to G1-Ts from G3-H (2.46 g) and 2 (0.41 g), and obtained as a white solids (1.89 g, 75%). m.p. > 250 °C. ¹H-NMR (300 MHz, CDCl₃, δ): 1.51 (s, 144H; CH₃), 2.53 (s, 3H; CH₃), 7.40 (d, J = 8.1 Hz, 17H; ArH), 7.50 (d, J = 7.2 Hz, 17H; ArH), 7.69 (d, J = 4.2 Hz, 16H), 7.86 (d, J = 8.4 Hz, 4H; ArH), 7.93 (d, J = 8.7 Hz, 4H; ArH), 8.09-8.17 (m, 4H; ArH), 8.22 (s, 16H; ArH), 8.34 (s, 8H; ArH), 8.59 (s, 2H; ArH), 8.66 (s, 4H; ArH), 8.93 (d, J = 8.7 Hz, 2H; ArH). 13 C-NMR (75 MHz, CDCl₃, δ) 10.95, 14.02, 22.97, 23.78, 28.94, 29.34, 29.69, 30.39, 31.61, 32.01, 34.69, 38.77, 68.18, 109.07, 111.03, 111.67, 116.17, 119.41, 120.06, 123.11, 123.52, 123.78, 123.94, 126.01, 128.80, 129.93, 130.86, 140.20, 141.39, 142.12, 142.51. IR (KBr disc, cm⁻¹), 3046 (s (=C-H aromatic)), 2865-2953 (s (CH₃)), 1487-1629 (s (C=C aromatic)), 1391, 1380, 1364 (vs (C-N aromatic)), 1324, 1295, 1281, 1262, 1231, 1187, 1173 (s (S=O)), 1104, 1090, 1033, 970, 920, 875 (vs (=C-H aromatic)), 838,, 808, 740, 689, 663, 610, 584, 543 . MALDI-TOF (m/z) (M[†]) calcd for C₂₅₁H₂₄₁N₁₅O₂S: 3528.8938, found: 3531.1599 (M[†]).

Synthesis of G4-H: G4-H was prepared in similar manner to G2-H from G4-Ts (1 g) and obtained by purification with by column chromatography over silica gel eluting with a mixture of dichloromethane and hexane (1:4) to give a white solid (0.91 g, 95%). m.p. > 250 °C. ¹H-NMR (300 MHz, CDCl₃, δ): 1.45 (s, 144H; CH₃), 7.34 (d, J = 8.4 Hz, 16 H; ArH), 7.45 (d, J = 8.4 Hz, 16 H; ArH), 7.67 (d, J = 8.4 Hz, 8H; ArH), 7.90-7.94 (m, 12H; ArH),8.16 (s, 16H; ArH), 8.28 (s, 8H; ArH), 8.60 (s, 4H; ArH), 8.63 (s, 2H; ArH),8.73 (s, 1H; Ar-NH). ¹³C-NMR (75 MHz, CDCl₃, δ): 32.05, 34.74, 109.30, 116.23, 123.37, 123.57, 127.77, 139.37, 142.91. IR (KBr disc, cm⁻¹), 3410 (s (N-H 2°-amine)), 3046 (s (=C-H aromatic)), 2852-2953 (s (CH₃)), 1484-1629 (s (C=C aromatic)), 1391, 1362, 1324, 1294 (vs (C-N aromatic)), 1280, 1262, 1233, 1153, 1130, 1033, 875 (w (N-H (2°-amine)), 805 (vs (=C-H aromatic)), 740, 655, 610, 571, 503. MALDI-TOF (m/z) (M[†]) calcd for C₂₄₄H₂₃₅N₁₅: 3374.8850, found: 3376.830 (M[†]).

Synthesis of G1CT: A mixture of 3 (0.30 g, 0.48 mmol), G1-H (0.67 g, 2.40 mmol), K_3PO_4 (0.38 g, 1.82 mmol) and CuI (0.14 g, 0.72 mmol) in toluene (30 ml) was stirred and degassed with N_2 for 5 min followed by an addition of (\pm)-trans-1,2-diaminocyclohexane. The reaction mixture was heated at 110 °C for 24 h. After being cooled to room temperature, the reaction mixture was filtrated through a plug of silica

gel washing with dichloromethane. After the solvent was evaporated to dryness, the residue was purified by column chromatography over silica gel eluting with a mixture of dichloromethane and hexane (1:4) followed by recrystallization with a mixture of dichloromethane and methanol to give a white solid (0.40 g, 78%). m.p. 228-230 °C. 1 H-NMR (300 MHz, CDCl₃, δ): 1.48 (s, 54H; CH₃), 7.48-7.58 (m, 24H; ArH), 8.19 (s, 6H; ArH). 13 C-NMR (75 MHz, CDCl₃, δ) 21.78, 32.09, 34.78, 76.64, 77.06, 77.48, 109.10, 110.98, 116.29, 116.79, 119.52, 123.19, 123.62, 124.07, 126.16, 127.92, 127.16, 127.51, 130.30, 131.15, 133.61, 138.24, 140.18, 142.66, 145.90. IR (KBr disc, cm $^{-1}$), 3041 (s (=C-H aromatic), 2861-2953 (s (CH₃)), 1504-1627 (s (C=C aromatic)),1487, 1472, 1392, 1363, 1313, 1292 (vs (C-N aromatic)), 1262, 1232, 1193, 1103, 1033, 875 (vs (=C-H aromatic)), 808. UV-Vis (CH₂Cl₂) λ_{max} (ϵ , 10 5 dm 3 mol $^{-1}$ cm $^{-1}$) 298 nm (2.76), 326 nm (2.07). MALDI-TOF (m/z) (M $^{+}$) calcd for C_{79} H₉₄N₄: 1076.6696, found: 1076.131 (M $^{+}$).

Synthesis of G2CT: G2CT was prepared in similar manner to G1CT from 3 (0.07 g, 0.12 mmol) and G2-H (0.45 g, 0.62 mmol), and obtained as a white solid (0.20 g, 77%). m.p. > 250 °C. ¹H-NMR (300 MHz, CDCl₃, δ): 1.48 (s, 108H; CH₃), 7.36 (d, J = 8.7 Hz, 12H; ArH), 7.49 (d, J = 8.4 Hz, 12H; ArH), 7.66-7.84 (m, 24H; ArH), 8.18 (s, 12H; ArH), 8.26 (s, 6H; ArH). ¹³C-NMR (75 MHz, CDCl₃, δ): 32.04, 34.74, 109.06, 111.15, 116.25, 119.42, 123.17, 123.57, 124.03, 125.75, 126.03, 128.57, 131.04, 132.67, 140.16, 140.52, 142.63, 146.88. IR (KBr disc, cm⁻¹), 3046 (s (=C-H aromatic), 2865-2953 (s (CH₃)), 1504-1629 (s (C=C aromatic)), 1484, 1392, 1363, 1315, 1292 (vs (C-N aromatic)), 1280, 1262, 1233, 1162, 1104, 1033, 875 (vs (=C-H aromatic)), 839, 807. UV-Vis (CH₂Cl₂) λ_{max} (ε, 10⁵ dm³mol⁻¹cm⁻¹) 298 nm (2.34), 326 nm (1.17). MALDI-TOF (m/z) (M[†]) calcd for C₁₇₄H₁₇₄N₁₀:2403.3923, found: 2403.405 (M[†]).

Synthesis of G3CT: G3CT was prepared in similar manner to G1CT from 3 (0.02 g, 0.03 mmol) and G3-H (0.50 g, 0.14 mmol), and obtained as a white solid (0.12 g, 75%). m.p. > 250 °C. ¹H-NMR (300 MHz, CDCl₃, δ): 1.48 (s, 216H; CH₃), 7.36 (d, J = 7.2 Hz, 22H; ArH), 7.47 (d, J = 8.1 Hz, 26H; ArH), 7.66 (d, J = 3.9 Hz, 24H; ArH), 7.90-7.98 (m, 24H; ArH), 8.18 (s, 24H; ArH), 8.30 (s, 12H; ArH), 8.62 (s, 6H; ArH). ¹³C-NMR (75 MHz, CDCl₃, δ) 29.72, 32.05, 34.74, 109.08, 111.01, 111.74, 116.25, 119.50, 120.21, 123.15, 123.56, 123.86, 124.28, 125.97, 126.08, 126.52, 128.82, 130.27, 130.88, 132.56, 140.21, 141.24, 141.37, 124.60, 147.17. IR (KBr disc, cm⁻¹), 3046 (s (=C-H aromatic), 2861-2953 (s (CH₃)), 1489-1629 (s (C=C aromatic)), 1391, 1362, 1323, 1259 (vs (C-N aromatic)), 1230, 1181, 1103, 871 (vs (=C-H aromatic)), 807. UV-Vis (CH₂Cl₂) λ_{max} (ε, 10^5 dm³ mol⁻¹cm⁻¹) 298 nm (3.8389), 326 nm (1.3383). MALDI-TOF (m/z) (M[†]) calcd for C₃₆₆H₃₅₄N₂₂:5056.8377, found: 5057.529 (M[†]).

Synthesis of G4CT: G4CT was prepared in similar manner to G1CT from 3 (0.015 g, 0.03 mmol)) and G4-H (0.50 g, 0.14 mmol), and obtained as a white solid (16 mg, 5%). m.p. > 250 °C. ¹H-NMR (300 MHz, CDCl₃, δ): 1.47 (s, 432H; CH₃), 7.33 (d, J = 8.4 Hz, 48H; ArH), 7.43 (d, J = 8.4 Hz, 48H; ArH), 7.58-7.73 (m, 60H; ArH), 7.84 (d, J = 8.7 Hz, 12H; ArH), 7.88 (d, J = 10.2 Hz, 12H; ArH), 8.02 (s, 12H; ArH), 8.15 (s, 48H; ArH), 8.27 (s, 24H; ArH), 8.60 (s, 12H; ArH), 8.72 (s, 6H; ArH). ¹³C-NMR (75 MHz, CDCl₃, δ);

29.72, 32.09, 34.70, 109.06, 111.00, 116.20, 119.45, 123.11, 123.53, 123.80, 126.02, 130.88, 140.18, 141.66 142.60. IR (KBr disc, cm⁻¹), 3046 (s (=C-H aromatic), 2857-2953 (s (CH₃)), 1489-1616 (s (C=C aromatic)), 1362, 1324, 1294, 1261 (vs (C-N aromatic)), 1232, 1098, 1022, 920, 876 (vs (=C-H aromatic)), 805. UV-Vis (CH₂Cl₂) λ_{max} (ϵ , 10⁵ dm³ mol⁻¹ cm⁻¹) 298 nm (5.1547), 326 nm (1.4577). MALDI-TOF (m/z) (M⁺) calcd for C₇₅₀H₇₁₄N₄₆: 10363.7285, found: 10436.618 (M⁺ + solvent).

Device Fabrication and Charaterization. Alq3-based green OLED devices using GnCT and NPB as HTL with configuration ITO/PEDOT:PSS/HTL(40 nm)/Alq3(50 nm)/LiF(0.5 nm):Al(150 nm) were fabricated and characterized as followed. The patterned indium tin oxide (ITO) glass substrate with a sheet resistance 14 Ω/\Box (purchased from Kintec Company) was thoroughly cleaned by successive ultrasonic treatment in detergent, deionised water, isopropanol, and acetone, and then dried at 60 °C in a vacuum oven. A 50 nm thick PEDOT:PSS hole injection layer was spin-coated on top of ITO from a 0.75 wt.% dispersion in water at a spin speed of 3000 rpm for 20 s and dried at 200 °C for 15 min under vacuum. Thin films of HTL were deposited on top of PEDOT:PSS layer by spin-coating chloroform:toluene solution of GnCT and NBP (1.5% w/v) on an ITO glass substrate at a spin speed of 3000 rpm for 30 second to get a 40 nm thick of hole-transporting layer (HTL). The film thickness was measured by using a Tencor α-Step 500 surface profiler. Then Alq3 was deposited onto the surface of the HTL film as lightemitting (EML) and electron-transporting layer (ETL) with a thickness of 50 nm by evaporation from resistively heated alumina crucibles at evaporation rate of 0.5-1.0 nm/s in vacuum evaporator deposition (ES280, ANS Technology) under a base pressure of ~10-5 mbar. The film thickness was monitored and recorded by quartz oscillator thickness meter (TM-350, MAXTEK). The chamber was vented with dry air to load the cathode materials and pumped back; a 0.5 nm thick LiF and a 150 nm thick aluminium layers were the subsequently deposited through a shadow mask on the top of EML film without braking vacuum to from an active diode areas of 4 mm2. The measurement of device efficiency was performed according to M. E. Thomson's protocol and the device external quantum efficiencies were calculated using procedure reported previously. 16 Current density-voltage-luminescence (J-V-L) characteristics were measured simultaneous by the use of a Keithley 2400 source meter and a Newport 1835C power meter equipped with a Newport 818-UV/CM calibrated silicon photodiode. The electroluminescent spectra were acquired by an Ocean Optics USB4000 multichannel spectrometer. All the measurements were performed under ambient atmosphere at room temperature.

PART IX

Novel D- π -A organic dyes for dye-sensitized solar cells

1. INTRODUCTION

Since their report on dye-sensitized solar cells (DSSCs) with dramatically increased in the light harvesting efficiency by O'Reagan and Grätzel in 1991, this type of solar cells has attracted considerable and sustained attention due to it offers the possibility of low-cost conversion of the photoenergy. Up to date, DSSC with a validated efficiency record of >11% has been obtained with ruthenium complexes dyes such as the black dye. More recently, DSSC submodule of 17 cm² constituted of eight parallel cells with conversion efficiency of >9.9% was fabricated by Son. Though there is still room for improvement of the efficiency of ruthenium-based DSSCs, ruthenium dyes are nevertheless costly, hardly attained and normally have moderate absorption intensity. Enormous effort is also being dedicated to develop new and efficient dyes suitable for their modest cost, ease of synthesis and modification, large molar extinction coefficient, and long-term stability. Ruthenium-free dyes or organic dyes meet all these criteria. Therefore, there is remarkable development in organic dye-based DSSCs in recent years, and efficiencies exceeding 10% have been achieved using dyes which have broad, red-shifted and intense spectral absorption in the visible light region, 400–800 nm. Although remarkable progress has been made in the organic dyes as sensitizers for DSSCs, it is still needed to optimize their chemical structures for further improvement in performances. Most of developed organic dyes are constituted by donor, π -conjugation and acceptor moieties, thereby forming a D- π -A structure, and broad ranges of conversion efficiencies were achieved. Most of the highly efficient DSSCs based on organic dyes was found to have long π -conjugated spacers between the donor and acceptor, resulting broad and intense absorption spectra, aromatic amines as donor moieties and strong electron withdrawing group (cyanoacrylic acid) as acceptor and anchoring moieties. However, introduction of long π -conjugation segments outcomes the prolonged rod-like molecules, which may facilitate the recombination of the electrons to the triiodide and magnify aggregation between molecules. The close π - π aggregation can not only lead to self-quenching and reduction of electron injection into TiO,, but also to instability of the organic dyes due to the formation of excited triplet states and unstable radicals under light irradiation. On the basis of these criteria, recently, organic dyes with 2D- π -A structure are reported by several groups. Their studies suggest that good performance for organic dyes based on 2D- π -A structure over the simple D- π -A configuration could be achieved by molecular design. We expect that a further improvement could be made by introducing additional donor moiety into the

aromatic amine donor to form the D-D- π -A structure, and believe that the absorption region can be extended and the molar extinction coefficient can be enhanced with lower tendency to aggregate and better thermal stability comparing with the D- π -A structure. There are rare reports on organic dyes with structure of this type.

Chart 1. Structure of the dyes

In our design (Chart 1), diphenylamine and 3,6-di-tert-butylcarbazole moiety are employed as the aromatic and additional donors, respectively because of their electron rich nitrogen hetero atom, thereby forming a 3,6-di-tert-butylcarbazol-9-ylphenyl-N-dodecylaniline donor moiety (D-D). Recently, many groups have reported that DSSCs with various triphenylamine and carbazole-based dyes have shown the n up to 9.1%, indicating the importance of their further investigation in DSSCs. In addition, it has been found that by incorporating electron donor triarylamine group into the dye molecule, the physical separation of the dye cation from the electrode surface will be increased, which fascinates to achieve high rate of charge separation and collection compared to interfacial charge-recombination processes. Furthermore, triphenylamine and carbazole molecules have aroused great interest for their excellent holetransport capability, and their derivatives have become classic hole-transporting materials. Moreover, the 3,6-di-tert-butylcarbazol-9-ylphenyl-N-dodecylaniline moiety is non-planar conformation in the ground state, which should prevent the aggregation of the dye molecules and enhance the open-circuit photovoltage by reducing recombination. As a result, π - π aggregation of long π -conjugated spacers can be inhibited. The bulky 3,6-di-tert-butyl substituents on the peripheral carbazole units aim at increasing the solubility of the dye and forming a hydrophobic layer on TiO₂ surface to prevent iodide/triiodide (I/I₃) in the electrolyte from recombining with injected electrons in the TiO₂. The cyanoacrylic acid moiety acts as the electron accepting and anchoring group. The two functional moieties are connected by oligothiophene segments rather than the p-phenylene and vinylene because of their chemical and environmental stability as well as their electronic tenability. Number of thiophene units in the segment is varied to tune the optical properties of the dye.

Nowadays, theoretical quantum calculations have been the famous and effective tools in field of chemistry because they can be used to rationalize the properties of known chemical compounds and also

predict those of unknown ones to guidance observed experimental synthesis. These methods included: (1) Density functional theory (DFT) a reliable tool including electron correlation based on density of electron, has been found to give satisfactory results especially electronic ground-state geometry prediction. (2) Time-dependent DFT (TDDFT) a developed tool from DFT, has been used to compute the spectroscopic properties including excitation energy, UV/Vis spectra, oscillator strength, and electronic composition. It is well-known that the use of standard density functional such as B3LYP results in severely underestimated charge-transfer excitation energies and incorrect asymptotic potential energy surfaces resulting from electron-transfer self-interaction. Therefore, in the present study, we used the promising approach, high-level symmetry-adapted cluster configuration interaction (SAC-CI), to prodict the spectroscopy of our dye molecules.

The SAC-CI method was developed by Nakatsuji to obtain a detailed interpretation and prediction of the molecular spectroscopy and photochemistry of the molecules. The SAC-CI method has been established as a reliable and useful method for investigating a wide variety of chemical phenom- ena through many successful applications. The method has been utilized for the accurate theoretical spectroscopy of many π -conjugated systems and has also been applied to the photochemistry of biological systems, such as porphyrins, photosynthetic reaction centers, retinal, and luciferin. Recently, the photophysical properties and excited state dynamics of fluorescent molecules, such as fluorene-thiophene oligomers that are useful for organic light-emitting diodes were investigated and the absorption/emission spectra of these molecules were elucidated. These works confirm that the SAC-CI method is useful for investigating the electronic excitations and excited state dynamics of large π -conjugated systems.

The photophysical properties and electronic structure of the present dye molecules, $UB4^-6$, were investigated by the high-level SAC-CI method which is based on cluster expansion theory. The method has been successfully applied to various kinds of molecular spectroscopies including the photofunctional molecules with large π -conjutgation like organic-light emitting diodes (OLED) and ultraviolet B blocking molecules. The UV-Vis absorption spectra in the range of 200 $^-$ 600 nm of $UB4^-6$ were calculated with the detailed characterization of the excited states. The DFT/TD-DFT calculations were also conducted with some functionals to obtain the ground-state geometry and to explore less computationally demanding approaches to this type of dyes as well as the solvent effect on the excited states. The electronic mechanism related to light-harvesting and charge transfer processes in dye/semiconductor was also simulated with the model prototype system consist of the dye adsorbed on the (TiO₂)₃₈ cluster by the DFT/TD-DFT calculations.

In this work, we report a detailed synthesis of compounds **UB4**⁻**6**. The physical and photophysical properties were studied by experimental characterizations and theoretical calculations using TD-DFT and SAC-CI methods. The functional dependence to the assignment and excitation energy of dye molecules

was examined using TD-DFT method. We showed that SAC-CI method provides the accurate results over all standard TD-DFT functionals. In addition, investigation on DSSC device fabrication and photovoltaic property are also reported.

2. RESULTS AND DISCUSSION

Synthesis and Characterization. The general synthetic routes to prepare **UB4-6** dyes are shown in **Scheme S1**, and the detailed synthetic procedures and characterization data are provided therein as well.

heme 1. Synthesis of UB4-6 dyes

All dyes can be crystallized in the deep color solids. The colors of these solid products tainted from orange to dark red solid as a number of thiophene units in the molecule increasing from **UB4**, **UB5** to **UB6**. These compounds show good solubility in organic solvents, resulting probably from the present of long *N*-dodecyl chain and their bulkiness.

Optical Properties. UV-vis absorption spectra of UB4-6 in dilute solution of CH₂Cl₂ are shown in Fig. 1a and the characteristic data are summarized in Table 1. In CH₂Cl₂ solution, all the dyes display three strong absorption bands appearing at 297-300, 330-340 and 450-600 nm, respectively. The first and second absorption bands are attributed to a localized $\pi \rightarrow \pi^*$ transitions of the carbazole and triphenylamine donors, respectively. The latter band is ascribed to intra-molecular charge transfer (ICT) transition from the 3,6-di-tert-butylcarbazol-9-ylphenylaniline donor moiety to the cyanoacrylic acid acceptor moiety. This assignment is supported by the solvatochromic behavior of the dyes. As shown in Fig. 1b, the $\pi \rightarrow \pi^*$ transition bands are nearly solvent polarity independent, whereas the ICT bands at xx nm display negative solvatochromism, i.e., blue shift of λ_{max} in more polar solvents. The molar extinction coefficients (ϵ) of the first and second absorption bands of all compounds are near identical ($\epsilon \sim 30400$ and ~19400 M⁻¹cm⁻¹, respectively), which is the result of all compounds bearing the same number of the donors. The molar extinction coefficients of the ICT bands of these compounds are moderate to high, ranging from 25174 to 30102 M⁻¹cm⁻¹. As a number of thiophene units in the molecules increasing from UB4, UB5 to UB6, the ICT bands show bathochromic shift and increased molar extinction coefficients. The absorption spectra and the molar extinction coefficients of conjugated chromophores are higher as the enhancement of the conjugation length. It should be noted that absorption spectrum of UB4 compared to that of (E)-3-(5-(4-(diphenylamino)phenyl)thiophen-2-yl)-2-cyanoacrylic acid ($\lambda_{\text{ICT}} = 379 \text{ nm}, \ \epsilon = 17000$ M⁻¹cm⁻¹ in CHCl₃) having D-π-A structure bathochromically shifts in the ICT peak together with significant increases in molar extinction coefficient (about 1.48 fold). The broader spectral response and higher molar extinction coefficient of UB4 mainly results from the present of peripheral carbazole units acting as additional or secondary donor to diphenylamine donor, which is desirable for harvesting more solar light. It is confirmed that the formation of D-D- π -A structure is an effective way to bathochromically shift the absorption spectrum and enhance the molar extinction coefficient. For the ICT transition of D- π -A compounds, the maximum absorption is bathochromically shifted and the molar extinction coefficients are higher as the presence of the additional donor. Moreover, the molar extinction coefficients of all dyes at the ICT band are considerably larger than that of the standard ruthenium dye N, at 518 nm ($\varepsilon = 13000$ M⁻¹cm⁻¹), indicating good light harvesting ability. The greater maximum absorption coefficients of the organic dyes allow a correspondingly thinner nanocrystalline film so as to avoid the decrease of the film mechanical strength. This also benefits the electrolyte diffusion in the film and reduces the recombination possibility of the light-induced charges during transportation. We observed that the dyes UB4-6 exhibited strong luminescence maxima of 598-635 nm when they are excited within their ICT bands in an airequilibrated solution at 298 K (Fig. 1c). Their fluorescence emission spectra in CH₂Cl₃ also show a redshift upon increased number of thiophene units in the molecules, which is roughly parallel to the trend of the absorption spectra (Fig. 1a and Table 1).

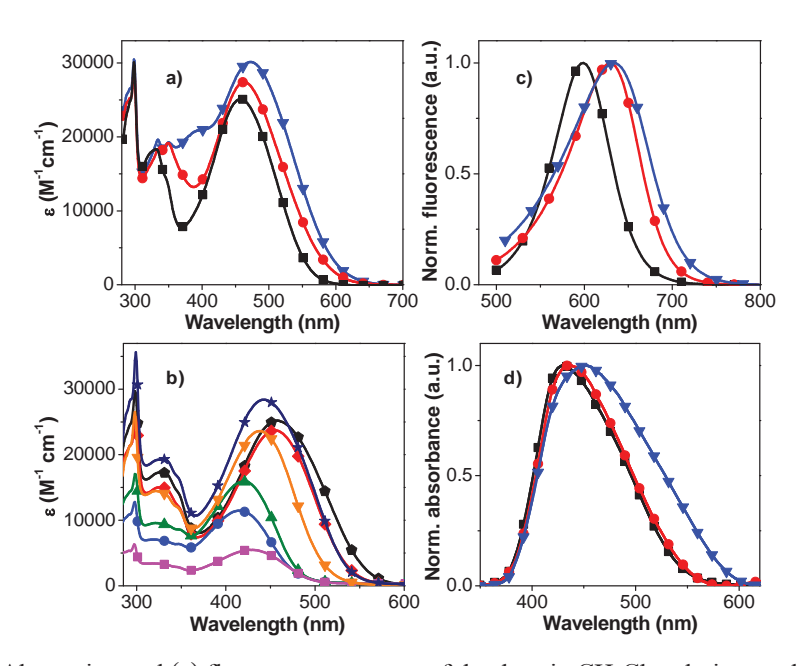


Figure 1. (a) Absorption and (c) fluorescence spectra of the dyes in CH₂Cl₂ solution, and (d) absorption spectra of the dyes on TiO₂ films: UB4 (black square), UB5 (red circle), and UB6 (blue inverted triangle).

(b) Absorption spectra of UB4 in different solvents: DCM (black pentagon), chloroform (red diamond), DMF (blue circle), DMSO (green triangle), EtOH (pink square), THF (orange invert triangle) and toluene (navy star).

The absorption spectra of $\mathbf{UB4-6}$ adsorbed on the $\mathrm{TiO_2}$ films are shown in $\mathbf{Fig. 1d}$. Absorption of the blank $\mathrm{TiO_2}$ film is subtracted from the curve. Absorption spectra of the dyes are broadened covering the region of 350-600 nm when anchored at the $\mathrm{TiO_2}$ surface compared to solution spectra. Such phenomenon is commonly observed in the spectral response of other organic dyes, which may be ascribed to the interaction of the anchoring groups of the dyes with the surface of $\mathrm{TiO_2}$. Absorption bands of all dyes on $\mathrm{TiO_2}$ film are slightly blue shifted (20–28 nm) compared to those of the corresponding solution spectra. From these results, we can explain that the *p*-substituted 3,6-di-*tert*-butylcarbazole unit of dyes can induce the non-planar structure by preventing aggregation via molecular stacking. In the series, the absorption spectrum of $\mathbf{UB6}$ is broadest, which is an advantageous spectral property for light harvesting of the solar spectrum.

Table 1. Optical, thermal and electrochemical and electronic properties of the dyes

_	Abs	E ^a	Abs ^b	Ema	E _{1/2} (0x) ^c	E _{1/2} (re) ^c	$\mathbf{E}_{1/2}(\mathbf{ox})^d$	T _{5d} e	HOMO/LUMO ^f	E ₀₋₀	E _{ox}	E _{ox} *i
Dye	(nm)	(M ⁻	(nm)	(nm)	(V)	(V)	(V)	(°C)	(eV)	(eV)	(V) vs	(V) vs
		¹ cm ⁻¹)									NHE	NHE
UB4	457	25174	429	598	0.85, 1.24	-1.71	0.85	284	-5.22/-2.92	2.31	1.07	-1.24
UB5	463	27460	435	630	0.80, 1.20, 1.39	-1.60	0.81	336	-5.13/-2.89	2.26	1.03	-1.23

หน้าที่ 148

^a Measured in CH_2Cl_2 solution. ^b Dyes adsorbed on TiO_2 film. ^c Measured by DPV with the dyes dissolved in CH_2Cl_2 and glassy carbon as working electrode ^d Measured by DPV with the dyes adsorbed on TiO_2 film as working electrode. ^e Measured by TGA. ^f Calculated from the onset oxidation potential (E_{onset}) of the dyes dissolved in CH_2Cl_2 with glassy carbon as working electrode: $HOMO = -(4.44 + E_{onset})$, $LUMO = HOMO + E_{0-0}$. ^g The 0–0 transition energy, E_{0-0} , estimated from the intercept of the normalized absorption and emission spectra of the dyes in CH_2Cl_2 : $E_{0-0} = 1240/\lambda_{intercept}$. ^h The ground-state oxidation potential (E_{ox}) or the first oxidation potential of the dyes adsorbed on TiO_2 film and was converted to normal hydrogen electrode (NHE) by addition of 0.22 V. ⁱ Estimated excited-state oxidation potential (E_{ox}^*) vs NHE calculated from the ground-state oxidation potential (E_{ox}) : $E_{ox}^* = E_{ox} - E_{0-0}$.

Electrochemical and Thermal Properties. The electrochemical properties of the dyes were studied by CV and DPV in CH₂Cl₂ with 0.1 M n-Bu₄N(PF₆) as a supporting electrolyte. The results are shown in Fig. S1 and all data are listed in Table 1. All dyes demonstrate multi quasireversible oxidation and one irreversible reduction processes. The reduction wave observed for all compounds is attributed to the reduction of the cyanoacrylic acid acceptor moiety, which is in the range of -1.55 to -1.71 V. UB4 displays well separated two quasireversible oxidation processes, whereas UB5-6 dyes show three quasireversible oxidation processes. The first oxidation wave corresponds to the removal of electrons from the peripheral carbazoles in the donor moiety to give radical cation and the rest to the oxidation of the remaining donor and oligothiophene segments. The potentials of the first oxidation decrease from 0.85, 0.80 to 0.74 V when a number of thiophene units in the molecules or length of the π -conjugated spacers increase from UB4, UB5 to UB6, respectively, as observed in other oligothiophenes. Their multiple CV scans reveal identical CV curves with no additional peak at lower potential on the cathodic scan (E_{nc}) being observed (Fig. S2). This indicates no oxidative coupling at the 3, 6 positions of the peripheral carbazole led to electro-polymerization. This is due to the present of 3,6-di-tert-butyl groups. This type of electrochemical coupling reaction can be detected in some carbazole derivatives with unsubstituted 3,6positions and might be occurred upon charge separation, which hampers the dye regeneration. Therefore, it is important that the dyes are electrochemically stable molecules. The HOMO energy levels of these dyes calculated from the oxidation onset potentials (E_{onset}) range from 5.22 to 5.08 eV. The optical intercept was utilized to derive the band gap and the LUMO energies.

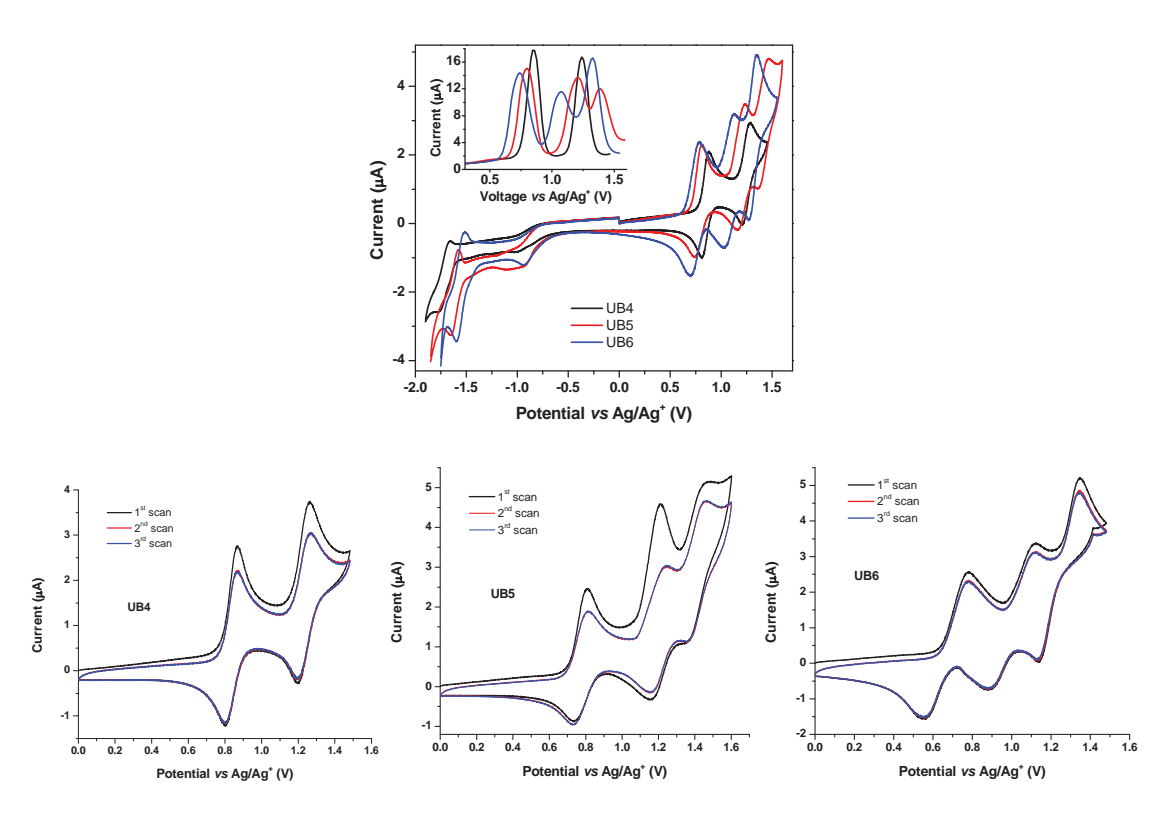


Fig. S4. Cyclic (CV) and differential pulse (DPV) (insert) voltammograms of the dyes (\sim 1 mM) in CH₂Cl₂ with 0.1 M n-Bu₄N(PF₆) at scan rate of 50 mV/s. Multiple CV scans of the dyes

While the CVs of the dyes UB4-6 adsorbed on TiO, film show one quasireversible oxidation with the potentials of 0.85, 0.81, and 0.76 V versus Ag/Ag⁺, respectively. From these oxidation potentials, the ground-state oxidation potentials (E_{ox}) of the dyes can be calculated according to the report method. The E_{ox} energy level of UB4 (1.07 V vs NHE) is more positive than that of both UB5 (1.03 V vs NHE) and **UB6** (0.98 V vs NHE), but all are much positive than the redox potential of the I/I₃ couple (0.4 V vs NHE), therefore, dye regeneration should be thermodynamically favorable and can complete efficiently with the recapture of the injected electrons by the dye radical cation. The excited-state oxidation potentials (E_{ox}^*) of the dyes were estimated from the ground-state oxidation potentials (E_{ox}) of the dyes and the 0-0 excitation energy (E_{0.0}). From the intersection of normalized absorption and emission spectra in CH₂Cl₂, $E_{0.0}$ energies of 2.31, 2.26 and 2.24 V were extracted for **UB4-6**, respectively. The E_{ox}^* potentials of these dyes (-1.24 - -1.26 V vs NHE) are more negative than the conduction band-edge energy level of the TiO₂ electrode (-0.5 V vs NHE) and the equivalent potential of N₃ dye (-0.88 V vs NHE). The energy level of the excited dye molecule should be > 0.3 V above the conduction band of the TiO₂ to ensure efficient charge injection. Therefore, all dyes have sufficient driving force for electron injection from the excited dyes to the conduction band of TiO2. As a result, all dyes have enough energetically driving force for efficient DSSCs using a nanocrystalline titania photocatalyst and the I/I_3 redox couple. Moreover, with high E₀₋₀* potentials (-1.26 V vs NHE) these dyes become very attractive for other metal oxide semiconductors having conduction bands more negative than the conduction band of TiO_2 such as ZnO, Nb_2O_3 , $SrTiO_3$ and their composites to achieve high open-circuit voltage (V_{oc}) resulting much improved cell efficiency.

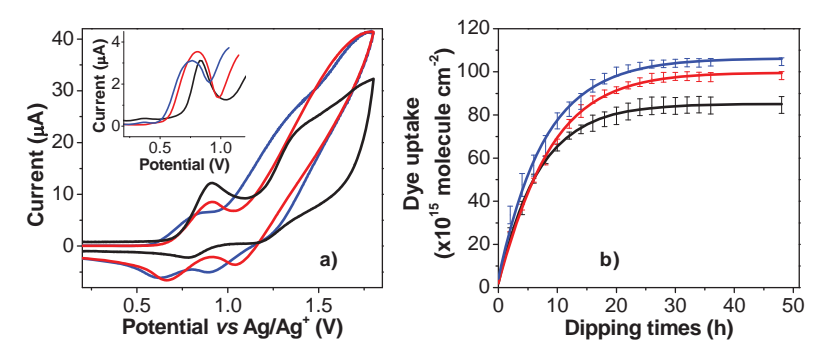


Figure 2. (a) Cyclic and differential pulse (insert) voltammograms using the dyes adsorbed on TiO_2 films as working electrode with 0.1 M n-Bu₄N(PF₆) at scan rate of 50 mV/s, and (b) the adsorption data for the dyes onto TiO_2 films measured over a period of 50 h (solid line represents the numerical regression fit).

UB4 (black line), UB5 (red line), and UB6 (blue line).

The thermal properties were investigated by the thermogravimetric analysis (TGA). Those results suggest that dyes **UB4-6** are thermally stable materials with temperature at 5% weight loss (T_{5d}) well over 284 °C (**Fig. S3**). The better thermal stability of the dye is important for the lifetime of the solar cells.

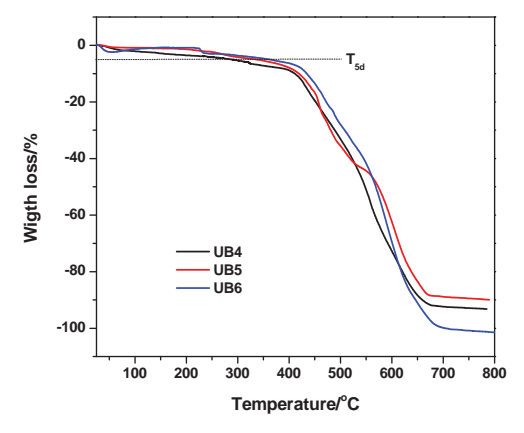


Fig. S5 TGA thermograms of the dyes measured at heating rate of 10 °C/min under N₂

Dye Adsorption on TiO₂ Film. The performance of a DSSC is not only based on the absorption of the harvesting dye but also on the total amount of dye present. Therefore, the dye uptake was determined. The TiO_2 photoelectrode (0.25 cm²) was immersed into a screw cap cuvette of dye solution (2.5 x 10^{-5} M) in CH_2Cl_2 , and the change in the absorbance of the dye solution at λ_{max} of the ICT band was measured *in situ* as a function of time. The dye uptake amount was then determined by comparison with standard solutions of known dye concentration. **Fig. 2b** shows the dye uptake profiles as a function of time for **UB4-6** dyes

(see also ESI; Fig. S3). In all case, rate of dye adsorption is initially rapid and eventually reaches a plateau. The plateau represents the equilibrium value related to maximum dye uptake. These profiles are typical for organic adsorbates into nano-porous inorganic matrices. The chemisorption of all dyes onto the surface of TiO, films was confirmed by FT-IR spectroscopy, which showed feature absorption peaks of both the dyes and TiO₂ at 2924 (C-H), 2213 (C≡N), 1603 (C=O), 1513 (C=C), 1364 (C=O), and 1238 cm⁻¹ (see ESI; Fig. S5). The characteristic vibration modes of carboxylate group, symmetric (1364 cm⁻¹) and asymmetric (1603 cm⁻¹), of all dyes are identical and in similar manner to that reported for other dyes independent of the molecular volume. This indicates that all dyes bind in the same way to the TiO2, therefore, difference observed in performance can be directly related to the effect of molecular volume and how much dye is absorbed. At the equilibrium, maximum uptakes of each dye are $84.4 \pm 3.8 \times 10^{15}$, $97.5 \pm 2.0 \times 10^{15}$, and $104.3 \pm 1.8 \times 10^{15}$ molecules cm⁻² for **UB4**, **UB5** and **UB6**, respectively (**Table 2**). In view of the lower dye uptake of UB4 dye on the TiO, film compared to UB5-6 dyes, such a result can be rationalized by steric hindrance of the donor moiety around the carboxylic acid anchoring group, which arises from a considerably shorter π -spacer of UB4 than that of both UB5-6. As a result, UB6 dyes with longer π conjugated spacers have more space to accommodate the donor moiety allowing larger dye uptake. The exact mechanism by which molecular volume affects dye uptake has been reported and the chemisorption (rather than bulk diffusion) has been recognized as the rate-determining step in the uptake process and kinetic hindrance also controls the initial rate. In summary, the kinetic studies of the adsorption show that at equilibrium the amount of dye uptake is controlled by the dye area occupancy, or in the other words, the dye uptake is directly related to the steric hindrance around the carboxylic acid binding site of the dye. Under this dye-loading result, the light-harvesting efficiency of UB4 is expected to be less than those of the other dyes, leading to small IPCE for the **UB4**-based cell.

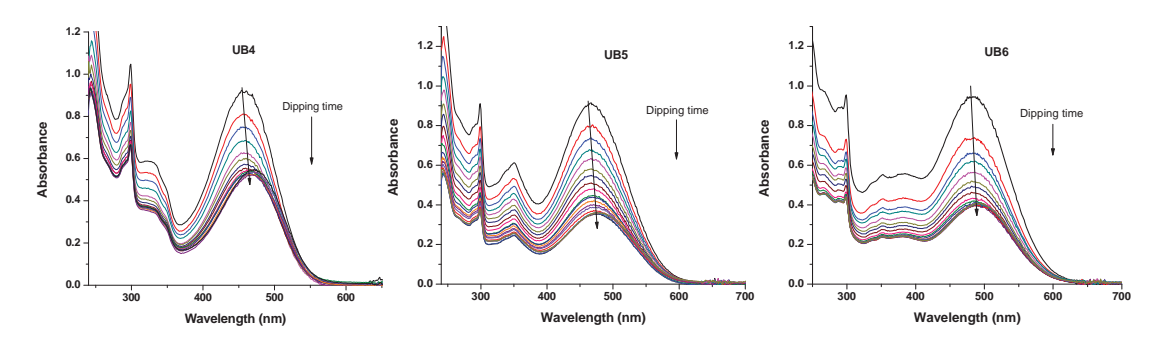


Fig. S6 The changes in UV-Vis absorption spectra as a function of time for dye adsorption measurements of the dyes

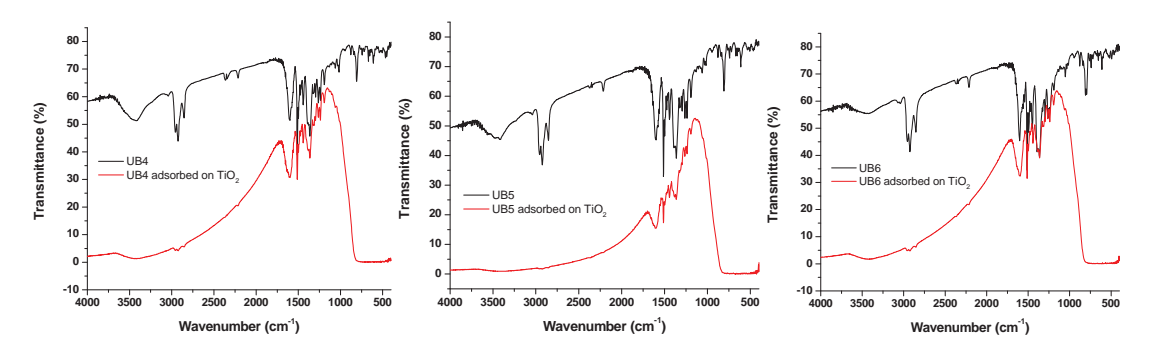


Fig. S7 FT-IR spectra of the dyes adsorbed in TiO₂ films

Photovoltaic Properties. UB4-6 dyes were used as the sensitizers for dye-sensitized nanocrystalline anatase TiO₂ solar cells (DSSCs). The cells with effective area of 0.25 cm² (0.5 cm x 0.5 cm) were fabricated with 11 μm (9.5 μm transparent + 1.5 μm scattering) thick TiO, working electrode, platinum (Pt) counter electrode and an electrolyte composed of 0.03 M I₂/0.6 M LiI/0.1 M guanidinium thiocyanate/0.5 M tert-butylpyridine in a 15/85 (v/v) mixture of benzonitrile/acetonitrile solution. The reference cell with the same structure based on N₃ dye, as the sensitizer, was made for comparison. For the measurement of the photovoltaic performance, five cells were prepared and measured under the standard conditions. The corresponding incident monochromatic photon-to-current conversion efficiency (IPCE) plots and current density-voltage (J-V) characteristics are shown in Figs. 3a and 3b, respectively, and the resulting photovoltaic parameters (average values) are summarized in **Table 2**. The IPCE spectra of **UB4-6** sensitizers plotted as a function of excitation wavelength are broadened and red-shifted as number of thiophene units in the molecule increased, which is coincident with the result of absorption spectra. The IPCE spectrum of UB5 dye show a high maximum value of 82%, which is slightly higher than the IPCE values of both UB4 (81%) and UB6 (80%). This observation deviates from our expectation on basis of the molar extinction coefficients of their absorption spectra. This was also observed in other types of organic dyes. The lower IPCE value of UB6 dye is probably due to extended π -conjugation elongation, which might lead to decreased electron-injection yield relative to that of UB5 dye. This suggests that the structure modification of the dyes strongly influences electron-injection and the collection efficiencies, in turn having a significant effect on the IPCE and overall conversion efficiency η of the devices. Moreover, the IPCE values of all dyes are higher than that of the N₃ dye due to the larger molar extinction coefficients of UB4-6 dyes, but N, dye shows broader IPCE spectrum, which is consistent with its wide absorption spectrum.

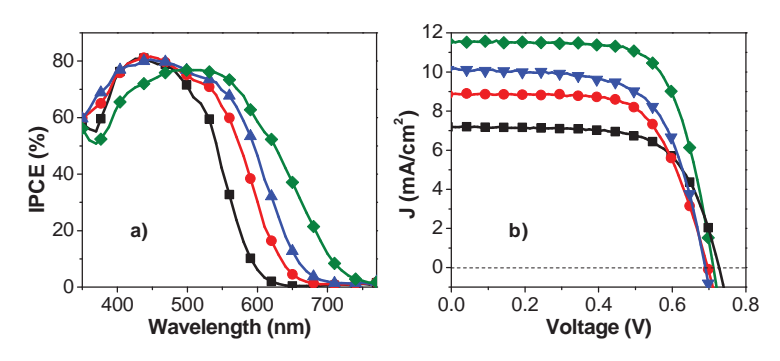


Figure 3. (a) Photocurrent action spectra, and (b) J–V characteristics of the DSSCs based on **UB4** (black square), **UB5** (red circle), **UB6** (blue inverted triangle), and N₃ (green diamond) dyes.

Table 2. Performance parameters of DSSCs constructed using the dyes^a

Dye	Dye uptake ^b	\mathbf{J}_{sc}	\mathbf{V}_{oc}	FF	η (%)	Cal. J _{sc} (mA cm ⁻²)
	(x10 ¹⁵ molecule cm ⁻²)	(mA cm ⁻²)	(V)			
UB4	84.4 ± 3.8	7.19	0.73	0.67	3.5	6.98
UB5	97.5 ± 2.0	8.88	0.70	0.66	4.1	8.61
UB6	104.3 ± 1.8	10.11	0.70	0.66	4.7	9.91
N_3	55.1 ± 1.0	11.54	0.71	0.70	5.7	11.29

^a Experiments were conducted in identical conditions using ${\rm TiO_2}$ photoanode with approximately 11 μm thickness and 0.25 cm² working area on the FTO (8 Ω/\square) substrates. ^b Obtained from dye adsorption measurement. ^c Obtained from integration of the corresponding IPCE spectra.

Under standard AM 1.5G 100 mW cm⁻² illumination, the UB6-sensitized cell shows the highest overall efficiency among the three dyes and gives a short-circuit photocurrent density (J_{sc}) of 10.11 mA cm⁻², open-circuit voltage (V_{oc}) of 0.70 V, and fill factor (FF) of 0.66, corresponding to an overall conversion efficiency η of 4.7%. The short-circuit photocurrent densities and efficiencies of the DSSCs are in the order of UB6 (10.11 mA cm⁻², 4.7%) > UB5 (8.88 mA cm⁻², 4.1%) > UB4 (7.19 mA cm⁻², 3.5%). The measured J_{sc} values of these solar cells were also cross-checked with the J_{sc} values calculated from integration of their corresponding IPCE spectra (Cal. J_{sc}), partly verifying the reported efficiency and the results found to be in agreement to within 3% (Table 4). The better solar cell performance (highest η and J_{sc}) of the UB6-based cell than other dyes in a series can be rationalized by the red-shift of the absorption spectrum of UB6 compared to UB4-5, that is, better light-harvesting efficiency of UB6. While the lower efficiency of the UB4-based cell compared to UB5-6 can be attributed to both the poorer spectral property and the lower dye content on TiO₂ film. The efficiency of UB6-based device reaches 82.5% of the standard ruthenium dye N₃-based cell (conversion efficiency = 5.7%). Interestingly, UB4-based cell also has efficiency reaching >61% of the N₃-based cell even though UB4 dye has a lower IPCE value and narrower IPCE spectrum than both UB5 and UB6. This can be uncertainly resulted from cascading electron transfer

from the additional or secondary carbazole donors to the acceptor moiety as stated earlier. The use of *tert*-butyl groups as the substituents on the peripheral carbazole donors and long N-dodecyl chain may also play the role in shielding the TiO_2 surface from the $I^{\prime}I_3^{-}$ in the electrolyte and thus reduce the charge recombination or dark reaction, leading to larger η of the device. From these results, it suggests that for D-D- π -A type organic dye the overall conversion efficiency of the solar cell increases when number of thiophene units in the molecule or in the other words π -conjugation length of the π -spacer increases. This condition leaves room for improvement of the cell performance for an organic dye-based DSSC to enhance its J_{sc} via molecular design based on the structure of **UB6** by fine-tuning the π -spacer to appropriate lengths or groups.

The stability of the solar cells was examined briefly by measuring the overall efficiency after a period of 28 days. The cell was irradiated for 30 min before measurement. Efficiency drops of 2–5% were observed after 28 days. The decrease in the efficiency was mainly caused by the decrease in $J_{\rm sc}$. Both leakage of the electrolyte and degradation of the organic dye may contribute to the decline in the efficiency.

Computational calculation

The present dye molecules, **UB4-6**, have bulky *tert*-butyl group and long dodecacyl side chain that are designed to prevent the charge recombination. Since these units are supposed to have less effect on the π -conjugation which determines the photophysical properties, we adopted model system without these units for the theoretical calculations, as shown in **Fig. 4**.

B3LYP/6-31G(d,p) in c-pcm model are displayed in **Fig. 4** with the top and side views. The bond lengths and dihedral angles between the connecting units are listed in **Table 3**. The molecules have bent structure due to N atom of diphenylamine unit, yet, the conjugation holds over the entire molecule as is clear in the side view. Although the *t*-butyl and dodecacyl units may affect the planarity of these compounds, this conjugation provides significant factor for the strong photoabsorption of these molecules as seen later in the oscillator strength. The non-planarity exist at carbazole and phenyl ring of diphenylamine (D1–D2) due to steric repulsion between H atoms with dihedral angle of ~63°, but, the planarity recovers at the single bond of diphenylamine. The conjugation also holds in the rest part of molecule; phenyl ring of diphenylamine (D2), thiophene (π-spacer), and accepter units are nearly planar. In **UB5** and **UB6**, the thiophene units have zigzag structure which keeps the near planarity of the molecules, although the zigzag structure is enhanced in **UB6** as seen in the dihedral angles at D2–T1 **UB5** (–17.62°) < **UB6** (–20.67°) and T1–T2 **UB5** (–1.28°) and **UB6** (5.09°). The inter-ring distances as well as bond distances within the units do not differ so much among these molecules, but the inter-ring distances at diphenylamine-thiophene (D2–T1) and thiophene-thiophene (T1–T2) are slightly larger for large molecule.

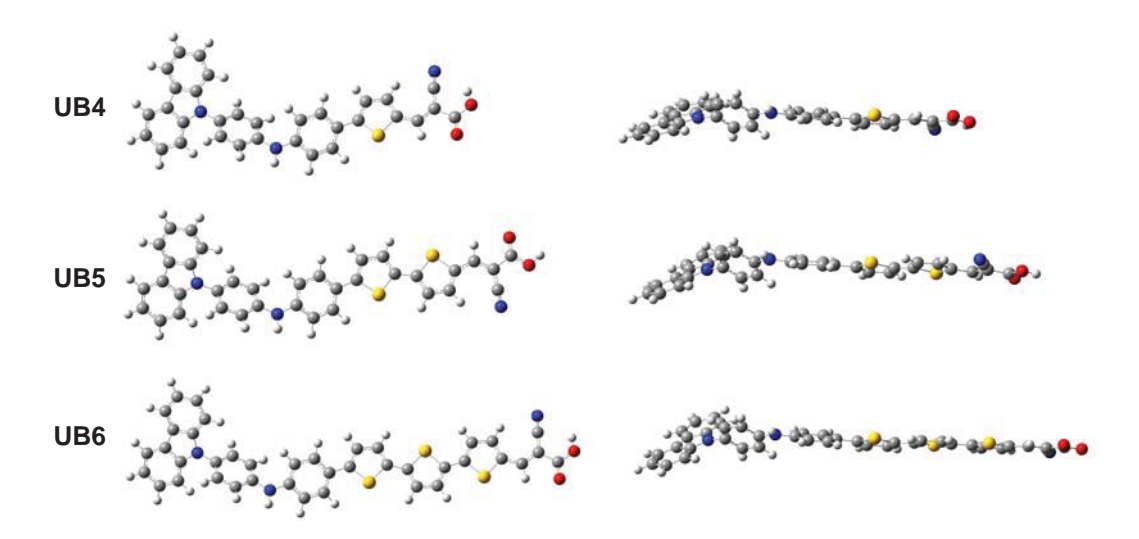


Figure 4. Front (left) and side (right) views of ground state geometries for **UB4**, **UB5** and **UB6** optimized by B3LYP/6-31G(d,p) level of theory.

Table 3. The selected bond lengths and dihedral angles for ground state geometries of dye molecules optimized by B3LYP/6-31G(d,p) level of theory.

Parameter ^a	UB4	UB5	UB6
Bond length (Å)			
$\mathbf{D_1}\!\!-\!\!\mathbf{D_2}$	1.425	1.425	1.426
D_2 – T_1	1.454	1.459	1.461
T_1 – T_2	-	1.437	1.440
T_2 – T_3	-	-	1.435
T-A	1.417	1.420	1.418
Dihedral Angle (degree)			
$\mathbf{D_1}\!\!-\!\!\mathbf{D_2}$	-63.12	-63.34	-63.20
Ph–Ph ^b	41.87	40.10	40.55
D_2 – T_1	-8.82	-17.62	-20.67
T_1-T_2	-	-1.28	5.09
$T_2 - T_3$	-	-	-0.96
T-A	1.27	0.25	0.38

^a D1=carbazole unit; D2=diphenylamine unit; T₁, T₂, and T₃=thiophene unit; A=cyanoacrylic acid, ^b

Ph-Ph = dihedral angle between phenyl and phenyl rings of diphenylamine moiety

Table 4 lists the HOMO and LUMO orbital energies of UB4-6 calculated by the CAM-B3LYP/6-31G(d,p) method. The HOMO energy level increase as the thiophene unit becomes longer, while the LUMO energy decrease. The calculated Δ HOMO-LUMO energy trends to decrease from 4.81 eV (UB4) > 4.59 eV (UB5) > 4.31 eV (UB5), [B3LYP provides 2.46 eV (UB4) > 2.25 eV (UB5) > 2.05 eV (UB5)] which is consistent to the trend of the 0–0 transition energy (2.31 V (UB4) > 2.26 V (UB5) > 2.24 V (UB5)), see also Table 1. The decreased electrochemical oxidation potential from 1.07 V (UB4) > 1.03 V

(UB5) > 0.98 V (UB5) is directly related to the calculated HOMO destabilization when insertion of thiophene unit to the linker of dye molecules.

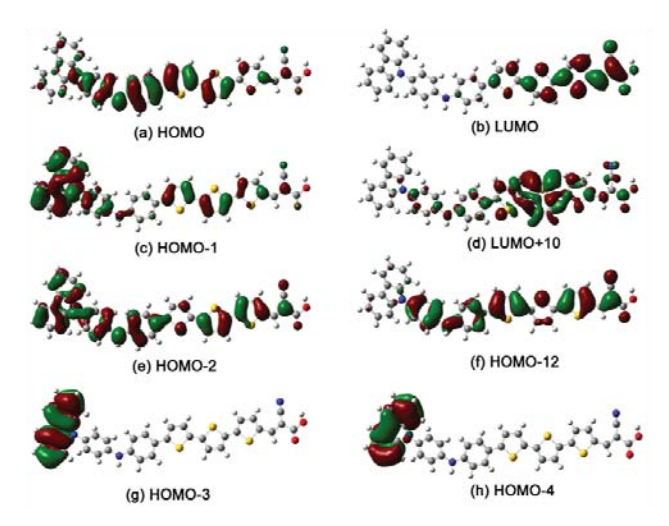


Figure 5. Frontier molecular orbitals of **UB6** related to excitation characters in S_1 state calculated by HF/LanL2DZ+(p)/B3LYP/6-31G(d,p) level of theory.

Table 4. Energy and electron contribution of HOMO and LUMO of UB4, UB5 and UB6 calculated by CAM-B3LYP /6-31G (d,p) level of theory.

Drya	electronic	Energy level (eV)	Electron contribution (%)					
Dye	level		D_1	D_2	π-spacer	A		
UB4	LUMO	-1.76	0	12	39	50		
	HOMO	-6.57	47	44	6	3		
UB5	LUMO	-1.81	0	5	55	40		
	HOMO	-6.40	18	48	30	4		
UB6	LUMO	-2.03	0	2	61	37		
	НОМО	-6.34	11	42	44	3		

 D_1 =carbazole unit; D_2 =diphenylamine unit; π -spacer=thiophene unit; A=cyanoacrylic acid

Provided that the relevant photoabsorption in these dyes are characterized as H⁻L transition as shown later, the characterization of HOMO and LUMO is essential issue. Orbital density analysis using GausSum program⁸⁴ was carried out for the HOMO and LUMO of all dyes. Decomposition of orbital density of these MOs for the present molecules are listed in **Table 4** (see also **Fig. 5**). Orbital densities of HOMO of these dyes are distributed over the donor moiety, which are calculated to be 91%, 66%, and 53% for **UB4**, **UB5**, and **UB6**, respectively. In HOMO of **UB4**, the major contribution comes from the carbazole unit (47%), while the diphenylamine unit is the major contribution for **UB5** (48%) and **UB6** (42%). Orbital densities of LUMO, on the other hand, are delocalized across the π -spacer and acceptor (A) moieties, which are decomposed as 39% (π -spacer), 50% (A) for **UB4**, 55% (π -spacer), 40% (A) for **UB5**, and 61% (π -spacer), 37% (A) for **UB6**, respectively. These values show that the distribution of the HOMO and LUMO of dyes

is well-separated suggesting that the H⁻L transition can be regarded as an intermolecular charge-transfer (ICT) that is a major characteristics of D- π -A based dyes. This feature also enabled the desirable efficient electron transfer with strong photoabsorption.

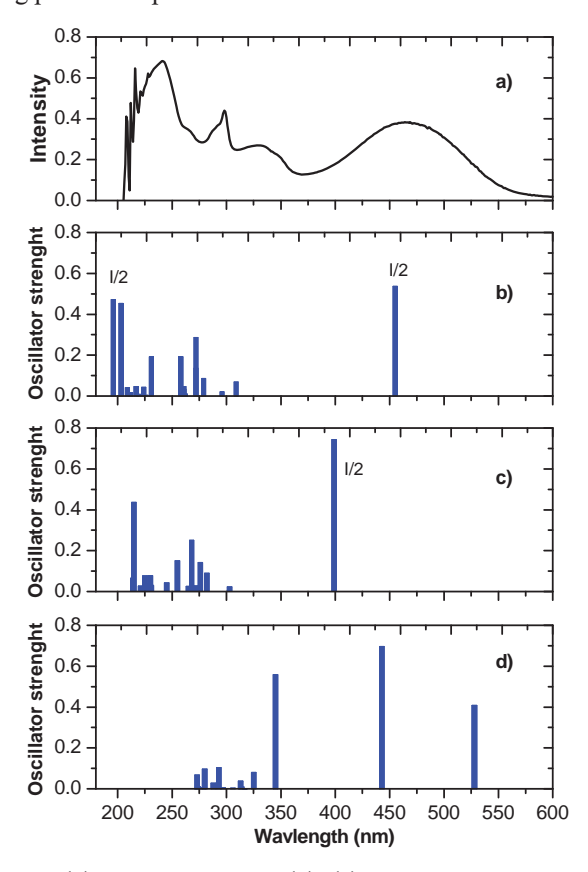


Figure 6. (a) Experimental, (b) SAC-CI/lanl2dz+(p), (c) TD-CAM-B3LYP/6-31G(d,p), and (d) TD-B3LYP/6-31G(d,p) absorption spectra of UB4. I/2 means haft-height of oscillator strength presented.

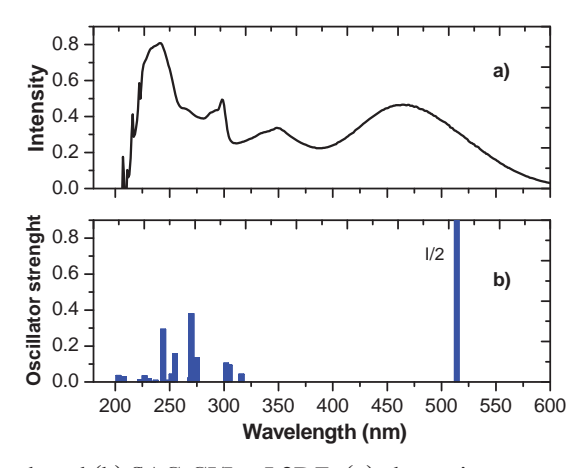


Figure 7. (a) Experimental, and (b) SAC-CI/LanL2DZ+(p) absorption spectra of UB5. I/2 means haft-height of oscillator strength presented.

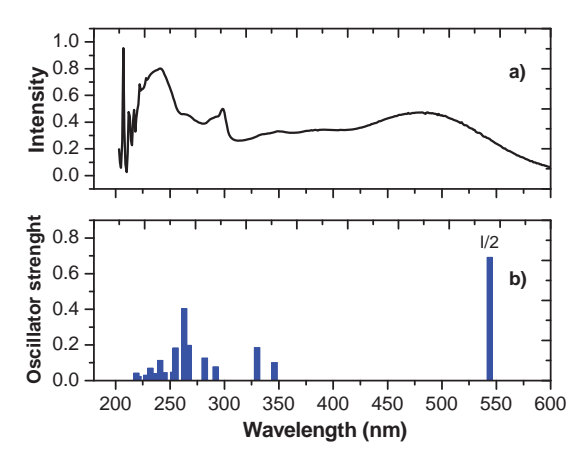


Figure 8. (a) Experimental, and (b) SAC-CI/Lanl2DZ+(p) absorption spectra of UB6. I/2 means haft-height of oscillator strength presented.

Table 5. Absorption energy (ΔE /eV, nm), dipole moment ($\Delta \mu$, D), dipole moment change ($\Delta \mu$, D), oscillator strength (f), and transition character of the singlet excited states of UB4 calculated by SAC-CI/LanL2DZ+(p) levels of theory.

	47	, or une ory.				
State	Expt. Δ E, eV (nm)	$\Delta \text{E, eV (nm)}$	μ (D)	$\Delta\mu$ (D) $^{\mathrm{a}}$	f	Transition character
1	2.71 (457)	2.72 (455)	19.62	11.31	1.074	0.67 (H →L)
2	3.75 (331)	4.02 (309)	7.19	-1.12	0.069	$0.66 (H \rightarrow L+5) + 0.31 (H-1 \rightarrow L+12)$
3		4.19 (296)	32.71	24.40	0.020	$0.53 (H \longrightarrow L) + 0.32 (H-2 \longrightarrow L)$
4		4.45 (279)	13.57	5.26	0.086	0.70 (H−8→L)
5	4.16 (298)	4.55 (272)	9.89	1.58	0.137	$0.50 \text{ (H-1} \rightarrow \text{L+5)} + 0.32 \text{ (H-8} \rightarrow \text{L)}$
6		4.56 (272)	9.07	0.76	0.287	$0.70 (H-1 \longrightarrow L+5)$
7		4.74 (262)	60.19	51.88	0.010	$0.85 (H-1 \longrightarrow L)$
8		4.75 (261)	25.11	16.80	0.046	$0.41 \text{ (H-1} \longrightarrow \text{L)} + 0.27 \text{ (H-10} \longrightarrow \text{L)}$
9		4.76 (261)	11.90	3.58	0.033	$0.44 (H-10 \longrightarrow L) + 0.30 (H \longrightarrow L+8)$
10		4.77 (260)	10.12	1.80	0.046	0.65 (H−10→L)
11		4.81 (258)	26.92	18.61	0.192	$0.44 (H \longrightarrow L+4) + 0.28 (H \longrightarrow L)$
12	5.15 (241)	5.36 (231)	12.23	3.91	0.191	$0.43 \text{ (H-2} \rightarrow \text{L+1)} + 0.36 \text{ (H} \rightarrow \text{L+4)}$
13		5.50 (226)	9.25	0.94	0.004	$0.53 (H-4 \longrightarrow L+5) + 0.32 (H \longrightarrow L+4)$
14		5.53 (224)	16.39	8.08	0.043	0.62 (H→L+2)
15		5.66 (219)	17.72	9.40	0.009	0.59 (H→L+3)
16		5.72 (217)	22.16	13.85	0.046	0.72 (H−6→L)
17		5.84 (212)	14.59	6.28	0.016	$0.36 (H \rightarrow L+8) + 0.30 (H \rightarrow L+1)$
18		5.94 (209)	13.67	5.36	0.041	$0.46 \ (H \longrightarrow L+9) + 0.27 \ (H \longrightarrow L+8)$
19		6.11 (203)	7.45	-0.86	0.453	$0.76 (H-1 \longrightarrow L+12)$
20		6.34 (196)	6.99	-1.32	0.945	$0.60 (H \rightarrow L+12) + 0.43 (H-4 \rightarrow L+5)$

^a Values show the changes in the dipole moments from the ground state (GS) to excited states (ES), $\Delta\mu$ = $|\mu_{\rm ES}|$ – $|\mu_{\rm GS}|$, and the ground state dipole.

Table 6. Absorption energy ($\Delta E/eV$, nm), oscillator strength (f), and transition character of the singlet excited states of UB5 calculated by SAC-CI/lanl2dz+(p) level of theory.

Q	Expt.			SAC-CI
State	Δ E, eV (nm)	Δ E, eV (nm)	f	Transition character
1	2.68 (463)	2.41 (514)	1.245	0.84 (H →L)
2		3.92 (316)	0.043	$0.52 (H-3 \longrightarrow L) + 0.30 (H-5 \longrightarrow L)$
3		4.07 (305)	0.095	$0.51 \ (H \longrightarrow L+1) + 0.26 \ (H-5 \longrightarrow L)$
4	3.57 (348)	4.11 (302)	0.105	0.78 (H−1→L+8)
5		4.51 (275)	0.135	$0.65 \text{ (H-11} \longrightarrow \text{L)} + 0.29 \text{ (H-1} \longrightarrow \text{L)}$
6	4.16 (298)	4.59 (270)	0.380	0.87 (H−2→L+8)
7		4.61 (269)	0.024	0.61 (H→L+10)
8		4.61 (269)	0.005	$0.72 (H-1 \longrightarrow L) + 0.26 (H-3 \longrightarrow L)$
9		4.87 (255)	0.156	$0.54 (H-8 \longrightarrow L) + 0.31 (H-9 \longrightarrow L)$
10		4.92 (252)	0.043	$0.37 (H \longrightarrow L+10) + 0.33 (H \longrightarrow L+11)$
11		5.00 (248)	0.010	0.81 (H→L+2)
12	5.15 (241)	5.07 (244)	0.295	$0.45 \text{ (H} \longrightarrow \text{L+3)} + 0.28 \text{ (H} \longrightarrow \text{L+1)}$
13		5.22 (237)	0.010	$0.51 (H-11 \longrightarrow L) + 0.37 (H-5 \longrightarrow L)$
14		5.28 (235)	0.001	0.65 (H→L+4)
15		5.36 (231)	0.019	$0.46 \ (H \longrightarrow L+7) + 0.33 \ (H \longrightarrow L+11)$
16		5.47 (227)	0.035	0.58 (H→L+7)
17		5.55 (223)	0.012	0.54 (H→L+4)
18		5.57 (233)	0.014	$0.53 (H-4 \longrightarrow L+8) + 0.34 (H-2 \longrightarrow L+22)$
19		5.96 (208)	0.030	$0.40 \text{ (H-3} \longrightarrow \text{L+1)} + 0.25 \text{ (H-5} \longrightarrow \text{L+1)}$
20		6.12 (203)	0.037	0.47 (H−2→L+15)

Table 7. Absorption energy ($\Delta E/eV$, nm), oscillator strength (f), and transition character of the singlet excited states of UB6 calculated by SAC-CI/lanl2dz+(p) level of theory.

G	Expt.			SAC-CI
State	Δ E, eV (nm)	Δ E, eV (nm)	f	Transition character
1	2.63 (472)	2.28 (544)	1.382	$0.82 \text{ (H} \longrightarrow \text{L)} + 0.30 \text{ (H-1} \longrightarrow \text{L)}$
2		3.59 (346)	0.100	$0.70 (H \longrightarrow L+2) + 0.31 (H-4 \longrightarrow L)$
3	3.56 (349)	3.75 (330)	0.184	$0.45 (H-3 \longrightarrow L) + 0.43 (H-4 \longrightarrow L)$
4		4.24 (292)	0.076	0.57 (H−1→L+10) + 0.34 (H-2→L+19)
5	4.16 (298)	4.40 (282)	0.126	0.60 (H−12→L)
6		4.65 (267)	0.197	$0.45 \text{ (H-10} \longrightarrow \text{L}) + 0.30 \text{ (H-3} \longrightarrow \text{L+1)}$
7		4.70 (264)	0.034	$0.43 \text{ (H-8} \longrightarrow \text{L)} + 0.31 \text{ (H-4} \longrightarrow \text{L)}$
8	5.15 (241)	4.71 (263)	0.404	0.65 (H−2→L+10)
9		4.71 (263)	0.006	0.81 (H→L+2)
10		4.85 (255)	0.181	$0.47 \ (H \longrightarrow L+14) + 0.25 \ (H-3 \longrightarrow L+14)$
11		4.89 (253)	0.047	$0.46 \text{ (H-12} \longrightarrow \text{L}) + 0.30 \text{ (H} \longrightarrow \text{L+13)}$
12		5.07 (245)	0.043	$0.35 (H \longrightarrow L+13) + 0.30 (H-1 \longrightarrow L+13)$
13		5.15 (241)	0.113	0.75 (H→L+6)
14		5.22 (238)	0.003	0.72 (H→L+3)
15		5.26 (236)	0.039	$0.39 (H-9 \longrightarrow L) + 0.29 (H-10 \longrightarrow L)$
16		5.30 (234)	0.004	0.73 (H→L+5)
17		5.34 (232)	0.069	$0.45 (H-3 \longrightarrow L+1) + 0.25 (H-4 \longrightarrow L+1)$
18		5.45 (228)	0.029	$0.34 (H \longrightarrow L+7) + 0.24 (H \longrightarrow L+8)$
19		5.61 (221)	0.023	$0.49 (H-1 \longrightarrow L+19) + 0.36 (H-2 \longrightarrow L+26)$
20		5.65 (219)	0.041	$0.47 (H-13 \longrightarrow L) + 0.24 (H-4 \longrightarrow L)$

Absorption Spectra of Dyes. The control of photoabsorption in both energy position and strength is one of the key factors for the development of the DSC molecules. Thus, the theoretical prediction and characterization of absorption spectra is relevant issue. The absorption spectra of **UB4-6** were computed by the SAC⁻CI and TD-DFT methods. **Fig. 6** shows the UV-Vis adsorption spectrum of **UB4** in the energy range of 200–600 nm compared with the calculated adsorption spectrum by SAC-CI/LanL2DZ+(p). The SAC-CI reproduced the UV-Vis spectrum satisfactorily in spite of the limited basis sets providing the reliable assignment and characterization of the electronic spectrum. The comparison with the TD-CAM-B3LYP and TD-B3LYP spectra was done. TD-B3LYP provides much lower peaks suggesting that the long-range correlation (LC) is substantially important for describing both the low-lying ICT and higher $\pi \rightarrow \pi^*$ states. The related excitation energy, oscillator strength, dipole moment and transition character for the 20 lowest transitions ($S_0 \rightarrow S_n$, n=1-20) calculated by SAC-CI are summarized in **Table 5** while those calculated by TD-CAM-B3LYP and TD-B3LYP are listed in **Table S2** (see **ESI**).

Although the first absorption band is the most relevant in the present DSC molecules, we perform the assignment of the absorption spectra in the entire energy region below ionization threshold. The UV-Vis

absorption spectrum of UB4 measured in CH₂Cl₂ solution show three absorption peaks and one shoulder between the first and second peaks. The first broad absorption peak has an absorption center at 2.71 eV (457 nm). The lowest excited state was calculated at 2.72 eV (455 nm) by SAC-CI in excellent agreement with experiment and characterized as H→L transition that is ICT as explained in previous section. This excitation is responsible for the electron transfer from the carbazole and diphenylamine donors to the thiophene π -spacer and cyanoacrylic acid acceptor. One shoulder and two higher absorption peaks are observed at 3.75 (331), 4.16 (298), and 5.15 (241) eV (nm). The SAC-CI method reproduces and characterizes these peaks better than the TD-DFT calculations do, as illustrated in Fig. 6. The SAC-CI calculates the shoulder at 4.02 eV (309 nm) which is assigned to the H→L+5 transition. The L+5 MO is delocalized mostly in diphenylamine unit as seen in Fig. 5 suggesting that this shoulder is characterized as $\pi \rightarrow \pi^*$ transition. The higher absorption peak is predicted at around 4.55 eV (272 nm) which is attributed to the linear combination between H-1 \rightarrow L+5 and H-8 \rightarrow L. The highest-energy peak providing the most intense absorption is calculated at 5.36 eV (231 nm) and is attributed to the linear combination of H-2→L+1 and H→L+4. Around this energy region, many electronic states with considerable intensity were obtained by the SAC-CI calculations. These higher excitations related to the contributions of $\pi \rightarrow \pi^*$ and ICT transitions. The MOs related to these transitions are shown in Fig. 5. For the characterization of the excited states, we also evaluated the dipole moment for the ground and excited states which are included in **Table 5**. From μ and $\Delta\mu$, the excited states with considerable oscillator strength are assigned to ICT in the low energy region and the mixture of $\pi \rightarrow \pi^*$ and ICT in the high energy region.

The basis set dependence of the excitation energy was examined by comparing the SAC-CI results calculated using LanL2DZ+(p) and 6-31G(d,p) basis sets, which are listed in **Table 5** and **Table S2**, respectively. The diffuse p function is important to describe both the ICT and $\pi \rightarrow \pi^*$ transitions. Focusing the first ICT excitation, the calculation with 6-31G(d,p) provides the first peak at 3.04 eV (408 nm) resulting an overestimated excitation energy by +0.33 eV (50 nm) compared with the experimental value. This trend also holds in the higher π - π^* transitions and both basis sets provide the similar transition character. It is difficult to examine the convergence of the results with further higher basis sets systematically because of the computational cost, but, the present calculations could reproduce the experimental spectra of the present dye compounds.

We observed that the feature of absorption spectra calculated by TD-B3LYP is significantly different from the SAC-CI spectra while that of TD-CAM-B3LYP which includes long-range effect is more likely to SAC-CI as seen in **Fig. S7**. This is what we have expected because the transitions are ICT or $\pi \rightarrow \pi^*$ in large system, and therefore, the long-range correction is indispensable for this type of dyes with large π conjugation. Other DFT functionals, i.e., PBE and M06-2x were also used to examine the functional dependence for the application to **UB4** in both gas phase and solvent phase. The effect of solvent was

Table 5. The dipole moments of the excited state were larger than that of the ground state, which cause the small red-shift of the peaks in a CH₂Cl₂ solvent as shown in Table S3. The calculated vertical excitation energies and transition characters are also compiled in Table S3. It is noted that the trend of calculated transition energies are increased in the order of PBE < B3LYP < Expt. ~ SAC-CI < M06-2x < CAM-B3LYP which may relate to the amount of the Hartree-Fock exchange included in the applied functionals. The difficulty in predicting the higher absorption peaks by the TD-DFT calculations shows that the SAC-CI and other related coupled cluster methods are useful for the spectroscopy in the entire energy region provided the high computational costs.

Let us next discuss the absorption spectra of UB5 based on the SAC-CI results. Fig. 7 compares the UV-Vis and SAC-CI absorption spectra of UB5 and Table 6 summarizes the transition energies and characters. Four absorption peaks were also observed at 2.64 (463), 3.57 (348), 4.16 (298) and 5.15 (241) eV (nm) as in **UB4**. The spectrum is very similar to that of **UB4**; the first and second peaks are red-shifted, while the third and fourth appear at the same positions compared with those of **UB4**. The SAC-CI result shows that the first absorption peak is attributed to the $H \rightarrow L$ transition which corresponds to the ICT process. The HOMO orbital density is distributed over the diphenylamine and thiophene moieties (see Fig. S8; ESI). This excitation induces the electron transfer to cyanoacrylic acid anchoring group which is similar to the case of UB4. For the second broad peak observed at 3.57 eV, three excited states with considerable oscillator strength were calculated in the region of 3.92⁻⁴.11 eV. These states are assigned to the mixtures of the $\pi \rightarrow \pi^*$ and ICT processes. The third absorption peak which is calculated at 4.59 eV (270 nm) is attributed to H⁻² \rightarrow L+8 and characterized as the $\pi\rightarrow\pi^*$ excitation; the orbital densities of H -2 and L+8 MOs are delocalized in carbazole moiety. The fourth peak calculated at 5.07 eV (244 nm) is assigned as the linear combination of H \rightarrow L+3 and H \rightarrow L+1, which correspond to the $\pi\rightarrow\pi^*$ transition within entire backbone. We note that the higher transitions are characterized as the $\pi \rightarrow \pi^*$ excitations within the donor moiety or entire backbone and therefore, the lowest excitation of dyes is dominantly responsible for the dye sensitization in the DSC system.

The UV-Vis and SAC-CI absorption spectra of **UB6** are compared in **Fig. 8**. The experimental spectrum shows two broad peaks and two strong peaks at 2.63 (472), 3.56 (349), 4.16 (298) and 5.15 (241) eV (nm). **Table 7** summarizes the SAC-CI results of the absorption energy, oscillator strength, and transition character for **UB6**. The broad absorption band of the first peak is effective for sensitization as mentioned above. The corresponding state was calculated at 2.28 eV (544 nm) with the character of $H \rightarrow L$ ICT transition; the deviation from the experiment may be attributed to the long π -spacer with flexible distortion. The relevant MOs for the present assignment are depicted in **Fig. S9** (see **ESI**). The HOMO is delocalized mostly on the diphenylamine donor and thiophene π -spacer in contrast to **UB4**, while the

LUMO is distributed on acceptor moiety. The oscillator strength for this transition becomes larger as the elongation of the thiophene unit, which accords with the experimental findings of high efficiency of **UB6**. The small broad structure at around 380 nm may be attributed to the second excited state calculated at 3.59 eV (346 nm) and the weak broad peak at 3.56 eV is assigned to the third excited state at 3.75 eV. These states are characterized as $H \rightarrow L+2$ and the linear combination of $H^-3 \rightarrow L$ and $H^-4 \rightarrow L$ which are the mixture of ICT and $\pi \rightarrow \pi^*$ transitions. For the most intense peak observed at 5.15 eV, many excited states were calculated in this energy region with considerable oscillator strength. Most of the transitions are characterized as the π - π^* transitions some of which are accompanied with the charge reorganization such as $H^-2 \rightarrow L+10$; H^-2 orbital is delocalized over the entire structural backbone, while L+10 orbital is mostly contributed in π -spacer moiety (see **Fig. S9; ESI**).

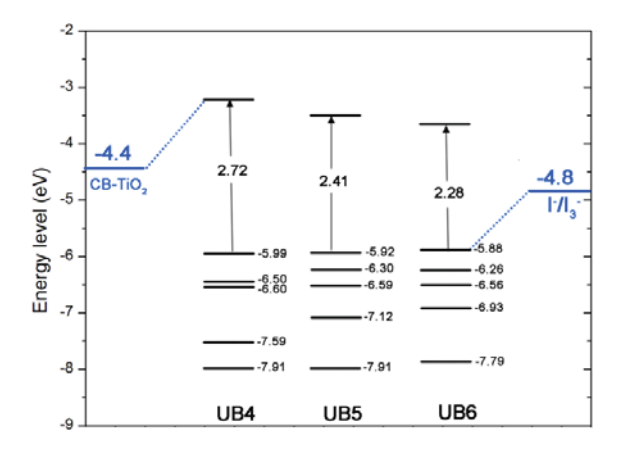


Figure 9. Energy levels of UB4, UB5, and UB6 compared with experimental energies (blue values) of TiO₂ conduction band and I/I₃ redox couple electrolyte. Energy levels are derived from the ionization and excitation energies calculated by SAC-CI/LanL2DZ+(p).

Fig. 9 shows the energy levels of UB4-6 derived from ionization/excitation energies calculated by SAC-CI method, compared with the experimental energies of TiO_2 conduction band and redox couple of I and I electrolyte. This diagram is well used to explain the conversion process of solar to electric energy in the DSC system with DFT KS levels, while the present energy levels are given by *ab initio* correlated method. Our novel synthesized dyes pose the first ionization energy levels (-5.99 - -5.88 eV) below the redox couple of I/I₃ electrolyte, and the LUMO energy levels above the conduction band of I which meet the properties of the practical dyes. The conversion process in DSC can be explained that when dye adsorbed light, electrons are ionized and then quickly injected into I conduction band (energy level is I and I electrolyte solution (energy level is I electrolyte solution (energy level is I electrolyte and the counter electrode. At the counter electrode, I ions are regenerated by reduction of I₃, which completes the circuit.

Dye/Semiconductor prototype system. To gain a better understanding of the electronic structure involved in dye/semiconductor charge transfer process in prototype system, we model the prototype system with dye adsorbed on the (TiO₂)₃₈ cluster. Carboxylic acid anchoring group can bind to the TiO₂ surface in both physisorption and chemisorption modes. We found that our dyes chemisorbed on the TiO₂ surface confirmed by FT-IR spectroscopy, see **Fig. S5**, which agrees with other experimental study. Thus, we calculated only the chemisorption configuration which is formed by the two carboxylate oxygen atoms of dye bonded with the two Ti atoms of TiO₂ surface, while proton of dye forms hydroxyl group with surface oxygen, see **Fig. 10**. The adsorption complex was first fully optimized using the PBE functional together with the all-electron core treatment performed in the DMol³ program. Two Ti⁻O bonds form with the Ti⁻O bond distances ranging 2.07⁻2.20 Å indicating the bidentate chemisorption. This mode has been accepted as the interaction between dye having carboxylic acid as anchoring group and TiO₂. The adsorption energies of **UB4**, **UB5**, and **UB6** on TiO₂ cluster are calculated to be ⁻10.30, ⁻13.86, and ⁻13.13 kcal/mol, respectively, indicating the strong interactions between dyes and TiO₂ surface.

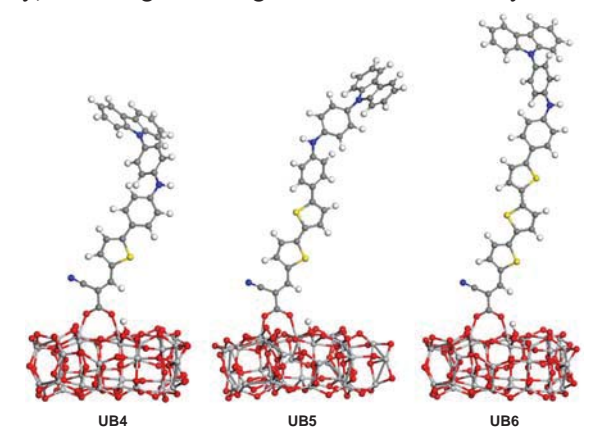


Figure 10. Bidentate chemisorptions of **UB4**, **UB5**, and **UB6** on the (TiO₂)₃₈ cluster. Black, gray, red, blue, yellow, and white spheres represent C, Ti, O, N, S, and H atoms, respectively.

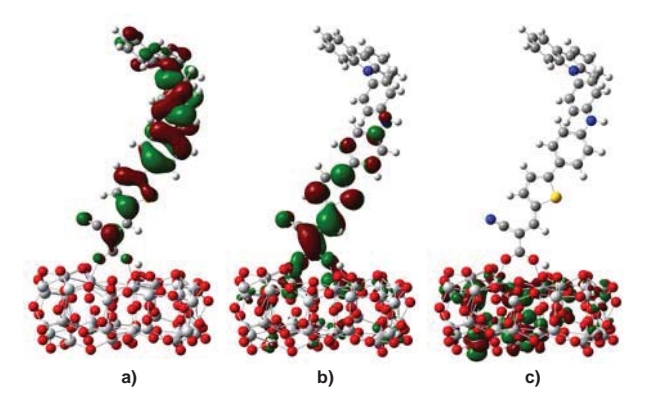


Figure 11. Frontier molecular orbitals a) HOMO, b) LUMO+1 and c) LUMO+2 of TiO_2 -UB4 adsorption complex. The transition characters for the absorption peak is assigned to $S_0 \longrightarrow S_2$ which is related the linear combination of 0.65 (H \longrightarrow L+2) + 0.23 (H \longrightarrow L+1).

Next, the HOMO, LUMO and excitation energies in the present dye—(TiO₂)₃₈ model systems were examined by the DFT/TD-DFT calculations with the Gaussian09 program at the DMol3 optimized geometries. The experimental absorption spectrum of each dye adsorbed on TiO₂ shows the strong peaks at 2.89 (429), 2.85 (435) and 2.75 (452) eV (nm) for dye UB4, UB5, and UB6, respectively, as shown in Fig. 1b and Table 1. The absorption peaks were characterized using TD-B3LYP with small basis set of 3-21G* because of the computational cost. In (TiO₂)₃₈-UB4 complex, for example, the transition of the linear combination of 0.65 (H \rightarrow L+2) and 0.23 (H \rightarrow L+1) has large oscillator strength of f=0.953 and is responsible for the photoabsorption (see ESI). The Kohn-Scham (KS) orbitals relevant to this transition and conduction band are shown in Fig. 11. The HOMO is delocalized over the adsorbed dye, while the LUMO+1 is delocalized over the TiO, cluster representing the conduction band. It is of interest that the LUMO+2 is distributed at the dye—(TiO₂)₃₈ interface. The direct electronic transitions from dye to TiO₂ surface like the H→L transition in this model system has small oscillator strength, so that the present calculation show that the photoabsorption occurs via ICT and the excited electron relaxes to the conduction band as expected. For the $(TiO_2)_{38}$ —UB5 and $(TiO_2)_{38}$ —UB6 complexes, similar picture was obtained as the H→L+1 transition has large oscillator strength of f=1.137 and 1.214, respectively, while those of other transitions are small (see Fig. S10; ESI). In both complexes, the HOMO is delocalized over the adsorbed dye, while the LUMO+1 is delocalized at the junction region of the adsorbed dye and (TiO₂)₃₈ part. These transition characters and KS-obitals of (TiO₂)₃₈—dye complexes show that the sensitization mechanism in prototypes is interfacial charge transfer process corresponding to electron injection from the excited dyes to the conduction band of TiO₂ surface. Similar behaviors are also found in the bare dyes and the prototype systems in which the carbazole and diphenylamine moieties are contributed to the sensitization.

3. CONCLUSIONS

In conclusion, we have developed a series of novel D-D- π -A type organic sensitizers using 3,6-ditert-butylcarbazol-9-ylphenyl-N-dodecylaniline as electron donor moiety (D-D), oligothiophene segments as π -conjugated spacers (π) and cyanoacrylic acid as the electron acceptor (A), which demonstrate the effect of the π -spacer length on controlling optical and photovoltaic properties. These dyes exhibit high thermal and electrochemical stability, which can enhance the stability of the solar cell. In this type of donor architecture (D-D), electrochemical, cell performance studies suggest that both peripheral 3,6-ditert-butylcarbazole donor and N-dodecyl chain not only can contribute electron injection into TiO_2 upon photo-excitation, either directly or indirectly by internal conversion to the lowest excited state, but also inhibit aggregation between dye molecules and prevent iodide/triiodide in the electrolyte from recombining with injected electrons in the TiO_2 , leading to increased overall conversion efficiency.

The photophysical properties and electronic structure of the dye molecules are investigated by

the high-level SAC-CI method which is based on cluster expansion theory. The method could reproduced the UV-Vis absorption spectra satisfactorily providing the reliable and detailed assignment of the spectra in the energy region of 200^-600 nm below ionization threshold. The low-lying light harvesting state was assigned to the ICT state, while the higher absorption was to the mixture of the ICT and $\pi \rightarrow \pi^*$ excited states. The characterization of the excited states in particluar the charge polarization is performed with the dipole moment. The TD-DFT calculations were conducted with some functionals and the results show that the functional including long-range correction is indispensable for the ICT and $\pi \rightarrow \pi^*$ excited states of the present dye molecules with large π conjugation.

The electronic mechanism related to light-harvesting and charge transfer processes in dye/semiconductor was also simulated with the model prototype system consist of the dye adsorbed on the $(TiO_2)_{38}$ cluster. The present dyes are exothermically adsorbed on the TiO_2 surface with chemisorption. The photoabsorption is shown as the interfacial charge transfer processes regarding to electron injection from the excited dyes to the conduction band of TiO_2 . The carbazole and diphenylamine moieties are contributed to the sensitization both for the bare dyes and the prototype systems.

This work suggests that the organic dyes based on double donor moiety are promising candidates for improvement of the performance of the DSSCs. DSSCs using these dyes exhibit efficiencies ranging from 3.5–4.7% under AM 1.5G illumination. The best performance among these dyes was found in **UB6**, which shows a maximal IPCE value of 80%, J_{sc} value of 10.11 mA cm⁻², V_{oc} value of 0.70 V, and FF value of 0.66, that correspond to an overall conversion efficiency of 4.7% (82.5% of the N₃-based cell). This work suggests that the organic dyes based on this type of donor moiety or donor molecular architecture are promising candidates for improvement of the performance of the DSSCs. Moreover, structural modification of **UB6** dyes to increase the molar extinction coefficient and red-shift the absorption spectrum is anticipated to give even better performance.

4. EXPERIMENTAL SECTION

Materials and Synthesis. All reagents were purchased from Aldrich, Acros or Fluka, and used without further purification. All solvents were supplied by Thai companies and used without further distillation. Tetrahydrofuran (THF) was refluxed with sodium and benzophenone, and distilled prior to use. Dichloromethane (CH₂Cl₂) for electrochemical measurements was washed with conc. H₂SO₄ and distilled twice from calcium hydride. Chromatographic separations were carried out on silica gel Merk Silica gel 60 (0.0630-0.200 mm). 3,6-Di-tert-butylcarbazole was prepared by adopting literature procedure. Detailed procedures for preparation of precursor compounds and dyes molecules are provided in the Supporting Information.

General Methods and Instrumentation. NMR spectra were recorded on a Brüker AVANCE 300 MHz spectrometer with tetramethylsilane as the internal reference using CDCl₃ as solvent in all cases. Infrared

(IR) spectra were measured on a Perkin-Elmer FTIR spectroscopy spectrum RXI spectrometer as potassium bromide (KBr) disc. Ultraviolet-visible (UV-Vis) spectra were recorded as a diluted solution in spectroscopic grade CH₂Cl₂ on a Perkin-Elmer UV Lambda 25 spectrometer. The diffuse reflectance spectra of the dye-sensitized TiO₂ were performed at room temperature with a Shimadzu UV-3101 spectrophotometer. Barium sulfate was used as a standard. The measured reflectance spectra were then conversed to absorption spectra by Kubelka-Munk method. Thermogravimetry analyses (TGA) were performed on a Rigaku TG-DTA 8120 thermal analyser with heating rate of 10 °C/min under nitrogen atmosphere. Cyclic voltammetry (CV) and differential pulse voltammetry (DPV) measurements were carried out on an Autolab potentiostat PGSTAT 12 with a three electrode system (platinum counter electrode, Ag/Ag+ reference electrode, and glassy carbon or dyes adsorbed on TiO₂ film as working electrode) and 0.1 M tetrabutyl ammonium hexafluorophosphate (n-Bu₄NPF₆) as supporting electrolyte in CH₂Cl₂ at scan rate of 50 mV/s under argon atmosphere.

DSSC Fabrication and Characterization. The photoanodes composed of nanocrystalline TiO, were prepared by using a previously reported procedure. Fluorine-doped SnO₂ (FTO) conducting glasses (8 Ω/\square , TCO30-8, Solaronix) were used for transparent conducting electrodes. The double nanostructure thick film (~11 µm thickness) consisting of a transparent (Ti-Nanoxide 20T/SP, Solaronix) and a scattering (Ti-Nanoxide R/SP, Solaronix) TiO, layers were screen-printed on TiCl₄ treated FTO. The thickness of the TiO, film was controlled by selection of screen mesh size and repetition of printing. Prior to dye sensitization, the TiO₂ electrode with cell geometry of 0.5 x 0.5 cm² were treated with an aqueous solution of 4 x 10⁻² M TiCl₄ at 70 °C in a water saturation atmosphere, heated to 450 °C for 30 min and then cooled to 80 °C. The TiO₂ electrodes were immersed in the dye solution (3 x 10⁻⁴ M N₃ in ethanol, and 5×10^{-4} M organic dyes in CH₂Cl₂) in the dark at room temperature for 24 h to stain the dye onto the TiO₂ surfaces. Excess dye was removed by rinsing with appropriated solvent. To ensure maximum dye adsorbed on TiO, film, higher dyes concentration (>10 fold) than that used for dye adsorption experiment was used. The Pt counter electrode was prepared on a predrilled TCO30-8 FTO glass (Solaronix) via the thermal decomposition of 7 x 10⁻³ M H₂PtCl₆ in isopropanol solution at 385 °C. The dye-adsorbed TiO₂ photoanode and Pt counter electrode were assembled into a sealed cell by heating a gasket Meltonix 1170-25 film (25 μm thickness, Solaronix) as a spacer between the electrodes. An electrolyte solution of 0.6 M LiI, 0.03 M I₂, 0.1 M guanidinium thiocyanate, and 0.5 M tert-butylpyridine in 15/85 (v/v) mixture of benzonitrile and acetonitrile was filled through the predrilled hole by a vacuum backfilling method. The hole was capped by using hot-melt sealing film (Meltonix 1170-25, 25 µm thickness, Solaronix) and a thin glass cover. Finally, the Schotch 3M conducting tape and the silver paint (SPI supplies) were coated on the electrodes to enhance the electric contact. For each dye, five devices were fabricated and measured for consistency and the averaged cell data was reported. The reference cells with the same device configuration based on N_3 dye, as the sensitizer, were also fabricated for comparison.

The current density-voltage of the DSCs was measured by using a Keithley 2400 source meter unit in a 4-terminal sense configuration. The data were averaged from forward and backward scans with a bias step and a delay time of 10 mV and 40 ms, respectively, according to the method of Koide and Han. The simulating sunlight was provides by Newport sun simulator 96000 equipped with an AM 1.5G filter. To minimize the error of measurements, the irradiation intensity of 100 mW cm⁻² was approximated with a calibrated BS-520 Si photodiode (Bunnkoukeiki Co., Ltd., Japan), which its spectral response was very similar to that of the DSSCs. The spectral output of the lamp was also matched to the standard AM 1.5G solar spectrum in region of 350-750 nm by the aid of KG-5 filter with spectral mismatch less than 2% as reported by Ito et al. Incident photon to electron conversion efficiency (IPCE) of the device under short-circuit condition were performed by mean of an Oriel 150W Xe lamp fitted with a CornerstoneTM 130 1/8 m monochromator as a monochromatic light source, a Newport 818-UV silicon photodiode as power density calibration and a Keithley 6485 picoammeter. All measurements were performed using a black plastic mask with an aperture area of 0.180 cm² and no mismatch correction for the efficiency conversion data.

Computational Details

Geometry optimization of free dyes. The dyes developed in the present work are double-donor- π -acceptor (D-D- π -A) based dyes as shown in **Chart 1**; The *tert*-buxyl group substituted at carbazole, and dodecacyl side chain substituted at diphenylamine were replaced by the –H atoms to reduce computational effort. The model systems with thiophene units (n) =1, 2 and 3 were represented **UB4**, **UB5** and **UB6**, respectively. The ground state geometries (S₀) of **UB4-6** were optimized without any constraint using B3LYP functional at 6-31G(d,p) basis set. The Conductor-like Polarized Continuum Model (C–PCM) was adopted for including the solvent effect of CH₂Cl₂ used in our experiment.

The UV-Vis absorption spectra of the present molecules in the energy range of 200 $^-600$ nm were investigated by the SAC-CI and TD-DFT methods. The 20 lowest excited states were solved to cover this energy range. In the TD-DFT calculations, various functionals such as B3LYP, CAM-(Coulomb-attenuating method) B3LYP, M06-2x and PBE0 were selected to examine the functional dependence on the excitations. In the SAC-CI calculations, the LanL2DZ basis set augmented with one polarized and one diffuse p function, namely LanL2DZ+(p), was adopted. The non-direct SAC-CI singles- and doubles-(SD)-R method was conducted with CIS vector as initial vectors. The perturbation selection technique was utilized to reduce the computational effort. The restricted active space (occupied MOs, unoccupied MOs) was used as **UB4** (44, 446), **UB5** (48, 506), and **UB6** (53, 566), which covers the MO energies in the range of $^-1.2$ to 2.0 au. The threshold of the linked terms for the ground state was set to $\lambda_a = 5.0 \times 10^{-6}$. For the

excited states, the threshold of the linked doubles was set to λ_e =5.0×10⁻⁷. The 6-31G(d,p) basis set was used in all the TD-DFT calculations. All calculations were performed on Gaussian09 suite of programs, Revision B.01.

The Dye/Semiconductor Adsorption Complex. We modeled the DSCs prototype system with the dye adsorbed on the $(TiO_2)_{38}$ cluster. The DFT calculations were performed by the DMol³ implemented in Material studio 4.3^{TM} . Spin-unrestricted calculations were employed using the generalized gradient approximation (GGA) with the Perdew–Burke–Ernzerhof (PBE) method. Double numerical polarization (DNP) basis set with all-electron core treatment was used. During the optimization, all atoms were allowed to relax without symmetry restriction. The convergence criterions of the energy, force and displacement convergence were 2×10^{-5} Ha, 4×10^{-3} Ha/Å and 5×10^{-3} Å, respectively. The adsorption energy was calculated as:

$$E_{ads} = E_{(TiO2)38 - Dve} - E_{(TiO2)38} - E_{dve}$$
 (1)

where $E_{(TiO_2)_{38} - Dye}$ is the total energy of $(TiO_2)_{38}$ —dye system, $E_{(TiO_2)_{38}}$ and E_{dye} are the total energy of $(TiO_2)_{38}$ cluster and dye molecule, respectively. A negative value of $E_{ads} < 0$ indicates stable adsorption.

Synthesis

Bis(4-iodophenyl)amine (1)

A mixture of diphenylamine (5.0 g, 29.5 mmol), KI (5.8 g, 35.4 mmol), KIO₃ (6.9 g, 32.5 mmol) in glacial acetic acid (250 ml) was heated at 70 $^{\circ}$ C for 12 h. The temperature was cooled and DCM (200 ml) was added. The organic phase was thoroughly washed with water (200 ml x 4), 0.2 M aqueous Na₂SO₃ (200 ml x 2) and aqueous NaHCO₃ (200 ml), brine solution (200 ml), dried over anhydrous Na₂SO₄ and filtered. After solvent evaporation, the pure compound was obtained by recrystallization from DCM/hexane mixture as light gray solids (9.7 g, 79%): m.p. 122-123 $^{\circ}$ C, FTIR (KBr, V, cm⁻¹): 3420 (N-H), 3075 (=C-H), 1585 (C=C), 1499, 1307, 815. 1 H NMR (300 MHz, CDCl₃, δ , ppm): 7.53 (4H, d, J = 8.7 Hz), 6.80 (4H, d, J = 8.7 Hz). 13 C NMR (75 MHz, CDCl₃, δ , ppm): 142.25, 138.24, 119.98, 83.24. HRMS calcd for C_{12} H9I₂N: m/z 420.8824; found: m/z 421.3671 [M⁺].

$N ext{-}Dodecyl-4 ext{-}iodo-N ext{-}(4 ext{-}iodophenyl)$ aniline (2)

A mixture of 1 (6.0 g, 14.2 mmol), 4-bromododecane (4.3 ml, 17.1 mmol), NaOH (4.6 g, 113.6 mmol) in 50 ml of DMSO was stirred at room temperature for 24 h. The solid residue was filtered out. Water (50 ml) was added to filtrate and then extracted with ethyl acetate. The organic phase was washed with water (100 ml x 2), aqueous HCl (2 M, 50 ml) and brine (50 ml), dried over anhydrous Na₂SO₄, filtered and evaporated to dryness. Purification by silica gel column chromatography using hexane as eluent gave colorless oil (7.6 g, 90%): FTIR (NaCl, V, cm⁻¹): 3061 (=C-H), 2922 (-C-H), 1585, 1575 (C=C), 1486, 1361, 1245, 1006, 810. ¹H NMR (300 MHz, CDCl₃, δ , ppm): 7.51 (4H, d, J = 8.7 Hz), 6.76 (4H, d, J = 8.7 Hz), 3.61 (2H, t, J = 7.5 Hz), 1.60 (2H, q, J = 6.3 Hz), 1.26 (18H, m), 0.89 (3H, t, J = 6.3 Hz). ¹³C NMR

(75 MHz, CDCl₃, δ , ppm): 147.30, 138.25, 123.10, 52.35, 32.00, 29.70, 29.66, 29.45, 27.34, 27.09, 22.78, 14.26. HRMS calcd for $C_{24}H_{33}I_3N$: m/z 589.0702; found: m/z 588.7832 [M⁺].

4-(3,6-Di-tert-butyl-9H-carbazol-9-yl)-N-dodecyl-N-(4-iodophenyl)aniline (3)

A mixture of **2** (8.9 g, 15.2 mmol), 3,6-di-*tert*-butylcarbazole (1.0 g, 3.8 mmol), CuI (0.4 g, 1.9 mmol), K_3PO_4 (2.0 g, 9.4 mmol), and (\pm)trans-1,2-diaminocyclohexane (0.2 ml, 1.9 mmol) in toluene (70 ml) was degassed with N_2 for 5 min and then heated at reflux under N_2 atmosphere for 24 h. After cooling, the solid residue was filtered out and washed with DCM (50 ml). The organic filtrate was washed with water (100 ml x 2) and brine solution (100 ml), dried over anhydrous Na_2SO_4 and evaporated to dryness. Purification by silica gel column chromatography using DCM/hexane (1:9) as eluent gave light gray wax (1.3 g, 46%): FTIR (NaCl, v, cm⁻¹): 3042 (=C-H), 2956 (-C-H), 1583, 1513 (C=C), 1487, 1363, 1262, 810. ¹H NMR (300 MHz, CDCl₃, δ , ppm): 8.13 (2H, d, J = 1.5 HZ), 7.56 (2H, d, J = 9.0 Hz), 7.33-7.47 (6H, m), 7.16 (2H, d, J = 8.7 Hz), 6.83 (2H, d, J = 9.0 Hz), 3.83 (2H, s), 1.60 (2H, s), 1.27 (18H, m), 0.86 (3H, t, J = 6.6 Hz). ¹³C NMR (75 MHz, CDCl₃, δ , ppm): 147.60, 146.37, 142.62, 139.52, 138.19, 131.79, 127.78, 123.48, 123.18, 122.96, 122.66, 122.25, 119.96, 116.18, 109.19, 83.33, 52.52, 34.72, 32.03, 31.92, 29.64, 29.60, 29.43, 29.3, 27.43, 27.08, 22.68, 14.10. HRMS calcd for $C_{44}H_{57}IN_2$: m/z 740.3566; found: m/z 741.0016 $[M^{+}]$.

4-(3,6-Di-tert-butyl-9H-carbazol-9-yl)-N-dodecyl-N-(4-(thiophen-2-yl)phenyl)aniline (4)

A mixture of **3** (2.5 g, 3.3 mmol), 2-thiopheneboronic acid (0.4 g, 3.3 mmol), Pd(PPh₃)₄ (0.07 g, 0.07 mmol), 2 M Na₂CO₃ aqueous (34 ml) in THF (57 ml) was degassed with N₂ for 5 min and then heated at reflux under N₂ atmosphere for 24 h. After cooling, DCM (100 ml) was added and the organic layer was washed with water (100 ml x 2) and brine solution (100 ml), dried over anhydrous Na₂SO₄, filtered and evaporated to dryness. Purification by silica gel column chromatography using DCM/hexane (1:9) as eluent gave colorless sticky gum (1.7 g, 71%): FTIR (NaCl, v, cm⁻¹): 3053 (=C-H), 2957 (-C-H), 1608, 1510 (C=C), 1502, 1362, 1261, 805. ¹H NMR (300 MHz, CDCl₃, δ , ppm): 8.23 (2H, s), 7.62 (2H, d, J = 8.4 Hz), 7.17-7.56 (12H, m), 6.10 (1H, t, J = 4.5 Hz), 3.85 (2H, t, J = 7.2 Hz), 1.83 (2H, m), 1.35-1.55 (18H, m), 0.94 (3H, t, J = 6.3). ¹³C NMR (75 MHz, CDCl₃, δ , ppm): 147.28, 146.98, 144.62, 142.75, 139.92, 131.29, 128.28, 128.20, 127.98, 127.25, 124.04, 123.77, 123.51, 122.31, 121.91, 121.51, 116.43, 109.60, 52.74, 34.97, 32.38, 32.24, 29.97, 29.94, 29.76, 29.68, 27.85, 27.41, 23.02, 14.49. HRMS calcd for $C_{48}H_{60}N_2$ S: m/z 696.4477; found: m/z 696.8625 [M⁺].

4-(5-Bromothiophen-2-yl)-N-(4-(3,6-di-tert-butyl-9H-carbazol-9-yl)phenyl)-N-dodecylaniline (5)

N-Bromosuccinamide (0.56 g, 3.2 mmol) was added in small portions to a solution of 4 (2.1 g, 3.0 mmol) in THF (30 ml). The mixture was stirred at room temperature under N_2 for a further 1 h. Water (30 ml) and DCM (100 ml) were added. The organic phase was separated, washed with water (100 ml x 2), brine solution (100 ml), dried over anhydrous Na_2SO_4 , filtered, and the solvents were removed to dryness.

Purification by silica gel column chromatography eluting with DCM/hexane (1:9) gave brominated product as colorless sticky gum (1.6 g, 68%): FTIR (NaCl, v, cm⁻¹): 3036 (=C-H), 2923 (-C-H), 1676, 1486 (C=C), 1362, 1253, 810. ¹H NMR (300 MHz, CDCl₃, δ , ppm): 8.17 (2H, s), 7.45-7.51 (H, m), 7.37 (2H, d, J = 8.4 Hz), 7.21-7.26 (3H, m), 7.01 (2H, d, J = 8.4 Hz), 6.96 (2H, dd, J = 8.4, 5.6 Hz), 3.77 (2H, t, J = 7.5 Hz), 1.77 (2H, m), 1.13-1.57 (18H, m), 0.87 (3H, t, J = 6.2). ¹³C NMR (75 MHz, CDCl₃, δ , ppm): 147.58, 146.44, 146.04, 142.62, 139.54, 131.75, 130.79, 127.78, 126.71, 126.50, 123.50, 122.42, 120.56, 116.20, 110.05, 109.23, 52.56, 37.13, 34.74, 32.78, 32.06, 31.94, 30.06, 29.73, 29.68, 29.63, 29.48, 29.38, 27.56, 27.13, 22.71, 19.76, 14.14. HRMS calcd for $C_{48}H_{59}BrN_2S$: m/z 774.3582; found: m/z 774.8591 [M[†]].

4-([2,2'-Bithiophen]-5-yl)-N-(4-(3,6-di-tert-butyl-9H-carbazol-9-yl)phenyl)-N-dodecylaniline (6)

Compound **6** was prepared from **5** with a method similarly to that described above for **4** and obtained as light green sticky gum (1.7 g, 73%): FTIR (NaCl, v, cm⁻¹): 3036 (=C-H), 2924 (-C-H), 1602, 1512 (C=C), 1499, 1363, 1262, 809. ¹H NMR (300 MHz, CDCl₃, δ , ppm): 8.14 (2H, d, J = 1.2 Hz), 7.54 (2H, d, J = 8.7 Hz), 7.01-7.49 (17H, m), 3.78 (2H, t, J = 7.2 Hz), 1.77 (2H, m), 1.26-1.47 (18H, m), 0.83 (3H, t, J = 6.2). ¹³C NMR (75 MHz, CDCl₃, δ , ppm): 147.32, 146.65, 143.32, 142.63, 139.67, 131.47, 127.87, 127.82, 127.31, 126.75, 124.69, 124.12, 123.58, 123.40, 123.28, 122.64, 121.94, 121.13, 116.26, 109.34, 52.61, 37.23, 34.80, 32.16, 32.05, 30.17, 29.83, 29.79, 29.75, 29.58, 29.49, 27.67, 27.23, 22.82, 14.25. HRMS calcd for $C_{52}H_{65}N_5S_2$: m/z 778.4354; found: m/z 779.2903 [M⁺].

4-(5'-Bromo-[2,2'-bithiophen]-5-yl)-N-(4-(3,6-di-tert-butyl-9H-carbazol-9-yl)phenyl)-N-dodecylaniline (7)

Compound 7 was prepared from **6** with a method similarly to that described above for **5** and obtained as light yellow-green sticky gum (1.1 g, 72%): FTIR (NaCl, v, cm⁻¹): 3029 (=C-H), 2923 (-C-H), 1589, 1576 (C=C), 1486, 1362, 1245, 810. ¹H NMR (300 MHz, CDCl₃, δ , ppm): 8.15 (2H, d, J = 1.8 Hz), 7.36-7.55 (8H, m), 7.21 (2H, d, J = 6.3 Hz), 7.06-7.14 (4H, m), 6.92 (2H, dd, J = 3.8, 12.6 Hz), 3.81 (2H, t, J = 7.2 Hz), 1.77 (2H, s), 1.27-1.55 (18H, m), 0.86 (3H, s). ¹³C NMR (75 MHz, CDCl₃, δ , ppm): 147.49, 146.47, 143.89, 142.61, 139.55, 139.15, 134.45, 131.69, 130.64, 127.78, 126.74, 124.90, 123.50, 123.36, 123.19, 122.53, 120.62, 110.57, 109.23, 52.56, 34.74, 32.0, 31.95, 29.69, 29.64, 29.48, 29.38, 27.58, 27.14, 22.71, 14.14. HRMS calcd for $C_{52}H_{61}BrN_2S_2$: m/z 856.3460; found: m/z 857.6411 [M⁺].

5-(4-((4-(3,6-Di-tert-butyl-9H-carbazol-9-yl)phenyl)(dodecyl)amino)phenyl)thiophene-2-carbaldehyde (8)

A mixture of 3 (0.6 g, 0.9 mmol), 5-formyl-2-thiopheneboronic acid (0.1 g, 0.6 mmol), $Pd(PPh_3)_4$ (0.016 g, 0.013 mmol), 2 M Na_2CO_3 aqueous solution (7 ml) in THF (20 ml) was degassed with N_2 for 5 min and then heated at reflux under N_2 atmosphere for 24 h. After cooling, DCM (50 ml) was added and the organic layer was washed with water (50 ml x 2) and brine solution (50 ml), dried over anhydrous Na_2SO_4 , filtered and evaporated to dryness. Purification by silica gel column chromatography using DCM/hexane

(1:4) as eluent gave yellow sticky gum (0.47 g, 54%): FTIR (NaCl, v, cm⁻¹): 3036 (=C-H), 2918 (-C-H), 1664 (C=O), 1600, 1510 (C=C), 1446, 1362, 1225, 805. HNMR (300 MHz, CDCl₃, δ , ppm): 9.85 (1H, s), 8.15 (2H, s), 7.70 (2H, d, J = 3.8 Hz), 7.58 (2H, d, J = 8.6 Hz), 7.26-7.53 (10H, m), 6.99 (2H, d, J = 8.6 Hz), 3.82 (2H, t, J = 7.5 Hz), 1.77 (2H, s), 1.26-1.54 (18H, m), 0.85 (3H, s). NMR (75 MHz, CDCl₃, δ , ppm): 182.52, 155.11, 149.14, 145.67, 142.83, 140.92, 139.37, 137.81, 133.54, 127.88, 127.52, 125.06, 124.21, 123.56, 123.31, 122.34, 117.96, 116.25, 109.18, 52.58, 34.73, 32.02, 31.91, 29.64, 29.44, 29.34, 27.55, 27.09, 22.68, 14.09. HRMS calcd for $C_{49}H_{60}N_2OS$: m/z 724.4426; found: m/z 724.6992 [M⁺].

5'-(4-((4-(3,6-Di-tert-butyl-9H-carbazol-9-yl)phenyl)(dodecyl)amino)phenyl)-[2,2'-bithiophene]-5-carbaldehyde (9)

Compound **9** was prepared from **5** with a method similarly to that described above for **8** and obtained as light yellow-green sticky gum (0.3 g, 57%): FTIR (NaCl, v, cm⁻¹): 3038 (=C-H), 2919 (-C-H), 1664 (C=O), 1607, 1511 (C=C), 1454, 1361, 1227. ¹H NMR (300 MHz, CDCl₃, δ , ppm): 9.85 (1H, s), 8.17 (2H, s), 7.65 (2H, d, J = 3.8 Hz), 7.18-7.51 (13H, m), 7.09 (2H, d, J = 8.6 Hz), 3.82 (2H, t, J = 7.5 Hz), 1.79 (2H, s), 1.29-1.49 (18H, m), 0.85 (3H, m). ¹³C NMR (75 MHz, CDCl₃, δ , ppm): 182.37, 148.02, 147.57, 146.62, 146.21, 142.72, 141.21, 139.50, 137.45, 133.76, 132.36, 127.82, 127.28, 126.91, 125.74, 123.65, 123.55, 123.34, 123.26, 122.85, 119.70, 116.24, 109.24, 52.57, 34.76, 32.07, 31.95, 29.69, 29.65, 29.49, 29.39, 27.60, 27.14, 22.72, 14.15. HRMS calcd for $C_{53}H_{62}N_{5}OS_{5}$: m/z 806.4304; found: m/z 806.7518 [M⁺].

5"-(4-((4-(3,6-Di-tert-butyl-9H-carbazol-9-yl)phenyl)(dodecyl)amino)phenyl)-[2,2':5',2"-terthiophene]-5-carbaldehyde (10)

Compound **10** was prepared from 7 with a method similarly to that described above for **8** and obtained as yellow-orange solid (0.28 g, 51%): m.p. > 250 °C, FTIR (KBr, v, cm⁻¹): 3059 (=C-H), 2914 (-C-H), 1659 (C=O), 1597, 1509 (C=C), 1454, 1356, 1225, 1046, 809, 791. ¹H NMR (300 MHz, CDCl₃, δ , ppm): 9.84 (1H, s), 8.26 (2H, s), 7.09-7.58 (18H, m), 3.82 (2H, s), 1.83 (2H, s), 1.36-1.63 (18H, m), 0.95 (3H, s). ¹³C NMR (75 MHz, CDCl₃, δ , ppm): 182.27, 147.67, 146.87, 146.39, 144.59, 142.74, 141.51, 139.60, 139.52, 137.39, 134.41, 134.10, 132.00, 127.81, 127.03, 126.79, 126.43, 125.53, 124.19, 123.94, 123.63, 123.34, 122.79, 122.74, 120.31, 116.30, 109.36, 52.59, 34.82, 32.17, 32.05, 29.79, 29.75, 29.58, 29.49, 27.68, 27.22, 22.82, 14.27. HRMS calcd for $C_{57}H_{64}N_2OS_3$: m/z 888.4181; found: m/z 889.4700 [MH⁺].

(E)-2-Cyano-3-(5-(4-((4-(3,6-di-tert-butyl-9H-carbazol-9-yl)phenyl)(dodecyl)amino)phenyl) thiophen-2-yl)acrylic acid (UB4)

A mixture of 8 (0.16 g, 0.2 mmol), cyanoacetic acid (0.04 g, 0.4 mmol) and piperidine (2 drops) in chloroform (20 ml) was degassed with N_2 for 5 min and then heated at reflux under N_2 atmosphere for 8 h. After cooling, the reaction was quenched with water (5 ml) and extracted with DCM (50 ml x 2). The combined organic layer was washed with water (50 ml x 2) and brine (50 ml), dried over anhydrous Na_2SO_4 , filtered and evaporated to dryness. Purification by silica gel column chromatography eluting with

MeOH:DCM (1:9) afforded orange solid (0.11 g, 61%): m.p. >250 °C, FTIR (KBr, ν, cm⁻¹): 3421 (O-H), 3042 (=C-H), 2925 (-C-H), 2213 (C≡N), 1598 (C=O), 1512 (C=C), 1363, 1225, 808. ¹H NMR (300 MHz, DMSO-D₆/CDCl₃, δ, ppm): 8.22 (3H, s), 7.77 (1H, s), 7.62 (2H, d, J = 8.1 Hz), 7.29-7.52 (9H, m), 7.04 (2H, d, J = 8.4 Hz), 3.81 (2H, s), 1.67 (2H, s), 1.19-1.40 (18H, m), 0.80 (3H, s). ¹³C NMR (75 MHz, DMSO/CDCl₃, δ, ppm): 164.42, 148.68, 145.88, 142.73, 139.20, 134.55, 132.41, 127.85, 127.59, 124.71, 124.45, 123.91, 123.29, 123.14, 119.15, 116.79, 109.51, 52.08, 34.88, 32.27, 31.77, 29.54, 29.49, 29.44, 29.26, 29.1, 27.49, 26.81, 22.56, 14.34. HRMS calcd for $C_{52}H_{61}N_3O_2S$: m/z 791.4484; found: m/z 791.9125 [M⁺].

(E)-2-Cyano-3-(5'-(4-((4-(3,6-di-tert-butyl-9H-carbazol-9-yl)phenyl)(dodecyl)amino)phenyl)-[2,2'-bithiophen]-5-yl)acrylic acid (UB5)

Compound **UB5** was prepared from **9** with a method similarly to that described above for **UB4** and obtained as red solid (0.12 g, 59%): m.p. > 250 °C, FTIR (KBr, v, cm⁻¹): 3420 (O-H), 3041 (=C-H), 2925 (-C-H), 2213 (C \equiv N), 1598 (C=O), 1512 (C=C), 1363, 1225, 809. ¹H NMR (300 MHz, DMSO-D₆/CDCl₃, δ , ppm): 8.14 (1H, s), 8.04 (2H, s), 7.87 (1H, s), 7.15-7.50 (13H, m), 6.97 (2H, d, J = 7.8 Hz), 3.71 (2H, s), 1.65 (2H, s), 1.17-1.37 (18H, m), 0.75 (3H, s). ¹³C NMR (75 MHz, DMSO/CDCl₃, δ , ppm): 167.00, 147.61, 146.15, 145.33, 143.82, 142.59, 139.22, 135.12, 133.87, 131.62, 127.52, 126.71, 125.84, 123.85, 123.67, 123.10, 120.04, 116.19, 109.37, 52.28, 34.70, 32.33, 31.67, 29.52, 29.48, 29.31, 29.22, 27.46, 26.93, 22.57, 14.22. HRMS calcd for $C_{56}H_{63}N_3O_2S_3$: m/z 873.4362; found: m/z 874.1042 [M⁺].

(E)-2-Cyano-3-(5"-(4-((4-(3,6-di-tert-butyl-9H-carbazol-9-yl)phenyl)(dodecyl)amino)phenyl)-[2,2':5',2"-terthiophen]-5-yl)acrylic acid (UB6)

Compound **UB6** was prepared from **10** with a method similarly to that described above for **UB4** and obtained as dark red solid (0.18 g, 47%): m.p. > 250 °C, FTIR (KBr, V, cm⁻¹): 3421 (O-H), 3036 (=C-H), 2924 (-C-H), 2212 (C \equiv N), 1602 (C=O), 1512 (C=C), 1363, 1225, 808. ¹H NMR (300 MHz, DMSO-D₆/CDCl₃, δ , ppm): 8.12 (1H, s), 8.02 (2H, s), 7.75-7.73 (3H, m), 7.07-7.51 (13H, m), 6.99 (2H, d, J = 8.4 Hz), 3.73 (2H, s), 1.66 (2H, s), 1.16-1.37 (18H, m), 0.75 (3H, s). ¹³C NMR (75 MHz, DMSO/CDCl₃, δ , ppm): 167.02, 147.31, 146.21, 143.82, 143.40, 142.55, 139.23, 138.29, 135.40, 134.29, 131.40, 127.47, 126.56, 126.27, 125.43, 124.14, 123.61, 122.97, 122.86, 122.54, 120.31, 116.12, 109.32, 52.28, 34.67, 32.09, 31.79, 29.55, 29.51, 29.47, 29.31, 29.22, 27.44, 26.93, 22.57, 14.19. HRMS calcd for C₆₀H₆₅N₃O₂S₃: m/z 955.4239; found: m/z 956.1763 [M⁺].

ภาคผนวก

ผลงานตีพิมพ์

- A Thangtong, D. Meunmart, T. Sudyoadsuk, S. Jungsuttiwong, N. Prachumrak, T. Keawin and V. Promarak, Bifunctional anthracene derivatives as non-doped blue emitters and hole-transporters for electroluminescent devices, *Chemical Communications*, 2011, 47, 7122-7124. (IF 5.80)
- A. Thangthong, D. Meunmart, N. Prachumrak, S. Jungsuttiwong, T. Keawin, T. Sudyoadsuk and V. Promarak, Synthesis and characterization of 9,10-substituted anthracene derivatives as blue light-emitting and hole-transporting materials for electroluminescent devices, *Tetrahedron*, 2012, 68, 1853-1861. (IF 3.01)
- A. Thangthong, N. Prachumrak, R. Tarsang, T. Keawin, S. Jungsuttiwong, T. Sudyoadsuk and V. Promarak, Blue Light-Emitting and Hole-Transporting Materials Based on 9,9-Bis(4-diphenylaminophenyl)fluorenes for Efficient Electroluminescent Devices, *Journal of Materials Chemistry*, 2012, 6869–6877. (IF 5.01)
- P. Moonsin, N. Prachumrak, R. Rattanawan, T. Keawin, S. Jungsuttiwong, T. Sudyoadsuk and V. Promarak, Carbazole Dendronised Triphenylamines as Solution Processed High Tg Amorphous Hole-Transporting Materials for Organic Electroluminescent Devices, *Chemical Communications*, 2012, 48, 3365-3464 (Inside cover image). (IF 5.80)
- J. Khunchalee, R.Tarsang, N. Prachumrak, S. Jungsuttiwong, T. Keawin, T. Sudyoadsuk and V. Promarak, Synthesis and Properties of Oligofluorene-thiophenes as Emissive Materials for Organic Electroluminescent Devices, *Tetrahedron*, 2012, submitted
- D. Muenmart, R. Tarsang, S. Jungsuttiwong, T. Keawin, T. Sudyoadsuk and V. Promarak, Synthesis
 and Properties of Fluorene-oligothiophenes Perylenediimide Triads and Their Electropolymerizations, *Journal of Materials Chemistry*, 2012, submitted
- N. Prachumrak, A. Thangthong, R. Tarsang, T. Keawin, S. Jungsuttiwong, T. Sudyoadsuk, and V. Promarak, Pyrene-Functionalized 9,9-Bis(4-diphenylaminophenyl)fluorene as Solution-Processed Blue Emitting and Hole-Transporting Materials for Efficient Electroluminescent Devices, *Organic Electronics*, 2012, submitted
- A. Thangthong, N. Prachumrak, S. Namuangruk, S. Jungsuttiwong, T. Keawin, T.Sudyoadsuk and V. Promarak, Synthesis, Properties and Applications of Biphenyl Functioned 9,9-Bis(4-diphenylaminophenyl)fluorene as Bifunctional Materials for Organic Electroluminescent Devices, Tetrahedron, 2012, submitted

- D. Meunmart, N. Prachumrak, T. Keawin, S. Jungsuttiwong, T. Sudyoadsuk and V. Promark, Bis(4-diphenylaminophenyl)carbazole end-capped fluorene as solution-processed deep blue light-emitting and hole-transporting materials for electroluminescent devices, *Tetrahedron Letters*, 2012, submitted
- 10. S. Namuangruk, M. Ehara, R.Fukuda, J. Meeprasert, T. Khanasa, S. Morada, T. Kaewin, S. Jungsuttiwong, T. Sudyoadsuk and V. Promarak, Synthesis, characterization, and theoretical investigation of D-D-π-A type organic dyes for dye-sensitized solar cells, *Jouranl of American Chemical Society*, 2012, in submission process

ผลงานเอกสารประกอบการประชุมวิชาการ

- V. Promarak, T. Sudyoadsuk, S. Jungsuttiwong, N. Prachumrak, D. Meunmart, and A. Phansuphon, Novel Blue Electroluminescence Materials Based on 9,10-Disubstituted Anthracenes for OLEDs, The 8th International Conference on Optical Probes of Conjugated Polymers and Organic Nanostructures, China, 2009, 133. (Oral presentation)
- 2. N. Prachumrak, T. Keawin, S. Jungsuttiwong, T. Sudyoadsuk and V. Promarak, 9,10-Substituted Anthracene Derivatives as Blue Light-Emitting and Hole-Transporting Materials for Electroluminescent Devices, International Symposium on Electronic/Optic Functional Molecules (ISEOFM2012) ระหว่างวันที่ 11 -13 มีนาคม 55 ณ ประเทศ China (Oral presentation)

รางวัล

1. รางวัล Wiley-CST Outstanding Publication Award 2011 ปี 2554 จากสมาคมเคมีแห่งประเทศไทย ในพระบรมราชูปถัมภ์ จากผลงานตีพิมพ์ เรื่อง Bifunctional anthracene derivatives as non-doped blue emitters and hole-transporters for electroluminescent devices, *Chemical Communications*, 2011, 47, 7122-7124. (IF 5.80)





หน้าที่ 177

2. ผลงานตีพิพ์ที่ได้รับการลงปกของวารสาร

จากผลงานที่พิมพ์ เรื่อง Carbazole Dendronised Triphenylamines as Solution Processed High Tg Amorphous Hole-Transporting Materials for Organic Electroluminescent Devices, *Chemical Communications*, **2012**, 48, 3365-3464

